



UNIVERSITAT_{DE}
BARCELONA

Nanoencapsulated antimicrobials to fight *Pseudomonas aeruginosa* respiratory infections in cystic fibrosis patients: a promising strategy

Eulàlia Sans Serramitjana



Aquesta tesi doctoral està subjecta a la llicència **Reconeixement 3.0. Espanya de Creative Commons.**

Esta tesis doctoral está sujeta a la licencia **Reconocimiento 3.0. España de Creative Commons.**

This doctoral thesis is licensed under the **Creative Commons Attribution 3.0. Spain License.**



UNIVERSITAT_{DE}
BARCELONA

PhD Thesis

**NANOENCAPSULATED ANTIMICROBIALS TO FIGHT
Pseudomonas aeruginosa RESPIRATORY INFECTIONS IN
CYSTIC FIBROSIS PATIENTS: A PROMISING STRATEGY**

DOCTORATE IN MEDICINE

AUTHOR: EULALIA SANS SERRAMITJANA

SUPERVISORS: Prof. Dr. MIQUEL VIÑAS CIORDIA AND

Dr. ESTER FUSTÉ DOMÍNGUEZ

L'Hospitalet de Llobregat, April 2017



UNIVERSITAT DE
BARCELONA

**DEPARTMENT OF PATHOLOGY AND EXPERIMENTAL
THERAPEUTICS**

Laboratory of Molecular Microbiology and Antimicrobials

Faculty of Medicine and Health Sciences

University of Barcelona

**NANOENCAPSULATED ANTIMICROBIALS TO FIGHT
Pseudomonas aeruginosa RESPIRATORY INFECTIONS IN
CYSTIC FIBROSIS PATIENTS: A PROMISING STRATEGY**

DOCTORATE IN MEDICINE

AUTHOR: EULALIA SANS SERRAMITJANA

SUPERVISORS: Prof. Dr. MIQUEL VIÑAS CIORDIA AND
Dr. ESTER FUSTÉ DOMÍNGUEZ

L'Hospitalet de Llobregat, April 2017



Miquel Viñas Ciordia, Catedràtic de Microbiologia del Departament de Patologia i Terapèutica Experimental i **Ester Fusté Domínguez**, professora lectora del Departament de Salut Pública, Salut Mental i Matern-infantil, ambdós de la Facultat de Medicina i Ciències de la Salut de la Universitat de Barcelona,

CERTIFIQUEN,

Que la Tesi Doctoral presentada per **Eulàlia Sans Serramitjana** i titulada "*Nanoencapsulated antimicrobials to fight Pseudomonas aeruginosa respiratory infections in cystic fibrosis patients: a promising strategy*" ha estat desenvolupada per l'autora sota la nostra supervisió en el laboratori de Microbiologia Molecular i Antimicrobians del Campus de Bellvitge.

Que la recerca desenvolupada i el manuscrit presentat compleix els requisits formals i conceptuals per a que pugui ser defensada davant del tribunal corresponent.

I per a que consti signen el present document a l'Hospitalet de Llobregat, el dia 28 d'abril del 2017

Prof.Dr. Miquel Viñas Ciordia

Dra. Ester Fusté Domínguez

Title: Nanoencapsulated antimicrobials to fight *Pseudomonas aeruginosa* respiratory infections in cystic fibrosis patients: a promising strategy.

Author: **Eulàlia Sans Serramitjana**

Setting: Laboratory of Molecular Microbiology and Antimicrobials. Dept. Pathology and Experimental Therapeutics. Faculty of Medicine and Health Sciences. University of Barcelona.

Supervisors: **Prof. Dr. Miquel Viñas Ciordia** (Full professor Dept. Pathology & Experimental Therapeutics) and **Dr. Ester Fusté Domínguez** (Lecturer Dept. Public Health, Mental Health and Perinatal Nursing). Faculty of Medicine and Health Sciences. University of Barcelona.

Evaluation Committee:

President: Prof. Dr. **Gaspar Lorén Egea** (Retired Full Professor of Microbiology).

Prof. Dr. **Roman Pallarés** (Full Professor Infectious diseases; Universitat de Barcelona).

Dr. **Paola Russo** (Associate Professor; Università degli studi di Salerno).

A Thesis submitted in fulfillment of the requirements for the degree of Doctor including the mention of "International Doctor" by the University of Barcelona.

Signed: Eulàlia Sans Serramitjana

L'Hospitalet de Llobregat, 28TH April 2017

“Hope is the dream of a waking man”.

Aristotle

“The important thing is not to stop questioning. Curiosity has its own reason for existing”.

Albert Einstein

A la meva família.

A la meva amiga Laura.

Perquè la teva valentia i perseverança inesgotables
han fet que avui estiguis gaudint de la llibertat. No et
rendeixis mai.

ACKNOWLEDGMENTS

ACKNOWLEDGMENTS

La realització d'aquesta Tesis Doctoral ha estat possible gràcies a un contracte de recerca realitzat pel grup liderat per el Prof. Dr. Miquel Viñas (Febrer 2012-Març 2017) i al contracte de professor associat vinculat a la Unitat de microbiologia del Departament de Patologia i Terapèutica Experimental del Campus de Bellvitge.

Els estudis realitzats en aquest treball s'han portat a terme mitjançant:

Projecte **Terfiquec-Innpacto**: "**Investigación integral de terapias efectivas para el tratamiento de la fibrosis quística y enfermedades conexas**".
Ministerio de Ciencia e Innovación; IPT-2011-1402-900000.

IMI (Innovative medicines initiative) - **ENABLE** (European Gram-negative Antibacterial engine) International Project; (IMI-ND4BB, <http://www.imi.europa.eu/content/enable>).

ACKNOWLEDGMENTS

Quan és moment de finalitzar una llarga etapa en la qual s'hi han viscut tantes experiències, m'adono de la quantitat de persones que m'han acompanyat en aquesta aventura i que m'han ajudat a aconseguir un dels meus somnis. Em sento immensament afortunada per l'aprenentatge tan a nivell professional com personal que he rebut de cada una d'elles. Gràcies a tots per compartir amb mi tant els moments amargs com els de felicitat plena.

Al Dr. Miquel Viñas, director d'aquesta tesi, per donar-me la oportunitat de formar part de la meravellosa família de la Unitat de microbiologia de Bellvitge. Gràcies per dipositar la confiança en mi i poder realitzar un dels meus somnis. Són molts els moments viscuts...que cada un d'ells han servit per donar-me consells, per aportar-me coneixements, per despertar-me l'esperit crític, per endinsar-me en el món de la microbiologia i de les noves alternatives terapèutiques com les nanopartícules, per transmetre'm la il·lusió necessària per seguir endavant en tot moment, i en definitiva, per créixer com a persona. Gràcies per aportar-me serenitat i experiència que són el premi de la maduresa per a una vida més plena.

A la Dra. Teresa Vinuesa, per fer-me sentir com a casa des de el primer dia que vaig arribar. Durant aquests anys hem compartit molts moments dins i fora de la feina... congressos, dinars, sopars, llargues converses al laboratori... tots ells han estat acompanyats d'afecte, generositat i comprensió. Gràcies per ajudar-me a resoldre i a afrontar diferents situacions viscudes en tot moment i contagiar-me la teva energia i vitalitat.

A la Dra. Ester Fusté, codirectora d'aquesta tesi, per tot el temps i esforç que li has dedicat a aquest treball i per ensenyar-me que la recerca científica et dona dies de tot tipus però que rendir-se mai és una opció. Gràcies per ensenyar-me que la microbiologia també et permet cultivar amistats .

M'agradaria ampliar aquest agraïment a la Dra. Blanca Martínez, per la seva ajuda i recolzament durant tots aquests anys. Les seves correccions són impecables. Gràcies per ser com ets, ha estat un plaer creuar-me amb tu i poder descobrir la teva essència.

ACKNOWLEDGMENTS

Al personal del Servei de Microbiologia del Hospital de Sant Joan de Déu i de l'hospital de la Vall d'Hebrón per cedir-nos les soques clíniques de *Pseudomonas aeruginosa* aïllades de pacients amb fibrosi quística, gràcies a això he pogut realitzar part de la tesi doctoral.

Al Dr. Eusebio Gainza de Praxis Pharmaceutical y a todo el equipo del Dr. José Luis Pedraz del Departamento de Farmacia y Tecnología Farmacéutica de la UPV/EHU, en especial a la Dra. Marta Pastor y a la Dra. María Moreno por la elaboración de las nanopartículas lipídicas y las colaboraciones que hemos realizados conjuntamente a lo largo de estos años. Reuniones, llamadas, correos electrónicos... han valido la pena para llegar hasta aquí. Marta, siempre recordaré el divertido día que compartimos en Palma de Mallorca.

Al Dr. Daniel Bachiller de la Fundación Caubet-Cimera, Centro Internacional de Medicina Respiratoria avanzada, y a todo su equipo por el buen trato recibido durante mi estancia en su laboratorio.

I would like to thank Prof. Dr. Roland Benz and his wonderful team, for accepting me to his laboratory in Würzburg during my undergraduate period, and for giving me the opportunity to be a coauthor of one of your publications. I really appreciate your help inside and outside the lab and the knowledge about the black lipid bilayer technique you taught me. Thanks to that experience I met Prof. Dr. Viñas and I've achieved one of my dreams.

Prof. Dr. Winterhalter, thank you very much for accepting me in your laboratory in Bremen in the forthcoming months. It will be a great experience for me.

Specially thanks to Dr. Michael Federle, for accepting me to his team in the Dept. of Medicinal Chemistry and Pharmacognosy at the University of Illinois at Chicago (UIC) and support my work. Mike and Juan, thanks a lot for introducing me to the complex world of bacterial *quorum sensing*.

ACKNOWLEDGMENTS

I would like to thank FEMS and SEM for giving me the opportunity to go to Dr. Mathias Winterhalter laboratory of Life Sciences & Chemistry in the Jacobs University (Germany) through the FEMS Research Fellowship 2016.

Vull agrair al Programa de Doctorat Medicina de la Universitat de Barcelona la concessió de l'ajut de mobilitat durant el curs 2014-2015 per a la obtenció de la menció internacional de doctor al laboratori del Dr. Michael Federle de la University of Illinois at Chicago (UIC).

També vull donar les gràcies a la extinta facultat d'Odontologia de la Universitat de Barcelona per concedir-me durant els cursos 2013 i 2016 un ajut per a estudiants de doctorat per a finançar material necessari per a la realització dels experiments.

A la unitat de Microbiologia del Departament de Patologia i Terapèutica Experimental per haver-me donat la oportunitat de formar part del seu equip docent. Gràcies per deixar-me gaudir d'aquesta experiència tan enriquidora. Lupe, gràcies per ensenyar-me tant durant tots aquests anys a les pràctiques de microbiologia. Ets una gran persona!

Milions de gràcies també a tot l'equip d'afers generals del Campus de Bellvitge per a la vostra ajuda i col·laboració sempre que ho he necessitat. Als que hi sou i als que ja no hi sou... Rosaura, Isa Gil, Isa Estradera, Carlos, Rosa, Susanna...Gràcies. Isa Estradera impossible oblidar-me de les llargues estones que hem passat organitzant factures!

I amb molt d'afecte, vull donar gràcies infinites a tots els meus companys i companyes de laboratori que he pogut conèixer i compartir moments immillorables. Estic molt contenta d'haver format part d'aquest gran equip humà que per davant de tot sempre ha prioritzat treballar amb molt bon ambient i on tothom sempre ha estat disposat a ajudar. Ester, Blanca, Josep Maria, Lupe, Eva, Lúdia, Iraida, Erica, Marina, Clara, Laura Oliver, Laura Giovannoni, Betty, Scarlett, Carme, Elena, Carolina, Sheila, Andrea, Maria, Michele... i en especial vull agrair enormement als meus amics i companys

ACKNOWLEDGMENTS

del “Lab Non Stop” per fer que m’aixequi cada dia amb ganes d’anar a la feina i de compartir moltes hores amb tots vosaltres. Viatges, sopars, vermouths, festes... i també ciència... sempre han sigut moments alegres. A l’Alex, per compartir amb mi aquest camí des del principi fins el final. Et desitjo el millor i aprofita totes les oportunitats que se’t presentin...perquè vals i molt. A la Rocío, per el suport i l’ajuda que sempre m’has ofert i per ser una de les persones més assertives que conec. A Héctor, por ser mi compañero de combate contra *P. aeruginosa*, por ser mi asesor informático, y por enseñarme la importancia de defender las ideas y valores. A l’Eva, per ser una de les persones més bondadoses que conec i per el teu suport incondicional. No canviïs mai. Al Pablo, por ser una persona tan especial y hacerme sonreír todos los días. A la Marta i a l’Elena, per compartir intensament el final d’aquesta etapa i el principi de la vostra. Gràcies per la vostra predisposició a ajudar-me sempre. Seguiu així que arribareu molt lluny. A la Isa i a l’Anna, per aportar frescor al laboratori i per les ganes d’aprendre i l’entusiasme que sempre despreneu.

A la meva família. Als meus avis per fer-me sentir la persona més estimada del món i per transmetre’m la seva il·lusió de viure i compartir amb mi el final d’aquesta aventura. Gràcies avi per preguntar-me cada diumenge com anava la tesi i per escoltar les meves explicacions. Sou el tresor més gran que tinc.

Als meus pares, per fer-me feliç cada dia. Sempre m’heu recolzat amb totes les meves decisions sense esperar res a canvi. Gràcies per abraçar-me quan he caigut i per saltar amb mi quan m’he aixecat. Per tots els valors que m’heu transmès, per tota l’estima que he rebut i per tots els consells que m’heu donat, he arribat fins aquí. Us estimo.

Al meu tiet Santi, per ser el meu tiet, segon pare, germà, amic... per ser-hi sempre i animar-me en tot moment a tirar endavant.

A tots els meus amics, per l’interès i suport que m’ han mostrat en tots aquests anys. Sóc una privilegiada de tenir-vos ben a prop a meu.

SCIENTIFIC PRODUCTION

The five years period employed in this thesis has allowed the participation in the research which production is presented in the following list:

Publications in international peer-reviewed journals

1. Bárcena-Uribarri I, Thein M, Barbot M, **Sans-Serramitjana E**, Bonde M, Mentele R, Lottspeich F, Bergström S, Benz R. Study of the protein complex, pore diameter, and pore-forming activity of the *Borrelia burgdorferi* P13 porin. **Journal of Biological Chemistry** 2014; 289:18614-24. **Impact Factor** according to 2014 Journal Citation Reports released by Thomson Reuters (ISI) is **4.258**.
2. Pastor M, Moreno-Sastre M, Esquisabel A, **Sans E**, Viñas M, Bachiller D, Asensio VJ, Pozo AD, Gainza E, Pedraz JL. Sodium colistimethate loaded lipid nanocarriers for the treatment of *Pseudomonas aeruginosa* infections associated with cystic fibrosis. **International Journal of Pharmaceutics** 2014; 477:485-94. **Impact Factor** according to 2014 Journal Citation Reports released by Thomson Reuters (ISI) is **3.650**.
3. Moreno-Sastre M, Pastor M, Esquisabel A, **Sans E**, Viñas M, Fleischer A, Palomino E, Bachiller D, Pedraz JL. Pulmonary delivery of tobramycin-loaded nanostructured lipid carriers for *Pseudomonas aeruginosa* infections associated with cystic fibrosis. **International Journal of Pharmaceutics** 2016; 498:263-73. **Impact Factor** according to 2015 Journal Citation Reports released by Thomson Reuters (ISI) is **3.994**.
4. **Sans-Serramitjana E**, Fusté E, Martínez-Garriga B, Merlos A, Pastor M, Pedraz JL, Esquisabel A, Bachiller D, Vinuesa T, Viñas M. Killing effect of nanoencapsulated colistin sulfate on *Pseudomonas aeruginosa* from cystic fibrosis patients. **Journal of Cystic Fibrosis** 2016; 15:611-8. **Impact Factor** according to 2015 Journal Citation Reports released by Thomson Reuters (ISI) is **3.853**.
5. Moreno-Sastre M, Pastor M, Esquisabel A, **Sans E**, Viñas M, Bachiller D, Pedraz JL. Stability study of sodium colistimethate-loaded lipid

nanoparticles. **Journal of Microencapsulation** 2016; 14:1-10. **Impact Factor** according to 2015 Journal Citation Reports released by Thomson Reuters (ISI) is **1.631**.

6. **Sans-Serramitjana E**, Jorba M, Pedraz JL, Vinuesa T, Viñas M. Determination of the spatiotemporal dependence of the *P.aeruginosa* biofilm viability after treatment with NLC-colistin. In press accepted manuscript. **International Journal of Nanomedicine**. **Impact Factor** according to 2015 Journal Citation Reports released by Thomson Reuters (ISI) is **4.320**.
7. **Sans-Serramitjana E**, Jorba M, Fusté E, Pedraz JL, Vinuesa T, Viñas M. Free and nanoencapsulated tobramycin: their effect on planktonic and biofilm cystic fibrosis *Pseudomonas*. Submitted to **Microorganisms**.

Congress participations

1. Gil-Martin I, **Sans E**, Fusté E, Vinuesa T, Viñas M. Poster presentation: Susceptibilidad a los antimicrobianos en *Pseudomonas aeruginosa* de enfermos de fibrosis quística. IV Congreso del Grupo Especializado Biología de Microorganismos Patógenos. 5-7 July 2012. Badajoz, Spain.
2. **Sans E**, Gil-Martin I, Fusté E, Vinuesa T, Viñas M. Poster presentation: Evaluación de la capacidad formadora de biofilm de cepas de *Pseudomonas aeruginosa* aisladas de enfermos de fibrosis quística. XXIV Congreso Microbiología SEM. 10-13 July 2013. L'Hospitalet de Llobregat, Spain.
3. Gil-Martin I, **Sans E**, Fusté E, Vinuesa T, Viñas M. Poster presentation: Análisis de la eficacia de nuevas formulaciones de antibióticos con nanopartículas frente a *Pseudomonas aeruginosa*, aisladas de enfermos de fibrosis quística. XXIV Congreso Microbiología SEM. 10-13 July 2013. L'Hospitalet de Llobregat, Spain.

4. Fusté E, Gil-Martin I, **Sans E**, Purello S, Bertuccio T, Cafiso V, Stefani S, Vinuesa T, Viñas M. Poster presentation: Comparison of Methods to Study Biofilm Formation by Cystic Fibrosis Isolates. XXIV Congreso Microbiología SEM. 10-13 July 2013. L'Hospitalet de Llobregat, Spain.
5. **Sans E**, Gil-Martin I. Oral communication: Study of antimicrobial activity of new formulations for the treatment of infections caused by *Pseudomonas aeruginosa* in Cystic fibrosis patients. Symposium AG Benz. 2-4 August 2013. Bremen, Germany.
6. Pastor M, Moreno-Sastre M, Esquisabel A, Herran E, Villullas S, Ibarrola O, del Pozo A, Aguirre JJ, Castresana M, **Sans E**, Viñas M, Bachiller D, Pedraz JL, Gainza E. Poster presentation: Lipid Nanoparticles as tobramycin and sodium colistimethate encapsulation alternative: towards improved anti-infective therapy against *Pseudomonas aeruginosa* infection. ImagineNano 2015. 10-13 March 2015. Bilbao, Spain.
7. **Sans-Serramitjana E**, Fusté E, Martínez-Garriga B, Pastor M, Pedraz JL, Vinuesa T, Bachiller D, Viñas M. Poster presentation: Nano-encapsulated colistin sulphate: antipseudomonal activity. 6th Congress of European Microbiologists. 7-11 June 2015. Maastricht, Holland.
8. **Sans-Serramitjana E**, Vinuesa T, Pedraz JL, Viñas M, Fusté E. Oral communication: Antibióticos nano-encapsulados en el combate contra las infecciones respiratorias por *Pseudomonas aeruginosa*. XXV Congreso Nacional de Microbiología. 7-10 July 2015. Logroño, Spain.
9. **Sans-Serramitjana E**, Fusté E, Martinez-Garriga B, Merlos A, Jorba M, Vinuesa T, Viñas M. Poster presentation: Nano-Encapsulated colistin sulphate to fight *Pseudomonas aeruginosa* infections. IMI Translocation meeting 2016 - Novel approaches to fight bacteria. 10-14 July 2016. Bremen, Germany.

10. Rudilla H, Fusté E, **Sans-Serramitjana E**, Rabanal F, Vinuesa T, Viñas M. Poster presentation: Antimicrobial synthetic cyclopeptides activity on *Staphylococcus aureus*. Microbiology and Infection 2017- 5th Joint Conference of the DGHM & VAAM. 5-8 March 2017. Würzburg, Germany.

ABSTRACT

P. aeruginosa is one of the major opportunistic pathogen colonizing the respiratory tract of cystic fibrosis (CF) patients and causing chronic airways infection. Once *P. aeruginosa* established chronically in the CF lung, bacterial density increases and the microorganism switches to a mucoid form and to a stable biofilm mode of growth in which susceptibility to antimicrobials decreases. The high resistance of *P. aeruginosa* to multiple antimicrobials led to scenarios in which almost no treatment options are available. In this regard, the research on the introduction of less toxic antimicrobials as well as the use of pharmaceutical forms enabling dose reductions, longer administration intervals, and reduced systemic toxicity has been stimulated.

Therefore, the aim of this thesis was to develop nanoencapsulated colistin and tobramycin in lipid nanoparticles (SLN: Solid Lipid Nanoparticles and NLC: Nanostructured Lipid Carriers) and explore their antimicrobial activity versus free drug against *P. aeruginosa* clinical isolates from CF patients and to investigate the efficacy of these novel formulations in the eradication of biofilms, one of the most relevant mechanisms involved in persistence and in chronic infections.

Elaboration and characterization

The main objective of the first part of this thesis was to elaborate and characterize lipid nanoparticles (SLN and NLC) as colistin and tobramycin carriers to treat *P. aeruginosa* lung infection.

The nanoparticles obtained displayed a 200–400 nm size, high drug encapsulation (79–94%) and a sustained drug release profile. The integrity of the nanoparticles was not affected by nebulization through a mesh vibrating nebulizer. Next, tobramycin-NLCs were able to overcome an artificial mucus barrier in the presence of mucolytic agents. Moreover, lipid nanoparticles loaded with both antimicrobials appeared to be less toxic than free drug in cell culture. Finally, an *in vivo* distribution experiment showed that nanoparticles spread homogenously through the lung and there was no migration of lipid nanoparticles to other organs, such as liver, spleen or kidneys.

Stability

The second essential point of this work concerns the stability of both types of lipid nanoparticles after freeze-drying.

The results showed that colistin-SLNs lost their antimicrobial activity at the third month; on the contrary, the antibacterial activity of colistin-NLCs was maintained throughout the study within an adequate range. In addition, colistin-NLCs exhibited suitable physic-chemical properties at 5 °C and 25 °C/60% relative humidity over one year. Altogether, colistin-NLCs proved to have better stability than colistin-SLNs.

Antimicrobial activity

The last part focuses on the study of the antimicrobial activity of SLN and NLC loaded with colistin and tobramycin against *P. aeruginosa* isolates from Sant Joan de Déu and Vall d'Hebrón hospitals CF patients.

Regarding the data documenting planktonic experiments, colistin nanoparticles had the same antimicrobial activity as free drug. The activity of tobramycin-loaded SLN was less than that of either tobramycin-loaded NLC or free tobramycin. However, in the relation to biofilms, nanoencapsulated antimicrobials were much more efficient than their free form. Moreover, the results showed the more rapid killing of *P. aeruginosa* bacterial biofilms by NLC-colistin than by free colistin. Nevertheless, the two formulations did not differ in terms of the final percentages of living and dead cells, which were higher in the inner than in the outer layers of the treated biofilms.

Since it seems clear that biofilms play a key role in respiratory infections in CF patients by *P. aeruginosa*, these formulations seem to us encouraging alternative to the currently available CF therapies.

RESUM

P. aeruginosa és un dels principals patògens oportunistes colonitzadors del tracte respiratori dels pacients amb fibrosi quística (FQ) causant una infecció crònica. Una vegada aquest microorganisme ja està establert de manera crònica al pulmó, la densitat bacteriana augmenta i *P. aeruginosa* canvia de morfologia no mucosa a mucosa afavorint la formació de biofilm en el qual la susceptibilitat als antibiòtics es veu enormement disminuïda. L'elevada resistència de *P. aeruginosa* a múltiples antimicrobians ens condueix a un escenari on gairebé no hi ha opcions de tractament disponibles. En aquest sentit, la recerca en la introducció d'antimicrobians menys tòxics així com l'ús de noves formes farmacèutiques amb la capacitat de reduir la dosi, allargar els intervals d'administració així com reduir la toxicitat adquireix molta rellevància.

Per tant, l'objectiu d'aquesta tesi va ser desenvolupar nanopartícules lipídiques (*Solid Lipid Nanoparticles*: SLN y *Nanostructured Lipid Carriers*: NLC) carregades amb colistina i tobramicina, explorar la seva activitat antimicrobiana comparant-la amb la seva forma lliure contra soques clíniques de *P.aeruginosa* aïllades de pacients amb FQ, i investigar l'eficàcia d'aquestes noves nanoformulacions en l'eradicació dels biofilms ja que és un dels mecanismes més rellevants associat a les infeccions cròniques.

Elaboració i caracterització

L'objectiu principal de la primera part d'aquesta tesi va ser l'elaboració i caracterització de nanopartícules lipídiques (SLN i NLC) carregades amb colistina i tobramicina per a tractar infeccions respiratòries causades per *P. aeruginosa*.

Les nanopartícules obtingudes van presentar un diàmetre d'entre 200 i 400 nm, una elevada eficiència d'encapsulació (79-94%) i un alliberament sostingut del fàrmac. La integritat de les nanoformulacions no es va veure afectada per el procés de nebulització mitjançant l'ús d'un nebulitzador de malla vibratòria. A continuació, també es va observar que les NLC amb tobramicina tenien la capacitat de travessar una barrera de moc artificial amb

la presència d'agents mucolítics. En relació a la toxicitat, cal destacar que les nanopartícules lipídiques carregades amb colistina i tobramicina van ser menys tòxiques que la seva forma lliure en cultius cel·lulars. Finalment, l'experiment de la distribució *in vivo* va demostrar que les nanopartícules es difonen homogèniament per els pulmons i eviten la migració cap a altres òrgans com el fetge, melsa o ronyons.

Estabilitat

El segon punt rellevant d'aquesta tesi està relacionat amb l'estabilitat de les ambdues formulacions després del procés de liofilització.

Els resultats van mostrar que mentre que les SLN amb colistina perdien activitat antimicrobiana al tercer mes de ser liofilitzades, l'activitat de les NLC es va mantenir constant durant tots els mesos d'estudi amb valors de CMI (concentració mínima inhibidora) acceptables. A més, les NLC-colistina van exhibir unes propietats fisicoquímiques molts adequades als 5 °C i 25 °C/60% d'humitat relativa durant un any. En general, es va poder concloure que les NLC-colistina eren més estables que les SLN.

Activitat antimicrobiana

La última part de la tesi està centrada en l'estudi de l'activitat antimicrobiana de les SLN i NLC amb colistina i tobramicina contra soques clíniques de *P. aeruginosa* aïllades de pacients amb fibrosis quística dels Hospitals de Sant Joan de Déu i de la Vall d'Hebrón.

En relació amb els experiments de *P. aeruginosa* en creixement planctònic, es va observar que la colistina nanoencapsulada presentava la mateixa activitat antimicrobiana que la colistina lliure. Pel que fa a la tobramicina, les SLN van tenir una bioactivitat inferior que les NLC i la seva forma lliure. No obstant, amb els experiments amb biofilm es va observar que les nanopartícules carregades amb colistina i tobramicina eren molt més eficients que la forma lliure en l'eradicació del biofilm. A més, els resultats també ens

van mostrar que les NLC-colistina tenen un efecte anti-biofilm més ràpid i potent que la colistina lliure. Per ambdues formulacions es va observar que el nombre de cèl·lules vives i mortes era superior a les capes més internes del biofilm que a les externes.

Prenent en consideració que els biofilms de *P. aeruginosa* juguen un paper rellevant en les infeccions respiratòries en els pacients amb FQ, els resultats obtinguts ens fan pensar que les nanoformulacions lipídiques podrien ser una alternativa terapèutica per millorar la qualitat de vida d'aquests pacients.

TABLE OF CONTENTS

Acknowledgements	XV
Scientific production	XXIII
Abstract	XXIX
Resum	XXXIII
1. INTRODUCTION	1
1.1. <i>Pseudomonas aeruginosa</i>	3
1.1.1. Highlights	3
1.1.2. Epidemiology	4
1.1.3. Pathogenesis	5
1.1.4. Manifestations	5
1.1.5. Identification	6
1.2. Cystic fibrosis (CF)	7
1.3. Microbial Infections in CF	9
1.4. <i>Pseudomonas aeruginosa</i> and cystic fibrosis	11
1.4.1. Hypermutable phenotype	12
1.4.2. Muroid phenotype	12
1.4.3. Modification of LPS	13
1.4.4. Loss of type III secretion	15
1.4.5. Loss of motility	15
1.4.6. Auxotrophy and metabolic adaptations	15

1.4.7. Small-colony variants (SCVs)	16
1.4.8. Defects in quorum sensing (QS)	16
1.4.9. Antimicrobial resistance	19
1.5. Microbial Biofilms	19
1.5.1. General aspects	19
1.5.2. The role of <i>P. aeruginosa</i> biofilms in respiration infections in CF patients.	21
1.6. Antimicrobial Treatment and Resistance	23
1.6.1. Treatment of <i>P. aeruginosa</i> respiratory infections in cystic fibrosis (CF).	23
1.6.2. Mechanisms of antimicrobial resistance in <i>P. aeruginosa</i>	28
1.6.2.1. Multidrug efflux systems	29
1.6.2.2. Resistance to β -lactams	30
1.6.2.3. Resistance to fluoroquinolones	32
1.6.2.4. Resistance to aminoglycosides	33
1.6.2.5. Resistance to polycations	35
1.6.2.6. Resistance to biocides	35
1.6.2.7. Biofilms	35
1.7. Nanoencapsulation of antimicrobials	36
1.7.1. The state of the art in nanoencapsulated antimicrobials	36
1.7.2. Lipid nanoparticles: SLN and NLC	39

2. OBJECTIVES	43
3. RESULTS	47
3.1. Elaboration and characterization	49
3.2. Stability	50
3.3. Antimicrobial activity	50
PAPER 1	55
PAPER 2	67
PAPER 3	81
PAPER 4	91
PAPER 5	105
PAPER 6	113
4. DISCUSSION	125
5. CONCLUSIONS	147
6. REFERENCES	153
7. ANNEXES	I
7.1. Annex I	III
7.2. Annex II	XIX

1. INTRODUCTION

1. INTRODUCTION

1.1. *Pseudomonas aeruginosa*

1.1.1. HIGHLIGHTS

Pseudomonas aeruginosa is part of the complex genus of bacteria named *Pseudomonas*. The genus *Pseudomonas*, which was firstly proposed by Migula in 1894, is rRNA homology group I, in the gamma subclass of the *Proteobacteria*. To date, 160 species are members of this genus, with only 12 of clinical interest (1)(2).

P. aeruginosa is a strict respirator and mainly aerobic, gram-negative, motile, non-spore-forming, straight or slightly curved bacilli capable of producing colorful water-soluble pigments and measuring 0.5 to 0.8 µm by 1.5 to 3.0 µm. The Gram stain and morphology does not permit easily distinguish the microorganism from other non-fermenting bacilli, even so it is thinner than *Enterobacteriaceae* (1)(2).

The microorganism grows with minimal requirements such as ammonia and carbon dioxide as sole nitrogen and carbon sources and can survive and multiply over a broad range of temperatures (20-42 °C) in almost any environment, including one with a high salt content (3)(4). The bacterium is oxidase-positive and catalase-positive. Although aerobic conditions are needed for optimal growth and metabolism, most strains can multiply slowly in an anaerobic atmosphere when nitrate is present as an electron acceptor (5)(6).

As a gram-negative bacterium, *P. aeruginosa* possesses the lipopolysaccharide (LPS) and the porin proteins, both located in the outer membrane. Porins are much less permeable to a wide range of molecules, including antibiotics than those of the *Enterobacteriaceae* family (7). *P. aeruginosa* also has a single polar flagellum that is essential for motility and chemotaxis.

In some strains, the secretion of alginate (copolymer of D-mannuronic and L-glucuronic acids) forms a mucoid exopolysaccharide slime layer outside the cell wall. This phenomenon affects the respiratory tract infected by *P. aeruginosa* of patients with cystic fibrosis (CF) (8) (more details in the section 1.4).

Multiple extracellular products are also produced, mainly including exotoxin A (ExoA), elastase and exoenzyme S (ExoS). All of them have been regarded as virulence factors of *P. aeruginosa* (1)(2).

ExoA is a secreted protein that inactivates eukaryotic elongation factor (EF-2) by ADP-ribosylation (ADPR), which leads to translation arrest and consequently, also leads to shutdown protein synthesis and cell death. ExoA action correlates with the primarily invasive and locally destructive lesions (9).

Elastase has tissue-damaging activity and can act on a variety of biologically relevant substrates such as elastin, immunoglobulins, coagulation and complement components, and some collagens. Once colonization and invasion have happened and septicemia has been established, its role become less important (10).

ExoS is an ADP-ribosylating enzyme and this activity is localized to its carboxy terminus. ExoS is translocated into human epithelial cells by the contact-dependent type III secretion system. Once inside the cell, this enzyme acts on regulatory G proteins effecting on eukaryotic cell function, including inhibition of DNA synthesis, alterations in cell morphology, microvillus effacement, and loss of cellular adherence, in addition to its antiphagocytic or anti-invasive effects (11).

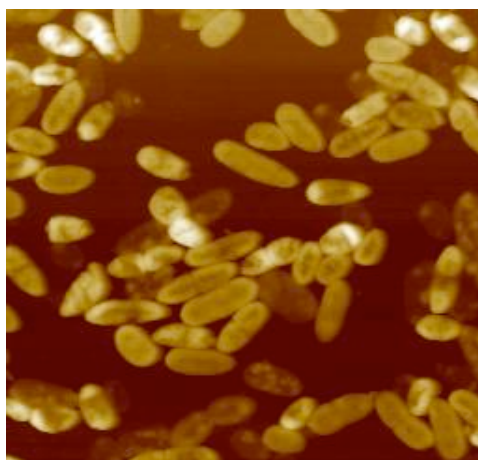


Fig.1. Atomic force microscopy (AFM) topography image of a *P.aeruginosa* CF clinical strain.

1.1.2. EPIDEMIOLOGY

The natural habitat of *P. aeruginosa* is the environment. It is found in water, soil and decaying vegetation (1)(2). Although infection by *P. aeruginosa* is rare among healthy persons, it is considered one of the most relevant causes of invasive infection in hospitalized patients with severe disease, such as leukemia, CF, and

extensive burns (12). Since it is a bacterium with minimal requirements it has the ability to survive and multiply in water with minimal concentration of solutes; this leads to contamination of humidifiers, respirators, medications, contact lens solutions, and even some disinfectants (13)(14)(15). In the case of humidifiers contamination, inhalation of aerosols from such sources can ignore the normal respiratory defense mechanisms and initiate pulmonary infection.

1.1.3. PATHOGENESIS

P. aeruginosa is an opportunistic pathogen and it is a frequent cause of nosocomial infections, many of which are responsible for high rates of illness and death.

To initiate infection, *P. aeruginosa* needs break first-line defenses (such as a wound) or a route past them (such as contaminated solution or intra-tracheal tube). The first step in the infection process is the attachment to epithelial cells. The adherence is mediated by pili, flagella, and the extracellular polysaccharide slime and favored by loss of fibronectin (16). *P. aeruginosa* expresses its pathogenicity with the activity of virulence determinants. Three virulence determinants are extensively studied: **quorum sensing (QS)**, **the type III secretion system (TTS)**, and **lipopolysaccharide (LPS) O-antigen**. QS allows bacteria to respond to their own population density by coordinately regulating their gene expressions patterns. When the bacteria cell population reaches a certain threshold, QS signaling leads to production of a set of toxins such as elastase, Exo A and the blue pigment pyocyanin which is detected in human lesions and shown to have a toxic effect on the respiratory ciliary function (17). TTS is a mechanism by which bacteria inject a set of toxins, such as ExoS and ExoU, directly into the cytosol of host cells (18). LPS O-antigen is a variable polysaccharide that decorates the outer surfaces of many bacteria and protects against complement-mediated lysis (19).

1.1.4. MANIFESTATIONS

P. aeruginosa can produce any of the opportunistic extra-intestinal infections caused normally by members of the *Enterobacteriaceae*. Burn, wound, urinary tract, skin, eye, ear, and respiratory infections all occur and may progress to bacteremia (20). *P. aeruginosa* pneumonia is a rapid and destructive infection particularly in patients with granulocytopenia. In contrast, pulmonary infection in CF patients is a

chronic infection that alternates between a state of colonization and more definite bronchitis or pneumonia (21).

1.1.5. IDENTIFICATION

P. aeruginosa grows efficiently on both standard broth and solid laboratory media, including tryptic soy agar, MacConkey agar, Columbia agar with 5% sheep blood, and chocolate agar. MacConkey agar is a differential medium useful in identifying different strains of *Pseudomonas* spp., underlining mucoid strains of *P. aeruginosa* from CF patients (1)(2).

Moreover, as mentioned previously, *P. aeruginosa* produces water-soluble pigments which are very useful in identification: pyoverdine (fluorescein) that fluoresces under short-wave length UV light, pyocyanin (blue), pyorubin (red) or pyomelanin (brown/black). When mixed together, pyoverdine and pyocyanin combine to create the bright green color characteristic of *P. aeruginosa* (1)(2). In addition, these two pigments are siderophores (Fe uptake components) and they are produced when the bacteria are grown in low iron conditions (22).

More relevant characteristics of *P. aeruginosa* can facilitate its identification. Fresh cultures have a grape-like odor, whereas the older ones may exhibit a corn taco-like odor. Colonies are usually flat and spreading and have a serrated edge and a metallic sheen that is often associated with autolysis of colonies. Other morphologies also exist, such as smooth, mucoid, and dwarf (small-colony variants). Furthermore, *P. aeruginosa* is different from the rest of the clinically relevant fluorescent pseudomonads in its ability to grow at 42 °C and because it can respire by using nitrates as terminal acceptors allowing the bacterium to grow in anaerobiosis. In addition to pigment production and oxidase and catalase positive tests, other test that confirms its identification is an alkaline over no-change reaction in triple-sugar iron agar slant (1)(2).

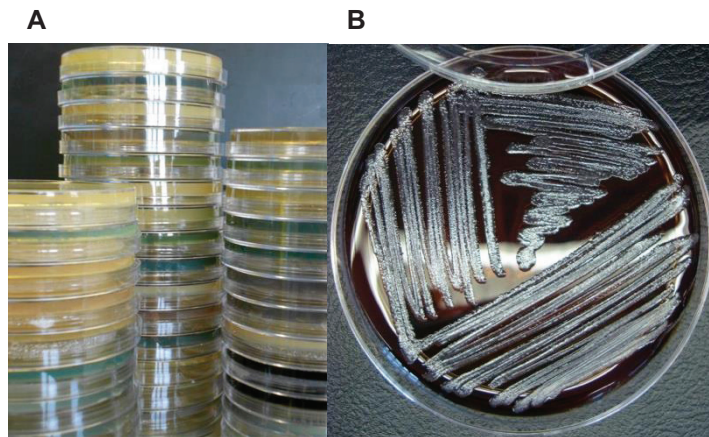


Fig.2. A. *P.aeruginosa* CF isolates growth on tryptic soy agar (TSA). Water-soluble pigments diffuse through the medium. **B.** *Pseudomonas aeruginosa* CF isolate on blood agar. Note the metallic sheen and ground glass appearance.

1.2. Cystic fibrosis (CF)

Cystic fibrosis (CF) is an inherited autosomal recessive disorder caused by mutations in the cystic fibrosis transmembrane conductance regulator (CFTR) gene located on the long arm (q) of chromosome 7 (7q31.2) encoding for the CFTR protein that functions as a chloride channel and regulates the transport of ions and the movement of water across the epithelial barrier (23). Four classes of CF-associated mutations causing a loss of CFTR chloride channel function are described. The most common mutation, deletion of phenylalanine at residue 508 ($\Delta F508$), is included in the class II mutations, and associated with a defective protein processing (24). This means that CFTR fails to be transported correctly. Dorothy H. Andersen described the disease in 1938 (25).

Progress in Pediatrics

CYSTIC FIBROSIS OF THE PANCREAS AND ITS RELATION TO CELIAC DISEASE

A CLINICAL AND PATHOLOGIC STUDY

DOROTHY H. ANDERSEN, M.D.
NEW YORK



Fig.3. Historical interest. The first report on the disease: Andersen,DH. Cystic fibrosis of the pancreas and its relation to celiac disease: a clinical and pathologic study. Am J Dis Child 1938; 56:344-399 (above). Dorothy Andersen is considered one of the most prominent medical doctors in US history. She was a heavily smoker and died from lung cancer at age 62. She entered in the National Women's Hall of Fame in 2002 (below).

Patients underlying such mutations tend to suffer recidivate respiratory infections caused by a wide variety of microorganisms, pancreatic dysfunction, high electrolytes level in sweat, male infertility, as well as intestine and biliary duct of the liver disorders. Loss of pancreatic exocrine function causes malnutrition and poor growth (26). It is estimated that 1 out of 2500 live births might be affected by CF, being the most common autosomal recessive disease worldwide (27). Over the last

years, the life expectancy of CF patients has increased to a median survival age of 39 years, with an early half of the populations being adults (28).

The absence of functional CFTR protein in the membrane of epithelial cells consists of a lack of transport of chloride and accompanying water across the airway epithelium and excessive sodium reabsorption, leading to dehydrated airway surface fluid, impaired mucociliary clearance, infection and inflammation. As a result, viscous mucus is secreted and gets accumulated in the airways that provokes the entrapment of bacteria and further complicates airway clearance causing chronic pulmonary disease, the main limiting factor of the disease in terms of morbidity and mortality (29). Lung transplantation is recognized as a last-resort treatment option for CF patients with end-stage disease (30).

CF pulmonary disease is initiated in airways that are normal at birth but that later become obstructed with mucus plugs. Early pathological findings include goblet-cell and mucus-gland hyperplasia. Afterwards, airway colonization and infection occur with diverse flora provoking an intense inflammatory reaction, which does not result in enhanced bacterial clearance. Airway obstruction results initially in hyperinflation, destruction of the airway walls and fibrosis, leading to decreased pulmonary function as measured by forced expiratory volume and vital capacity (26)(8).

1.3. Microbial infections in CF

CF airways are infected at an early age and opportunistic bacteria enter the lower airways from the environment. These bacteria form a chronic presence in the airways due to damaged innate immunity system and are related to chronic inflammatory response (26)(8).

Among these bacteria that affect the CF patients, *P.aeruginosa* is the most prevalent, but not the unique since many other microorganisms could be involved either as the sole microbe or in multi-specific infections. Thus, a part from *P. aeruginosa*, the most commonly pathogenic bacteria associated with CF include *Staphylococcus aureus*, *Hemophilus influenzae*, *Stenotrophomonas maltophilia*, *Achromobacter xylosoxidans*, *Burkholderia* species, the fungus *Aspergillus fumigatus*, nontuberculous mycobacteria (NTM) and even respiratory viruses can contribute to the progression of lung disease (31)(32).

The predisposition to infection by these microorganisms change with age (Fig.4).

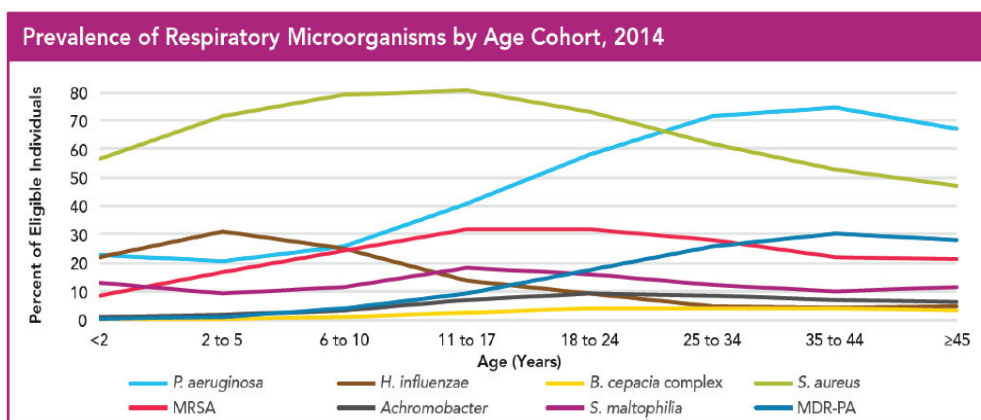


Fig.4. Prevalence of several common respiratory pathogens in CF as a function of age. (Adapted from the 2014 Annual Data Report of the Cystic Fibrosis Foundation Patient Registry, Bethesda, MD) (189).

Here is a summary of the microbial species associated with CF lung infections (31):

S. aureus is the pathogen most commonly isolated from CF sputum or cough swab in infants who do not receive long-term anti-staphylococcal prophylaxis. Currently, the existence of methicillin resistant *S. aureus* (MRSA) strains among CF patients does not seem to have clinical significance.

P. aeruginosa, particularly the mucoid colonial morphotype, causes a respiratory infection leading to an immediate and rapid reduction of lung function in CF patients.

Nonencapsulated *H. influenzae* persists in the lungs of these patients for prolonged periods of time due to its penetration into epithelial cells and subsequently, specific antibodies are present in the sputum and sera of CF individuals.

B. cepacia complex is a group of at least nine closely related bacterial species, which *B.cenocepacia* dominates in CF being highly transmissible and virulent in these patients. In addition, infections caused by *B. cepacia* are related to a markedly shortened median survival and characterized by high fever, bacteremia, rapid pulmonary deterioration and death.

The opportunistic human pathogens *A. xylosoxidans* and *S. maltophilia* have also been recovered with increasing frequency from respiratory tract cultures of patients with CF over the last years.

M. avium complex and *M. abscessus* among NTM group are the most common species in CF. Older age is the most significant predictor for isolation of NTM.

Also *A. fumigatus* causes bronchopulmonary aspergillosis (ABPA) in approximately 2% to 7.8% of patients with CF. Aspergilloma or invasive aspergillosis is unusual.

1.4. *Pseudomonas aeruginosa* and cystic fibrosis

P. aeruginosa is the most studied microorganism in the context of CF (33). About 50% of patients ≤ 18 years of age are infected with this microorganism and this prevalence rises to 80% when individuals are older than 18 years. The high prevalence is mainly due to the ability of *P. aeruginosa* to cause chronic infections.

Once established in the respiratory tract, *P. aeruginosa* resists eradication despite the activation of the host immune system and prolonged antimicrobial treatment. The main reason by which this bacterium successfully persists in the lungs is the ability to adapt to changes and stresses in its environment. Although initial infection can be facilitated by the extensive genome of *P. aeruginosa* and its ability to sense and respond to a broad variety of environmental conditions, later adaptation results at least in part from the selection of clonal lineages containing spontaneously arising mutations (31)(33).

Some adaptive characters such as mucoid phenotype, antibiotic resistance, alterations in lipopolysaccharide (LPS), loss of type III secretion system and motility, auxotrophy, small colonial variants (SCVs), defects in quorum sensing (QS), and hypermutability, frequently emerge during respiratory infection in CF (31)(33).

1.4.1. HYPERMUTABLE PHENOTYPE

P. aeruginosa isolates from CF patients exhibit a hypermutable phenotype. The same thing happened to *S. aureus* and *H. influenzae*, all of them responsible for lung injury in CF individuals (31).

In this context, mutations mostly occur in the *mutS*, *mutL*, and *uvrD* genes, which encode proof-reading proteins responsible for correcting errors that appear during DNA replication. Some studies have observed that the hypermutable phenotypes emerges late in CF, after mutations affecting such properties as alginate production and QS have already occurred (34).

Moreover, it has been considered that hypermutable strains tend to be more resistant to antimicrobials (35), more likely to be mucoid or defective in QS (36), more metabolically adapted to the CF respiratory tract, and in general more adaptable to the hard habitat of the CF airways (31).

1.4.2. MUCOID PHENOTYPE

The mucoid phenotype is the most studied adaptation of *P. aeruginosa* in CF and it is linked to overproduction of the exopolysaccharide alginate, a polymer of D-manuronic and L-glucuronic acid (37).

After a long period in the respiratory airways, *P. aeruginosa* gets mutations in the *mucA* gene, which results in loss of production of MucA and, consecutively, high levels of revealed AlgT leading to uncontrolled expression of *algD* cluster of genes, overproduction of alginate and a mucoid phenotype (34). The conversion to the mucoid phenotype is concomitant with the establishment of chronic respiratory infections in CF (38). Approximately, this phenotype comes out after 3 years of infection and at a median age of 13 years and it is commonly observed in respiratory samples from CF patients but also in bronchiectasis or ciliary dyskinesia sputum cultures from non-CF individuals (33).

Overproduction of alginate provides advantages to *P. aeruginosa* in the context of CF: biofilm formation enhancement which limits bacterial clearance by both host phagocytes and antimicrobial therapy and opsonization, phagocytosis, and killing are also inhibited causing a dysregulated immune response (39).

It is also noteworthy that non-mucoid isolates from chronically infected CF patients carry mutations in the *mucA* gene, suggesting that the mucoid phenotype reverts to non-mucoid phenotype (40).

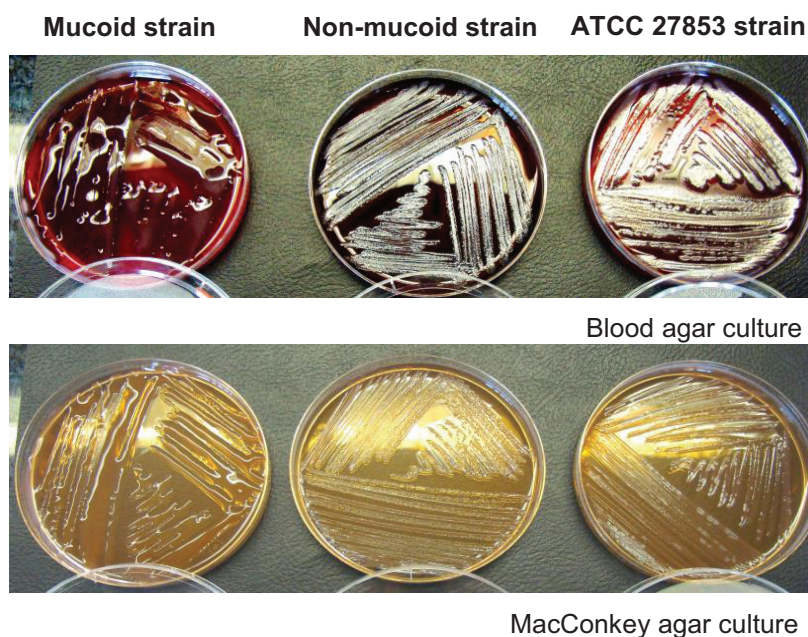


Fig.5. *P.aeruginosa* clinical isolates collected from sputum of CF patients.

1.4.3. MODIFICATION OF LPS

P. aeruginosa and the rest of members of gram-negative bacteria group are protected by an outer membrane that contains LPS, which is composed of three parts: lipid A, O- antigen, and central core oligosaccharide, which is attached to lipid A (41). The modified structure in *P. aeruginosa* isolates from CF is associated with O- antigen and lipid A (19).

There is a failure to produce O antigen during CF respiratory infections. Since O antigen is highly immunogenic and evokes a strong antibody response, its absence facilitates persistence within the respiratory airways (42).

Moreover, another lipid A alteration has been observed related to the addition of aminoarabinose, a positively charged amino sugar residue. Lipid A modifications

have substantial biological sequelae such as enhancement of resistance to antimicrobials peptides and some antibiotics due to addition of arabinose, and induction of proinflammatory response because of the acylation levels (43).

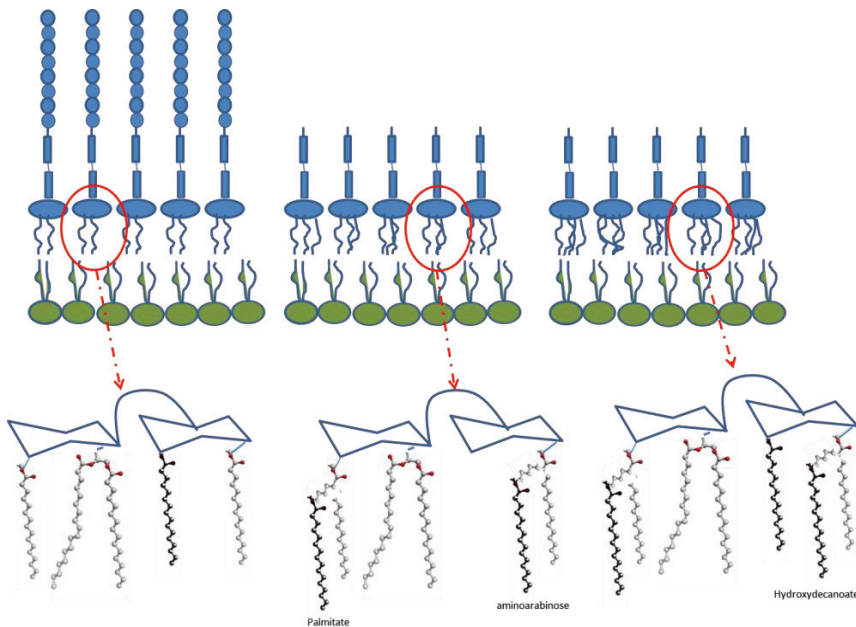


Fig.6. Modifications of *P. aeruginosa* LPS during CF respiratory infections. During early infection in individuals with CF, the O-antigen polysaccharide is frequently lost. Also, palmitate and aminoarabinose are added to the lipid A portion of LPS. Moreover, in patients with advanced CF, a hydroxydecanoate chain is retained, likely due to mutations in the *pagL* gene, which encodes a lipid A deacylase (31).

1.4.4. LOSS OF TYPE III SECRETION

Many *P. aeruginosa* isolates from the environment and from non-CF infections secrete a set of toxins (ExoS, ExoT, ExoU and Exo Y) that are delivered into the host cells through a type III secretion system (18). However, *P. aeruginosa* strains progressively lose the ability to secrete these toxin proteins in the CF lung infection context (44).

P. aeruginosa strains that secrete type III effector proteins seem to be at a selective disadvantage during chronic infection in CF, which means that individuals with CF mount an antibody response against type III proteins (18)(44).

Therefore, secretion-positive strains are cleared from CF patients over time whereas secretion-negative strains are not (44)(18).

1.4.5. LOSS OF MOTILITY

P. aeruginosa strains isolated from individuals with CF fail to produce fully functional flagella and consequently, they are defective in swimming motility (37).

The loss of motility happens during the course of infection, since *P. aeruginosa* isolates cultured early during infection are motile (37).

The main reason that explains the gradual loss of swimming motility is the acquisition of mutations in one of several genes that regulate production of flagella, including *rpoN*, *vfr*, and *fleQ* (45).

In addition, another movement named twitching motility is done by *P. aeruginosa* and it is mediated by the extension and retraction of type IV pili, proteinaceous filamentous appendages on the surface of this microorganism (46). Chronic infection in CF is related to this kind of movement (37).

1.4.6. AUXOTROPHY AND METABOLIC ADAPTATIONS

Most *P. aeruginosa* respiratory isolates from CF patients are auxotrophs meaning that they are unable to synthesize all amino acids to build proteins. Thus, they are unable to survive in the absence of externally provided amino acids which are not required by wild-type (prototroph) strains. Most of auxotrophs require only one given amino acid, although in some cases more than one auxotrophy can be found.

The high levels of free amino acids in CF respiratory infections like methionine, leucine and arginine, allow these auxotrophic strains to survive during infection. Furthermore, some *P. aeruginosa* isolates acquire mutations in the *lasR* gene, which enhance their ability to use exogenous amino acids and other nutrients, and therefore, they grow more rapidly than parenteral strains (47).

It has been noted that auxotrophic *P. aeruginosa* strains are more commonly cultured from CF patients with experiencing pulmonary exacerbations or with baseline lung disease than from those who are clinically stable or have mild underlying lung disease (48).

1.4.7. SMALL-COLONY VARIANTS (SCVs)

SCVs are present in about 10% of the respiratory specimens of CF patients. *P. aeruginosa* SCVs have special characteristics: they autoaggregate in liquid culture, they are hyperadherent to surfaces, exhibit reduced motility, and frequently enhance resistance to antimicrobials (49).

These characteristics promote a biofilm mode of growth in the CF respiratory airways. SCV phenotype is associated with mutations or changes in expression of chemosensory, exopolysaccharide, and two-component system response regulators. However, it has been observed that individual SCV's differ from one to another in their gene expressions patterns meaning that SCVs represent a group of bacteria that share only a subset of their phenotypes (50).

1.4.8. DEFECTS IN QUORUM SENSING (QS)

Quorum sensing (QS) is a mechanism activated by molecules called autoinducers or pheromones and consists of individual bacteria communicate with one another to modify gene expression in response to changes in population density. QS in *P. aeruginosa* involves the use of at least three signal molecules. Two small molecules have been broadly studied: 3-oxo-dodecanoyl homoserine lactone (3-oxo-C12-HSL), which is produced by the LasI/LasR system (51)(52), and butyryl homoserine lactone (C4-HSL), which is produced by the RhII/RhlR system (52).

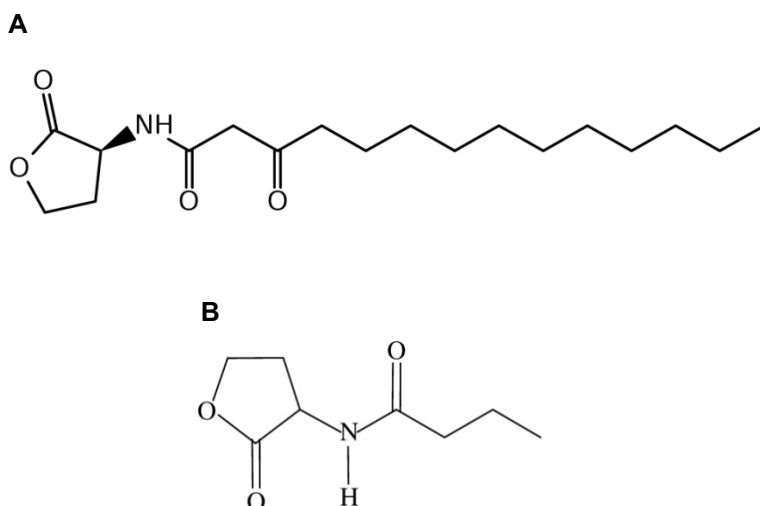


Fig.7. A. 3-oxo-dodecanoyl homoserine lactone (3-oxo-C12-HSL). **B.** Butyryl homoserine lactone (C4-HSL).

The third QS signal structurally based on 2-heptyl-3-hydroxy-4-quinolone, is designated the *Pseudomonas* quinolone signal (PQS) and it has been involved in cystic fibrosis (CF) disease with an increase of PQS production in early *P. aeruginosa* colonizers of the CF lung (53).

PQS is chemically unique from the N-Acyl homoserine lactones (AHLs) signals of the Las and Rhl systems and its signaling is also regulated differently from AHLs. Whereas AHLs are produced when bacteria reach a threshold density, PQS is produced in the late stationary phase of growth suggesting that PQS signaling is relevant when *P. aeruginosa* culture are under stressful conditions (54) (more details can be found in chapter 1.5). The PQS signaling system operates between the Las and Rhl systems in the QS regulatory system. This means that the production of PQS depends on LasR and that the Rhl QS system is associated with the PQS bioactivity. In addition, PQS induces expression of *LasB* (coding for elastase) and the Rhl QS system (55).

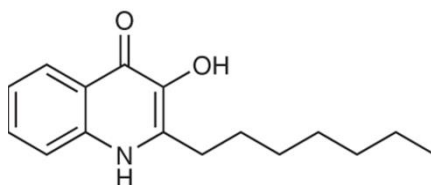


Fig.8. *Pseudomonas* quinolone signal (PQS): 2-heptyl-3-hydroxy-4-

These three QS systems are primarily involved in the regulation of virulence factors (pyocyanin, elastase, PA-IL lectin and rhamnolipids) as well as cellular processes such as chemotaxis and biofilm formation. Besides, QS molecules also modulate host responses (56). However, it has been observed the presence of mutations in the *lasR* and *rhlR* genes in *P. aeruginosa* isolates from CF patients, meaning that homoserine lactones are not detectable in many CF isolates, and subsequently, they do not have a functional quorum sensing system. These mutations appear generally 15 years after the initial lung infection (52).

Several reasons may explain these findings. One explanation is that QS play an important role in CF infections but that the metabolic cost of producing signaling molecules under the control of these systems promotes the emergence of cheater clones, which do not themselves respond to autoinducers but benefit from the autoinducer-induced factors synthesized by their neighbors. Another evidence is that loss-of-function mutations in *lasR* confer an advantage in CF modifying gene expression patterns and leading to an increased growth rate due to better utilization of amino acids found in high levels in the CF levels, to an increased ability to use nitrate instead of oxygen as an electron receptor during growth in the anaerobic conditions of the CF airways, and to increased resistance to antimicrobials. In fact, *lasR* mutants produce high levels of β -lactamases, culminating in increase tolerance to β -lactam antibiotics.

In any case, *P. aeruginosa* isolates lacking functional QS system are associated with the progression of lung disease in CF (51)(52).

1.4.9. ANTIMICROBIAL RESISTANCE

Antimicrobial resistance is commonly due to mutations in genes controlling the production of efflux pumps and β -lactamases.

Multidrug resistance is defined as the lack of susceptibility to all antimicrobials tested in at least two of the following classes: fluoroquinolones, β -lactams and aminoglycosides. Patients infected with MDR (multidrug resistant) *P. aeruginosa* have an increased risk of death or lung transplantation and a more rapid decline in FEV₁ (forced expiratory volume in 1 second) in comparison to those with antibiotic-susceptible *P. aeruginosa*.

More details of mechanisms of antimicrobial resistance in *P. aeruginosa* will be forthcoming in the next sections.

1.5. Microbial biofilms

1.5.1. GENERAL ASPECTS

In 2002, Donlan and Costerton stated that a biofilm is “a microbially derived sessile community characterized by cells that are irreversibly attached to a substratum or interface or to each other, are embedded in a matrix of extracellular polymeric substances that they have produced, and exhibit an altered phenotype with respect to growth rate and gene transcription” (57).

Microbial biofilms may form on a broad variety of surfaces, such as living tissues, indwelling medical devices, industrial or potable water system piping, or natural aquatic systems. This means that biofilms are of importance for several environmental processes, and also the elemental cause of persistent infections in numerous parts of the human body, such as the teeth, urinary tract, CF lungs, bones, or medical devices such as heart valves (58).

The formation of biofilms depends basically on the presence of bacteria-to-bacteria interconnecting extracellular substances that act as a biofilm matrix. Many components, such as exopolymers (e.g. polysaccharide), proteins and DNA are considered to form part of the biofilm matrix. Additionally, outer membrane proteins and a variety of bacterial cell appendages (e.g. fimbriae, pili, and flagella) also have bacteria-to-bacteria interconnecting functions, and can therefore be part of the

biofilm matrix. The extracellular biofilm matrix offers protection against immune responses and antibiotic treatment (59).

The formation of biofilm starts when bacteria attach to a surface or to each other and form aggregates. As it can be observed in Figure 9, five main stages are involved in biofilm development: i) transport of individual microbes to the surface or each other, ii) initial attachment of the microbes to the surface or each other, iii) formation of microcolonies, iv) maturation of the biofilm, v) dispersal of the biofilm.

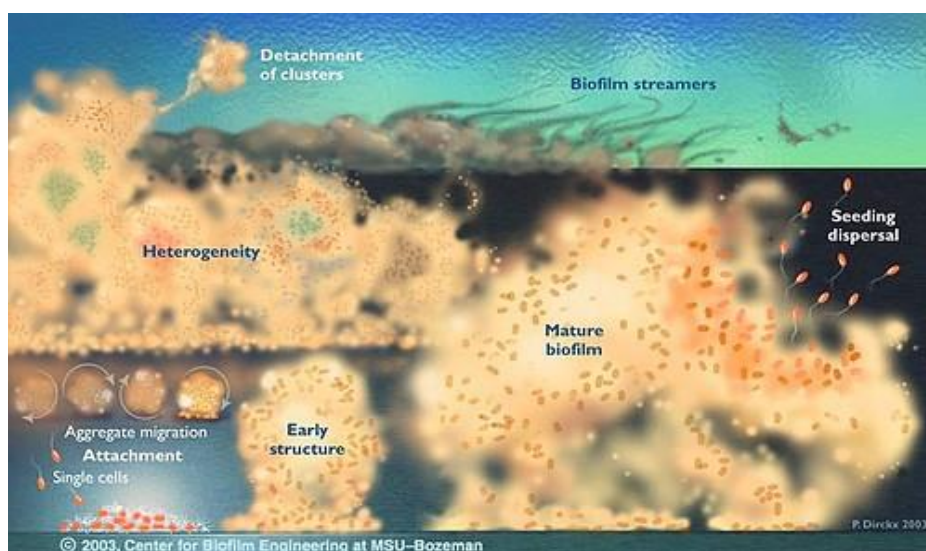


Fig.9. Phases of biofilm formation: reversible and irreversible attachment to the surface; growth and maturation state; dispersion state. (© Montana State University CBE).

The initiation of biofilm formation and the production of biofilm matrix components occur in response to high intrabacterial levels of the second messenger molecule c-di-GMP, whereas the last phase of the cycle occurs in response to low levels of c-di-GMP (60). It is also relevant to note that dispersal enables biofilms to spread to other locations where new biofilms can be formed (61).

Interestingly, the spatial structure of the biofilms is species dependent as well as dependent on the environmental conditions. As in the case of *P. aeruginosa*, it forms biofilms with mushroom shaped structure in flow-chambers perfused with

glucose-medium, whereas it forms flat biofilms in flow-chambers perfused with citrate medium (62).

At the earliest stage of the cycle, the sessile bacteria are still susceptible to antimicrobials, whereas more developed biofilms show confrontation to antibiotic treatment.

1.5.2. THE ROLE OF *P. aeruginosa* BIOFILMS IN RESPIRATION INFECTIONS IN CF PATIENTS

In the Fig.10 (63), it can be observed in detail the entire *P. aeruginosa* biofilm life cycle within the lungs. The conversion of *P. aeruginosa* from planktonic to biofilm mode of growth, and back again, involves a horde of physiological changes (64)(65).

P. aeruginosa planktonic bacteria adhere reversibly to the layer of gelatinous mucus of airway lining fluid utilizing their poles, flagella and pili. Then, irreversible attachment occurs to the bacterial axis, which divide and arrange themselves in clusters and consequently, an early biofilm is formed. This step is dependent on type 4 pili and the *las*IR encoded quorum sensing (QS) system which produce the signal molecule 3-oxododecanoyl-L-homoserine lactone (3-oxo-C12-HSL) (40).

The release of oxygen free radicals and elastase is involved in the polymorphonuclear leucocytes (PMN) activation due to the inflammatory reaction. This fact induces mutation in the *mucA* gene and, consequently alginate production occurs. In addition, the release of extracellular DNA at a later phase of biofilm formation is regulated by the *Pseudomonas* quinolone signal (Pqs) QS system, because of autolysis of PMN (66). As Häussler et al. observed (67), Pqs QS system enhances DNA release and fragmentation. Although PMN are the major effector responsible for the clearance of *P. aeruginosa* from the site of infection, this microorganism has the ability to confront with very high levels of reactive oxygen intermediates from the respiratory burst of human phagocytes as a defense strategy. It is at this point that PQS intensifies DNA fragmentation and DNA release in the presence of oxygen in *P. aeruginosa* steady-state biofilm.

Maturation of the biofilm leads to pillar-and-mushroom like-structures with water channels allowing for the exchange or waste nutrients. This step involves the *rh*IR

encoded QS system which produce the signal molecule N-butanoyl-homoserin lactone (C4-HSL) (40)(68).

Mature biofilms are complex and different microenvironments are created resulting in heterogeneity in metabolic and reproductive activity among bacteria located in different parts of the structure. Metabolically inactive bacteria are mostly found in deep layer (40)(68). Several (3-12) days after initial attachment, pieces of biofilm and planktonic bacteria are moved away from the surface of mature biofilms to start a new cycle of biofilm development (61).

Biofilm dispersal can be the result of various clues, including alterations in nutrients availability, oxygen fluctuations and increase of toxic products, or other stress-inducing conditions.

Most of the *P. aeruginosa* biofilms are found in sputum and the biofilm is depleted of oxygen, the viability of which needs *rhl* QS and nitric oxide reductase for preventing accumulation of toxic NO, a byproduct of anaerobic respiration (64).

It is important to note that the three QS systems known in *P. aeruginosa* are involved in biofilm lifestyle cycle (69).

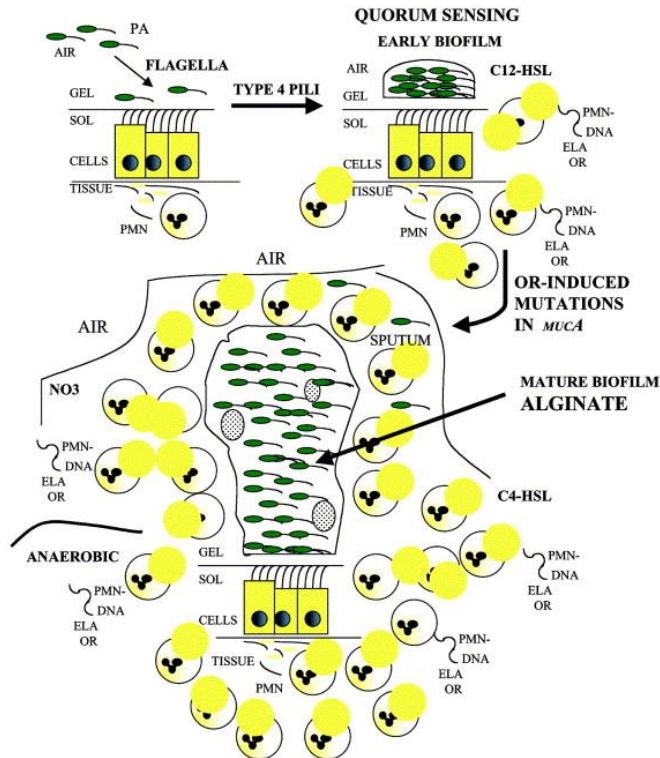


Fig.10. The biofilm life cycle in the lungs of CF patients (63).

1.6. Antimicrobial treatment and resistance

1.6.1. TREATMENT OF *P. aeruginosa* RESPIRATORY INFECTIONS IN CYSTIC FIBROSIS (CF)

Different situations for use of antimicrobial agents can be distinguished depending on the sequence of colonization and infection events involving *P. aeruginosa* in CF patients (70), each of which requires different therapeutic approach (Figure 11).

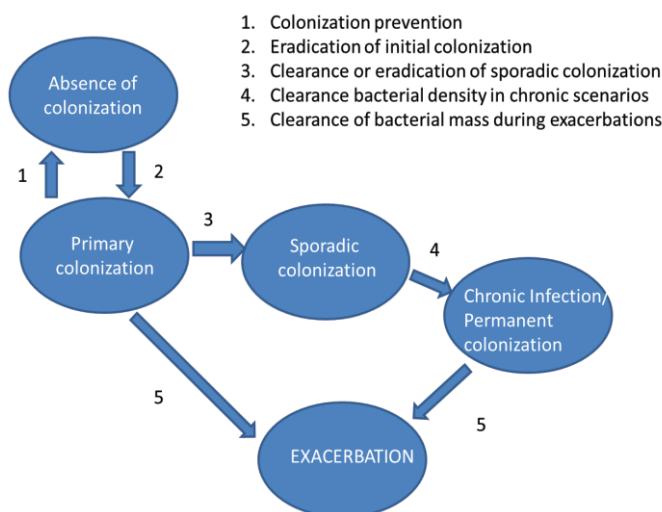


Fig.11. Summary of the sequence of colonization and infection events involving *P. aeruginosa* in cystic fibrosis patients, and the theoretical objectives of antimicrobial treatment of each stage (70).

The aim of the bactericidal antimicrobial agents in cases of CF should be to reduce bacterial population and to be fast-acting to avert the selection of resistant mutants and prevent phenotypic tolerance.

The bactericidal activity of β -lactams is obtained only after extended contact with the bacteria; independent of the concentration used, but with others, such as aminoglycosides, is quick and proportional to the dose. Bacterial death with fluoroquinolones is slower, and is also proportional to the dose, but perplexedly, very high doses can be less efficient. With colistin, the bactericidal effect is not quite as rapid, but is also proportional to the dose (70).

Reduction of the bacterial population is commonly achieved after the use of high doses and several successive, correctly spaced exposures to the bactericidal agents. Part of the bacterial mass may not be in full contact with the antimicrobial agent, or may enter a state of phenotypic tolerance, so at this stage and with the lack of antimicrobials during dose intervals or between cycles, the bacterial population reacquires the capacity for death (70).

The progressive occurrence of multidrug-resistant (MDR) *P. aeruginosa* led to scenarios in which almost no treatment options were available. This was particularly

clear after the widespread emergence of imipenem resistance of strains lacking the OprD porin (71). This is the reason why in the last few years old antibiotics, such as colistin, has been rescued and new technologies, such as nanotechnology, are being applied, to fight infections.

Colistin is a bactericidal cyclic polycationic peptide (Fig.12) (72) that interacts with anionic lipopolysaccharide in the outer membrane of gram-negative bacteria mainly displacing Ca^{2+} and Mg^{2+} , thus dramatically decreasing the stability of the outer membrane and allowing a secondary effect on the cytoplasmic membrane by increasing its permeability. This leads to cytoplasmic content leakage and subsequent bacterial death (73). From the fifties to the eighties, colistin was mainly administered intravenously. However, due to high nephrotoxicity and neurotoxicity, its use was restricted in the early 1970s (74). Nowadays, inhaled colistin is regarded as a useful therapeutic option for early antibiotic intervention in periodically colonized CF patients and in critically ill patients (75)(76).

Currently, at initial infection, inhaled colistin, tobramycin or aztreonam with or without oral ciprofloxacin are recommended. In chronic infections, treatment is based on continuous administration of colistin or with a 28-day on-off regimen with tobramycin or aztreonam.

During mild-moderate exacerbations oral ciprofloxacin can be administered while serious exacerbations must be treated with intravenous combination therapy (β -lactam with an aminoglycoside or fluoroquinolone) (77).

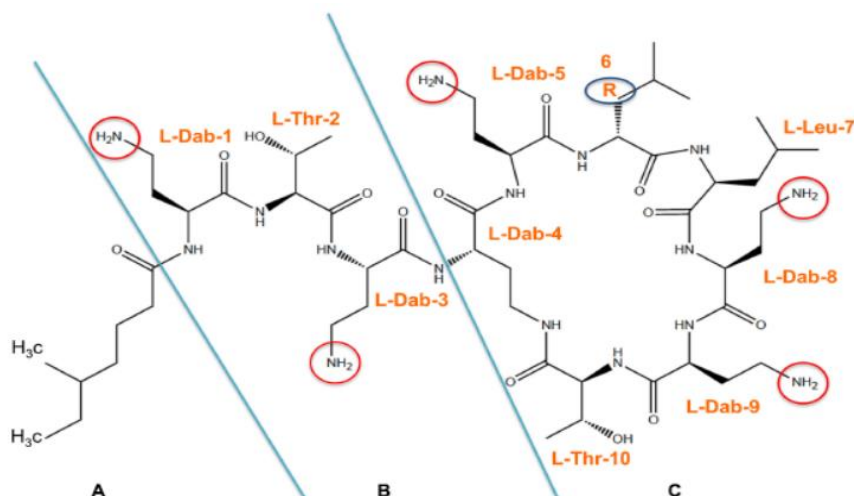


Fig.12. Molecular and chemical structure of colistin (polymyxin E). The chemical structure of colistin is composed of three parts: (A) hydrophobic acyl tail, (B) linear tripeptide segment (C) hydrophilic, heptapeptide ring. Arabic numeral indicates the position of amino acids on the structure and the reactive amino groups are encircled (190).

A summary of the antimicrobial agents which are being currently used to treat *P. aeruginosa* infections in CF patients is presented in Table 1. In addition, their mode of action and the primary *P. aeruginosa* resistance mechanisms are also explained. The resistance mechanisms of *P. aeruginosa* to antimicrobials will be treated in detail in the next section.

INTRODUCTION

Antipseudomonal agent	Mechanism of action	Resistance mechanism
Ceftazidime	<ul style="list-style-type: none"> • A third-generation cephalosporin • Binds to penicillin-binding proteins (PBPs) interfering with synthesis of peptidoglycan of the bacterial wall. • Produces bactericidal effects by triggering autolytic enzymes in the envelope of bacteria. 	<ul style="list-style-type: none"> • Derepression of AmpC • Up-regulation of: MexAB-OprM MexCD-OprJ MexEF-OprN MexXY-OprM
Aztreonam	<ul style="list-style-type: none"> • Monobactam • Binds to the PBP 3 disrupting bacterial wall synthesis. 	<ul style="list-style-type: none"> • Derepression of AmpC • Up-regulation of: MexAB-OprM MexCD-OprJ MexEF-OprN MexXY-OprM
Imipenem	<ul style="list-style-type: none"> • Carbapenem • Binds to PBP 1 and PBP 2 elongating the cell and causing lysis. 	<ul style="list-style-type: none"> • Up-regulation of: MexEF-OprN • Loss of OprD
Meropenem	<ul style="list-style-type: none"> • Carbapenem • Binds to PBP 1 and PBP 2 elongating the cell and causing lysis. 	<ul style="list-style-type: none"> • Up-regulation of: MexAB-OprM MexCD-OprJ MexEF-OprN MexXY-OprM • Loss of OprD
Ciprofloxacin	<ul style="list-style-type: none"> • A third-generation fluoroquinolone • Has two binding domains: DNA and DNA gyrase 	<ul style="list-style-type: none"> • Reduced affinity of: topoisomerase II topoisomerase IV

	<ul style="list-style-type: none"> • DNA gyrase-ciprofloxacin-DNA complex is associated with the inhibition of DNA replication. 	<ul style="list-style-type: none"> • Up-regulation of: MexAB-OprM MexCD-OprJ MexEF-OprN MexXY-OprM
Amikacin Tobramycin	<ul style="list-style-type: none"> • Aminoglycosides • Inhibit bacterial protein synthesis by binding reversibly to the 30S ribosomal subunit preventing mRNA translation during protein synthesis and leading bacteria to death. 	<ul style="list-style-type: none"> • Up-regulation of: MexXY-OprM • Reduced aminoglycoside transport
Colistin	<ul style="list-style-type: none"> • Polymyxin E • Interacts with the anionic LPS molecules displacing Ca^{2+} and Mg^{2+} from the OM of bacteria, leading to permeability changes in the cell envelope, leakage of cell contents, and cell death. 	<ul style="list-style-type: none"> • Membrane changes

Table 1. Summary of the antipseudomonal agents commonly used to treat *P. aeruginosa* infections in the context of CF.

1.6.2. MECHANISMS OF ANTIMICROBIAL RESISTANCE IN *P. aeruginosa*

The intrinsic resistance of *P. aeruginosa* to many antimicrobials and the ready selection of resistant isolates during antipseudomonal chemotherapy contribute to acquire multidrug resistance in this microorganism (78). The resistance mechanisms in *P. aeruginosa* are mainly associated with the presence of a highly impermeable outer membrane (OM) that restricts the entry of antimicrobials into the cell and the synergistic action of the outer membrane barrier and the activity of specific multidrug efflux systems that together restrict drug accumulation inside bacteria. Therefore, mutational overexpression of these systems and/or OM modifications that limit antimicrobial accumulation contribute to reinforce multidrug

resistance causing treatment failure (78)(79). A summary of the resistance mechanisms associated with *P. aeruginosa* in CF is presented in Table 2.

1.6.2.1. MULTIDRUG EFFLUX SYSTEMS

Chromosomally encoded multidrug efflux systems of the resistance-nodulation-division (RND) family seems to be the most significant in terms of export of and, thus, resistance to antimicrobials in *P. aeruginosa* and other gram-negative bacteria (78)(80).

RND pumps transport a broad range of compounds such as β -lactams and aminoglycosides. In addition, RND transporters form a multiprotein complex together with the OM channel of the outer membrane factor (OMF) family and the periplasmic linker protein of the membrane fusion protein (MFP) family permitting excretion drugs directly into the medium.

Seven RND-type multidrug efflux systems have been described to date in *P. aeruginosa*: MexAB-OprM, MexCD-OprJ, MexEF-OprN, MexXY-OprM, MexJK-OprM, MexHI-OpmD and MexVW-OprM (80). Efflux operon for each of these encodes for an RND transporter (MexB, MexD, MexF, MexY, MexK, MexI, MexW) in the inner membrane, a periplasmic MFP (MexA, MexC, MexE, MexX, MexJ, MexH, MexV), and in numerous cases an OM channel protein (OprM, OprJ, OprN, OpmD). Of these, MexAB-OprM and MexXY-OprM have a major role in the intrinsic resistance of *P. aeruginosa* to frequently used antimicrobial agents (81).

a. MexAB-OprM

The overproduction of MexAB-OprM confers high levels of acquired multidrug resistance seen with at least two types of mutants (*nalB* and *nalC*) selected either *in vitro* or *in vivo* (82)(83)(84)(7). The overexpression or deletion of the MexAB system, does not heavily alter the susceptibility to imipenem because it is likely a poor substrate of the pump. The presence of OprD channel in the OM allows rapid penetration of imipenem diminishing the effect of efflux (85). However, the susceptibility of other carbapenems such as meropenem are strongly influenced by the MexAB-OprM pump (83).

b. MexXY-OprM

The silence of *oprK* gene encoding the outer membrane protein OprM linked to the mexXY operon provokes a union between MexXY system and OprM from MexAB-OprM system (86). Overexpression of the MexXY-OprM pump is related to aminoglycoside resistance in impermeable-type *P. aeruginosa* clinical isolates (87).

ANTIMICROBIAL AGENT	PERMEABILITY AND EFFLUX ¹	INACTIVATION ²	CHANGES IN TARGET ³
β- lactams	+	+	+
Aminoglycosides	+	+	-
Fluoroquinolones	+	-	+
Polymyxins	-	-	+
Biocides	+	-	+

Table 2. Summary of the resistance mechanisms of *P.aeruginosa* in cystic fibrosis (CF).

¹ Permeability changes in the bacterial cell wall which restricts antimicrobial access to target sites. Active efflux of the antibiotic from the microbial cell.

² Enzymatic modification of the antimicrobial agent. Degradation of the antimicrobial agent.

³ Modification of antimicrobial agent targets.

1.6.2.2. RESISTANCE TO β-LACTAMS

The most prevalent mechanism of resistance to β-Lactams in *P. aeruginosa* is the production of β-lactam-hydrolyzing β-lactamases, though efflux systems or reduced outer membrane permeability can also be contributing factors.

a. β-lactamases

The first β -lactamase discovered was a cepalosporinase that now it is well known as the chromosomally encoded class C enzyme (AmpC) produced by many gram-negative bacteria, including *P. aeruginosa*. Apart from this endogenous β-lactamase, several plasmid-encoded β-lactamases have been described in *P. aeruginosa*, such as enzymes of molecular classes A, B and D.

i. AmpC

AmpC enzymes are broad-spectrum β -lactamases that hydrolyze and provide resistance to most β -lactams except carbapenems, and being the major determinant of resistance to cephalosporins in *P. aeruginosa*. Despite of carbapenems are good inducers of this enzyme, their speedy bactericidal activity and stability to AmpC hydrolysis provides them effective against this organism. The *ampC* gene expression is under the control of the AmpR regulator that inhibits *ampC* expression when the inducers are absent and triggers *ampC* expression when these are present (88). Therefore, mutations in *ampR* and as well as in *ampD* are associated with the production of AmpC in β -lactam-resistant clinical isolates of *P. aeruginosa*.

ii. Transferable narrow-spectrum β -lactamases

Carbenicillinases (enzymes of the PSE/CARB group) such as CARB-1 (PSE-4), CARB-2 (PSE-1), CARB 3, CARB-4 and CARB-5 are acquired β -lactamases responsible for the most common acquired β -lactamases in β -lactam-resistant *P. aeruginosa*. Moreover, acquired class D enzymes of the OXA group (oxacillinases) also predominate in isolates where acquired β -lactamases are implicated in resistance (89).

iii. Transferable extended-spectrum β -lactamases and carbapenemases

The extended spectrum β -lactamases (ESBLs) have a great interest since these enzymes can promote resistance to antipseudomonal cephalosporins (ceftazidime), ureido and carboxy penicillins (piperacillin and ticarcillin, respectively) and, frequently cefepime and/or aztreonam. ESBLs are plasmid- or chromosome-encoded and sometimes associated with integrons carrying additional resistance genes. β -lactamases with antcarbapenems activity are the class A and D carbapenemases and the class B metallo- β -lactamases hydrolyzing most β -lactams except monobactams. The more prevalent types of acquired metallo-enzymes in *P. aeruginosa* are VIM and IMP which are plasmid- or chromosome-encoded and associated with integrons carrying additions resistance genes.

b. Permeability and Efflux

Nonenzymatic and intrinsic resistance to β -lactams has also a key role in *P. aeruginosa* and involves impermeability and/or efflux. Certainly, several of the RND type multidrug efflux systems associated with fluoroquinolones (FQs) resistance are also implicated in accommodate β -lactams, including penicillins (MexAB-OprM), third (MexAB-OprM) and fourth (MexCD-OprJ) generation cephalosporins, monobactams (MexAB-OprM) and carbapenems (several Mex systems) (80). However, only MexAB-OprM is implicated in meropenem resistance in clinical strains, whereas none of Mex systems impact imipenem resistance (85)(90). Carbapenems resistance, especially imipenem, in *P. aeruginosa* is most commonly related to loss or mutation of outer membrane protein OprD, a portal for basic amino acids uptake that also accommodates carbapenems (71).

1.6.2.3. RESISTANCE TO FLUOROQUINOLONES

Despite the resistance to fluoroquinolones (FQs), especially ciprofloxacin, these agents have been a potent component of the antipseudomonal therapy. Resistance to FQs among almost all bacteria including *P. aeruginosa* is attributable to mutations in the genes encoding the DNA gyrase and/or topoisomerase IV targets of these antimicrobials. The most common modifications observed in FQs-resistant isolates are in the quinolone resistance determining region (QRDR) of the GyrA component of gyrase and ParC component of topoisomerase IV. It has also been reported that mutations in the GyrB and ParE components of gyrase and topoisomerase IV are much less frequently found (91). Moreover, FQs resistance is also related to several of the 3-component RND family multidrug efflux systems in *P. aeruginosa* provoking cross-resistance of many FQs-resistant isolates of this organism to multiple antimicrobial classes (92). Overexpression of the MexAB-OprM, MexCD-OprJ and MexEF-OprN play a relevant role in numerous FQs-resistant isolates, in many occasions together with target site mutations (92). There are also other efflux systems such as MexXY-OprM and MexVW-OprM associated with FQs transport, but no cases of FQs-resistant isolates hyperexpressing these efflux systems have not been observed.

1.6.2.4. RESISTANCE TO AMINOGLYCOSIDES

Aminoglycosides are commonly used in the treatment of *P. aeruginosa* pulmonary infections in CF patients. The most frequently aminoglycosides associated with resistance are gentamicin, tobramycin and to a lesser extent, amikacin. Resistance is typically due to drug inactivation by plasmid-or chromosome-encoded enzymes harbored by resistant strains and defects in drug uptake/accumulation (78).

a. Modifying Enzymes

Inactivation of aminoglycosides in resistant strains is related to their modification by enzymes that either phosphorylate, acetylate, adenylate or aminoglycoside adenyl-transferase these antimicrobials (93).

i. Aminoglycoside acetyltransferases (AAC)

Enzymes that modify the 3 and 6' positions of amino groups are the most common AACs in *P. aeruginosa*. Aminoglycoside acetyltransferases are generally encoded by integrons or transposons found in many aminoglycoside-resistant isolates. On one hand, the AAC (3)-I enzyme is a frequent determinant of gentamicin resistant in *P. aeruginosa*. On the other hand, the AAC (6') family of enzymes gives resistance to tobramycin, netilmicin, kanamycin, amikacin (-I subfamily) and gentamycin (-II). The most prevalent ACC in this organism is AAC (6')-II being in most cases the determinant of gentamicin and tobramycin (93).

ii. Aminoglycoside phosphotransferases (APH)

Several APH (3') enzymes are involved in resistance to kanamycin, neomycin and streptomycin because of their phosphorylation at the 3'-OH. In addition, other APH (3') enzymes have been described in *P. aeruginosa* providing resistance to amikacin (APH(3')-VI) and gentamicin and tobramycin (APH (2'')) (78).

iii. Aminoglycoside nucleotidyl transferases (ANT)

The most relevant ANT described in *P. aeruginosa* is the ANT (2'')-I enzyme, which with AAC (6') represents the most common determinant of enzyme-dependent aminoglycoside resistance in this organism. The ANT (2'')-I enzyme is associated

with gentamicin and tobramycin resistance. Genes for ANT enzymes can also be integron associated (93).

b. Impermeability and Efflux

The impermeability resistance (reduction of aminoglycoside accumulation as a consequence of reduced drug uptake owing to reduce resistance) has a key role in *P. aeruginosa* CF isolates resistant to aminoglycosides, which frequently occurs in alliance with modifying enzymes to promote broad-spectrum aminoglycoside resistance in this organism. The reduced of aminoglycoside accumulation is due to MexXY-OprM multidrug efflux system, since this system is the major efflux complex exporting aminoglycosides in *P. aeruginosa*, in addition to other antimicrobials such as tetracyclines and macrolides (94).

c. Adaptive Resistance

P. aeruginosa has the ability to adapt to and grow at elevated levels of aminoglycosides decreasing the susceptibility to all of them and loss the resistant phenotype in the absence of drug. Resistance appears during the first few hours of first-drug exposure and disappears a few hours after antimicrobial removal. Curiously, aminoglycoside resistance occurs because of the reduction of aminoglycoside accumulation and in addition, the MexXY efflux system is involved in the reduced accumulation that characterizes adaptive aminoglycoside resistance although the uptake reduction also contributes (95).

d. Outer Membrane

The OM protein called OprH has an apparent role in aminoglycoside (and polymyxin) resistance observing its expression under low Mg^{2+} growth conditions and its presence in certain mutants (93). It is also well known that OprH is encoded by the first gene of a 3-gene operon that includes *phoP* and *phoQ*. The low Mg^{2+} - dependent and mutational resistance to aminoglycosides previously related to OprH are, in fact, attributed to PhoP-PhoQ expression and activity and it may involve modification of LPS as for polycation resistance (96).

1.6.2.5. RESISTANCE TO POLYCATIONS

P. aeruginosa resistance to polymyxins (polycation antimicrobials such as polymyxin B and E) involves alterations to LPS, including modifications of the lipid A with aminoarabinose (78).

Mutations in the genes encoding the PmrA-PmrB two-component regulatory system are also implicated in adaptive polycation resistance that occurs with low levels of Mg^{2+} or the presence of polycations (97). A second two-component system called PhoP-PhoQ regulates *pmrAB* and mediates the low Mg^{2+} and polycation induction of resistance, so it is also associated with polycation resistance (96).

Remarkably, PmrA-PmrB/PhoP-PhoQ also regulates resistance to the cationic antimicrobial peptides of innate immunity that are being studied as chemotherapeutic agents and it is again related to aminoarabinose modification of LPS-polymyxin-resistant *pmrAB* mutants with the aminoarabinose modification increasing resistance to these peptides (97).

1.6.2.6. RESISTANCE TO BIOCIDES

P. aeruginosa has variable susceptibility to biocides (disinfectants, preservatives and antiseptics) such as triclosan, chlorhexidine and quaternary ammonium compounds (QACs). The intrinsic or adapted resistance to most biocides is involved in changes in membrane composition and ultrastructure limiting drug uptake. In fact, it has been observed that hyperexpression of a OM lipoprotein named OprR is correlated with QAC resistance (98).

1.6.2.7. BIOFILMS

Biofilms are the most common mode of life in the case of *P. aeruginosa* causing the chronic pulmonary infection that affects CF patients.

Increasingly, there is a close relationship between biofilm formation and antimicrobial resistance. Several mechanisms are involved in biofilm resistance. It has been reported that the restricted penetration of antimicrobials into biofilms is a main reason of resistance (99). In addition, some studies have suggested that *P. aeruginosa* within biofilms are metabolically less active and grow slowly than periphery layers because of limited access to nutrients and oxygen, contributing to increasing biofilm tolerance and considering that antimicrobials often target

antimicrobial resistance has been demonstrated with anaerobic biofilm-grown of *P. aeruginosa* from CF patients since many drugs are inactive or less active in anaerobic conditions (100) (101).

And the last but not least, the established theory of persister cells has a high association with multidrug tolerance of biofilms. Persisters are a small fraction of biofilm cells that become highly tolerant to antimicrobials and get to this state without suffering genetic alterations. Persisters in biofilms seem to be responsible for the relapsing nature of chronic infections, since antimicrobials eradicate most bacterial population; however, persisters remain viable and repopulate when the level of drugs drop (102).

Moreover, persisters have shown a reduced susceptibility to antimicrobials because bacteria are not undergoing cellular activities that antimicrobials corrupt resulting in tolerance which means no growth and slow death. On the contrary, resistant mechanisms emerge from genetic changes that block antimicrobial activity resulting in resistance which means that resistant bacteria grow in the presence of antimicrobials, whereas persister bacteria do not grow and are latent (102).

1.7. Nanoencapsulation of antimicrobials

1.7.1. THE STATE OF THE ART IN NANOENCAPSULATED ANTIMICROBIALS

Nowadays, both tobramycin and colistin are part of current inhaled therapy to treat respiratory infections in CF patients (29). Although both antibiotics proved to be effective against *P. aeruginosa*, they produced local side effects. Moreover, their administration is time consuming, is conditioned by unpredictable systemic drug absorption and needs education and training. All these facts together induce poor adherence to the treatment (29). Despite colistin is considered one of the most active antimicrobials to combat multidrug-resistance bacteria, recent studies have described the emergence of colistin-resistant bacteria in CF patients treated with long-term by inhalation (103)(104). All these evidences together have stimulated the research on the introduction of less toxic antimicrobials as well as the use of pharmaceutical forms that can diminish doses (74).

It has been widely shown that pharmaceutical form has a great influence in the antimicrobial action. This is due to several reasons. The first one derives from the

fact that the availability of antimicrobial in the site of infection strongly depends upon the pharmaceutical form and administration way. In some scenarios, this influence could be as relevant as to lead to a change in the microbial behavior, meaning that an antimicrobial being considered as non-active against a given microbe, could turn active when administered in the appropriate form.

Due to economic reasons, the research on new antimicrobials has been scarce in the last decades, although fortunately the report of President Barack Obama as well as the recent reports of World Health Organization (WHO) has changed this tendency (Fig.13). Subsequently, only a few new antimicrobials entities have been discovered over the last years (105).

Nanoencapsulation of antibiotics is being regarded as a good alternative for improving current treatments and represents a promising strategy to overcome the mucus barrier and to prolong the drug retention in the lung as other authors have also previously reported (106).

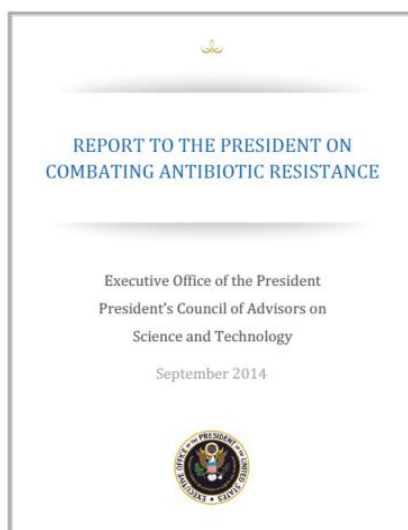


Fig.13. The report to the President Obama on combating antibiotic resistance (left) and the WHO report on Antimicrobial resistance (Global Report on surveillance) (right) have changed the tendency of the last years in which almost no funding was available to explore new antimicrobial drugs. ENABLE Project is the European basis of this change of tendency.

Nano-encapsulation of antibiotics is being regarded as a good alternative for improving current treatments and represents a promising strategy to overcome the

mucus barrier and to prolong the drug retention in the lung as other authors have also previously reported (106).

1.7.2. LIPID NANOPARTICLES: SLN AND NLC

Over the last decades, lipid nanoparticles have emerged as a very promising pulmonary drug delivery system presenting many advantages, such as: (i) mucoadhesion. The bioadhesion is defined as a mechanism by which two biological materials are maintained together due to forces in the interface. In pharmaceuticals, the term mucoadhesion is used to describe attractive forces between any material and mucus. In the case of respiratory tract of CF patients, the ability of antimicrobial to bind mucus is a crucial parameter. Mucus membranes strongly adhered to epithelial surfaces (gastrointestinal and respiratory tracts, vagina, eyes and others) are generally hydrophilic since numerous hydrogen bonds due to their high-water content (approximately 95%) within its composition. Understanding the hydrophilic bonding and adhesion mechanisms of mucus to biological material is of utmost importance to produce the most efficient applications. For instance, in drug delivery systems, the mucus layer must be penetrated to effectively transport micro-or nanosized drug particles into the body. Of interest is the so called first pass degradation which consisted in a phenomenon of drug metabolism whereby the concentration of a drug is greatly reduced before it reaches the systemic circulation and subsequently the site of infection. The fraction of drug lost during the process of absorption generally related to the liver and gut metabolisms. Avoidance of first pass effect and hence the possibility to reduce the dose, good tolerability, deep lung deposition of drug and a sustained release of the active pharmaceutical ingredient (API) leading to a much longer dosing interval (107) (108) or reduced doses.

The use of solid lipid nanoparticles (SLN) and nanostructured lipid carriers (NLC) are being explored to treat *P. aeruginosa* infections in CF. This should reduce systemic toxicity, diminish dose, and enlarge administration intervals.

In the 1990s, three working groups (109)(110)(111) developed SLN, the first generation of lipid nanoparticles. SLN are prepared from a lipid matrix that is solid at body and room temperature and are composed of 0.1-30% (w/w) lipid dispersed in an aqueous solution of 0.5-5% (w/w) surfactant as stabilizing agent. The mean diameter of the SLN ranges from 40 to 1000 nm approximately. Solid lipids and

surfactants used in our SLN formulations are glycerides (Precirol ATO 5=glyceryl distearate NF and poloxamer 88/polysorbate 80, respectively). SLN present the following characteristics: physical stability, protection of the incorporated drug from degradation, the possibility to incorporate lipophilic but also hydrophilic drugs, controlled release and low cytotoxicity, if well tolerated excipients are used. In addition, preparation methods at industrial scale are available (e.g. spray drying, high shear mixing, ultra-sonication, and high pressure homogenization) and these methods can be carried out organic solvent free (112). Mainly, disadvantages of SLN are low drug loading capacity because of the formation of a perfect lipid crystal matrix, and drug expulsion during storage due to the complexity of the physical state of the lipid.

To solve these SLN related problems, the second generation of lipid nanoparticles (NLC) was developed. NLC have a solid lipid matrix at room and body temperature that consists of a blend of a solid lipid (Precirol ATO 5 = glyceryl distearate NF) and oil (Miglyol 812 = medium-chain triglycerides). Through mixing different kinds of lipids, a less ordered lipid matrix with more space for active compounds is achieved. Thus, the lipid matrix gives more flexibility for modulation of drug release, increasing the drug loading and preventing its leakage (108) (Fig.14).

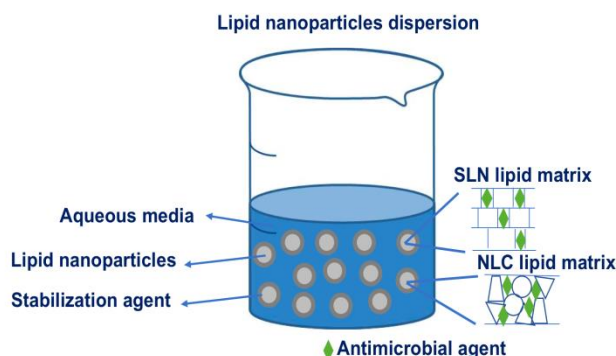


Fig.14. SLN and NLC. SLN are composed of solid lipids. NLC are prepared from a blend of a solid lipid with a liquid lipid.

SLN and NLC present several advantages for pulmonary application with all the features mentioned above. Firstly, good tolerability in the airways and

biodegradability. Secondly, due to their size, nanoparticles can be easily aerosolized into droplets which enables sufficient deep lung deposition of an active compound. Furthermore, nanoparticles adhere to the mucosal surface of lung for a long period. Thus, particle adhesion, accumulation and retention in the lung as well as prolonged release properties SLN and NLC result in a longer dosing interval and better patient compliance (108).

It has been pointed out that both SLNs and NLCs are more stable than liposomes both *in vitro* and *in vivo*, they have better biocompatibilities and lower potential toxicity (both acute and chronic) than polymeric nanoparticles or other synthetic nanoformulations and are relatively to produce (113). The use of nanoparticles could overcome pre-existing drug resistance mechanisms, including decreased uptake and increased efflux of drug as well as biofilm formation (114)(115). Lipid nanoparticles loaded with aminoglycosides are significantly more effective than free formulations against *P. aeruginosa* clinical isolates (116)(117).

These are the reasons why we are basically going to focus on exploring the antimicrobial activity of the nanoencapsulated colistin and tobramycin (in both SLN and NLC) versus free drug against *P. aeruginosa* clinical isolates from CF patients and investigation the efficacy of these novel formulations in the eradication of biofilms, the most common mode of life of *P. aeruginosa* causing pulmonary infections.

2. OBJECTIVES

2. JUSTIFICATION OF THE STUDY AND OBJECTIVES

P.aeruginosa predominantly infects the respiratory tract of cystic fibrosis (CF) patients causing significance decline of pulmonary functions and increasing morbidity and mortality. Multidrug-resistant phenotypes and high capacity to form stable biofilms are common. The use of nanoparticles containing antimicrobials has gained increasing attention as a way to overcome drug resistance mechanisms. Moreover, despite tobramycin and colistin are part of current inhaled therapy to treat respiratory infections in CF patients, they produce local side effects as well as the emergence of colistin-resistant bacteria. The goal standard of our studies was the exploration of the antimicrobial activity of lipid nanoparticles (SLN and NLC) with colistin and tobramycin for pulmonary delivery as an alternative treatment of *P. aeruginosa* in the context of respiratory infections in CF patients.

The main objectives are summarized below:

- 1. Preparation and characterization of lipid nanoparticles (SLN and NLC) as colistin and tobramycin carriers to treat *P. aeruginosa* lung infections.**
 - 1.1. Determination of the size, drug entrapment and drug release profile of both type of lipid nanocarriers.
 - 1.2. Study of the toxicity effect of SLN and NLC.
 - 1.3. Study of the nebulization effects on lipid nanoparticles properties (size distribution, polydispersity index, zeta potential and morphology).
 - 1.4. Determination of how lipid nanoparticles could overcome an artificial mucus barrier in the presence of mucolytic agents.
 - 1.5. Study of the *in vivo* distribution of lipid nanoparticles in lungs.
- 2. Exploration of the stability of nanoencapsulated colistin in freeze dried SLN and NLC.**
 - 2.1. Study of the stability of their physical and chemical properties over time.

OBJECTIVES

- 2.2. Investigation of the effect of the storage temperature of nanoparticles over time.
- 2.3. Study of how the trehalose and mannitol acting as cryoprotectants in freeze-dried formulations influence stability.
- 3. **Study of the antimicrobial activity of SLN and NLC loaded with colistin and tobramycin against respiratory *P.aeruginosa* isolates from Sant Joan de Déu and Vall d'Hebron hospitals CF patients.**
 - 3.1. Determination of the antimicrobial effect of colistin and tobramycin loaded in lipid nanoparticles on planktonic *P.aeruginosa* cultures.
 - 3.2. Study of the effect of nanoencapsulated colistin and tobramycin on *P.aeruginosa* biofilm mode of growth.
 - 3.3. Determination of their efficacy in biofilm eradication.
 - 3.4. Dertermination of their efficacy in prevention of biofilm formation.
 - 3.5. Determination of the time dependence of the biofilm viability after treatment of NLC-colistin.

3. RESULTS

3. RESULTS

All papers presented in this work are enumerated according to the publication date.

3.1. ELABORATION AND CHARACTERIZATION

Objective 1 : To elaborate and characterize lipid nanoparticles (SLN and NLC) as colistin and tobramycin carriers to treat *P. aeruginosa* lung infections.

- 1.1. To determine size, drug entrapment and drug release profile of both type of lipid nanocarriers.
- 1.2. To study the toxicity effect of SLN and NLC.
- 1.3. To study whether the nebulization could affect lipid nanoparticles properties.
- 1.4. To analyze whether lipid nanoparticles could overcome an artificial mucus barrier in the presence of mucolytics agents.
- 1.5. To study the *in vivo* distribution of lipid nanoparticles in lungs.

Paper 1: Sodium colistimethate loaded lipid nanocarriers for the treatment of *Pseudomonas aeruginosa* infections associated with cystic fibrosis.

Pastor M, Moreno-Sastre M, Esquisabel A, **Sans E**, Viñas M, Bachiller D, Asensio VJ, Pozo AD, Gainza E, Pedraz JL. Int J Pharm. 2014 Dec 30;477:485-94. doi: 10.1016/j.ijpharm.2014.10.048.

Paper 2: Pulmonary delivery of tobramycin-loaded nanostructured lipid carriers for *Pseudomonas aeruginosa* infections associated with cystic fibrosis.

Moreno-Sastre M, Pastor M, Esquisabel A, **Sans E**, Viñas M, Fleischer A, Palomino E, Bachiller D, Pedraz JL. Int J Pharm. 2016 Feb 10;498:263-73. doi: 10.1016/j.ijpharm.2015.12.028.

3.2. STABILITY

Objective 2 : To investigate the stability of colistin nanoencapsulated in SLN and NLC after freeze-drying.

- 2.1.** To study the maintenance of their physicochemical properties over time.
- 2.2.** To test the effect of the storage temperature of nanoparticles over time.
- 2.3.** To study whether trehalose and mannitol could act as cryoprotectants in freeze-dried formulations.

Paper 1: Sodium colistimethate loaded lipid nanocarriers for the treatment of *Pseudomonas aeruginosa* infections associated with cystic fibrosis.

Pastor M, Moreno-Sastre M, Esquisabel A, **Sans E**, Viñas M, Bachiller D, Asensio VJ, Pozo AD, Gainza E, Pedraz JL. Int J Pharm. 2014 Dec 30;477:485-94.

Paper 3: Killing effect of nanoencapsulated colistin sulfate on *Pseudomonas aeruginosa* from cystic fibrosis patients.

Sans-Serramitjana E, Fusté E, Martínez-Garriga B, Merlos A, Pastor M, Pedraz JL, Esquisabel A, Bachiller D, Vinuesa T, Viñas M. J Cyst Fibros. 2016 Sep;15:611-8.

Paper 4: Stability study of sodium colistimethate-loaded lipid nanoparticles.

Moreno-Sastre M, Pastor M, Esquisabel A, **Sans E**, Viñas M, Bachiller D, Pedraz JL. J Microencapsul. 2016 Nov; 33: 636-645.

3.3. ANTIMICROBIAL ACTIVITY

Objective 3 : To study the antimicrobial activity of SLN and NLC loaded with colistin and tobramycin against respiratory *P.aeruginosa* isolates from Sant Joan de Déu and Vall d'Hebron hospitals CF patients.

Paper 1: Sodium colistimethate loaded lipid nanocarriers for the treatment of *Pseudomonas aeruginosa* infections associated with cystic fibrosis.

Paper 2: Pulmonary delivery of tobramycin-loaded nanostructured lipid carriers for *Pseudomonas aeruginosa* infections associated with cystic fibrosis.

Paper 3: Killing effect of nanoencapsulated colistin sulfate on *Pseudomonas aeruginosa* from cystic fibrosis patients.

Paper 5: Determination of the spatiotemporal dependence of the *P. aeruginosa* biofilm viability after treatment with NLC-colistin.

Paper 6: Antipseudomonal activity of free and nanoencapsulated tobramycin (NLC and SLN).

Objective 3.1: To determine the antimicrobial effect of colistin and tobramycin loaded in lipid nanoparticles on planktonic *P.aeruginosa* cells.

Paper 1: Sodium colistimethate loaded lipid nanocarriers for the treatment of *Pseudomonas aeruginosa* infections associated with cystic fibrosis.

Pastor M, Moreno-Sastre M, Esquisabel A, **Sans E**, Viñas M, Bachiller D, Asensio VJ, Pozo AD, Gainza E, Pedraz JL. Int J Pharm. 2014 Dec 30;477:485-94.

Paper 2: Pulmonary delivery of tobramycin-loaded nanostructured lipid carriers for *Pseudomonas aeruginosa* infections associated with cystic fibrosis.

Moreno-Sastre M, Pastor M, Esquisabel A, **Sans E**, Viñas M, Fleischer A, Palomino E, Bachiller D, Pedraz JL. Int J Pharm. 2016 Feb 10;498:263-73.

Paper 3: Killing effect of nanoencapsulated colistin sulfate on *Pseudomonas aeruginosa* from cystic fibrosis patients.

Sans-Serramitjana E, Fusté E, Martínez-Garriga B, Merlos A, Pastor M, Pedraz JL, Esquisabel A, Bachiller D, Vinuesa T, Viñas M. J Cyst Fibros. 2016 Sep;15:611-8.

Paper 6: Free and nanoencapsulated tobramycin: their effect on planktonic and biofilm cystic fibrosis *Pseudomonas*.

Sans-Serramitjana E, Fusté E, Jorba M, Pedraz JL, Vinuesa T, Viñas M. Submitted to Microorganisms.

Objective 3.2: To analyze the key role of nanoencapsulated colistin and tobramycin on *P.aeruginosa* biofilm mode of growth.

Objective 3.2.1: To determine their efficacy in biofilm eradication.

Objective 3.2.2: To determine their efficacy in prevention of biofilm formation.

Paper 3: Killing effect of nanoencapsulated colistin sulfate on *Pseudomonas aeruginosa* from cystic fibrosis patients.

Sans-Serramitjana E, Fusté E, Martínez-Garriga B, Merlos A, Pastor M, Pedraz JL, Esquisabel A, Bachiller D, Vinuesa T, Viñas M. J Cyst Fibros. 2016 Sep;15:611-8.

Paper 6: Free and nanoencapsulated tobramycin: their effect on planktonic and biofilm cystic fibrosis *Pseudomonas*.

Sans-Serramitjana E, Fusté E, Jorba M, Pedraz JL, Vinuesa T, Viñas M. Submitted to Microorganisms.

Objective 3.2.3: To determine the time dependence of the biofilm viability after treatment with NLC-colistin.

Paper 5: Determination of the spatiotemporal dependence of *P.aeruginosa* biofilm viability after treatment with NLC-colistin.

Sans-Serramitjana E, Jorba M, Pedraz JL, Vinuesa T, Viñas M. In press accepted manuscript. International Journal of Nanomedicine.

PAPER 1



Sodium colistimethate loaded lipid nanocarriers for the treatment of *Pseudomonas aeruginosa* infections associated with cystic fibrosis



Marta Pastor^{a,b}, María Moreno-Sastre^{a,b}, Amaia Esquisabel^{a,b}, Eulàlia Sans^c, Miguel Viñas^c, Daniel Bachiller^{d,e}, Víctor José Asensio^d, Ángel Del Pozo^f, Eusebio Gainza^f, José Luis Pedraz^{a,b,*}

^a NanoBioCel Group, Laboratory of Pharmaceutics, University of the Basque Country, School of Pharmacy, Paseo de la Universidad 7, Vitoria-Gasteiz 01006, Spain

^b Biomedical Research Networking Center in Bioengineering, Biomaterials and Nanomedicine (CIBER-BBN), Vitoria-Gasteiz, Spain

^c Department of Pathology and Experimental Therapeutics, Medical School, University of Barcelona – IDIBELL, Barcelona, Spain

^d Fundación Investigaciones Sanitarias Islas Baleares (FISIB), Development and Regeneration Program, Ctra. Sóller km 12, Bunyola (Balearic Islands) 07110, Spain

^e Consejo Superior de Investigaciones Científicas (CSIC), Ctra. Sóller km 12, Bunyola (Balearic Islands) 7110, Spain

^f B.R.A.I.E., Hermanos Lumiere 5, Miñao 01510, Spain

ARTICLE INFO

Article history:

Received 16 September 2014

Received in revised form 20 October 2014

Accepted 21 October 2014

Available online 24 October 2014

Keywords:

Sodium colistimethate

Lipid nanoparticles

NLC

Pseudomonas aeruginosa

Cystic fibrosis

Nanomedicine

ABSTRACT

Lung impairment is the most life-threatening factor for cystic fibrosis patients. Indeed, *Pseudomonas aeruginosa* is the main pathogen in the pulmonary infection of these patients. In this work, we developed sodium colistimethate loaded lipid nanoparticles, namely, solid lipid nanoparticles (SLN) and nanostructured lipid carriers (NLC), as a strategy to enhance the antimicrobial therapy against *P. aeruginosa* in cystic fibrosis patients. The nanoparticles obtained displayed a 200–400 nm size, high drug entrapment (79–94%) and a sustained drug release profile. Moreover, both SLN and NLC presented antimicrobial activity against clinically isolated *P. aeruginosa*. The integrity of the nanoparticles was not affected by nebulization through a mesh vibrating nebulizer. Moreover, lipid nanoparticles appeared to be less toxic than free sodium colistimethate in cell culture. Finally, an *in vivo* distribution experiment showed that nanoparticles spread homogeneously through the lung and there was no migration of lipid nanoparticles to other organs, such as liver, spleen or kidneys.

© 2014 Elsevier B.V. All rights reserved.

1. Background

Cystic fibrosis (CF) is an autosomal recessive disorder caused by mutations in the gene encoding for the CF transmembrane conductance regulator (CFTR) protein (Gibson et al., 2003). The absence of functional CFTR protein in the membrane of epithelial cells leads to chronic pulmonary disease, recidivant respiratory infections, pancreatic dysfunction, high electrolytes level in sweat and male infertility (WHO, 2002). It is estimated that 1 out of 2500 Caucasian newborns might be affected by CF, being the most common autosomal recessive disease (Sims et al., 2005). CFTR mutations cause malfunctioning of the membrane-bound cAMP

regulated chloride channel, which in turn, produces plugs of mucus, obstruction and bronchial infections in the lung, constituting the main limiting factor of the disease in terms of morbidity and mortality (Heijerman et al., 2009; Ratjen et al., 2009). Among the pathogens that affect the CF patients, *Pseudomonas aeruginosa* (PA) is the most prevalent, but the treatment of its infections is often difficult due to the wide range of antimicrobial resistance of this species. This resistance to antimicrobials is a well documented phenomenon due to several molecular mechanisms such as the restricted outer membrane permeability, the presence of integron, insertion sequences, and the biosynthesis of degrading-enzymes (Fuste et al., 2013; Ruiz-Martinez et al., 2011a; Ruiz-Martinez et al., 2011b). *P. aeruginosa* infections usually start as an acute infection that finally becomes chronic. One of the main pathogenicity factors that favors *P. aeruginosa* colonization and resistance is its ability to develop a biofilm-like mucus layer in the viscous hypoxic media of CF patients' respiratory tract (Koch, 2002; Worlitzsch et al., 2002).

Currently, the preferred treatment is a high dose of inhaled antibiotic along with oral ciprofloxacin (Proesmans et al., 2013).

* Corresponding author at: NanoBioCel Group, Laboratory of Pharmaceutics, University of the Basque Country, School of Pharmacy, Paseo de la Universidad 7, Vitoria-Gasteiz 01006, Spain. Tel.: +34 945 013 091; fax: +34 945 013 040.

E-mail addresses: marta.pastor@ehu.es (M. Pastor), maria.moreno@ehu.es (M. Moreno-Sastre), amaia.esquisabel@ehu.es (A. Esquisabel), joseluis.pedraz@ehu.es (J.L. Pedraz).

The spread of multi-resistant bacteria strains together with the lack of new antibacterial agents drove the recovery of old antibiotics to treat CF patients and to apply new technologies, such as nanotechnology, to fight infections. Nowadays, both tobramycin and sodium colistimethate are the first-choice option for inhaled therapy to treat respiratory infections in CF patients (Heijerman et al., 2009). Although both the antibiotics proved to be effective against *P. aeruginosa*, they produced local side effects. Moreover, their administration is time consuming, is conditioned by an unpredictable systemic drug absorption and needs education and training. All these facts together induces poor adherence to the treatment (Heijerman et al., 2009).

Over the last decades, lipid nanoparticles have emerged as a promising drug delivery system that could overcome some limitations of the already existing drugs. Since only a few new antimicrobial entities have been discovered over the last years (Gould and Bal, 2013), nano-encapsulation of antibiotics is a good alternative for improving current treatments. Pulmonary delivery of lipid nanoparticles presents many advantages, such as, mucoadhesion, biodegradability, avoidance of first pass effect and hence the possibility to reduce the dose, good tolerability, deep lung deposition of drug and a sustained release of the API that leads to a longer dosing interval (Andrade et al., 2013; Weber et al., 2014). Many research groups have focused their efforts in developing inhalable nanoparticles to fight against bacterial resistances by encapsulating different drugs, such as amikacin (Ghaffari et al., 2011), tobramycin (Ungaro et al., 2012), ciprofloxacin (Chono et al., 2008; Wong et al., 2003), itraconazole (Alvarez et al., 2007) or amphotericin B (Gilani et al., 2011).

Taking the above into consideration, the aim of this work is to elaborate and fully characterize sodium colistimethate loaded lipid nanoparticles to be used in the treatment of infections in CF patients. Furthermore, the antimicrobial activity of the nanoparticles was assessed against a collection of *P. aeruginosa* strains isolated from CF patients. Finally, the *in vivo* pulmonary distribution was assessed.

2. Methods

2.1. Preparation of lipid nanoparticles

Two sodium colistimethate loaded formulations were elaborated, namely solid lipid nanoparticles (Colist-SLN) and nano-structured lipid carriers (Colist-NLC). An emulsion solvent evaporation technique was chosen for the preparation of Colist-SLN by modifying the procedure reported elsewhere (Soares et al., 2013). Briefly, 10 mg of antibiotic (Sigma–Aldrich, St. Louis, MO, USA) were mixed with a 5% (w/v) Precirol[®] ATO 5 (Gattefossé, Madrid, Spain) dichloromethane solution. Then, the organic phase and an aqueous surfactant containing solution (Poloxamer 188 at 1% w/v and Polysorbate 80 at 1% w/v) were mixed and emulsified by sonication at 20 W for 30 s (Branson Sonifier 250, Danbury, CT, US). The solvent was allowed to evaporate by magnetic stirring for 2 h at room temperature. Subsequently, the resulting SLNs were washed by centrifugation in Amicon[®] centrifugal filtration units (100,000 MWCO, Merck Millipore) at 2500 rpm for 15 min three times. For the Colist-NLC elaboration, a hot melt homogenization technique was selected (Beloqui et al., 2013; Obeidat et al., 2010). In brief, Precirol[®] ATO 5 and Miglyol[®] 812 (Sasol, Johannesburg, South Africa) were selected as the lipid core. Those lipids were mixed with the API and heated above the melting temperature of the solid lipid. The surfactant solution consisted of 1.3% (w/v) of Polysorbate 80 and 0.6% (w/v) of Poloxamer 188. The lipid and aqueous solutions were heated to the same temperature and then emulsified by sonication for 15 s at 20 W. Nanoparticles were stored at 4 °C overnight to allow lipid re-crystallization and particle

formation. Then, a washing step was undergone by centrifugation at 2500 rpm in Amicon[®] centrifugal filtration units (100,000 MWCO) three times. All the nanoparticles prepared were freeze-dried with two different cryoprotectants, either D-mannitol or trehalose (15%).

For the preparation of infrared (IR) labeled NLC, the IR-783 dye was selected (Sigma–Aldrich). The use of IR-labeled NLC enables particle observation in the near infra-red (NIR) region that it is known to avoid tissue auto-fluorescence problems. NIR dye has been previously encapsulated in heparin–folic conjugates and demonstrated its ability to remain inside the nanoparticles (Yue et al., 2013). The NLCs were prepared just as mentioned previously, but by adding 50 mg of IR-783 instead of the antibiotic. The washing step was performed three times by centrifugal filtration and trehalose 15% (w/w) was added prior to the freeze drying.

2.2. Characterization of lipid nanoparticles

2.2.1. Size and zeta potential

The particle size and zeta potential (ζ) were measured in a Zetasizer Nano ZS (Malvern Instruments, Worcestershire, UK) based on dynamic light scattering (DLS).

2.2.2. Microscopy analysis

Lipid nanoparticles were analyzed under transmission electron microscopy (TEM). Firstly, a negative staining was performed and after that the samples were observed.

In addition, lipid nanoparticles were imaged in air by using an Atomic Force Microscope (AFM) XE-70 (Park Systems, Suwon, Korea). All images were collected in a non-contact mode. Four types of images were simultaneously acquired with several scan sizes (100 μm^2 , 25 μm^2 and 6.25 μm^2) at a scan rate of 0.3–0.5 Hz.

2.2.3. Encapsulation efficiency

Non-entrapped sodium colistimethate was determined from the supernatants recollected after centrifugation. The amount of non-encapsulated drug was detected by HPLC (see Section 2.2.4). For the IR-labeled nanoparticles, dye loading was calculated spectrophotometrically at 800 nm. The supernatant samples were diluted to 10 ml and compared to a calibration curve (5–80 $\mu\text{g}/\text{ml}$). In both cases, the encapsulation efficiency (EE) was calculated following this equation,

$$\text{EE (\%)} = 100 \times \frac{(\text{initial amount of drug or dye} - \text{non-encapsulated drug or dye})}{\text{initial amount of drug or dye}}$$

2.2.4. Determination of sodium colistimethate by HPLC

The quantification of sodium colistimethate was conducted by a high performance liquid chromatographic (HPLC) technique adapted from Cancho Grande et al. (2000) and using a Waters 1525HPLC Binary Pump, UV-detector Waters 2487 and Waters 717 plus autosampler (Waters Corp., Milford, USA). The system was controlled by the Empower software. The column selected was a Novapak C18 \times 150 mm with a 4 μm pore size. The mobile phase consisted of 77% of an aqueous solution and 23% of acetonitrile. The aqueous phase was prepared by dissolving (7.1 g) sodium sulphate, (0.6 g) acetic acid and (2.2 g) phosphoric acid and adjusted to pH 2.5 with triethylamine up to 1 l. Sodium colistimethate was detected at 206 nm wavelength. The flow rate was fixed at 1.5 ml/min for isocratic elution, and 50 μl were set as an injected sample volume. This analytic technique was validated following EMA guidance for bioanalytical methods (Committee for Medicinal

Products for Human Use, CHMP, 2011). The assay was found to be linear for 100–800 µg/ml. Absence of interference was confirmed as the mobile phase and surfactant presented no peak under these conditions at this wavelength.

2.2.5. In vitro release profile

An amount ranging from 25 to 35 mg of each formulation was accurately weighed and incubated in 4 ml of PBS. At pre-established time points samples were centrifuged in Amicon[®] centrifugal filtration units (100,000 MWCO) for 15 min. The supernatants were then analyzed for drug quantification by HPLC. The PBS withdrawn was replaced with fresh medium. Results were expressed as percentage of drug released compared to the total encapsulated drug. The assay was run in triplicate for each formulation, Colist-SLN, Colist-NLC and IR-NLC.

2.2.6. Nebulization study

In order to study whether the nebulization through a mesh vibrating equipment (eFlow[®] rapid, PARI GmbH, Starnberg, Germany) could affect lipid nanoparticles properties, different analysis were performed after nebulization, i.e., size and zeta potential determination and TEM observation, as previously mentioned at Sections 2.2.1 and 2.2.2.

2.2.7. Microbiological experiment

2.2.7.1. Isolation of *P. aeruginosa* strains. Samples were recovered from the sputum of CF patients. Further steps were performed in order to select and identify the different *P. aeruginosa* strains (Ruiz et al., 2004). In brief, the samples obtained were harvested and microbiological assays were performed, i.e., morphology observation of short Gram-negative bacilli. Moreover, colony observation was performed in McConkey agar, Blood agar, TSA and MHA. At 37 °C for 24–48 h. Furthermore, several biochemical assays were conducted such as, oxidase test, oxidative/fermentative test (O/F), and Kliger medium assay. These isolated strains were compared to control strains *P. aeruginosa* ATCC 27853, *E. coli* ATCC 25922, *Staphylococcus aureus* ATCC 29213 and *Enterococcus faecalis* ATCC 29212.

2.2.7.2. MIC determination. Nanoparticles and free sodium colistimethate were tested in 31 *P. aeruginosa* isolates from patients (see Section 2.2.7.1) selected for these experiments, among whose 13 were mucoid and 18 non-mucoid.

Freeze-dried nanoparticles were resuspended in MHBCA and placed in the first row of 96-well plates. Next, starting from 32 µg/ml of antimicrobial agent, decreasing concentrations of nanoparticles were obtained by serial two-fold dilutions. Then, 5 µl of 10⁴ CFU/ml of bacteria was used as inoculum, and added to each well. Finally, plates were incubated for 24 h at 37 °C. Negative controls were defined as well without both bacteria and antimicrobial whereas positive bacterial growth controls were antibiotic-lacking wells. In addition, free antibiotic was also assessed. The minimum inhibitory concentration (MIC) was defined as the lowest antibiotic concentration that can prevent visible bacterial growth. The assay was run by triplicates.

2.2.8. Cell experiments

2.2.8.1. Inhibition concentration 50, IC₅₀. Cells were grown in Dulbecco's Modified Eagle Growth Medium (DMEM) supplemented with 10% foetal bovine serum (FBS), 1% L-glutamine, 1% penicillin/streptomycin solution and 1% of minimum essential medium-non essential amino acids 100× (MEM-NEAA) at 37 °C and 5% CO₂. The median inhibition concentration (IC₅₀) was determined for Colist-SLN and Colist-

NLC on A549 and H441 cells (ATCC). For this purpose, decreasing concentrations of nanoparticles starting from 10 mg/ml to 0.07812 mg/ml were added to the cells and incubated at 37 ± 2 °C and 5% CO₂ for 24 h. First, cells were seeded at a density of 12,000 cells per well in a 96-well plate and after overnight incubation, lipid nanoparticles were added to the wells and diluted in DMEM supplemented with 0.5% serum. Cell viability was assessed by means of the Cell Counting Kit 8 (CCK-8, Sigma-Aldrich) after a washing step. With this aim, 10% of CCK-8 reagent was added to each well and incubated in a wet chamber for 4 h at 37 ± 2 °C and 5% CO₂. Subsequently, the absorbance was read at 450 nm and at 650 nm as the reference wavelength. The absorbance was directly proportional to the number of living cells in culture. The results are given as 50% of living cells (IC₅₀), meaning that this dose inhibits the growth of the 50% of the population. The test was run in triplicates for each sample.

2.2.8.2. In vitro cytotoxicity. The cytotoxicity of Colist-SLN and Colist-NLC was determined against A549 and H441 cells by incubating them with different concentrations of nanoparticles for 24, 48 and 72 h at 37 ± 2 °C and 5% CO₂. Cells were seeded at a density of 12,000 cells per well and after overnight incubation, lipid nanoparticles, diluted in DMEM supplemented with 0.5% serum, were added to the wells from 78.1 up to 2500 µg/ml. After performing a washing step, cell viability was analyzed by means of the CCK-8. Subsequently, 10% of CCK-8 reagent was added to each well and incubated in a wet chamber for 4 h at 37 ± 2 °C and 5% CO₂. The test was run in triplicates for each sample.

2.3. In vivo biodistribution study

Mice were treated in accordance with the Directive 2010/63/EU of the European Parliament and of the Council of 22 September 2010 on the protection of animals used for scientific purposes. This animal study was approved by the Bioethics Committee of the Balearic Islands University (CEEA 06/11/13). Certified animal technicians observed mice regularly in all the studies and took steps to maintain animal welfare and prevented undue suffering. The animals were maintained under controlled environmental conditions (20–24 ± 1 °C, 40–65% ± 5% humidity, and 12-hour light/dark cycle), with free access to standard food (A04 diet, Panlab) and tap water in makrolon III cages (Tecniplast). Eight B6SJLF1 males (Charles River) were used to study the biodistribution of IR-labeled lipid nanoparticles.

Each mouse was administered 1.66 mg of IR-labeled NLCs by means of an inhalation tower (Buxco, Wilmington, NC, USA). At 0, 2.5, 4, 24 and 48 h after inhalation, groups of two mice were sacrificed by ketamin/xylazin anaesthesia overdose. Skin and peritoneal tissue were removed and lungs dissected for imaging. IR recordings were performed with a LI-COR Pearl[®] impulse small animal imaging system (LI-COR Corporate). The image J (NIH, USA) Java-based image analysis program was chosen for RGB brightness measurement of the images of the 800 nm channel. In brief, the whole lung area was selected and the mean brightness value of the green channel in ABU (arbitrary brightness units) was calculated.

2.4. Statistical analysis

All data are expressed as mean ± standard deviation (SD). All statistical calculations were carried out using the SPSS[®] 19.0 (SPSS[®] Inc., Chicago, IL, US). Kruskal–Wallis and one-way ANOVA program and post-hoc test were used for multiple group comparisons.

Table 1
Characteristics of sodium colistimethate loaded lipid nanoparticles.

Formulation	Cryoprotectant	Size (nm) ^a	Polydispersity index (PDI) ^a	Zeta potential (mV) ^a
Colist-NLC	Trehalose	412.5 ± 13.9	0.442	−21.97 ± 1.72
	D-mannitol	254.5 ± 20.3	0.339	−26.1 ± 7.05
Colist-SLN	Trehalose	303.4 ± 39.5	0.276	−20.80 ± 1.63
	D-mannitol	302.6 ± 20.5	0.361	−20.5 ± 6.09
IR-NLC	Trehalose	439.3 ± 20.1	0.439	−23.03 ± 1.8

^a The results are expressed as the mean ± S.D (n = 3).

3. Results

3.1. Nanoparticles characterization

Nanoparticles displayed a mean diameter size of 412.5 ± 13.9 nm and 303.4 ± 39.5 nm, for Colist-NLC and Colist-SLN, respectively, when trehalose was used as cryoprotectant. The addition of D-mannitol led to particle sizes of 254.5 ± 20.3 nm for Colist-NLC and 302.6 ± 20.5 nm for Colist-SLN. In addition, the polydispersity index was below 0.5, i.e., 0.442 and 0.276 for trehalose containing Colist-NLC and Colist-SLN and 0.361 and 0.339 for D-mannitol Colist-NLC and Colist-SLN, respectively. All the nanoparticles elaborated presented a negative zeta potential, around −21 mV. Likewise, IR-labeled NLC displayed a 439.3 ± 20.1 nm size and -23.03 ± 1.8 mV of charge, very similar to the antibiotic loaded NLCs. Table 1 summarizes the characterization data of the nanoparticles prepared.

As Fig. 1 shows TEM images revealed that the nanoparticles presented an almost spherical shape. Similarly, in the topography images obtained by AFM it becomes possible to observe the shape, structure and differences of the sample surface, confirming that the particles were spherical and presented a smooth surface. Amplitude images accentuating the edges give roughness and

height information, showing that particles were mainly smooth and flat. Finally, the phase images showed variations in elasticity and viscoelasticity of the sample.

The impact of nebulization on the properties of lipid nanoparticles was studied in terms of size, zeta potential and TEM. A mesh vibrating nebulizer was selected for this purpose. Size distribution and polydispersity index varied from the pre-nebulization to the post-nebulization sample, i.e., from 488 nm to 573 nm. Similarly, zeta potential changed from −20.8 to −25.3 mV, although it remained to be negative. These slight variations were not statistically significant. As TEM images showed (Fig. 1), nebulization did not affect nanoparticles morphology.

Once the nanoparticles were prepared, the supernatants were quantified by HPLC in order to calculate the EE indirectly (Fig. 2). High encapsulation efficiencies were achieved for Colist-SLN, Colist-NLC and IR-NLC, i.e., $79.70 \pm 6.06\%$, $94.79 \pm 4.20\%$ and $98.94 \pm 0.01\%$, respectively.

Regarding the release profile, a sustained release of the antibiotic was detected for both Colist-SLNs and Colist-NLCs. As Fig. 2C displays, an initial burst release was detected for all the nanoparticles. By the end of the study, a 49.3% and 85.6% of sodium colistimethate was released from Colist-SLN and Colist-NLC, respectively. With regard to the IR-labeled NLC, a slower profile

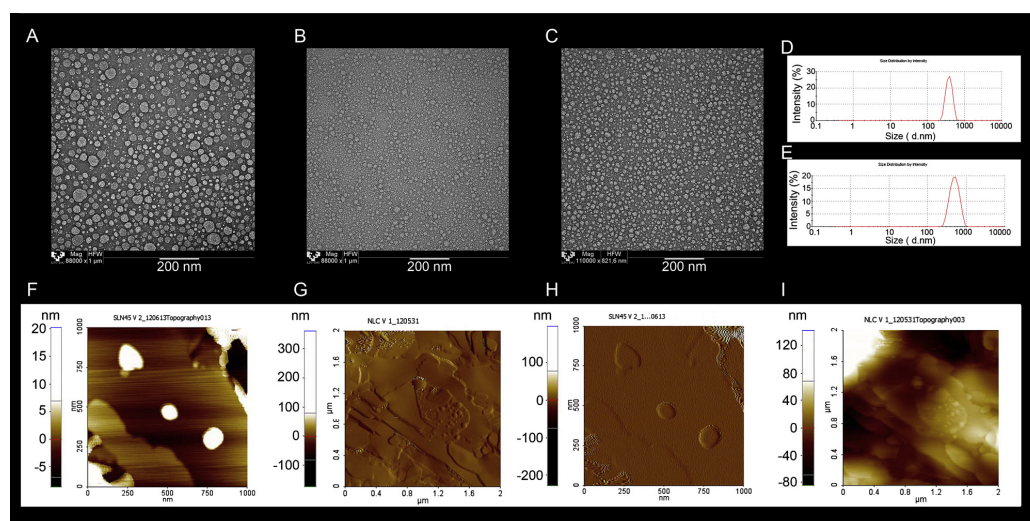


Fig. 1. Electron microscopy.

Transmission electron microscopy images of sodium colistimethate loaded lipid nanoparticles, (A) SLN, (B) NLC after reconstitution, and (C) NLC after nebulisation with vibrating mesh nebulizer. Size analysis results, (D) Colist-NLC after reconstitution, and (E) Colist-NLC after nebulisation with vibrating mesh nebulizer. F-I atomic force microscopy images, (F and G) sodium colistimethate loaded SLN and H, and (I) sodium colistimethate loaded NLC.

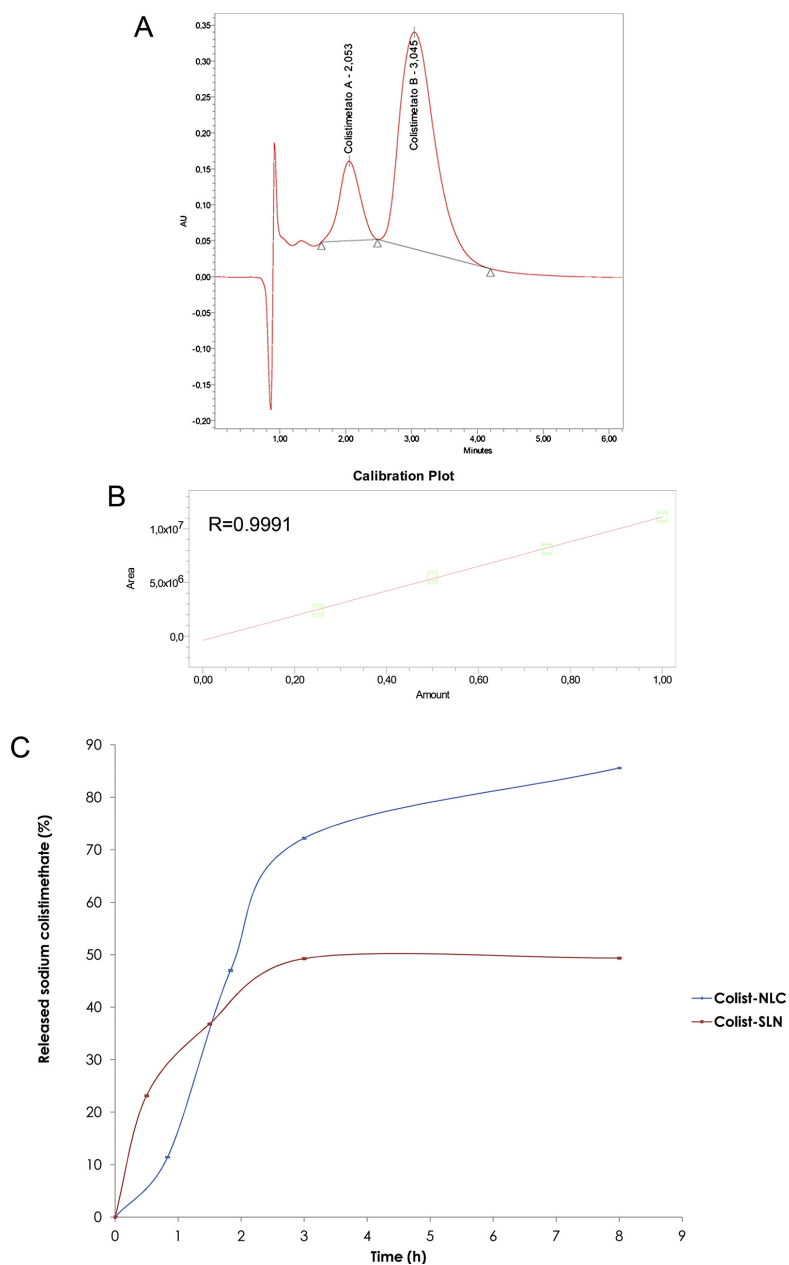


Fig. 2. Sodium colistimethate determination.

(A) The 2 peak chromatogram of the API from the supernatants of the lipid nanoparticles. (B) Calibration plot of the standard. (C) Release profile of sodium colistimethate from the lipid nanoparticles.

was detected, releasing $18.9 \pm 1.1\%$ at the 8th hour and the $25.47 \pm 0.68\%$ of the dye content in 48 h, the end of the *in vivo* sampling time points.

3.2. Microbiological experiments

P. aeruginosa is frequently isolated from sampling the respiratory tract of cystic fibrosis patients. It is also well known that both

mucoid and non-mucoid types can be isolated. Fig. 3 shows petri dishes containing both types of colonies. These species are characterized by its shape and size (short Gram-negative rods). Moreover, when grown on McConkey agar, lactose negative, greyish colonies were detected. In blood agar, bacterial growth was noticed, presenting beta-hemolysis in most cases. In TSA (Trypticase Soy Agar) at 42 °C bacterial growth is disclosed and green coloring is detected in most of the isolates. Regarding biochemical

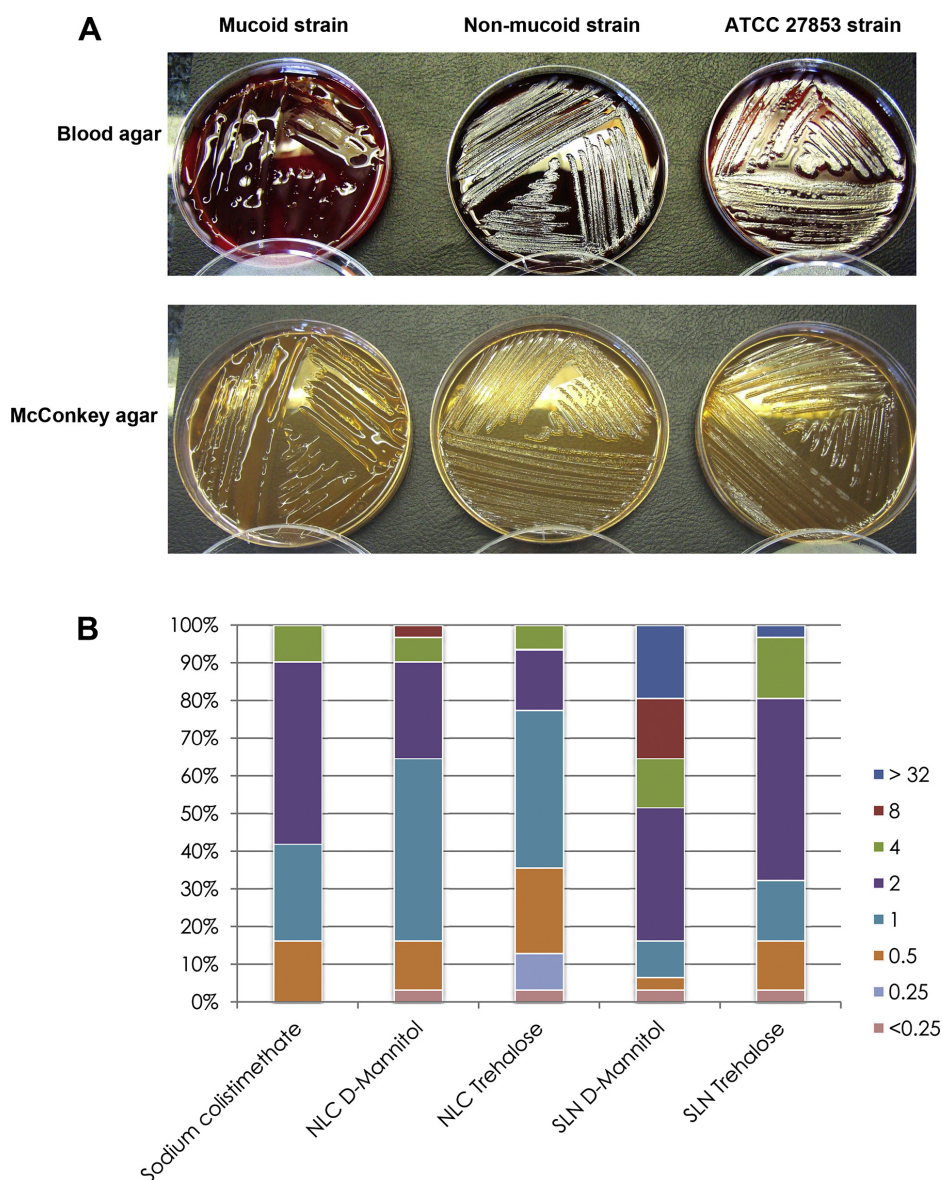


Fig. 3. Microbiological experiments.

(A) Isolated *Pseudomonas aeruginosa* strains. Left column, mucoid strain, middle column no-mucoid strains and right column control *P. aeruginosa* from ATCC. First row represents the morphology in blood agar and second row growth in McConkey Agar. (B) Bioactivity of elaborated lipid nanoparticles in terms of MIC determination in 31 strains of clinically isolated *P. aeruginosa* samples.

testing, all strains presented oxidase positive results, oxidative metabolism and were strictly aerobic.

Turning to MIC determination, both Colist-NLCs and Colist-SLNs showed to be active against clinically isolated *P. aeruginosa* growth. Fig. 3 exhibits the free antibiotic solution presented a mode of 2 µg/ml, whereas NLCs (irrespective of the cryoprotectant) displayed a 1 µg/ml MIC. The inhibitory concentration found for Colist-SLNs was 2 µg/ml. When nanoparticles were freeze dried with D-mannitol, a lower activity was determined in both cases. Although the MIC remained similar for both Colist-NLC and Colist-SLN, the final percentage of isolates susceptible to the formulation was lower when D-mannitol was incorporated, i.e., 64% vs 77% of isolates were susceptible to D-mannitol Colist-NLC and trehalose Colist-NLC, respectively, at 1 µg/ml. In the case of SLNs, 51% of isolates incubated with D-mannitol Colist-SLN and 80% of those with trehalose Colist-SLN were not able to grow at a 2 µg/ml concentration. It is noteworthy that free sodium colistimethate was unable to inhibit microorganism growth below 0.5 µg/ml, while lipid nanoparticles presented antimicrobial activity at 0.25 µg/ml. It should be also underlined that lipid nanoparticles were able to prevent microbial growth of the mucoid *P. aeruginosa* isolates.

As the D-mannitol containing lipid nanoparticles led to higher MIC values, trehalose was defined as the cryoprotectant to use in the following experiments. Finally, it should be underlined that NLCs presented most satisfactory results, compared to the SLNs.

3.3. Cell experiments

The IC₅₀ of the lipid nanoparticles developed was estimated by CCK8 assay in two cell lines, H441 human lung papillary adenocarcinoma and A549 human lung carcinoma, as showed in Fig. 4A. It has been previously analyzed and reported in a systemic review by Doktorovova et al. that in terms of toxicity studies no differences in susceptibility could be achieved to the fact of employing normal or cancer cell lines. Therefore, we chose these cell lines as they came from a lung cell lineage that is the intended route of administration for the nanoparticles elaborated (Doktorovova et al., 2014). The IC₅₀ represents half of the maximum inhibitory concentration. Hence, the lower the IC₅₀ value, the higher the toxicity. Firstly, it could be concluded that the H441 cell line presented a more sensitive behavior displaying a lower

IC₅₀ compared to the A549 cell line. For both cell lines, sodium colistimethate showed the lowest IC₅₀, therefore displaying the highest toxicity, 0.0065 ± 0.0007 mg/ml and 0.080 ± 0.103 mg/ml for H441 and A549, respectively. Among the lipid nanoparticles, Colist-NLC exhibited the lowest IC₅₀ ($p < 0.01$) 1.08 ± 0.19 mg/ml and 2.59 ± 0.87 mg/ml for H441 and A549, respectively. Interestingly, these IC₅₀ values are far from the 1–2 µg/ml that was estimated as MIC in Section 3.2., therefore, it could be inferred that lipid nanoparticles might be a safe product. These results were statistically significant compared to sodium colistimethate ($p < 0.01$). Overall, it should be pointed out that enclosing the antibiotic in lipid nanoparticles led to a huge decrease in toxicity, as NLCs presented 160-fold less toxicity in H441 cells and 28-fold less toxicity in A549 cells than the free antibiotic. Moreover, it should be highlighted that Colist-NLC was statistically less toxic than Colist-SLN ($p < 0.01$).

Regarding the cytotoxicity of the formulations three exposure times, 24 h, 48 h and 72 h, and six different concentrations were assessed (78.13–2500 µg/ml). Both the H441 and A549 cell lines were used in the test. In the CCK8 assay the number of living cells was estimated by the bio-reduction of the reagent leading to formazan. The results obtained suggest that sodium colistimethate encapsulation enhances cell viability especially at concentrations below 1250 µg/ml. As described in Fig. 4B–D, it could be observed that at the lowest concentration, sodium colistimethate exhibited lower absorbance values than the nano-encapsulated formulation, thus, less living cells. On the other hand, the absorbance value of sodium colistimethate became even lower as the exposure time was longer. NLCs presented higher absorbance values than SLNs when assessed in the A549 cell line. Nevertheless, the cell viability was quite similar for Colist-SLN and Colist-NLC when tested in H441 cell line. Blank lipid nanoparticles showed to be less toxic than antibiotic loaded nanoparticles when testing in H441 cells. Nevertheless, under the A549 cell line, unloaded lipid nanocarriers displayed almost the same absorbance value than loaded ones.

3.4. In vivo biodistribution study

Due to a more suitable release profile of NLCs along with a lower MIC and IC₅₀, the IR-labeled NLCs were selected for the *in vivo* distribution experiment. Similarly, trehalose was chosen as cryopreservation agent. In this work, an inhalation tower was

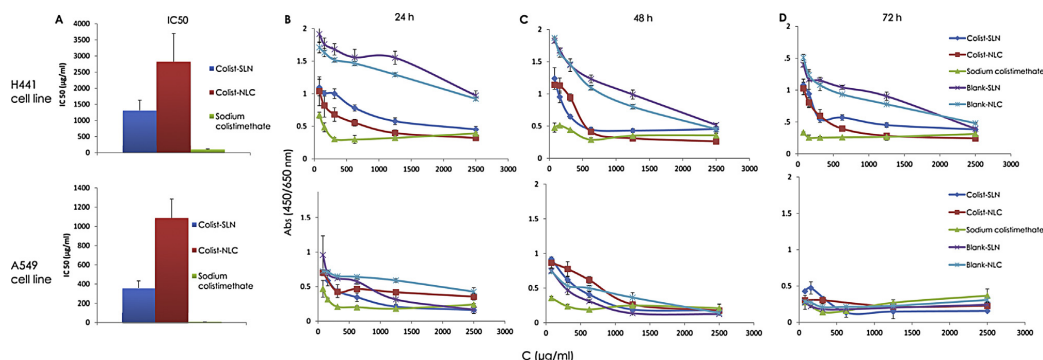


Fig. 4. Cell experiments results data.

(A) Represents the IC₅₀ value of the formulation in both cell lines. *** Describes statistically significant difference between the formulation and the free sodium colistimethate, $p < 0.01$ and **** represents differences between Colist-NLC and Colist-SLN, $p < 0.01$ (B–D). *In vitro* cytotoxicity measured by means of CCK8 at 24 h (B), 48 h (C) and 72 h (D). Upper row: cytotoxicity tested against H441 cell line, second row: cytotoxicity in the A549 cell line (B–D). *In vitro* cytotoxicity at 24 h, 48 h and 72 h. Upper row represents results of formulation cytotoxicity tested against H441 cell line and second row describes the results of the A549 cell line.

used to administer the nebulized lipid nanoparticles to mice. The inhalation tower enables a homogeneous dose distribution among the experimental animals. Moreover, the more aggressive intra-tracheal administration was avoided and the associated anaesthesia eluded. Each mouse was administered 1.66 mg of IR-labeled NLCs and IR images were recorded (Fig. 5). At 0 h, immediately after the nebulization was completed, the whole body images showed abundant NLC presence in the snout and the oropharyngeal cavity, the most exposed areas to the inhalation device. Two and half hours later, swallowing and breathing have displaced most NLCs to the respiratory and digestive tracks; at this time point NLCs were homogeneously distributed in both lungs and remained there until the end of the study. When comparing brightness intensities in the lungs at different time points, it could be observed that the strongest signal was displayed after 2.5 h (Fig. 5). In fact, a 1.5-fold increase in the arbitrary brightness units (ABU) value could be measured when comparing time 0 and time 2.5 h. The signal at 4 h remained strong, whereas recordings at 24 h and 48 h showed a progressive decrease in intensity. No IR emission was detected in other organs, such as liver, kidney, or spleen at any

time point during the experiment. It is also worth mentioning that in spite of the relatively high doses of NLCs detected in lungs and intestine, the animals did not show any symptomatology association with the uptake. It is likely, therefore, that the nanocarriers have negligible systemic toxicity. Nevertheless, further animal experiments would be required to confirm the safety of the formulation.

The use of an inhalation tower to administer nanoparticles to mice enabled a homogeneous dose delivery throughout the lungs of the animals. Furthermore, this method led to a broad distribution of NLCs across the organ that could be detected up to 48 h after nebulization. It remains to be studied, however, whether the residual dose detected after 48 h could have an impact on the clinical outcome of the treatment of the disease.

4. Discussion

As detailed in this work, we prepared sodium colistimethate loaded lipid nanoparticles focusing on the treatment of *P. aeruginosa* in cystic fibrosis patients. The use of lipid nanoparticles

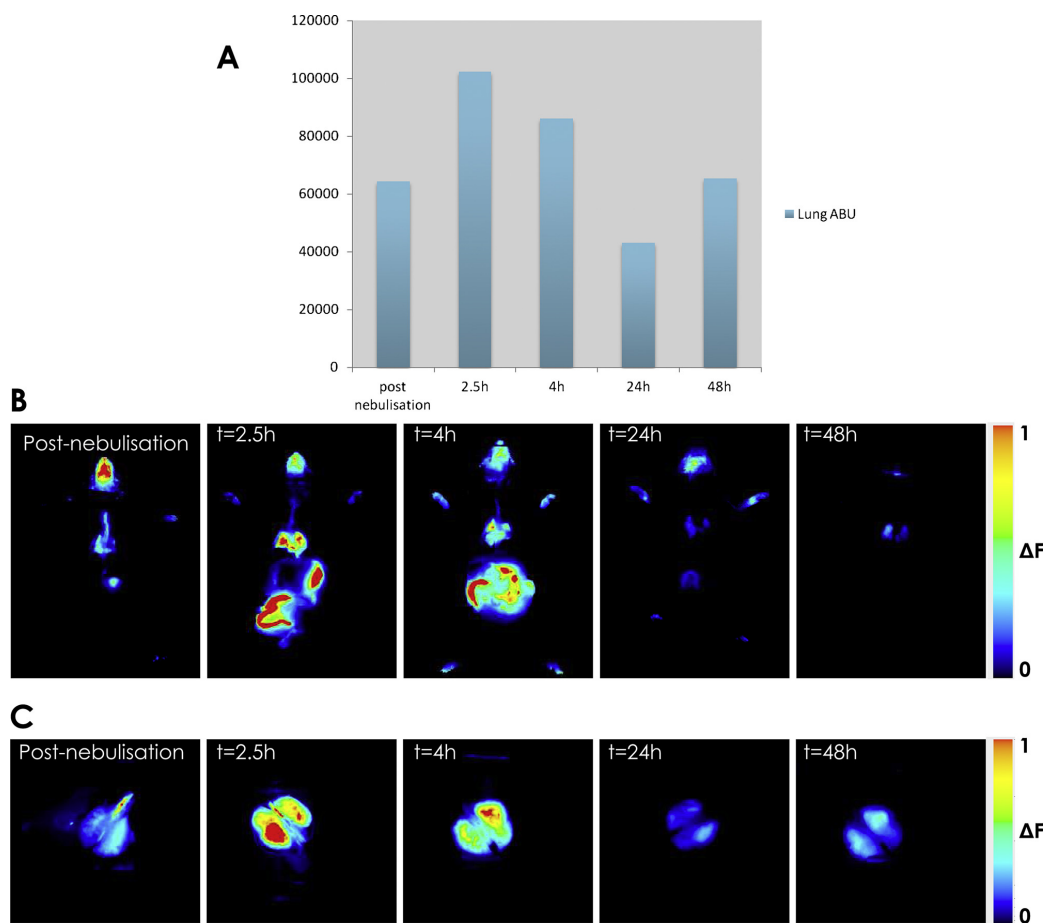


Fig. 5. *In vivo* results of IR-NLC distribution after inhalation.

(A) Bar graph showing the mean brightness intensity in arbitrary brightness units (ABU) of the whole area of each lung pair. (B and C) <***>Pseudo-color image representing the spatial distribution of photon counts in whole animals and lungs, respectively, immediately after nebulization and at 2.5, 4, 24 and 48 h after IR-NLC inhalation. Fluorescence intensity in the 800 nm channel is related to an external reference to make images of different animals and time points comparable.

gave rise to a potential enhancement of the treatment. We obtained high encapsulation efficiencies (SLN 79.7% and NLC 94.8%) that are in accordance with the results reported by Martins et al. who also described high EE values (>90%) for camptothecin loaded SLN. Their slightly higher results are likely to be related to the higher lipophilicity of camptothecin compared to sodium colistimethate (Martins et al., 2012). Likewise, Patlolla et al. (2010) reported similar encapsulation efficiency values when encapsulating Celecoxib in NLCs, >90%. Hence, the lipid nanoparticles described in this work presented acceptable EE values, comparable to those reported previously. Turning to the release profile of the nanoparticles, NLCs released a 86% of sodium colistimethate in 8 h and SLNs a 50%, data that were similar to those reported by Silva et al. (2012) for risperidone loaded SLN, i.e., 40% drug released by the 8th hour, similarly, Zheng et al. also detected almost a 100% of drug release from their NLCs (Zheng et al., 2013). Remarkably, it could be observed that almost all the drug was released from the Colist-NLC under the assayed conditions. This sustained release, especially the one presented by the Colist-NLC, could reduce the number of doses, improving patient adherence to the treatment and, thus, life quality. The release profile of the dye was much slower than that observed for sodium colistimethate, very likely due to its lipophilicity (Yue et al., 2013). Indeed, this delayed release is very helpful for the *in vivo* imaging in order to ensure that the IR dye detected in mice is closely related to the dye incorporated into the NLCs.

Regarding the microbiological assays, other authors, such as Omri, described much higher MIC values for *P. aeruginosa* ATCC 27853, $4.0 \pm 1.0 \mu\text{g/ml}$, when incorporating Polymixin B in liposomes. Nevertheless, the MIC values were even higher when the free Polymixin B was assessed (Omri et al., 2002). Wang et al. (2012) reported also the utility of lipid nanoparticles for tilimicosin, a macrolide, encapsulation reporting a MIC of $4.0 \mu\text{g/ml}$ (.). It is should be underlined that the lipid nanoparticles described in this work presented MIC values around 1–2 $\mu\text{g/ml}$ and were active against the mucoid strains.

As far as cell experiments are related, it should be remarked that, in agreement with our finding, Nassimi et al. reported that blank SLN displayed very high IC50 values (analysed by MTT, (3-(4,5-dimethylthiazole-2-yl)-2,5-diphenyltetrazolium bromide, and NRU, Neutral Red Uptake), that is 2–3 mg/ml. Although the assays were conducted under the same cell line, the results could not be directly compared as they used other techniques for determination of cell viability (Nassimi et al., 2010). On an average, as reported by Doktorovova after the analysis of their published data concerning IC50, this value is usually within 0.1–1 mg/ml for lipid nanoparticles, being in our case slightly superior for Colist-NLC, 2.82 mg/ml and 1.08 mg/ml for A549 and H441, respectively (Doktorovova et al., 2014). In terms of cell viability, Ribeiro de Souza described that praziquantel-loaded SLN presented a time and dose-dependent cell viability in a hepatoma cell line, reaching up to a 70% decrease of cell viability for the free drug and 45% decrease for the loaded SLN (Souza et al., 2014). Overall, it could be concluded that sodium colistimethate encapsulation led to lower toxicity values. Sodium colistimethate is transformed to colistin that is the active molecule and it is known to present an increased toxicity. Lately, due to the Gram-negative resistance, the use of colistin has re-emerged despite its side effects and toxicity (Sukhadeve et al., 2012). Hence, based on these *in vitro* results, it could be postulated that enclosing sodium colistimethate into lipid nanoparticles decreases the toxicity of both the pro-drug, sodium colistimethate, and the drug, colistin, mainly because they are released in a controlled manner over time.

Finally, as the *in vivo* biodistribution has shown, NLCs displayed a suitable tissue disposition, spreading extensively throughout the lungs. Similarly, Taratula et al. (2013) reported that NLC presented

a uniform distribution through the lungs 24 h post-nebulization, whereas i.v. administration led to only 23% of NLCs retained in the lungs.

5. Conclusions

Taking into account the results described in this work, in terms of antimicrobial activity and toxicity, lipid nanoparticles seem to us an encouraging alternative to the currently available cystic fibrosis therapies. NLCs distributed homogeneously through the respiratory tract and remained in the target tissue for at least 48 h. Furthermore, it is remarkable that both Colist-SLNs and Colist-NLCs are effective against mucoid *P. aeruginosa*. Besides, the side effects of the active drug, colistin, could be ameliorated because of the sustained drug release. Moreover, based on the release of the antibiotic and the homogeneous distribution through the lungs, the results suggest that the number of doses could be diminished. Yet other studies should be conducted in order to assess the bioavailability of sodium colistimethate and to transform the elaborated lipid nanoparticles into an optimized inhalable CF therapy.

Acknowledgements

This work was carried out under the TERFIQEC Project, Comprehensive Research On Effective Therapies For The Treatment Of Cystic Fibrosis And Associated Diseases; IPT-2011-1402-900000 was funded by the Ministry of Economy and Competitiveness. Technical and human support provided by SGIker (UPV/EHU, MICINN, GV/EJ, ERDF and ESF) is gratefully acknowledged. M. Moreno-Sastre thanks the University of the Basque Country for the ZabaldUz fellowship grant. The authors gratefully acknowledge the support of University of the Basque Country UPV/EHU (UFI11/32), of University of Barcelona (UB) as to the CSIC and FISIB.

References

- Alvarez, C.A., Wiederhold, N.P., McConville, J.T., Peters, J.I., Najvar, L.K., Graybill, J.R., Coalson, J.J., Talbert, R.L., Burgess, D.S., Bocanegra, R., Johnston, K.P., Williams III, F., 2007. Aerosolized nanostructured itraconazole as prophylaxis against invasive pulmonary aspergillosis. *J. Infect.* 55, 68–74.
- Andrade, Rafael, D., Videira, M., Ferreira, D., Sosnik, A., Sarmento, B., 2013. Nanotechnology and pulmonary delivery to overcome resistance in infectious diseases. *Adv. Drug Deliv. Rev.* 65, 1816–1827.
- Beloqui, A., Solinís, M.A., Gascón, A.R., del Pozo-Rodríguez, A., des Rieux, A., Prétat, V., 2013. Mechanism of transport of saquinavir-loaded nanostructured lipid carriers across the intestinal barrier. *J. Control. Release* 166, 115–123.
- Cancho Grande, B., García Falcón, M., Pérez-Lamela, C., Rodríguez Comesaña, M., Simal Gándara, J., 2000. Quantitative analysis of colistin and tiamicin in liquid and solid medicated premixes by HPLC with diode-array detection. *Chromatographia* 53, S460–S463.
- Chono, S., Tanino, T., Seki, T., Morimoto, K., 2008. Efficient drug targeting to rat alveolar macrophages by pulmonary administration of ciprofloxacin incorporated into mannolyated liposomes for treatment of respiratory intracellular parasitic infections. *J. Control. Release* 127, 50–58.
- Committee for Medicinal Products for Human Use, CHMP, 2011. European Medicines Agency. Guideline on Bioanalytical Method Validation. Available at: http://www.ema.europa.eu/docs/en_GB/document_library/Scientific_guideline/2011/08/WC500109686.pdf, (accessed 04.11.14).
- Doktorovova, S., Souto, E.B., Silva, A.M., 2014. Nanotoxicology applied to solid lipid nanoparticles and nanostructured lipid carriers – a systematic review of *in vitro* data. *Eur. J. Pharm. Biopharm.* 87, 1–18.
- Fuste, E., Lopez-Jimenez, L., Segura, C., Gainza, E., Vinuesa, T., Viñas, M., 2013. Carbapenem-resistance mechanisms of multidrug-resistant *Pseudomonas aeruginosa*. *J. Med. Microbiol.* 62, 1317–1325.
- Chaffari, S., Varshosaz, J., Saadat, A., Atyabi, F., 2011. Stability and antimicrobial effect of amikacin loaded SLN. *Int. J. Nanomed.* 6, 35–43.
- Gibson, R.L., Burns, J.L., Ramsey, B.W., 2003. Pathophysiology and management of pulmonary infections in cystic fibrosis. *Am. J. Respir. Crit. Care Med.* 168, 918–951.
- Gilani, K., Moazeni, E., Ramezani, T., Amini, M., Fazeli, M.R., Jamalifar, H., 2011. Development of respirable nanomicelle carriers for delivery of amphotericin B by jet nebulization. *J. Pharm. Sci.* 100, 252–259.

- Gould, I., Bal, A., 2013. New antibiotic agents in the pipeline and how they can help overcome microbial resistance. *Virulence* 4, 185–191.
- Heijerman, H., Westerman, E., Conway, S., Touw, D., 2009. Inhaled medication and inhalation devices for lung disease in patients with cystic fibrosis: a European consensus. *J. Cyst. Fibros.* 8, 295–315.
- Koch, C., 2002. Early infection and progression of cystic fibrosis lung disease. *Pediatr. Pulmonol.* 34, 232–236.
- Martins, S., Tho, I., Reimold, I., Fricker, G., Souto, E., Ferreira, D., Brandl, M., 2012. Brain delivery of camptothecin by means of solid lipid nanoparticles: formulation design, *in vitro* and *in vivo* studies. *Int. J. Pharm.* 439, 49–62.
- Nassimi, M., Schleh, C., Lauenstein, H.D., Hussein, R., Hoymann, H.G., Koch, W., Pohlmann, G., Krug, N., Sewald, K., Rittinghausen, S., Braun, A., Müller-Goymann, C., 2010. A toxicological evaluation of inhaled solid lipid nanoparticles used as a potential drug delivery system for the lung. *Eur. J. Pharm. Biopharm.* 75, 107–116.
- Obeidat, W.M., Schwabe, K., Müller, R.H., Keck, C.M., 2010. Preservation of nanostructured lipid carriers (NLC). *Eur. J. Pharm. Biopharm.* 76, 56–67.
- Omri, A., Suintres, Z.E., Shek, P.N., 2002. Enhanced activity of liposomal polymyxin B against *Pseudomonas aeruginosa* in a rat model of lung infection. *Biochem. Pharmacol.* 64, 1407–1413.
- Patlolla, R.R., Chougule, M., Patel, A.R., Jackson, T., Tata, P.N.V., Singh, M., 2010. Formulation: characterization and pulmonary deposition of nebulized celecoxib encapsulated nanostructured lipid carriers. *J. Control. Release* 144, 233–241.
- Proesmans, M., Vermeulen, F., Boulanger, J., Verhaegen, J., De Boeck, K., 2013. Comparison of two treatment regimens for eradication of *Pseudomonas aeruginosa* infection in children with cystic fibrosis. *J. Cyst. Fibros.* 12, 29–34.
- Ratjen, F., Brockhaus, F., Angyalosi, G., 2009. Aminoglycoside therapy against *Pseudomonas aeruginosa* in cystic fibrosis: a review. *J. Cyst. Fibros.* 8, 361–369.
- Ruiz, L., Domínguez, M.A., Ruiz, N., Viñas, M., 2004. Relationship between clinical and environmental isolates of *Pseudomonas aeruginosa* in a hospital setting. *Arch. Med. Res.* 35, 251–257.
- Ruiz-Martínez, L., López-Jiménez, L., d'Ostun, V., Fusté, E., Vinuesa, T., Viñas, M., 2011a. A mechanism of carbapenem resistance due to a new insertion element (ISPa133) in *Pseudomonas aeruginosa*. *Int. Microbiol.* 14, 51–58.
- Ruiz-Martínez, L., López-Jiménez, L., Fuste, E., Vinuesa, T., Martínez, J.P., Viñas, M., 2011b. Class 1 integrons in environmental and clinical isolates of *Pseudomonas aeruginosa*. *Int. J. Antimicrob. Agents* 38, 398–402.
- Silva, A.C., Kumar, A., Wild, W., Ferreira, D., Santos, D., Forbes, B., 2012. Long-term stability: biocompatibility and oral delivery potential of risperidone-loaded solid lipid nanoparticles. *Int. J. Pharm.* 436, 798–805.
- Sims, E.J., McCormick, J., Mehta, G., Mehta, A., 2005. Neonatal screening for cystic fibrosis is beneficial even in the context of modern treatment. *J. Pediatr.* 147, S42–S46.
- Soares, S., Fonte, P., Costa, A., Andrade, J., Seabra, V., Ferreira, D., Reis, S., Sarmiento, B., 2013. Effect of freeze-drying cryoprotectants and storage conditions on the stability of secondary structure of insulin-AT solid lipid nanoparticles. *Int. J. Pharm.* 456, 370–381.
- Souza, A.L.R.D., Andreani, T., de Oliveira, R.N., Kiill, C.P., Santos, d.F.K., Allegretti, S.M., Chaud, M.V., Souto, E.B., Silva, A.M., Gremião, M.P.D., 2014. *In vitro* evaluation of permeation, toxicity and effect of praziquantel-loaded solid lipid nanoparticles against *Schistosoma mansoni* as a strategy to improve efficacy of the schistosomiasis treatment. *Int. J. Pharm.* 463, 31–37.
- Sukhadeve, K., Apte, M., Waghmare, P., 2012. Colistin for bad bugs. *Pediatr. Infect. Dis.* 4, 168–171.
- Taratula, O., Kuzmov, A., Shah, M., Garbuzenko, O.B., Minko, T., 2013. Nanostructured lipid carriers as multifunctional nanomedicine platform for pulmonary co-delivery of anticancer drugs and siRNA. *J. Control. Release* 171, 349–357.
- Ungaro, F., d'Angelo, I., Coletta, C., d'Emmanuele di Villa Bianca, R., Sorrentino, R., Peretto, B., Tufano, M.A., Miro, A., La Rotonda, M.L., Quaglia, F., 2012. Dry powders based on PLGA nanoparticles for pulmonary delivery of antibiotics: modulation of encapsulation efficiency release rate and lung deposition pattern by hydrophilic polymers. *J. Control. Release* 157, 149–159.
- Wang, X.F., Zhang, S.L., Zhu, L.Y., Xie, S.Y., Dong, Z., Wang, Y., Zhou, W.Z., 2012. Enhancement of antibacterial activity of tilmicosin against *Staphylococcus aureus* by solid lipid nanoparticles *in vitro* and *in vivo*. *Vet. J.* 191, 115–120.
- Weber, S., Zimmer, A., Pardeike, J., 2014. Solid lipid nanoparticles (SLN) and nanostructured lipid carriers (NLC) for pulmonary application: a review of the state of the art. *Eur. J. Pharm. Biopharm.* 86, 7–22.
- WHO, 2002. The Molecular Genetic Epidemiology of Cystic Fibrosis. Report of a Joint Meeting of WHO/ECFTN/ICF(M)/A/ECFS, 1–26.
- Wong, J.P., Yang, H., Blasetti, K.L., Schnell, G., Conley, J., Schofield, L.N., 2003. Liposome delivery of ciprofloxacin against intracellular *Francisella tularensis* infection. *J. Control. Release* 92, 265–273.
- Worlitzsch, D., Tarran, R., Ulrich, M., Schwab, U., Cekici, A., Meyer, K.C., Birrer, P., Bellon, G., Berger, J., Weiss, T., Botzenhart, K., Yankaskas, J.R., Randell, S., Boucher, R.C., Döring, G., 2002. Effects of reduced mucus oxygen concentration in airway *Pseudomonas* infections of cystic fibrosis patients. *J. Clin. Invest.* 109, 317–325. 10.1172/JCI13870.
- Yue, C., Liu, P., Zheng, M., Zhao, P., Wang, Y., Ma, Y., Cai, L., 2013. IR-780 dye loaded tumor targeting theranostic nanoparticles for NIR imaging and photothermal therapy. *Biomaterials* 34, 6853–6861.
- Zheng, M., Falkeborg, M., Zheng, Y., Yang, T., Xu, X., 2013. Formulation and characterization of nanostructured lipid carriers containing a mixed lipids core. *Colloids Surf. Physicochem. Eng. Aspects* 430, 76–84.

PAPER 2



Pulmonary delivery of tobramycin-loaded nanostructured lipid carriers for *Pseudomonas aeruginosa* infections associated with cystic fibrosis



María Moreno-Sastre^{a,b}, Marta Pastor^{a,b}, Amaia Esquisabel^{a,b}, Eulàlia Sans^c, Miguel Viñas^c, Aarne Fleischer^{d,e}, Esther Palomino^{d,e}, Daniel Bachiller^{d,e}, José Luis Pedraz^{a,b,*}

^a NanoBioCel Group, Laboratory of Pharmaceutics, University of the Basque Country (UPV/EHU), School of Pharmacy, Paseo de la Universidad 7, Vitoria-Gasteiz 01006, Spain

^b Biomedical Research Networking Center in Bioengineering, Biomaterials and Nanomedicine (CIBER-BBN), Vitoria-Gasteiz, Spain

^c Department of Pathology and Experimental Therapeutics, Medical School, University of Barcelona – IDIBELL, Barcelona, Spain

^d Fundación Investigaciones Sanitarias Islas Baleares (FISIB), Development and Regeneration Program, Ctra. Sóller km 12, Bunyola (Balearic Islands) 07110, Spain

^e Consejo Superior de Investigaciones Científicas (CSIC), Ctra. Sóller km 12, Bunyola (Balearic Islands) 7110, Spain

ARTICLE INFO

Article history:

Received 6 October 2015

Received in revised form 8 December 2015

Accepted 10 December 2015

Available online 15 December 2015

Keywords:

Tobramycin

Lipid nanoparticles

Nanocarriers

Cystic fibrosis

Pulmonary administration

Pseudomonas aeruginosa

ABSTRACT

Among the pathogens that affect cystic fibrosis (CF) patients, *Pseudomonas aeruginosa* is the most prevalent. As a way to fight against this infection, nanotechnology has emerged over the last decades as a promising alternative to overcome resistance to antibiotics in infectious diseases. The goal of this work was to elaborate and characterize lipid nanoparticles for pulmonary delivery of tobramycin.

Tobramycin-loaded nanostructured lipid carriers (Tb-NLCs) were prepared by hot melt homogenization technique. In addition, nanoparticles labeled with infrared dye (IR-NLCs) were used to investigate their *in vivo* performance after pulmonary administration.

Tb-NLCs displayed a mean diameter size around 250 nm, high drug encapsulation (93%) and sustained release profile. Tb-NLCs showed to be active against clinically isolated *P. aeruginosa*. Moreover, Tb-NLCs did not decrease cell viability and were able to overcome an artificial mucus barrier in the presence of mucolytic agents. During the *in vivo* assay, IR-NLCs were administered to several mice by the intratracheal route using a Penn Century[®] device. Next, the biodistribution of the nanoparticles was analyzed at different time points showing a wide nanosystem distribution in the lungs.

Altogether, tobramycin-loaded NLCs seem to us an encouraging alternative to the currently available CF therapies.

© 2015 Elsevier B.V. All rights reserved.

1. Introduction

Cystic fibrosis (CF) is a genetic disorder that affects nearly 70,000 patients worldwide. It is caused by mutations in the cystic fibrosis transmembrane conductance regulator (CFTR) gene that encodes a protein that form an ion channel in epithelial cell membranes whose dysfunction leads to the secretion and accumulation of a viscous mucus in the airways that become thick and sticky causing bronchial obstruction (Moreau-Marquis et al., 2008). The tenacious mucus enables chronic bacterial infection by

an opportunist gram-negative bacterium, which is the most frequent pathogen identified in CF patients (Ratjen et al., 2009). Mucoid strains of *P. aeruginosa* usually develop community of microbes in an exopolysaccharide matrix called biofilm. Although CF patients routinely take antibiotics, the mucus plugs and bacterial biofilm contribute to the poor lung penetration of antimicrobial agents, leading to clinical exacerbations (Okusanya et al., 2009). Therefore the eradication of these organisms is a difficult but essential endpoint to achieve. Furthermore, over the last decades, antibiotic-resistant strains have increased due to the misuse and overuse of anti-infectious drugs (Andrade et al., 2013). As a consequence, there is a high morbidity and mortality associated to the respiratory manifestations of the CF disease hampered by the lack of effective therapies (Savla and Minko, 2013).

* Corresponding author at: NanoBioCel Group, Laboratory of Pharmaceutics, School of Pharmacy, University of the Basque Country (UPV/EHU), Paseo de la Universidad 7, 01006 Vitoria-Gasteiz, Spain. Fax: +34 945 013 040.

E-mail address: joseluis.pedraz@ehu.es (J.L. Pedraz).

In this regard, nanotechnology has emerged as a new alternative to drug encapsulation to overcome the limitations of conventional drugs. Nanoformulations such as nanostructured lipid carriers (NLCs) are made up of a solid lipid core stabilized by surfactants and have the possibility to incorporate both lipophilic and hydrophilic drugs. NLCs provide several advantages over other drug delivery systems (DDSs) such as good biocompatibility, biodegradable properties, higher drug loading, controlled drug release, long-term stability, as well as scaling-up feasibility (Weber et al., 2014).

Nanoparticles (NPs) are currently being extensively investigated for antibiotic inhalation therapy. Pulmonary drug delivery has gained much attention as a non-invasive route for the delivery of high amounts of therapeutic agents directly to the desired site of action minimizing systemic exposure and adverse effects (Patil and Sarasija, 2012). This route is a preferred route for agents such as aminoglycosides in CF patients. The inhalation of tobramycin is part of current CF therapies as it presents strong bactericidal activity against planktonic cells (Thellin et al., 2015). For instance, TOBI[®] or TIS (tobramycin inhalation solution) and TIP (tobramycin inhalation powder) have recently become commercially available for the treatment of chronic lung infections caused by *P. aeruginosa* (Waters and Smyth, 2015). However, the efficacy of free drug administration in CF patients is not high enough to achieve therapeutics levels at the site of infection due to its rapid clearance and poor mucus penetration (Tseng et al., 2013). These drawbacks could be overcome by nanotechnology. Encapsulation of antibiotics into nanocarriers has attracted considerable interest to improve the therapeutic index of antimicrobial drugs and for their benefits in the context of combating bacteria (Hajipour et al., 2012). Moreover, many cystic fibrosis patients present an accumulation of dehydrated and thicker mucus within the airways causing respiratory problems, therefore, it is important for therapeutic agents to penetrate into this mucus in order to distribute the drug and maximize its antibacterial effect (Yang et al., 2011). Nano-antibiotic represents a promising strategy to overcome the mucus barrier and to prolong the drug retention in the lung as other authors have also previously reported (Poyner et al., 1995).

Taking the above into account, the goal of this work was to elaborate and characterize tobramycin-loaded lipid nanocarriers (Tb-NLCs) for pulmonary delivery for the treatment of respiratory infectious diseases; in particular CF. Two different solid lipids were selected as core agents for the NLCs (Precirol[®] ATO 5 and Compritol[®] ATO 888). The antimicrobial activity against *P. aeruginosa* was investigated as well as the capability of the nanoparticles to cross the mucus barrier *per se* or after adding mucolytic agents. Finally, the NPs biodistribution was analyzed after intratracheal administration in mice.

2. Material and methods

2.1. Materials

Precirol[®] ATO 5 (glycerol distearate, type I) and Compritol[®] 888 ATO (glyceryl dibehenate) were kindly provided by Gattefossé (Madrid, Spain). Kolliphor[®] P188 (Poloxamer 188) was a gift from BASF (Ludwigshafen, Germany). Polysorbate, Tween[®] 80 was purchased from Panreac Química (Castellar del Vallès, Barcelona, Spain). Miglyol[®] 812 was provided by Sasol (Hamburg, Germany). Tobramycin, fluorecamine, IR-783 dye, gelatine from bovin skin type B, diethylenetriaminepentaacetic acid (DPTA), type II mucine from porcine stomach, egg yolk enrichment, amino acids and were purchased from Sigma–Aldrich Chemicals (St. Louis, MO, USA). Coomassie Brilliant Blue was provided from Bio-Rad Laboratories (Hercules, CA, USA). PBS, DPBS, DMEM, MEM-NEAA, FBS, DMSO and Trypsin-EDTA Gibco[®] were supplied by Life Technologies

(Thermo Fisher Scientific, Waltham, MA). Blood agar was provided by Oxoid (Microbiological Products Thermo Fisher, Hampshire, UK). Mannitol (Pearlitol PF) and L-lysine-S-carboxymethyl-L-cysteine salt were provided from Roquette and Pharmazell (India), respectively. Hydroxyethylcellulose was purchased from Vencaser S.A (Bilbao, Spain). Other chemicals were all analytical grade.

2.2. Methods

2.2.1. Preparation of nanostructure lipid carriers (NLCs)

The nanostructured lipid carriers, NLCs, were elaborated by a hot melt homogenization technique (Pastor et al., 2014). In brief, Precirol[®] ATO 5 (NLC P) or a 50:50 Compritol[®] 888 ATO and Precirol[®] ATO 5 mixture (NLC PC) together with Miglyol[®] 812 were selected as lipid core. These lipids were mixed with tobramycin (Tb) and heated above the melting temperature of the solid lipid until its fusion. As tobramycin is a hydrophilic drug, it was dispersed in the molten lipids. The aqueous phase was prepared by dispersing 1.3% (w/v) of Tween[®] 80 and 0.6% (w/v) of Poloxamer 188 in Milli-Q water and heating to the same temperature as the lipid phase. Straightaway, the hot aqueous phase was added to the oily phase, and then sonicated for 30 s at 20 W (Branson Sonifier 250, Danbury, CT, USA). The formed emulsion was stored for 12 h at 4 °C to allow the re-crystallization of the lipids and the nanoparticle formation. Then, Tb-NLCs were washed by centrifugation at 2500 rpm in Amicon[®] centrifugal filtration units (100,000 Da MWCO, Merck Millipore, Darmstadt, Germany) for 15 min three times. All the nanoparticles prepared were freeze-dried for 39 h (Telstar Lyobeta freeze-dryer, Terrasa, Spain) using trehalose at 15% (w/w) as cryoprotectant. Different batches of blank nanoparticles without the drug (Blank-NLCs) were also prepared for comparison.

Two types of dyes were used to label NLCs. Firstly, Coomassie blue (CB) labeled NLCs (CB-NLCs) were prepared for the artificial mucus (AM) penetration assay. NLCs were prepared just as mentioned above but instead of the drug, 1.3% (w/w) of CB was added. Secondly, to prepare labeled NLCs, an infrared dye (IR-783) was embedded into the nanoparticles by adding 50 mg of IR instead of the antibiotic. This dye is an excellent stain for the observation in the near infrared region (NIR). In both cases, the nanoparticles were washed by centrifugal filtration units and trehalose 15% (w/w) was added prior to the lyophilization step.

2.2.2. Characterization of lipid nanoparticles

2.2.2.1. Size and Zeta potential. The particle size and polydispersity index (PDI) were measured in a Zetasizer Nano ZS (Malvern Instruments, Worcestershire, UK) based on dynamic light scattering. Zeta potential was also determined by Doppler velocimetry by means of the Zetasizer Nano ZS. Prior to the measurements NPs were dispersed in Milli-Q water at optimal intensity. All the measurements of each sample were performed in triplicate.

2.2.2.2. Microscopy analysis. NPs morphology was examined by Transmission Electron Microscope (TEM, Philips CM120) after negative staining with 2% uranyl acetate.

2.2.2.3. Encapsulation efficiency. The encapsulation efficiency (EE) of tobramycin into NLCs was determined by indirect and direct methods. By the indirect method, the supernatants obtained during the centrifugation in Amicon[®] devices were analyzed for Tb content by UV-vis spectrophotometer after derivatization with fluorecamine (Sampath and Robinson, 1990; Ungaro et al., 2012). Briefly, NLCs samples were diluted 1:2 (v/v) in fluorecamine solution at 0.5% (w/v) in ethanol and incubated at room

temperature protected from light for one hour before analysis. The absorbance of these samples was measured at 390 nm using a Shimadzu UV-1800 spectrophotometer (Shimadzu Co., Kyoto, Japan) fitted out with a 0.1-cm quartz cell. The absorbance of the supernatants collected from blank particles displayed no absorption at 390 nm. The tobramycin content in the supernatants samples was calculated using a calibration curve that present linearity from 5 to 100 µg/mL ($r^2 \geq 0.999$). Encapsulation efficiency was calculated following this equation: EE (%) = $100 \times (\text{initial drug or dye amount} - \text{non-encapsulated drug or dye}) / \text{initial drug or dye amount}$.

In order to evaluate the total amount of tobramycin into NLCs by a direct method, a known mass of NLCs (10 mg) was dissolved in a mixture of CHCl_3 : MeOH (1:1, v/v) and analyzed by UV–vis spectrophotometric method after derivatization with fluorescamine as mention before. NLCs particles without drug were used as background signal.

On the other hand, the encapsulation efficiency of CB-NLCs and IR-NLCs was measured by determining the absorbance of the dye from the supernatants and comparing it to a calibration curve 10–100 µg/mL using a plate reader (Infinite® 200 PRO, Tecan, Männedorf, Switzerland) at 590 and 800 nm, respectively.

2.2.2.4. In vitro drug release studies. In-vitro drug release studies were conducted using Quix-Sep Micro Dialyzers (Membrane Filtration Products Inc, Seguin, Texas, USA) at 37 °C under magnetic stirring in phosphate buffer saline (PBS). A dialysis regenerated cellulose tubular membrane having a molecular weight cut-off (MWCO) between 12,000 and 14,000 Da was used. First, cellulose membranes were soaked in the dissolution medium (PBS) for 20 min prior to its use to ensure thorough wetting of the membrane before placing it in a Quix-Sep cell. To carry out this study, the Tb-NLCs suspension (50 mg/mL) was placed in the cell system which was immersed in 50 mL of PBS solution at pH 7.4 as the dissolution medium. At fixed time intervals up to 96 h, samples (500 µL) were withdrawn from the incubation and evaluated by UV–vis spectrophotometer. The release study was carried out under sink conditions and the removed PBS was replaced with equal volumes of fresh medium. Results were expressed as percentage of tobramycin released compared to the total drug encapsulated in the sample. The experiments were run in triplicate for each point of release kinetics.

2.2.3. Determination of minimum inhibitory concentration (MIC)

P. aeruginosa strains isolated from adult CF sputum patients were selected for the MIC determination of the nanoparticles. The patient group consisted of 34 individuals, and each of them provided one sputum sample resulting in 17 of them mucoid and 17 non-mucoid strains. *P. aeruginosa* strains were cultivated routinely on blood agar (Sigma–Aldrich, Gillingham, UK) for 24 h at 37 °C. Furthermore, *P. aeruginosa* ATCC 27853 strain was also assessed as control.

Nanoparticles and free antibiotic were tested against *P. aeruginosa* strains by broth microdilution method in 96-well

microplates. The formulations were serially diluted 2-fold in Mueller–Hinton II Broth Cation-Adjusted (MHBCA) from a starting concentration of 128–0.125 µg/mL in a final volume of 100 µL. Then, 5 µL of *P. aeruginosa* inoculum were added to each well to produce a bacterial cell suspension of 10^4 cfu/mL (colony-forming units) and samples were incubated for 24 h at 37 °C. Negative and positive growth controls were included. The minimum inhibitory concentration represents the lowest antibiotic concentration that inhibits a visible planktonic bacterial growth after an overnight incubation at 37 °C. The assay was run in triplicate.

2.2.4. Cell experiments

2.2.4.1. Cell culture. Human lung adenocarcinoma epithelial cell line (A549 cells) and human lung papillary adenocarcinoma epithelial cell line (H441 cells) were purchased from the American Type Culture Collection (ATCC; Manassas, USA). Cells were grown and maintained in Dulbecco's Modified Eagle Growth Medium (DMEM) pH 7.4, supplemented with 10% (v/v) inactivated fetal bovine serum (FBS), 1% glutamine and 1% antibiotic/antimycotic and 1% Minimum Essential Medium non-essential amino acids 100× (MEM-NEAA) and incubated at 90% humidity, 5% (v/v) CO_2 atmosphere at 37 °C. The cells were allowed to grow until confluence, then they were trypsinized (Trypsin-EDTA) and seeded in plates for each experiments.

2.2.4.2. In vitro cytotoxicity studies. The cytotoxicity of Tb-NLCs was evaluated in the A549 and H441 cell lines as reported earlier. The cells were plated in 96-well microtiter plates at a density of 10,000 cells per well in a final volume of 100 µL of DMEM medium (supplemented with 10% serum). The cells were treated with Blank-NLCs or NLCs formulations (Tb-NLC P or Tb-NLC PC) diluted in DMEM medium at concentrations of 0.25, 0.5 and 1 mg/mL for 24 h at 37 ± 2 °C, 90% humidity and 5% CO_2 . Controls were set with dimethyl sulfoxide (DMSO) as negative or death control, and medium without formulation as positive control. Free antibiotic was added for comparison. After overnight incubation, the determination of cell viability was carried out using the Cell Counting Kit 8 (CCK-8, Sigma–Aldrich, St. Louis, MO; USA). Wells were washed with sterile PBS and then 10% of CCK-8 in medium was added to each well and incubated in a wet chamber for 4 h at 37 ± 2 °C and 5% CO_2 . The resulting colored solution was quantified using a microplate reader (Infinite® 200 PRO, Tecan, Männedorf, Switzerland). The spectrophotometric absorbance was measured at 450/650 nm wavelength. Results were calculated in relation to the untreated wells (100% viability) and are expressed as percent of cell vitality \pm SD of values collected from three separate experiments performed in triplicate for each sample.

2.2.4.3. Cell viability. To confirm the CCK-8 data, a second independent cell viability test was assessed using a Live/Dead® kit that consisted of two stains, calcein acetoxy-methyl and ethidium homodimer-1 (calcein AM/EthD-1) (Invitrogen, Karlsruhe, Germany). Live cells were distinguished by enzymatic conversion of calcein AM to intensely green fluorescent and EthD-

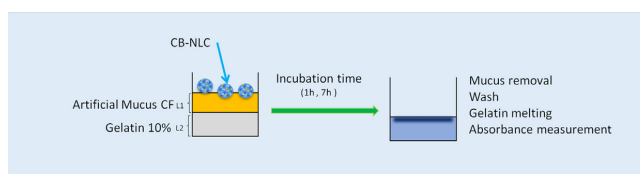


Fig. 1. Scheme of the mucus penetration study. Layer 1 (L1) and 2 (L2).

1 produced intracellular red fluorescence in nucleus of dead cells allowing to differentiate the population of live cells from the dead-cells (Nassimi et al., 2010).

In brief, after 24 h the adherent cells (A549 and H441) cultured on 96 well-plate treated with both nanoparticles and free antibiotic were washed with Dulbecco's phosphate buffered saline (DPBS) to limit the background fluorescence and then, 100 μ L of a combined reagent solution of calcein (0.5 μ M) and ethidium homodimer (0.5 μ M) in DPBS was added to each well. After 45 min of incubation at room temperature and protected from light, the fluorescence emission from both fluorophores was observed simultaneously using a conventional fluorescence microscope (Nikon Eclipse TE2000-S, TSM) equipped with an excitation filter. Both positive (living cells without formulation) and negative (dead cells treated with DMSO) controls were also assessed by dying with live/dead stained and observed.

2.2.5. Penetration of NPs through artificial mucus

The purpose of this study was to test whether mannitol or S-carboxymethylcysteine (CMC) as mucolytic agents, improved nanoparticle diffusion through artificial mucus (AM) and could enhance the antibacterial activity. The penetration of CB-NLCs (Coomassie Blue-NLCs) through a mucus layer was carried out using an artificial mucus model as previously reported Yang et al. (2011) (Fig. 1). Briefly, 50 mL of artificial mucus was elaborated by adding 500 mg of DNA in 32.5 mL DNAase-free water complemented with 250 μ L of sterile egg yolk emulsion and an autoclaved solution of 250 mg of mucin, 0.295 mg diethylenetriaminepentaacetic (DTPA), 250 mg NaCl, 110 mg KCl and 12.5 mg amino acids dissolved in 17.5 mL of water. The dispersion was stirred until a homogenous mixture was obtained and the pH of the AM was adjusted to 7.0 using NaOH solution. On the other hand, a 10% (w/v) gelatin solution was prepared in hot water; one milliliter of this solution was placed in each well of a 24-well plate, solidified at room temperature and stored at 4 °C until use (layer 2). 0.5 mL of artificial mucus was placed on the top of the hardened gelatin gel (layer 1). Then, 500 μ L of an aqueous dispersion of CB-NLC (containing 75 μ g of CB) at different proportions of mucolytics (75:25, 50:50 and 25:75, NLC:mucolytic, w/w) were placed on the artificial mucus layer and incubated in a closed chamber maintaining 100% relative humidity, emulating the humid environment of airways (Marini and Slutsky, 1998) until pre-determinate sampling points. The upper layer (layer 1), that is, the artificial mucus layer plus the nanoparticles that have not crossed the mucus barrier, was removed after 1 and 7 h, and gelatin plates were washed three times with water and subsequently melted at 100 °C for homogenous mixing of gelatin and CB. The amount of CB in gelatin was evaluated at 590 nm using a plate reader. The absorbance values were compared to a standard CB curve from 1 to 100 μ g/mL. Results are reported as percentage of the dye penetrated through artificial mucus [(amount of CB in gelatine plates/total amount of CB in NPs) \times 100] \pm SD.

2.2.6. In vitro permeation study

2.2.6.1. Rheological properties of artificial mucus. As AM was too fluid to carry on permeation studies, another mucus model named AM1 was prepared by adding 1% (w/v) of hydroxyethylcellulose (HEC) as an inert thickening agent to the preceding formula. Viscosity of AM1 was conducted using a rotational viscometer (AR1000, TA instruments, New Castle, DE, USA) based on the measurements of the torque of a rotating spindle in a sample at a specified velocity (from 1 to 1000 rpm). The probe applied was a cone plate with a 2° angle. Data were reported as Pascals per second (Pas) related to the rotor velocity and all the viscosity

values were always between 15% and 100% of the torque range, as requested.

2.2.6.2. In vitro permeation experiment. A permeation assay was carried out to evaluate the permeation properties of Tb-NLCs formulations through AM1 by using Franz cells (Hanson Research Corporation, CA, USA), as previous reported by Donnelly et al. (2007). The AM1 was kept for 12 h at room temperature before use. The receptor and donor chamber were divided by means of a cellulose membrane (pore size: 0.45 μ m) that was applied between the two compartments (permeation area 0.785 cm²). The receptor compartment was filled with 5 mL of PBS. Then, a thin layer (3 mm) of artificial mucus (AM1) was interposed between the membrane and the drug deposition area forming a film. A suspension of Tb-NLCs diluted in water and mixtures of NLC: mucolytics agents at 75:25 were uniformly added on the top. In addition, free tobramycin in presence of mucus or not was assayed as control. The cell system was stored under continuous stirring at 37 °C and samples were removed (500 μ L) at defined times, 1 and 7 h, replacing the same volume with PBS. Samples were analyzed for tobramycin content by UV-spectrophotometric method as mention in Section 2.2.2.3 and results are reported by Tb permeated versus time.

On the other hand, the amount of the drug permeated per area (Q) for each time was calculated using the following equation:

$$Q \left(\frac{\text{mg}}{\text{cm}^2} \right) = \frac{V_R \times C_n + \sum_{i=0}^{n-1} V_p \times C_i}{A}$$

where V_R is the receiver volume; C_n is the drug concentration in the receiver at the time n ; V_p is the volume of the removed sample; C_i is the drug concentration in the receiver at the time $n - 1$ and A is the permeation area (cm²). Permeation data were reported as the quantity of drug in the receptor chamber per permeation area (mg/cm²) related to time (Russo et al., 2013).

2.2.7. In vivo biodistribution study

Female BALB/c OlaHsd mice (12 weeks old; Harlan Laboratories, Barcelona, Spain) were used for *in vivo* pulmonary administration of IR-labeled lipid nanoparticles. The animals were maintained under controlled environmental conditions of temperature (20–24 °C) humidity (40–65%) and lighting (12-h light-darkness cycle), with free access to standard food (A04 diet, Panlab, Barcelona, Spain) and tap water in makrolon III cages (Tecniplast, Rome, Italy). The procedures were approved by the Bioethics Committee of the Balearic Islands University and carried out in accordance with the Directive 2010/63/EU of the European Parliament and of the Council of 22 September 2010 on the protection of animals used for scientific purposes.

Once mice were anesthetized intra-peritoneally by ketamine/xylazine, 1 mg of IR-NLCs (both types, IR-NLC P and IR-NLC PC) resuspended in PBS was administered intratracheally to each mouse by a MicroSprayerTM aerosolizer (Penn Century[®] Liquid, Philadelphia, PA, USA). Free IR was used as a control. The mice were placed in an intubation platform for the right administration of drugs and the trachea and epiglottis of the animals were visualized by using a small animal laryngoscope. The formulations were spray-instilled into the lungs by pushing the syringe plunger of the Penn Century[®] device. MicroSprayerTM aerosolizer can deliver liquid in the form of aerolized droplets (Bivas-Benita et al., 2005). At given time points after intratracheal instillation (5 min, 2, 24 and 48 h), mice were sacrificed by ketamine/xylazine anesthesia overdose and cervical dislocation. After that, respiratory tissue (trachea, and lung) and other tissues such as heart, liver, spleen and kidneys were removed and

analyzed by LI-COR Pearl[®] impulse small animal imaging system (LI-COR Corporate, Bad Homburg, Germany) at 800 nm channel.

2.2.8. Statistical analysis

The results are expressed as the mean \pm S.D. (standard deviation) for each experimental group. To evaluate the data from the different *in vitro* penetration and permeability experiments, the normal distribution of samples was assessed with the *t*-test and one way ANOVA, respectively. All statistical analyses were calculated using the IBM SPSS[®] 20.0 Statistics software (Chicago, IL, USA). $P < 0.05$ was considered as significant.

3. Results

3.1. Nanoparticle characterization

The particle characterization of Blank-NLCs, Tb-NLCs, CB-NLCs and IR-NLCs is summarized in Fig. 2A. All formulations displayed sizes between 250 and 300 nm after the freeze-drying step using trehalose as cryoprotectant, with polydispersity indexes below 0.4, demonstrating a narrow size distribution. In addition, all the NPs presented a negative charge of around -23 mV. Likewise, CB-labeled NLCs displayed a similar size and Zeta potential, ≈ 293 nm and -26 mV, respectively and IR-NLCs nearly 289 nm and -26 mV. The entrapment efficiency of tobramycin was around 94% for both Tb-NLCs and 99% for stained-NLCs. Moreover, all the EE values analyzed by direct method were consistent with the indirect values. The encapsulation of the drug did not affect the size of NPs, which remained substantially unchanged compared to unloaded NP formulations. It could be observed that the Zeta potential of NLCs decreased in presence of tobramycin but without significant changes.

The pH of the nanosuspension was also measured presenting an appropriate pH value, 8, within the limits that European Pharmacopeia states for liquid preparations for pulmonary administration (European Council, 2014).

TEM images (Fig. 2B) revealed that nanoparticles had a regular homogeneous spherical shape without significant differences between the batches prepared.

Results from the *in vitro* release studies performed at physiological pH and temperature (pH 7.4 and 37 °C, respectively) are reported in Fig. 2C as percentage of tobramycin release over the time. An initial rapid release phase was observed for Tb-NLC P and Tb-NLC PC during the first 24 h ($\approx 80\%$ of drug release). Following the initial burst, a sustained release of the antibiotic is detected in both cases and by the end of the study (92 h) almost 100% of tobramycin was released from both NPs.

3.2. Microbiological experiments

To examine the antimicrobial effect of the nano-formulated tobramycin, MIC values were calculated against clinical isolated *P. aeruginosa*. Both Tb-NLCs showed to be active against bacterial growth, displaying a MIC value of 0.5 $\mu\text{g/mL}$ in most of the planktonic bacteria tested. In the same experimental conditions, free tobramycin displayed the same or higher MIC value indicating that the encapsulation of the drug did not affect the antimicrobial activity (Table 1). According to the controls, Blank-NLCs had no discernible inhibitory activity on the visible growth of bacteria.

3.3. Cell assays

The cytotoxicity of the optimized formulations was investigated on A549 and H441 as models of pulmonary epithelium cells. The exposition of NLCs at three different concentrations, 0.25, 0.5 and 1 mg/mL, for 24 h was studied. The results of CCK-8 are described in Fig. 3 as the percentage of viability compared to control cells (100% of viability), obtained at the same time and in the same experimental conditions. It was observed that none of these formulations presented toxic effects on the cells; at least at the concentrations studied considering that the negative control (DMSO) viability was less than 8%. On the other hand, NLCs

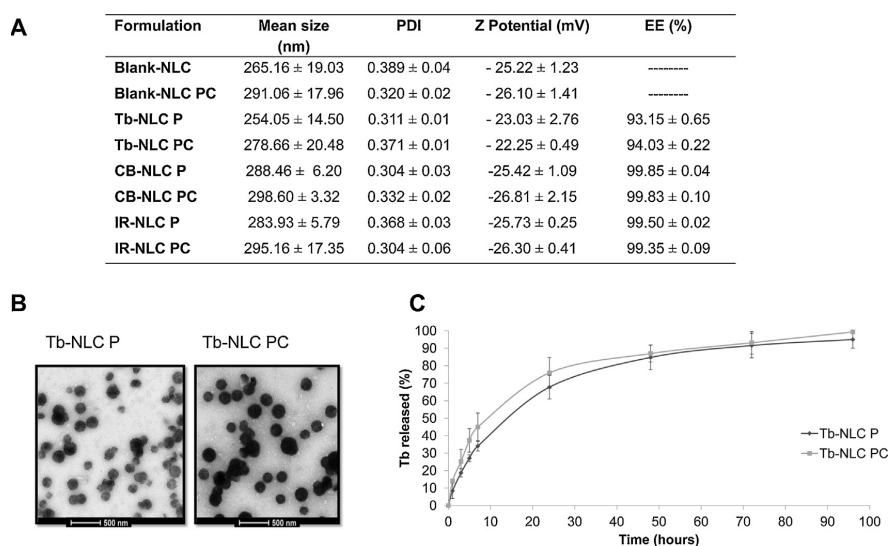


Fig. 2. Characterization of NLCs: (A) summary table displaying the main properties of the NLCs after freeze-drying, particle size, zeta potential, polydispersity index (PDI) and encapsulation efficiency (EE). (B) Transmission electron microscopy images of Tb-NLCs. (C) *In vitro* release profiles of tobramycin from NLCs (Tb-NLC P and Tb-NLC PC). Data represent mean \pm SD values calculated on 3 different batches.

Table 1

Bioactivity of Tb-NLCs and free drug in terms of MIC determination in 34 strains of clinically isolated *P. aeruginosa* samples. MIC, minimum inhibitory concentration, PA, *Pseudomonas aeruginosa*, M, mucoid clinical strain and NM, non-mucoid clinical strain. P, precirol and PC, precirol + compritol.

MIC ($\mu\text{g/mL}$)	PA ATCC 27853	PA 852 (NM)	PA 056 (NM)	PA 760 (NM)	PA458 (M)	PA 428 (M)	PA 086 (M)
Free tobramycin	0.5	0.5	1	1	0.5	4	2
Tb-NLC P	0.5	0.5	0.5	0.5	0.5	2	1
Tb-NLC PC	0.5	0.5	0.5	0.5	0.5	4	1

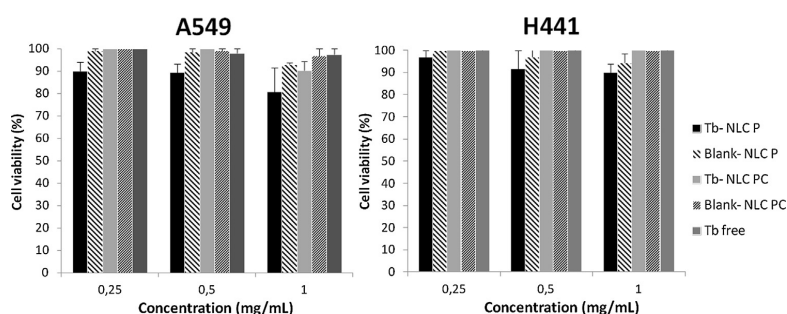


Fig. 3. Effect of Tb-NLCs, Blank-NLCs and free drug at different concentrations (0.25, 0.5 and 1 mg/mL) on the viability of A549 and H441 cell lines at 24 h.

presented higher absorbance values in both cell lines when Compritol[®] ATO 188 was also included in the lipid core (Tb-NLC PC). Higher Tb-NLC P concentrations showed lower viability, but always above 80%, and this phenomenon was more remarkable when tested in the A549 cell line. Besides, under the H441 cell line, Tb-NLC PC, unloaded lipid nanocarriers, and free tobramycin displayed the same absorbance values over all concentrations representing a desired biocompatibility (100%). Blank-NLC formulations displayed no effect on cell viability after 24 h of treatment, in all cases the viability value range over 80%. Hence, all nanoparticles elaborated were safe in terms of cell viability.

Regarding the cell viability assay, the use of calcein-AM and ethidium homodimer reagents allowed the simultaneous determination of live and dead cells. After the treatment, the cells were examined under a fluorescence microscope and the results obtained in our previous study were confirmed (Fig. 4), i.e.,

tobramycin-loaded NLCs presented no toxicity even at higher doses as predominate the green color. As expected, the negative control solutions (DMSO) were highly toxic to the cells, as noted by the red fluorescent staining.

3.4. Artificial mucus penetration assay

Two mucolytic agents, mannitol and carboxymethylcysteine (CMC), presenting the property of decreasing the mucus viscosity were used to compare the effect on drug diffusion through an artificial mucus (AM). Fig. 5 shows the amount of CB (%) captured in the gelatin gel that was proportional to particle penetration. According to the results, CB-NLC P particles with CMC penetrated the AM faster at the ratio 50:50 (NLC:mucolytic agent) than nanoparticles with mannitol (60% at 7 h versus 50% at the same time). Similarly, NLC P:CMC at 25:75, the penetration values were

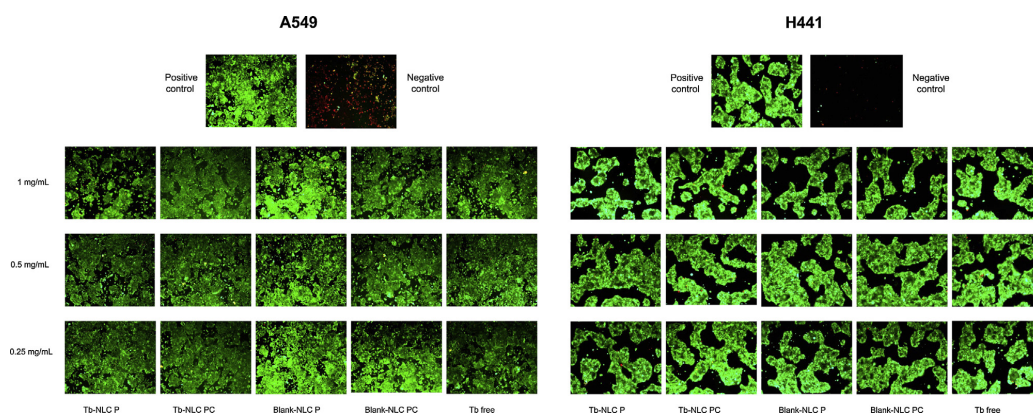


Fig. 4. A549 and H441 cells (under 20 \times magnification) examined by fluorescent microscopy after 24 h of incubation with Tb-NLCs, Blank-NLC and free drug at different concentrations (0.25, 0.5 and 1 mg/mL). Red color shows cell nucleus of dead cells and green color the cytoplasm of viable cells.

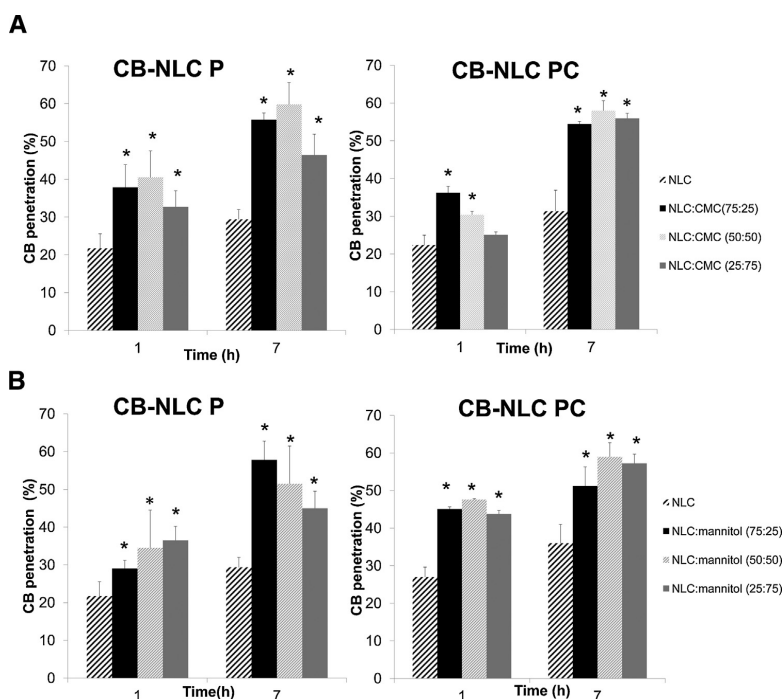


Fig. 5. Ability of Coomassie Blue-loaded nanoparticles (CB-NLCs) to penetrate through artificial mucus (AM). (A) CB-NLCs alone and mixture of CB-NLCs plus CMC (carboxymethylcysteine) at 75:25, 50:50 and 25:75. (B) CB-NLCs alone and mixture of CB-NLCs plus mannitol at 75:25, 50:50 and 25:75. Left column, represents CB-loaded NLC Precirol[®] ATO 5 and right column, CB-NLC with Precirol[®] ATO 5 and Compritol[®] ATO 188.

almost the same, around 57%. On the other hand, CB recovered from NLC PC was around 55–60% at 7 h with both excipients independent of the proportions. In all cases, the amount of CB was higher in presence of mucolytic agents. According to these results, no significant differences were found when using various NLC: mucolytic agent ratios, therefore, for further studies, the proportion NLC: mucolytic 75:25 was selected as it contained a higher proportion of nanoparticles.

3.5. Permeation study

In order to estimate the permeability of nanoparticles through artificial mucus, AM1 was used to better simulate the pulmonary environment in CF patients. First, its rheological behavior was analyzed and then the Tb-NLCs permeability was studied.

AM1 presented a pseudo-plastic behavior (Fig. 6A), the shear stress increases while viscosity decreases. Moreover, this artificial mucus was able to be retained on the membrane surface throughout the study period. In the second part of the study, Tb-NLCs with different mucolytics agents were added on the top of the mucus layer and results of the permeation through the mucus are reported in Fig. 6B. It was observed that the addition of CMC enhance the permeability of the drug significantly reaching 73% (7 h) for Tb-NLC PC, whereas using mannitol only 42% crossed the AM1 at the same time. In both types of Tb-NLCs, the addition of a mucolytic agent led an increase in permeation. According to the free antibiotic, AM1 reduced significantly the permeability of tobramycin from around 85 to 30%. As Fig. 6C shows, tobramycin, a very soluble and polar drug, showed a high dissolution rate from the beginning of the experiment reaching the 100% in less than 5 h

and achieving 1 mg/cm² permeation rate, however the presence of a mucus layer reduced it to less than 0.4 mg/cm². Tb-NLCs with mannitol and CMC (75:25) demonstrated an improved permeation rate than the free drug, due to the mucolytic effect of the excipients. In this case, CMC-containing formulations showed higher permeability than mannitol-containing NPs over the time reaching 0.9 mg/cm² with Tb-NLCs PC. In both cases tobramycin was locally available to exert its antibiotic activity.

3.6. In vivo biodistribution study

IR-NLCs were used for the *in vivo* distribution study as they allow the observation of the NLCs *in vivo* avoiding the auto-fluorescence of the tissues. After intratracheal administration to mice by the Penn Century[®] device, each mouse was sacrificed at determinate time points and images from LI-COR Pearl[®] were recorded. IR emission associated with nanoparticles was detected at different levels of the pulmonary tree, suggesting a wide distribution in the lungs until 48 h (Fig. 7A). Immediately after the administration, a high concentration of IR-NLCs in the lungs was observed (Fig. 7B). According to the intense red color of the images, IR signal was totally dispersed throughout the entire lung lobes including alveoli. After 2 h of administration, a systemic absorption of NLCs could be detected in other organs such as liver and kidneys, and less intensively in spleen. At 48 h, the nanoparticles remained in the lungs while the IR signal disappeared in all other organs suggesting that the lung functions as a NP-trapping organ. Both formulations displayed a similar behavior *in vivo*. The only difference was the lack of signal in the liver at 48 h in the case of NLCs PC. According to Fig. 7A, free dye was faster cleared from

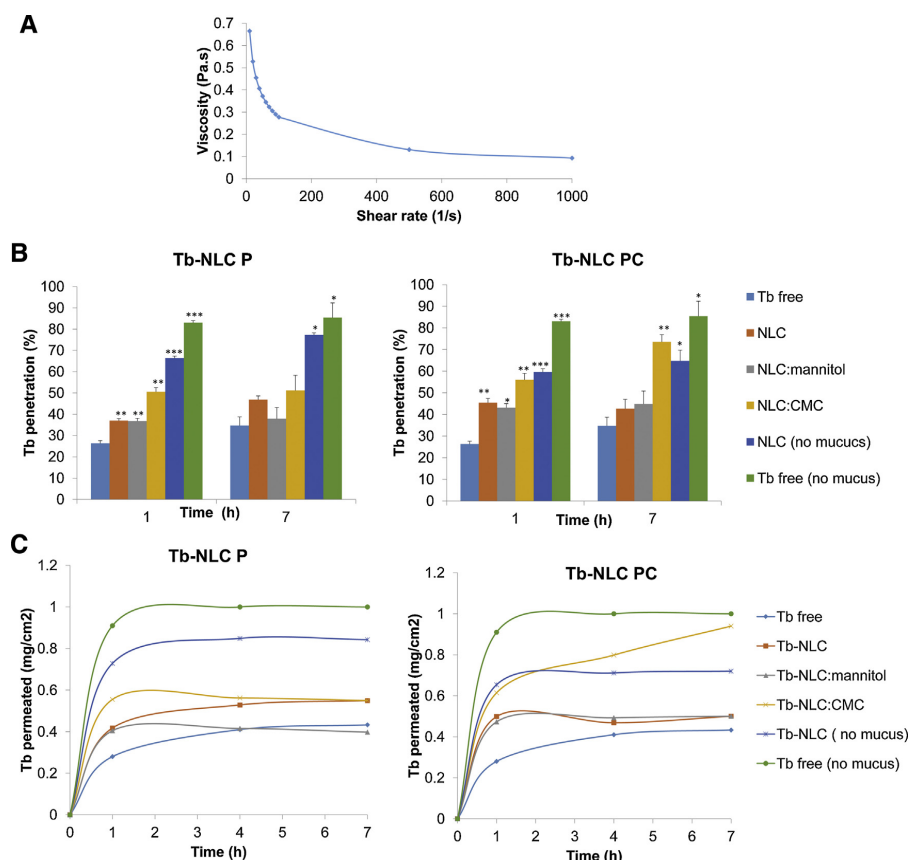


Fig. 6. (A) Viscosity values versus shear rate of artificial mucus (AM1). (B) Percentage of tobramycin permeation from NLCs through the AM1 layer. (C) Mucus permeation profile of tobramycin (mg/cm²) from Tb-NLCs through AM1 at 1, 4 and 7 h. Legends for B and C: Tb free, Tb-NLC, Tb-NLC: mannitol (75:25), Tb-NLC:CMC (carboxymethylcysteine) (75:25) are formulations tested in presence of a mucus layer. Tb-NLC (no mucus) and Tb free (no mucus) are used as controls without AM1.

the lung and distributed more quickly to other organs such as kidneys and liver (e.g., at 48 h there was almost no signal in the lungs) compared to NLC formulations. No IR emission was detected in mice before the administration of the formulations.

4. Discussion

As described in this work, we developed antibiotic-loaded NLCs as pulmonary delivery system focusing on the treatment of cystic fibrosis patients. In this case, tobramycin was selected as it is an antibiotic of choice in the treatment of CF associated *P. aeruginosa* infection (Smyth et al., 2014). Some clear advantages of these nanoparticles are the use of biocompatible and biodegradable lipids and the avoidance of organic solvents during their preparation leading to economic efficiency and an environmental friendly process. In addition, it has been reported that the presence of residual solvents in the final product could lead to pulmonary toxicity (Patil and Sarasija, 2012).

Nanoparticles displayed a diameter size ranging from 250 to 300 nm using trehalose as cryoprotectant. Based on our previous studies, 15% (w/w) of trehalose was chosen as cryoprotectant as it was found to be the most suitable one for the lyophilization process (Pastor et al., 2014). The particle size of the nanoparticles

allows them to escape from phagocytosis by macrophages, as it is generally thought that particles of 0.5–3 µm in diameter are taken by macrophages (Mansour et al., 2009). The low PDI achieved meant that the particles are distributed uniformly within the formulation. The negative Zeta potential of the nanoparticles, around –24 mV, predicts good physical stability of nanoparticle dispersions (Das et al., 2012). High encapsulation efficiencies (≥93%) were achieved for both nanoparticles. Many other studies have been reported regarding the encapsulation of tobramycin into SLN (Cavalli et al., 2000, 2002), liposomes (Messiaen et al., 2013), and polymeric nanoparticles (Deacon et al., 2015; Ungaro et al., 2012), and those were also able to achieve nanometric size although with less encapsulation efficiencies.

According to the release studies, results showed a biphasic profile characterized by an initial rapid release followed by a modulated and progressive release of tobramycin lasting at least for three days, in both types of formulations. The burst release could be attributed to the drug adsorbed onto or close to the surface of the nanoparticles (Nandakumar et al., 2013). This profile release is very similar to the one reported by Patlolla et al. (2010) where Colecoxib-NLCs formulation incorporating Compritol® were able to release the drug in a controlled manner and almost completely (over 80% of the drug) during 72 h. The sustained

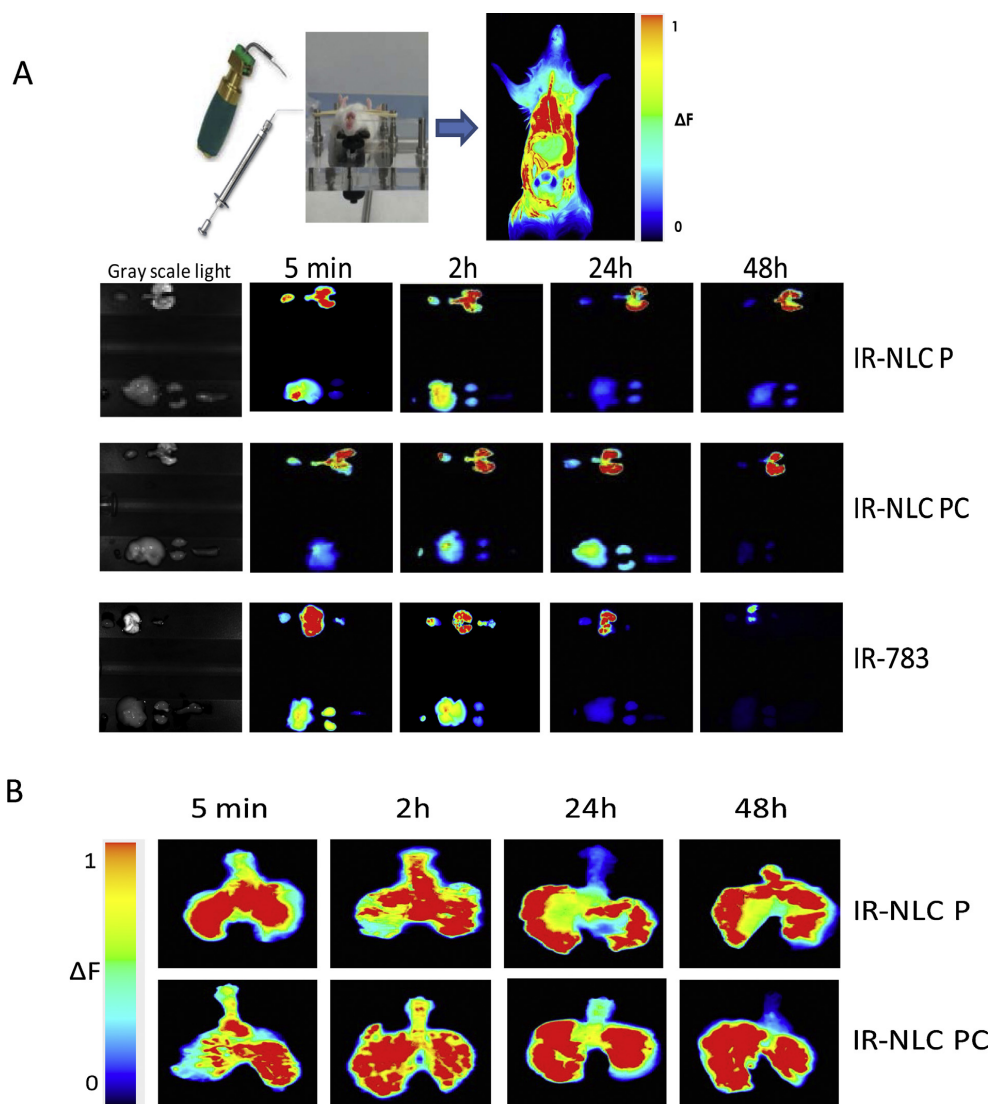


Fig. 7. (A) Biodistribution of IR-NLCs and free IR after intratracheal administration to mice. IR-intensity image of selected organ excised (upper row from left to right: heart, trachea and lungs, lower row from left to right: gallbladder, liver, kidneys and spleen) at different time points (5 min, 2 h, 24 h and 48 h). (B) Biodistribution of IR-NLCs in the lungs.

release of tobramycin via a nanocarrier delivery system may provide the opportunity to maintain prolonged targeted lung exposures and enhance the uptake of drug to the site of infection. Moreover, in case of a biofilm development, the biphasic release profile might be beneficial, where the fast antibiotic release in the beginning ensures a high initial antibiotic concentration enough to inhibit the biofilm growth, followed by a sustained antibiotic concentration above the MIC value that permits the eradication of the surviving cells minimizing the exacerbation (Cheow et al., 2010). It is remarkable that the number of doses could be reduced or longer the dosing interval and therefore enhance patient compliance.

CF patients usually suffer for chronic infections caused by *P. aeruginosa*, which frequently become resistant to antibiotics. For that reason, the efficacy of Tb-NLCs was evaluated using a *P. aeruginosa* strain from CF patients finding the same or higher antipseudomonal activity than free tobramycin. Similar results were reported by Deacon et al. (2015), who found that tobramycin NPs and free tobramycin reflected the same MIC values against *P. aeruginosa* PA01 (0.625 µg/mL). According to Mugabe et al. (2005), the MIC of liposomal gentamicin formulations were significantly lower than the MICs of free gentamicin against resistant mucoid and non-mucoid clinical strains of *P. aeruginosa* (≤ 8 µg/mL versus ≥ 32 µg/mL). This phenomenon was explained

by the liposome-bacterial membrane fusion mechanism that led to the deformation of bacterial membrane.

To determine whether Tb-NLCs exerted cell toxicity, *in vitro* cytotoxicity and viability assays using human epithelial cell (A549 and H441) lines was performed after 24 h of exposition. None of the formulations tested presented toxicity, at least at the concentrations studied. This finding is in accordance with other reports that demonstrated the good tolerability of lipid nanoparticles *in vitro* using A549 cell lines (Hu and Jia, 2010; Liu et al., 2008; Patlolla et al., 2010). Furthermore, the concentration of 1 mg/mL is 2000 times higher than the MIC of Tb-NLCs against *P. aeruginosa* (MIC 0.5 µg/mL). In the next step, cell viability was analyzed under fluorescent microscopy where the predominance of green color in all the samples confirmed the safety of the lipid nanoparticles.

Mucus covers many body surfaces forming a gel-like barrier to protect the body from pathogens and other kind of environmental ultrafine particles (Cone, 2009). However, in CF patients this natural mucus becomes tenacious housing many bacterial pathogens that hinder the penetration of antibiotics and the efficiency of therapies. In order to overcome this abnormal mucus barrier and to prolong the NLCs retention in the lung two mucolytic agents, i.e. mannitol and carboxymethylcysteine were selected. We tested whether our particles could cross the mucus and facilitate the drug transport through it using the AM model, reported before by Yang et al. (2011) CB dye was chosen as the active ingredient because the gelatin interfered with the amino groups of the tobramycin and it was impossible to quantify. As the nanoparticle diffusion across the mucus is dictated by the size of the mucus pores, Tb-NLCs particles with an approximate diameter of 250 nm, theoretically, should be able to overcome the mucus barrier as they are small enough to diffuse through the mucus pores which typically fall in the range of 200–500 nm in chronically infected lungs (Suk et al., 2009). Forier et al. (2013) also reported that negatively charged nanoparticles exhibited superior mucus penetration. As expected, the penetration of the particles across the mucus layer was improved by the addition of mucolytic agents that facilitated the drug transport through it. Suk et al. also demonstrated an increased in particle penetration through CF sputum when using another mucolytic, *N*-acetylcysteine (Suk et al., 2011).

To carry out permeation studies for tobramycin quantification, another artificial mucus (AM1) was elaborated with similar physico-chemical properties to the mucus that have CF patients as described by Shur et al. (2008). This model reproduces pulmonary environment and allows *in vitro* experiments performing because AM passed through membranes pores. According to our previous penetration study, the highest proportion of NLC: mucolytic agent was selected (75:25). The permeability assay revealed that the maximum drug permeation across the mucus layer was observed for the Tb-NLC PC incorporating carboxymethylcysteine (CMC), whereas the addition of mannitol did not improve significantly the drug permeability at 7 h. Similarly, Suk et al. (2011) also reported a close to 13-fold improvement in the diffusion velocity of NPs through a sputum layer upon the addition of acetylcysteine. The presence of tobramycin in the receptor compartment suggests that the drug from NLCs may slowly release, permeate and distribute into the abnormal mucus layer being locally available for its antimicrobial activity. According to these results, we developed a mucus penetrating drug carrier that after formulate with appropriate mucolytic agents, could offer sustained levels of antibiotic at the mucus barrier. However, a complementary studies incubating *P. aeruginosa* with AM should be performance in order to find out what could happen in an infection scenario such as in CF patient sputum.

Finally, the administration of IR-NLCs exerted a strong IR signal in the lungs of the mice lasting until 48 h allowing the drug release from the lipid matrix. The intratracheal instillation by Penn Century® device provides a fast and quantifiable technique for drug delivery directly to the lungs (Patil and Sarasija, 2012) presenting large distribution and minimal drug loss during application compared to nebulization processes (Bivas-Benita et al., 2005). Nevertheless, intratracheal instillation does not reflect the natural inhalation mechanism because the formulation is required to be administered to anesthetized animals (Nahar et al., 2013). Regarding to the free drug Poyner et al. (1995), reported that the endotracheal administration of radiolabeled tobramycin led to a higher dissemination to the kidney and in a lower extent at the lung tissue compared to liposomal and microcapsular tobramycin which were primarily retained in the lungs, thus decreasing nephrotoxicity. Similar results were reported by Varshosaz et al. (2013) who confirmed that amikacin-loaded SLNs remained 6 h longer in lungs after pulmonary administration by microsyringe compared to i.v. route. Moreover, in another study by Patlolla et al. (2010), authors also showed that celecoxib-loaded NLCs deposited in the alveolar region with prolonged residence time, up to 24 h, after inhalational administration in mice. Therefore, it might be concluded that tobramycin encapsulation within nanoparticulate DDS may represent an advantage for prolonging lung residence time of the encapsulated drug that would be slowly released to the media allowing continuous bacterial killing.

5. Conclusions

In this work, we report the development and the characteristics of a new tobramycin nanocarrier formulation. Tb-NLCs (both Tb-NLC P and Tb-NLC PC) demonstrated efficacy against *P. aeruginosa* *in vitro*, mucus penetration ability and large pulmonary distribution and retention in the *in vivo* studies. Tb-NLCs can provide the advantage of a sustained drug release in the target site, resulting in reduced-dose schedule and improved patient compliance. Therefore, Tb-NLCs could represent an alternative drug delivery system for pulmonary infection treatment. As yet, the results presented in this study are not sufficient to predict the effectiveness of the lipid-based nanosystem in CF patients although the features of the developed formulation so far examined could be considered promising in a perspective of an efficacious CF inhalable therapy.

Acknowledgments

The production and characterization of nanoparticles has been performed by the ICTS “NANBIOSIS”, more specifically by the Drug Formulation Unit (U10) of the CIBER in Bioengineering, Biomaterials & Nanomedicine (CIBER-BBN) at the University of the Basque Country (UPV/EHU).

This work was supported by the TERFIQEC Project, IPT-2011-1402-900000 (funded by the Ministry of Economy and Competitiveness MINECO, Spain). The authors gratefully acknowledge the support of University of the Basque Country UPV/EHU (UFI11/32), University of Barcelona (UB), UIB and CSIC-FISIB Caubet-Cimera. M. Moreno-Sastre thanks UPV/EHU for the ZabaldUz fellowship grant. Technical and human support provided by Sara Vallejo and SGIKer (UPV/EHU) is gratefully acknowledged.

References

- Andrade, F., Rafael, D., Videira, M., Ferreira, D., Sosnik, A., Sarmento, B., 2013. Nanotechnology and pulmonary delivery to overcome resistance in infectious diseases. *Adv. Drug Deliv. Rev.* 65, 1816–1827. doi:http://dx.doi.org/10.1016/j.addr.2013.07.020.

- Bivas-Benita, M., Zwier, R., Junginger, H.E., Borchard, G., 2005. Non-invasive pulmonary aerosol delivery in mice by the endotracheal route. *Eur. J. Pharm. Biopharm.* 61, 214–218. doi:http://dx.doi.org/10.1016/j.ejpb.2005.04.009 S0939-6411(05)00153-0 [pii].
- Cavalli, R., Zara, G.P., Caputo, O., Bargini, A., Fundarò, A., Gasco, M.R., 2000. Transmucosal transport of tobramycin incorporated in SLN after duodenal administration to rats. Part I—a pharmacokinetic study. *Pharmacol. Res.* 42, 541–545. doi:http://dx.doi.org/10.1006/phrs.2000.0737.
- Cavalli, R., Gasco, M.R., Chetoni, P., Burchiassi, S., Saettone, M.F., 2002. Solid lipid nanoparticles (SLN) as ocular delivery system for tobramycin. *Int. J. Pharm.* 238, 241–245.
- Cheow, W.S., Chang, M.W., Hadinoto, K., 2010. Antibacterial efficacy of inhalable antibiotic-encapsulated biodegradable polymeric nanoparticles against *E. coli* biofilm cells. *J. Biomed. Nanotechnol.* 6, 391–403.
- Cone, R.A., 2009. Barrier properties of mucus. *Adv. Drug Deliv. Rev.* 61, 75–85. doi:http://dx.doi.org/10.1016/j.addr.2008.09.008.
- Das, S., Ng, W.K., Tan, R.B.H., 2012. Are nanostructured lipid carriers (NLCs) better than solid lipid nanoparticles (SLNs): development, characterizations and comparative evaluations of clotrimazole-loaded SLNs and NLCs? *Eur. J. Pharm. Sci.* 47, 139–151. doi:http://dx.doi.org/10.1016/j.ejps.2012.05.010.
- Deacon, J., Abdelghany, S.M., Quinn, D.J., Schmid, D., Megaw, J., Donnelly, R.F., Jones, D.S., Kissenpennig, A., Elborn, J.S., Gilmore, B.F., Taggart, C.C., Scott, C.J., 2015. Antimicrobial efficacy of tobramycin polymeric nanoparticles for *Pseudomonas aeruginosa* infections in cystic fibrosis: formulation, characterisation and functionalisation with dornase alfa (DNase). *J. Control. Release* 198, 55–61. doi:http://dx.doi.org/10.1016/j.jconrel.2014.11.022.
- Donnelly, R.F., McCarron, P.A., Cassidy, C.M., Elborn, J.S., Tunney, M.M., 2007. Delivery of photosensitisers and light through mucus: investigations into the potential use of photodynamic therapy for treatment of *Pseudomonas aeruginosa* cystic fibrosis pulmonary infection. *J. Controlled Release* 117, 217–226. doi:http://dx.doi.org/10.1016/j.jconrel.2006.11.010.
- European Council, 2014. European Pharmacopoeia 8.0. Council of Europe: European Directorate for the Quality of Medicines and Healthcare, Strasbourg, pp. 363–365.
- Forier, Messiaen, A.S., Raemdonck, K., Deschout, H., Rejman, J., De Baets, F., Nelis, H., De Smedt, S.C., Demeester, J., Coenye, T., Braeckmans, K., 2013. Transport of nanoparticles in cystic fibrosis sputum and bacterial biofilms by single-particle tracking microscopy. *Nanomedicine (Lond.)* 8, 935–949. doi:http://dx.doi.org/10.2217/nmm.12.129.
- Hajipour, M.J., Fromm, K.M., Ashkarran, A.A., Jimenez de Aberasturi, D., de Larramendi, I.R., Rojo, T., Serposhan, V., Parak, W.J., Mahmoudi, M., 2012. Antibacterial properties of nanoparticles. *Trends Biotechnol.* 30, 499–511. doi:http://dx.doi.org/10.1016/j.tibtech.2012.06.004.
- Hu, L., Jia, Y., 2010. Preparation and characterization of solid lipid nanoparticles loaded with epirubicin for pulmonary delivery. *Die Pharmazie-Ann Int. J. Pharm. Sci.* 65, 585–587.
- Liu, J., Gong, T., Fu, H., Wang, C., Wang, X., Chen, Q., Zhang, Q., He, Q., Zhang, Z., 2008. Solid lipid nanoparticles for pulmonary delivery of insulin. *Int. J. Pharm.* 356, 333–344. doi:http://dx.doi.org/10.1016/j.ijpharm.2008.01.008.
- Mansour, H.M., Rhee, Y.S., Wu, X., 2009. Nanomedicine in pulmonary delivery. *Int. J. Nanomed.* 4, 299–319.
- Marini, J.J., Slutsky, A.S., 1998. *Physiological Basis of Ventilatory Support*. Marcel Dekker, New York.
- Messiaen, A., Forier, K., Nelis, H., Braeckmans, K., Coenye, T., 2013. Transport of nanoparticles and tobramycin-loaded liposomes in *Burkholderia cepacia* complex biofilms. *Nanomedicine* 8, 895–949.
- Moreau-Marquis, S., Stanton, B.A., O'Toole, G.A., 2008. *Pseudomonas aeruginosa* biofilm formation in the cystic fibrosis airway. *Pulm. Pharmacol. Ther.* 21, 595–599. doi:http://dx.doi.org/10.1016/j.pupt.2007.12.001.
- Mugabe, C., Azghani, A.O., Omri, A., 2005. Liposome-mediated gentamicin delivery: development and activity against resistant strains of *Pseudomonas aeruginosa* isolated from cystic fibrosis patients. *J. Antimicrob. Chemother.* 55, 269–271. doi:http://dx.doi.org/10.1093/jac/dkh518.
- Nahar, K., Gupta, N., Gauvin, R., Absar, S., Patel, B., Gupta, V., Khademhosseini, A., Ahsan, F., 2013. In vitro, in vivo and ex vivo models for studying particle deposition and drug absorption of inhaled pharmaceuticals. *Eur. J. Pharm. Sci.* 49, 805–818. doi:http://dx.doi.org/10.1016/j.ejps.2013.06.004.
- Nandakumar, V., Geetha, V., Chittaranjan, S., Doble, M., 2013. High glycolic poly (DL lactic co glycolic acid) nanoparticles for controlled release of meropenem. *Biomed. Pharmacother.* 67, 431–436. doi:http://dx.doi.org/10.1016/j.biopha.2013.02.004.
- Nassimi, M., Schlegel, C., Lauenstein, H.D., Hussein, R., Hoymann, H.G., Koch, W., Pohlmann, G., Krug, N., Sewald, K., Rittinghausen, S., Braun, A., Muller-Goymann, C., 2010. A toxicological evaluation of inhaled solid lipid nanoparticles used as a potential drug delivery system for the lung. *Eur. J. Pharm. Biopharm.* 75, 107–116. doi:http://dx.doi.org/10.1016/j.ejpb.2010.02.014.
- Okusanya, O.O., Bhavnani, S.M., Hammel, J., Minic, P., Dupont, L.J., Forrest, A., Mulder, G.J., Mackinson, C., Ambrose, P.G., Gupta, R., 2009. Pharmacokinetic and pharmacodynamic evaluation of liposomal amikacin for inhalation in cystic fibrosis patients with chronic pseudomonal infection. *Antimicrob. Agents Chemother.* 53, 3847–3854. doi:http://dx.doi.org/10.1128/AAC.00872-08.
- Pastor, M., Moreno-Sastre, M., Esquisabel, A., Sans, E., Viñas, M., Bachiller, D., Asensio, V.J., Pozo, A.D., Gainza, E., Pedraz, J.L., 2014. Sodium colistimethate loaded lipid nanocarriers for the treatment of *Pseudomonas aeruginosa* infections associated with cystic fibrosis. *Int. J. Pharm.* 477, 485–494. doi:http://dx.doi.org/10.1016/j.ijpharm.2014.10.048.
- Patil, J.S., Sarasija, S., 2012. Pulmonary drug delivery strategies: a concise, systematic review. *Lung India* 29, 44–49. doi:http://dx.doi.org/10.4103/0970-2113.92361.
- Patlolla, R.R., Chougule, M., Patel, A.R., Jackson, T., Tata, P.N., Singh, M., 2010. Formulation, characterization and pulmonary deposition of nebulized celecoxib encapsulated nanostructured lipid carriers. *J. Control. Release* 144, 233–241. doi:http://dx.doi.org/10.1016/j.jconrel.2010.02.006.
- Poyner, E.A., Alpar, H.O., Almeida, A.J., Gamble, M.D., Brown, M.R.W., 1995. A comparative study on the pulmonary delivery of tobramycin encapsulated into liposomes and PLA microspheres following intravenous and endotracheal delivery. *J. Control. Release* 35, 41–48. doi:http://dx.doi.org/10.1016/0168-3659(95)00017-3.
- Ratjen, F., Brockhaus, F., Angyalosi, G., 2009. Aminoglycoside therapy against *Pseudomonas aeruginosa* in cystic fibrosis: a review. *J. Cyst. Fibros.* 8, 361–369. doi:http://dx.doi.org/10.1016/j.jcf.2009.08.004.
- Russo, P., Stigliani, M., Protta, L., Aurieemma, G., Crescenzi, C., Porta, A., Aquino, R.P., 2013. Gentamicin and leucine inhalable powder: what about antipseudomonal activity and permeation through cystic fibrosis mucus? *Int. J. Pharm.* 440, 250–255. doi:http://dx.doi.org/10.1016/j.ijpharm.2012.05.077.
- Sampath, S.S., Robinson, D.H., 1990. Comparison of new and existing spectrophotometric methods for the analysis of tobramycin and other aminoglycosides. *J. Pharm. Sci.* 79, 428–431.
- Savla, R., Minko, T., 2013. Nanotechnology approaches for inhalation treatment of fibrosis. *J. Drug Target.* 21, 914–925. doi:http://dx.doi.org/10.3109/1061186X.1.2013.829078.
- Shur, J., Nevell, T.G., Ewen, R.J., Price, R., Smith, A., Barbu, E., Conway, J.H., Carroll, M. P., Shute, J.K., Smith, J.R., 2008. Cospray-dried unfractionated heparin with L-leucine as a dry powder inhaler mucolytic for cystic fibrosis therapy. *J. Pharm. Sci.* 97, 4857–4868. doi:http://dx.doi.org/10.1002/jps.21362.
- Smyth, A.R., Bell, S.C., Bojcin, S., Bryon, M., Duff, A., Flume, P., Kashirskaya, N., Munck, A., Ratjen, F., Schwarzenberg, S.J., Smeret-Gaudelou, I., Southern, K.W., Taccetti, G., Ullrich, G., Wolfe, S., 2014. European Cystic Fibrosis Society, 2014. European Cystic Fibrosis Society standards of care: best practice guidelines. *J. Cyst. Fibros.* 13 (Suppl. 1), S23–S42. doi:http://dx.doi.org/10.1016/j.jcf.2014.03.010.
- Suk, J.S., Lai, S.K., Wang, Y.Y., Ensign, L.M., Zeitlin, P.L., Boyle, M.P., Hanes, J., 2009. The penetration of fresh undiluted sputum expectorated by cystic fibrosis patients by non-adhesive polymer nanoparticles. *Biomaterials* 30, 2591–2597. doi:http://dx.doi.org/10.1016/j.biomaterials.2008.12.076.
- Suk, J.S., Lai, S.K., Boylan, N.J., Dawson, M.R., Boyle, M.P., Hanes, J., 2011. Rapid transport of muco-inert nanoparticles in cystic fibrosis sputum treated with N-acetyl cysteine. *Nanomedicine (Lond.)* 6, 365–375. doi:http://dx.doi.org/10.2217/nmm.10.123.
- Theillin, O., Zorzi, W., Jolios, O., Elmoualij, B., Duysens, G., Cahay, B., Streel, B., Charif, M., Bastin, R., Heinen, E., Quatresouz, P., 2015. In vitro approach to study the synergistic effects of tobramycin and clarithromycin against *Pseudomonas aeruginosa* biofilms using prokaryotic or eukaryotic culture media. *Int. J. Antimicrob. Agents* 46, 33–38. doi:http://dx.doi.org/10.1016/j.ijantimicag.2015.02.010.
- Tseng, B.S., Zhang, W., Harrison, J.J., Quach, T.P., Song, J.L., Penterman, J., Singh, P.K., Chopp, D.L., Packman, A.I., Parsek, M.R., 2013. The extracellular matrix protects *Pseudomonas aeruginosa* biofilms by limiting the penetration of tobramycin. *Environ. Microbiol.* 15, 2865–2878. doi:http://dx.doi.org/10.1111/1462-2920.12155.
- Ungaro, F., d'Angelo, I., Coletta, C., d'Emmanuele di Villa Bianca, R., Sorrentino, R., Perfetto, B., Tufano, M.A., Miro, A., La Rotonda, M.I., Quaglia, F., 2012. Dry powders based on PLGA nanoparticles for pulmonary delivery of antibiotics: modulation of encapsulation efficiency, release rate and lung deposition pattern by hydrophilic polymers. *J. Control. Release* 157, 149–159. doi:http://dx.doi.org/10.1016/j.jconrel.2011.08.010.
- Varshosaz, J., Ghaffari, S., Mirshojaei, S.F., Jafarian, A., Atyabi, F., Kobarfard, F., Azarmi, S., 2013. Biodistribution of amikacin solid lipid nanoparticles after pulmonary delivery. *Biomed. Res. Int.* 13685, 9. doi:http://dx.doi.org/10.1155/2013/136859.
- Waters, V., Smyth, A., 2015. Cystic fibrosis microbiology: advances in antimicrobial therapy. *J. Cyst. Fibros.* 14, 551–560. doi:http://dx.doi.org/10.1016/j.jcf.2015.02.005 S1569-1993(15)00043-0 [pii].
- Weber, S., Zimmer, A., Pardeike, J., 2014. Solid lipid nanoparticles (SLN) and nanostructured lipid carriers (NLC) for pulmonary application: a review of the state of the art. *Eur. J. Pharm. Biopharm.* 86, 7–22. doi:http://dx.doi.org/10.1016/j.ejpb.2013.08.013.
- Yang, Y., Tsifansky, M.D., Shin, S., Lin, Q., Yeo, Y., 2011. Mannitol-guided delivery of ciprofloxacin in artificial cystic fibrosis mucus model. *Biotechnol. Bioeng.* 108, 1441–1449. doi:http://dx.doi.org/10.1002/bit.23046.

PAPER 3

Original Article

Killing effect of nanoencapsulated colistin sulfate on *Pseudomonas aeruginosa* from cystic fibrosis patients



E. Sans-Serramitjana ^a, E. Fusté ^{a,b}, B. Martínez-Garriga ^a, A. Merlos ^a, M. Pastor ^c, J.L. Pedraz ^c,
A. Esquisabel ^c, D. Bachiller ^d, T. Vinuesa ^a, M. Viñas ^{a,e,*}

^a Dept. Pathology and Experimental Therapeutics, Medical School, University of Barcelona, Barcelona, Spain

^b Dept. Public Health, Mental Health and Perinatal Nursing, US of Nursing, University of Barcelona, Barcelona, Spain

^c Laboratory of Pharmaceutics, University of the Basque Country (UPV/EHU) and CIBER-BBN, Vitoria-Gasteiz, Spain

^d Fundación Investigaciones Sanitarias Islas Baleares (FISIB), Development and Regeneration Program (CSIC), Bunyola, Spain

^e CESPU, INNFACTS, Gandra, Portugal

Received 15 September 2015; revised 18 November 2015; accepted 2 December 2015

Available online 18 December 2015

Abstract

Pseudomonas aeruginosa frequently infects the respiratory tract of cystic fibrosis (CF) patients. Multidrug-resistant phenotypes and high capacity to form stable biofilms are common. Recent studies have described the emergence of colistin-resistant isolates in CF patients treated with long-term inhaled colistin. The use of nanoparticles containing antimicrobials can contribute to overcome drug resistance mechanisms.

The aim of this study was to explore antimicrobial activity of nanoencapsulated colistin (SLN-NLC) versus free colistin against *P. aeruginosa* clinical isolates from CF patients and to investigate their efficacy in biofilm eradication. Susceptibility of planktonic bacteria to antimicrobials was examined by using the broth microdilution method and growth curve assay. Minimal biofilm eradication concentration (MBEC) and biofilm prevention concentration (BPC) were determined to assess antimicrobial susceptibility of sessile bacteria. We used atomic force microscopy (AFM) to visualize treated and untreated biofilms and to determine surface roughness and other relevant parameters. Colistin nanoparticles had the same antimicrobial activity as free drug against planktonic bacteria. However, nanoencapsulated colistin was much more efficient in the eradication of biofilms than free colistin. Thus, these formulations have to be considered as a good alternative therapeutic option to treat *P. aeruginosa* infections.

© 2015 European Cystic Fibrosis Society. Published by Elsevier B.V. All rights reserved.

Keywords: Colistin sulfate; Lipid nanoparticles; Antimicrobial effect; *Pseudomonas aeruginosa*; Cystic fibrosis

1. Introduction

Pseudomonas aeruginosa is the predominant pathogen infecting the respiratory tract of cystic fibrosis (CF) patients causing significant decline of pulmonary functions and increasing morbidity and mortality [1]. Early colonizers are generally a few individuals forming non-mucoid colonies. Once bacteria

colonize the lung, eradication becomes difficult; bacterial density increases, and the microorganism switches to a mucoid form and to a stable biofilm mode of growth in which susceptibility to antimicrobials decreases [2]. It is well-known that *P. aeruginosa* has a high metabolic versatility, genetic plasticity, and ability to acquire genes carried both in plasmids and transposons from mainly Gram-negative bacteria; these genes often encode for antimicrobial resistance [3]. In addition, outer membrane of *P. aeruginosa* has low permeability to most antimicrobials. Thus, multidrug-resistant (MDR) phenotypes frequently emerge. One of the main goals of CF treatment is to prevent, limit, and eradicate *P. aeruginosa* from the respiratory tract of patients. This

* Corresponding author at: Laboratory of Molecular Microbiology, Faculty of Medicine, University of Barcelona, Feixa Llarga s/n, 08907 Hospitalet de Llobregat, Barcelona, Spain. Tel.: +34 934024265.

E-mail address: mvinyas@ub.edu (M. Viñas).

could enlarge survival and improve health-related quality of life [4].

The emergence of multidrug-resistant *P. aeruginosa* led to the rescue of colistin (a bactericidal cyclic polycationic peptide) [5]. Colistin interacts with anionic lipopolysaccharide in the outer membrane of gram-negative bacteria mainly displacing Ca^{2+} and Mg^{2+} , thus dramatically decreasing the stability of the outer membrane and allowing a secondary effect on the cytoplasmic membrane by increasing its permeability. This leads to cytoplasmic content leakage and subsequent bacterial death [6]. From the fifties to the eighties, colistin was mainly administered intravenously. However, due to high nephrotoxicity and neurotoxicity, its use was restricted in the early 1970s [7]. This has also stimulated the research on the introduction of less toxic antimicrobials as well as the use of pharmaceutical forms that can diminish doses [8].

The progressive occurrence of MDR *P. aeruginosa* led to scenarios in which almost no treatment options were available. This was particularly clear after the widespread emergence of imipenem resistance of strains lacking the OprD porin. This is the reason why in the last few years, colistin use recommenced. Nowadays, inhaled colistin is regarded as a useful therapeutic option for early antibiotic intervention in periodically colonized CF patients and in critically ill patients [9,10].

Despite that colistin is considered one of the most active antimicrobials to combat multidrug-resistant bacteria, it is noteworthy that recent studies have described the emergence of colistin-resistant bacteria in CF patients treated with long-term by inhalation [11,12].

Currently, new delivery strategies, such as the use of solid lipid nanoparticles (SLN) and nanostructured lipid carriers (NLC) are being explored to treat *P. aeruginosa* infections in CF. In principle, this should reduce systemic toxicity, diminish dose, and enlarge administration intervals. Simultaneously, search for alternative methods of antibiotic administration is being done [13,14]. Since the lung offers a large surface area for drug absorption, aerosolization of drugs ensures rapid drug distribution; moreover, when treating respiratory infections, inhalation delivers the antimicrobial in the precise site of infection. Nebulization of antimicrobials carried in lipid nanoparticles improves drug bioavailability and allows reducing the dosing frequency. It has been pointed out that both SLNs and NLCs are more stable than liposomes both *in vitro* and *in vivo*, they have better biocompatibilities and lower potential toxicity (both acute and chronic) than polymeric nanoparticles or other synthetic nanoformulations and are relatively easy to produce [15]. The use of nanoparticles could overcome pre-existing drug resistance mechanisms, including decreased uptake and increased efflux of drug as well as biofilm formation [16,17]. The *in vitro* activity of sodium colistimethate on similar isolates in planktonic form was reported recently [18]. Lipid nanoparticles loaded with aminoglycosides are significantly more effective than free formulations against *P. aeruginosa* clinical isolates [19,20]. The aim of this study was to explore the antimicrobial activity of the nanoencapsulated colistin (in both SLN and NLC) versus free drug against *P. aeruginosa* clinical isolates from CF patients and to investigate the efficacy of these novel formulations in

the eradication of biofilms, the most common mode of life of *P. aeruginosa* causing pulmonary infections.

2. Material and methods

2.1. Bacterial isolates

Thirty-four clinical isolates of *P. aeruginosa* (19 non-mucoid and 15 mucoid) from sputum and pharyngeal exudates of cystic fibrosis patients collected between January 2012 and April 2012 from Hospital de la Vall d'Hebron and Hospital Sant Joan de Déu (Barcelona, Spain) were included in this study. The age of patients ranged from 9 to 50 and the mean age of the patients was 27. As much as 41% of patients were male and 59% of patients were female. *P. aeruginosa* ATCC 27853 and *P. aeruginosa* PAO1 were used as control strains in drug susceptibility testing assays and in biofilm studies, respectively. Two colistin-resistant clinical isolates (P19 and P20) were used to be compared with susceptible bacterial isolates.

2.2. Chemicals and bacteriological media

Colistin sulfate was obtained from Zhejiang Shenghua Biok Biology Co., LTD. (China). Mueller–Hinton II broth cation adjusted (MHBCA) was from Becton Dickinson and Company (Sparks, MD, US) and Tryptone Soy Agar (TSA) and Tryptone Soy Broth (TSB) were purchased from Scharlau (Sentmenat, Barcelona, Spain). Precirol® ATO 5 was kindly provided by Gattefossé (Madrid, Spain). Poloxamer 188 and Lutrol LF68 were a kind gift from BASF (Ludwigshafen, Rhineland-Palatinate, Germany). Polysorbate and Tween 80 were purchased from Panreac Química (Castellar del Vallès, Barcelona, Spain) and Miglyol 182 N/F was provided by Sasol (Hamburg, Germany).

2.3. Preparation of lipid nanoparticles

Solid lipid nanoparticles (SLN) were prepared as previously described [16]. Briefly, amounts of 10 mg of colistin sulfate were mixed with Precirol® ATO 5 dichloromethane solution at 5% (w/v). Then, a mixture of organic phase and an aqueous surfactant containing antimicrobial solution (Poloxamer 188 at 1% w/v and Polysorbate 80 at 1% w/v) was prepared and subsequently emulsified under ultrasonic treatment at 20 W for 30 s (Branson Sonifier 250, Danbury, CT, US). Then, solvent was evaporated under magnetic stirring for 2 h at 20 °C. Once prepared, nanoparticles (SLNs) were filtered through Amicon® centrifugal filtration units (100,000 Da MWCO) at 2500 rpm for 15 minutes. Nanostructured lipid carriers (NLC) were prepared by using the so-called hot melt homogenization technique [19,20]. Lipid core was formed by Precirol® ATO 5 and Miglyol® 812. They were mixed with the API (active pharmaceutical ingredients) and then temperature gradually increased up to melting temperature of the solid lipid. The surfactant solution was 1.3% (w/v) Polysorbate 80 and 0.6% (w/v) Poloxamer 188. Emulsification was performed by sonication for 30 s at 20 W. Nanoparticles were stored at 4 °C overnight to re-crystallize and to stimulate particle formation. Washing step was accomplished by centrifugation at

2500 rpm in Amicon® centrifugal filtration units (100,000 Da MWCO) three times. All prepared nanoparticles were freeze-dried with two different cryoprotectants, either D-mannitol or trehalose (15%).

2.4. Characterization of lipid nanoparticles

Solid lipid nanoparticles (SLN) and nanostructured lipid carriers (NLC) were characterized for size, polydispersity index (PDI), and Zeta potential by means of Zetasizer Nano ZS (Malvern Instruments, Worcestershire, UK). Encapsulation efficiency and release profile were determined by HPLC as reported elsewhere [18].

2.5. Antimicrobial susceptibility of planktonic bacteria

Susceptibility to free colistin and two formulations of nanoencapsulated colistin of all isolates was determined by using the broth microdilution method (in MHBCA) in accordance with the Clinical Laboratory Standards Institute (CLSI) [21]. Minimal inhibitory concentrations (MICs) were determined in triplicate in at least three different experiments. Moreover, antimicrobial susceptibility was examined in two clinical isolates (the mucoid 086SJD and the non-mucoid 056SJD isolates) and the control strain to test the effect of the storage temperature (4 °C, 25 °C, 30 °C, and 40 °C) of nanoparticles over time [18].

2.6. Antimicrobial susceptibility of sessile bacteria

Minimal biofilm eradication concentration (MBEC) determinations were performed as described by Moskowitz et al [22] with a few modifications. Briefly, bacterial biofilms were formed by immersing the pegs of a modified polystyrene microtiter lid (catalog no. 445497; Nunc TSP system) into 96-well microtiter plates containing 200 µL of MHBCA each, followed by incubation at 37 °C for 24 h with no movement. Pegs were then gently rinsed in 0.9 % NaCl solution and biofilms exposed to different concentrations of free and nanoencapsulated colistin sulfate, and the combination of free colistin and empty nanoparticles for 24 h at 37 °C. Pegs were again rinsed with 0.9% NaCl solution and biofilms removed by 10 min sonication. Recovered bacteria were incubated for 24 h at 37 °C. Optical densities at 620 nm were measured in order to determine MBEC values, defined as the lowest concentration of antimicrobial that prevented bacterial regrowth from the treated biofilm. All experiments were performed in triplicate on at least three occasions.

A modification of MBEC assay was implemented to determine the Biofilm Prevention Concentration (BPC) [23]. Peg lids were immersed into 96-well microtiter plates containing 100 µL of dilution 1/100 of an overnight planktonic *P. aeruginosa* culture and 100 µL of a range of antibiotic concentrations in MHBCA. After 24 h incubation at 37 °C, pegs were rinsed with 0.9% NaCl solution and biofilms sonicated for 10 min. Detached bacteria were incubated at 37 °C for 24 h and optical densities (620 nm) were measured to determine the minimal concentration of antimicrobial that prevented the formation of biofilm.

These experiments were carried out with six *P. aeruginosa* clinical isolates. Four colistin-susceptible (ATCC 27853, PAO1, 056SJD, and 086SJD) and two colistin resistant (P19 and P20).

2.7. Effect of free and nanoencapsulated colistin on *P. aeruginosa* growth

The colistin-susceptible isolate 056SJD and colistin-resistant isolate P19 were used to examine the effect of free and nanoencapsulated colistin, and the combination of free colistin and empty nanoparticles on growth. Antimicrobials were added to logarithmic-phase liquid cultures (in TSB) with $1-5 \times 10^8$ CFU/mL and concentrations of $1/4 \times$ MIC, MIC, and $8 \times$ MIC.

Bacteria were incubated for 4 h at 37 °C and 2000 rpm in RTS-1C real-time cell growth loggers (Biosan) and growth measured as optical density (850 nm) in real time. All measurements were carried out in triplicate.

2.8. Atomic force microscopy (AFM) imaging and measurements

AFM was used to visualize 056SJD biofilm after 2, 6, and 24 h exposure to free and nanoencapsulated colistin, and the combination of free colistin and empty nanoparticles at concentrations of 128 µg/mL. We used 128 µg/ml since it is a concentration in between MIC and MBEC, in other words, the biofilm was not fully destroyed and still could be visualized. Moreover, the concentration of colistin in sputum after nebulization is situated between 50 and 500 µg/ml [24].

The culture was used to inoculate 24-well culture plates containing 2 mL of growth medium (MHBCA) to yield a bacterial concentration of 10^7 CFU/mL. Each well contained a Thermanox coverslip previously coated with a 0.01% (w/v) poly-L-lysine hydrobromide (Sigma–Aldrich, Dorset, UK) solution to enhance bacterial cell adhesion and to prevent biofilm removal during experiments. Plates were incubated at 37 °C for 24 h. Samples were imaged in air by using an Atomic Force Microscope XE-70 (Park Systems, Korea). All images were collected in non-contact mode using pyramidal-shaped silicon cantilevers with a spring constant of ± 40 N/m and a resonance frequency of ± 300 kHz, with the upper side coated with aluminum to enhance the laser beam reflectivity. The acquired data during the surface scanning were converted into images of topography and amplitude and analyzed by using XEP and XEI software (Park Systems, Korea). On topography images, it was feasible to observe the shape, structure, and surface of bacteria embedded in biofilms. Furthermore, amplitude images allow the visualization of fine surface details of bacteria that form biofilms [25]. AFM images were acquired with a scan size of $7 \mu\text{m}^2$ at a scan rate of 0.3–0.6 Hz. AFM was also used to measure the surface roughness of the treated and untreated biofilms. The roughness average (R_a), defined as the average distance from the roughness profile to the center plane of the profile, was calculated from the topography images obtained in this experiment. To obtain topography images and nanomechanics of the cells, the AFM was run in contact mode and controlled by software XEP (Park Systems, Korea) in order to measure force/distance curves

between the bare tip and bacterial cells (control group and treated group) in PBS at room temperature. Probes used for imaging and measuring force curves were DNP-S10 (Cantilever D) (Bruker); made of silicon nitride, the triangular cantilever was 205 μm long, coated in reflective gold, and held a nominal spring constant of 0.06 N/m. All cantilevers used in these experiments were individually calibrated by thermal tune method. Tip height was 2.5 μm with a curvature radius of 10 nm. The approach and retraction speed through all force–distance curves was $0.3 \mu\text{m s}^{-1}$, with an applied force of 2 nN at $t = 0$ s and $t = 10$ s. Values for adhesion forces—detachment force between the bare AFM tip and cell membrane in the process of AFM cantilever retracting—were extracted from the obtained measurement of the cantilever deflection versus the distance curves. Data were reported as mean \pm SD.

2.9. Statistical analysis

Comparisons of antimicrobial susceptibilities, for free and nanoencapsulated colistin stabilized with mannitol or trehalose, were statistically analyzed using the Cochran's Q test. Differences were considered significant when $p < 0.05$.

3. Results and discussion

3.1. Lipid nanoparticles

All the elaborated nanoparticles displayed nanometric size, around 300–427 nm, where NLC displayed slightly bigger size than SLNs. Both formulations presented PDI below 0.5 (NLCs 0.4 and SLNs 0.3), meaning that the sample was monodisperse. In addition, encapsulation efficiency values were also high, 80–95%, meaning that almost all the drug added to the formulation was encapsulated. Finally, antibiotic-loaded SLN and NLC showed sustained release profile, liberating at least 50% of the drug content during the first 24 h.

3.2. Antimicrobial activity of free and nanoencapsulated colistin sulfate

All the isolates were susceptible ($\text{MIC} \leq 4 \mu\text{g/mL}$) to free colistin and to NLC-colistin prepared by using trehalose as cryoprotectant. On the other hand, almost all (97%) were susceptible to NLC-colistin stabilized with mannitol a value identical to the one obtained when the isolates were assayed in SLN-colistin with trehalose. When comparing both types of nanoparticles (SLN and NLC) stabilized by mannitol, it

becomes apparent that NLC were much more active than SLN accounting 3 and 19 % of survival ($p < 0.05$). Moreover, the comparison between SLN-colistin stabilized by mannitol and trehalose, one can conclude that differences were also significant ($p < 0.05$). In conclusion, it was demonstrated that NLC were more active than SLN and that trehalose was more adequate to be used as cryoprotectant in the preparation of nanoparticulated colistin.

Empty lipid nanoparticles had no antibacterial activity (Table 1). Based on the results showed in Table 1, the effect of the temperatures of storage over time was only tested for nanoparticles stabilized with trehalose. After storages of 3 months at 25 $^{\circ}\text{C}$, 30 $^{\circ}\text{C}$, and 40 $^{\circ}\text{C}$, SLN nanoparticles loose antimicrobial activity (MICs increased between 1 and 2 dilutions). In contrast, NLC maintained similar levels of activity after storage at different conditions for 9 months. Mucoid isolate 086SJD was initially less susceptible to SLN-colistin than non-mucoid isolates, suggesting that the mucoid state could alter the effect of SLN but not NLC. After 3 months, storage at different temperatures, MICs of isolates to NLC-colistin became lower than those of SLN-colistin. Antibacterial activity of NLC-colistin remained stable for all isolates and tested temperatures, giving MIC values similar to those of fresh nanoparticles. Our results showed that NLC were more stable than SLN and that they can be employed in a wider range of storage temperatures without relevant modifications on their antimicrobial activity. Thus, NLC stabilized with trehalose was the chosen formulation for further experiments. According to some authors[26,27], NLC, which are a second generation of lipid nanoparticles, have higher drug loading capacity than SLN (first generation of lipid nanoparticles) and do not present drug expulsion during storage.

3.3. Effect of free and nanoencapsulated colistin on growth

Both isolates (056SJD and P19) had similar susceptibilities to free colistin, nanoencapsulated colistin, and empty nanoparticles with free colistin at all concentrations tested (Fig. 1).

At subinhibitory concentrations of antimicrobials ($1/4 \times \text{MIC}$), no differences were observed among the formulations tested, being rates of growth slightly lower than those of the drug-free control (Fig. 1a,d). At MIC, the inhibitory effect was higher on the susceptible isolate although none of the formulations were able to fully inhibit bacterial growth of the resistant isolate after 4 h of antimicrobial exposure (Fig. 1b,e). At concentrations above MIC, bacterial growth was immediately inhibited after the addition of the antimicrobial (Fig. 1c,f). Empty lipid nanoparticles did not have antibacterial activity (data not shown).

Table 1
Free and nanoencapsulated colistin susceptibility in CF *P. aeruginosa* isolates.

Susceptibility range	Percentage of resistant clinical strains (%)					
	Free Colistin	NLC Colistin (mannitol)	NLC Colistin (trehalose)	SLN Colistin (mannitol)	SLN Colistin (trehalose)	Empty NLC
Resistant ($\text{MIC} \geq 8 \mu\text{g/mL}$)	0.0	3.0	0.0	19.0	3.0	100.0

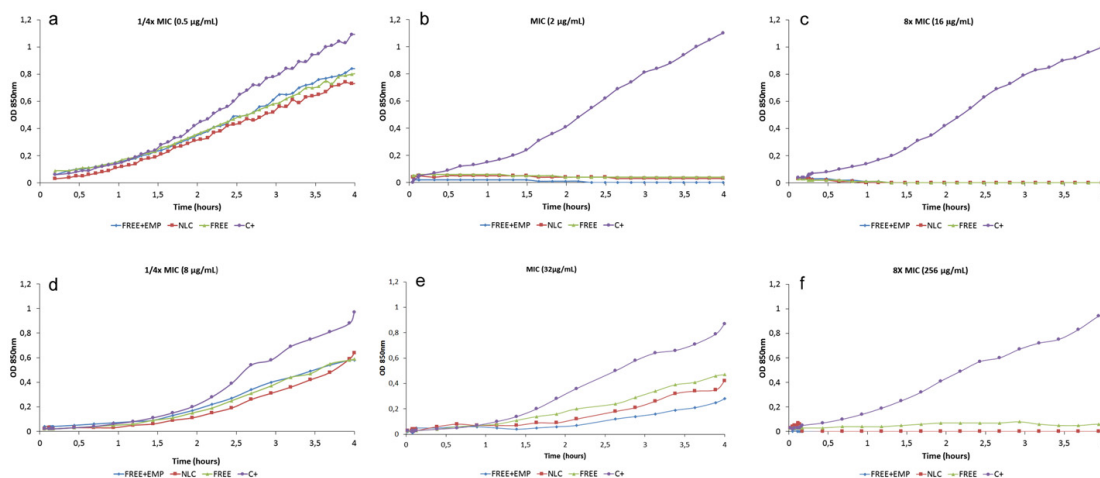


Fig. 1. Effect of free colistin, NLC of colistin, and mixtures of empty nanoparticles and free colistin on *P. aeruginosa* growth. (a) 056SJD at 1/4 × MIC (0.5 µg/mL); (b) 056SJD at MIC (2 µg/mL); (c) 056SJD at 8 × MIC (16 µg/mL); (d) P19 at 1/4 × MIC (8 µg/mL); (e) P19 at MIC (32 µg/mL), and (f) P19 at 8x MIC (256 µg/mL). All incubations were at 37 °C with shaking at 2000 rpm and bacteria were in the exponential phase of growth.

3.4. Anti-biofilm efficacy of free and nanoencapsulated colistin

To test the influence of the NLC nanoparticles on colistin's ability to kill sessile bacteria, biofilms of six *P. aeruginosa* were exposed to free and nanoencapsulated colistin at concentrations between 0 and 2560 µg/mL. NLC-colistin had higher antibiofilm activity than free colistin in both susceptible and resistant isolates (Table 2). Whereas concentrations of free colistin and also when empty nanoparticles and free colistin were used together, colistin concentrations required to completely eradicate biofilm ranged from 640 to 2560 µg/mL, in contrast, concentrations of NLC-colistin needed for biofilm removal were much lower (160 and 320 µg/mL, respectively). These values were quite similar either in mucoid, non-mucoid, and reference strain as well. Since it seems clear that biofilms play a key role in respiratory infections in CF patients by *P. aeruginosa*, NLC-colistin could open new frontiers in the treatment of such infections. Despite the intimate mechanism by which colistin in NLC is so efficient in biofilm removal remains unknown, data clearly show that it is directly derived from the nanopharmaceutical form since free colistin plus empty NLC do not have significant effect on MBEC values (at maximum one dilution) whereas NLC-colistin gave MBEC values up to four dilutions. As Pamp et al. [28] pointed out, free colistin acts

preferentially on bacteria with low metabolic rates, that is to say in a biofilm free colistin is going to be more active on the microbes located deep in the multilayered biofilm, since metabolic activity decreases when distance to surface increases. It could be also feasible that nanoencapsulated colistin would not distinguish between metabolically active bacteria and starved individuals, but this has not been experimentally demonstrated. Another possibility is in close relation with the charge distribution. NLC-colistin has a negative net charge, whereas free colistin has a positive net charge. Lipopolysaccharide has also negative charge, and this charge is higher at stationary phase of growth, than at exponential phase; subsequently, NLC-colistin (negatively charged) action on exponentially growing bacteria would be favored. It is well known that *P. aeruginosa* exposed for long periods to colistin exhibits a mechanism of resistance based on the up-regulation of a two-component system (or more). This leads to the addition of 4-aminoarabinose to lipid A of the LPS molecule reducing the net negative charge of LPS and limiting its interaction with polycationic antibiotics (adaptive resistance) [29]. When resistant strains (P19 and P20) were tested by their susceptibility to free and nanoencapsulated colistin, results demonstrate that also in this case nanoencapsulated colistin was more active against biofilms than free colistin. This is in agreement with the hypothesis that net charge would be the main reason of different activities.

Table 2
MBEC values for free and NLC of colistin.

Isolate	MBEC (µg/mL)					
	ATCC 27853	PAO1	056SJD	086SJD	P19	P20
Free colistin	2560	2560	1280	640	1280	2560
FREE + EMP ^a	1280	1280	1280	1280	1280	2560
NLC-colistin	320	160	320	160	320	320

^a FREE + EMP = Free colistin and empty NLC nanoparticles.

Table 3
Biofilm prevention concentration (BPC) values for free and NLC of colistin.

Isolate	BPC (µg/mL)					
	ATCC 27853	PAO1	056SJD	086SJD	P19	P20
Free colistin	2	8	2	4	32	16
FREE + EMP ^a	2	8	2	4	32	16
NLC-colistin	2	8	2	4	32	16

^a FREE + EMP = Free colistin and empty NLC nanoparticles.

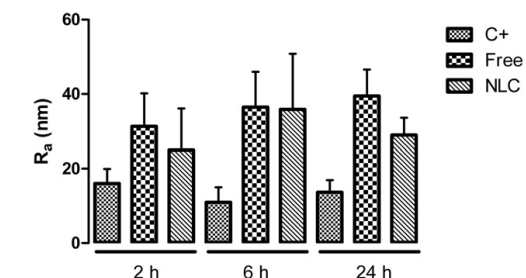
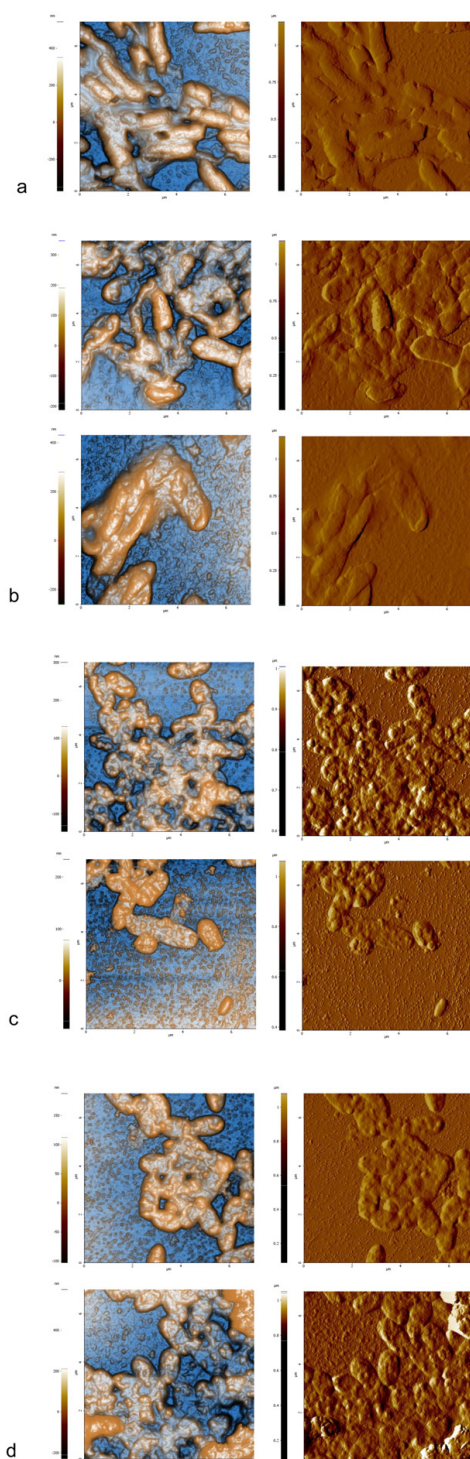


Fig. 3. Graphical representation of surface roughness (R_a) in nanometers, according to the different formulations tested and surface scans. Bars represent the standard deviation of the mean.

There are no previously reported data on the antimicrobial activity of NLC-colistin against *P. aeruginosa* biofilms.

3.5. Prevention of *P. aeruginosa* biofilm formation with free and nanoencapsulated colistin

To test the efficacy of NLC-colistin to prevent the biofilm formation, *P. aeruginosa* biofilms were exposed to free and nanoencapsulated colistin, and the combination of free colistin and empty nanoparticles (at ranges between 0 and 256 $\mu\text{g/mL}$).

As shown in Table 3, for all the isolates tested, BPC values of NLC-colistin were identical to values for free colistin and the mixture of empty NLC and free colistin. All formulations had BPCs coincident with MICs. Whereas NLC-colistin was more effective than free colistin in eradicating biofilms, both free and nanoencapsulated colistin did not show any differences on the prevention of biofilm formation.

3.6. Visualization of *P. aeruginosa* 056SJD treated with free and nanoencapsulated colistin

AFM topography and amplitude images of *P. aeruginosa* 056SJD biofilms after treatment with free and nanoencapsulated colistin at 2, 6, and 24 h, as well as AFM images of untreated bacterial biofilms are shown in Fig. 2. Topography images gave information about surface and structure differences whereas amplitude images allowed a better observation of surface characteristics and fine details [30]. Based on AFM images, untreated biofilms were compared to a control and presented the typical *P. aeruginosa* bacilli shape without alterations in its surface (Fig. 2a). After both free and nanoencapsulated colistin treatment, biofilm forming bacteria resulted severely altered. Moreover, these alterations in biofilm gradually increased over time. However, it was also observed that non-relevant differences existed between free and nanoencapsulated colistin (Fig. 2b, c, and d). AFM is an

Fig. 2. AFM images obtained at 7 μm^2 of scan size of (a) untreated *P. aeruginosa* biofilms; (b) after treatment with 128 $\mu\text{g/mL}$ of free (first row) and nanoencapsulated (second row) colistin sulfate at 2 h; (c) after treatment with 128 $\mu\text{g/mL}$ of free (first row) and nanoencapsulated (second row) colistin sulfate at 6 h; (d) after treatment with 128 $\mu\text{g/mL}$ of free (first row) and nanoencapsulated (second row) colistin sulfate at 24 h. First column shows topography images, whereas amplitude images are shown in second column.

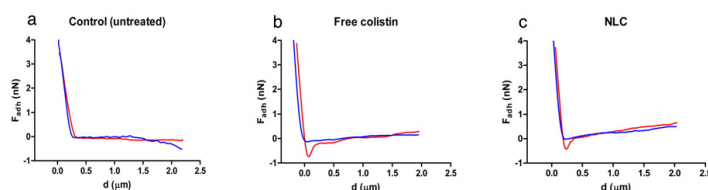


Fig. 4. Typical force–distance curves of untreated and colistin and NLC-colistin-treated *P. aeruginosa* 056SJD.

excellent tool widely used to shed some light not only in imaging parameters—topography, error signal, phase—but also in cell mechanics at the nanoscale resolution—adhesion forces, elasticity, etc.—and roughness, being extremely sensitive due to its ability to detect a large range of forces, from nN to pN. One of the main goals of the fight against biofilm is to induce changes that could decrease the physical stability of biofilm. We have used such measurements to explore the eventual differences in adhesion forces due to the treatment with colistin and nanoencapsulated colistin. As can be seen, surface nanoroughness varied (Fig. 3) being the lower those of control whereas both free and NLC-colistin induce drastic increases in cellular surface roughness. Fig. 4 shows time–force curves generated by bacteria also treated with free and NLC-colistin. Tip–cell–surface adhesion force of untreated, as well as NLC-colistin- and free-colistin-treated bacteria resulted to be 145 ± 33 , 885 ± 195 , and 701 ± 239 , respectively. We found that values in NLC-colistin-treated bacteria were higher than those of control and that colistin-treated were even higher than those measured in NLC-colistin-treated biofilms although very similar. This is in agreement with the hypothesis that nanoparticles do not have direct effect on biofilm but facilitate the direct antimicrobial effect of colistin, and also with the results recorded when empty nanoparticles were tested.

4. Conclusions

New antimicrobial formulations are being developed to improve survival of patients with cystic fibrosis, reduce antimicrobial resistance, enhance intrapulmonary concentrations of drugs, and fight bacterial biofilms [31,32]. Design of new delivery strategies such as lipid nanoparticles may help in fighting multidrug-resistant bacteria as well as microbial biofilms. Here, we have investigated the application of colistin-charged lipid nanoparticles toward *P. aeruginosa* in planktonic cultures and biofilms. Although colistin nanoparticles presented the same *in vitro* antimicrobial activity as free drug against planktonic bacteria, nanoencapsulated colistin was much more efficient in the eradication of biofilms. *In vivo* experiments would be necessary to further examine the suitability of the use of NLC on *P. aeruginosa* infections.

Conflict of interest and sources of funding statement

The authors declare that there are no conflicts of interest in this study.

Acknowledgments

Authors specially thank the generous gift of colistin sulfate by Shenghua Biok Biology Co., LTD. (China). Bacterial strains were generously given by Hospital Vall d'Hebron and Hospital Sant Joan de Déu. This work was carried out under the Comprehensive Research on Effective Therapies for the Treatment of Cystic Fibrosis and Associated Diseases (TERFIQEC); IPT-2011-1402-900000 funded by the Spanish Ministry of Economy and Competitiveness. The authors gratefully acknowledge the support of University of the Basque Country UPV/EHU (UFI11/32) and the support of the Basque Government by IT 428-10 consolidated group.

References

- [1] Ramsey BW. Management of pulmonary disease in patients with cystic fibrosis. *N Engl J Med* 1996;335:179–88.
- [2] Drenkard E, Ausubel FM. *Pseudomonas* biofilm formation and antibiotic resistance are linked to phenotypic variation. *Nature* 2002;416:740–3.
- [3] Fusté E, López-Jiménez L, Segura C, Gainza E, Vinuesa T, Viñas M. Carbapenem-resistance mechanisms of multidrug-resistant *Pseudomonas aeruginosa*. *J Med Microbiol* 2013;62:1317–25.
- [4] Westerman EM, Heijerman HG, Frijlink HW. Dry powder inhalation versus wet nebulisation delivery of antibiotics in cystic fibrosis patients. *Expert Opin Drug Deliv* 2007;4:91–4.
- [5] Döring G, Conway SP, Heijerman HG, Hodson ME, Hoiby N, Smyth A, et al. Antibiotic therapy against *Pseudomonas aeruginosa* in cystic fibrosis: a European consensus. *Eur Respir J* 2000;16:749–67.
- [6] Bergen PJ, Landersdorfer CB, Zhang J, Zhao M, Lee HJ, Nation RL, et al. Pharmacokinetics and pharmacodynamics of 'old' polymyxins: what is new? *Diagn Microbiol Infect Dis* 2012;74:213–23.
- [7] Nicolau DP. Carbapenems: a potent class of antibiotics. *Expert Opin Pharmacother* 2008;9:23–37.
- [8] Beringer P. The clinical use of colistin in patients with cystic fibrosis. *Curr Opin Pulm Med* 2001;7:434–40.
- [9] Lim LM, Ly N, Anderson D, Yang JC, Macander L, Jarkowski III A, et al. Resurgence of colistin: a review of resistance, toxicity, pharmacodynamics, and dosing. *Pharmacotherapy* 2010;30:1279–91.
- [10] Döring G, Hoiby N. Early intervention and prevention of lung disease in cystic fibrosis: a European consensus. *J Cyst Fibros* 2004;3:67–91.
- [11] Gales AC, Jones RN, Sader HS. Contemporary activity of colistin and polymyxin B against a worldwide collection of Gram-negative pathogens: results from the SENTRY Antimicrobial Surveillance Program (2006–09). *J Antimicrob Chemother* 2011;66:2070–4.
- [12] Carmeli Y, Troillet N, Eliopoulos GM, Samore MH. Emergence of antibiotic-resistant *Pseudomonas aeruginosa*: comparison of risks associated with different antipseudomonal agents. *Antimicrob Agents Chemother* 1999;43:1379–82.
- [13] Li J, Turnidge J, Milne R, Nation RL, Coulthard K. *In vitro* pharmacodynamic properties of colistin and colistin methanesulfonate

- against *Pseudomonas aeruginosa* isolates from patients with cystic fibrosis. *Antimicrob Agents Chemother* 2001;45:781–5.
- [14] Ghaffari S, Varshosaz J, Saadat A, Atyabi F. Stability and antimicrobial effect of amikacin-loaded solid lipid nanoparticles. *Int J Nanomedicine* 2010;6:35–43.
 - [15] Abdelghany SM, Quinn DJ, Ingram RJ, Gilmore BF, Donnelly RF, Taggart CC, et al. Gentamicin-loaded nanoparticles show improved antimicrobial effects towards *Pseudomonas aeruginosa* infection. *Int J Nanomedicine* 2012;7:4053–63.
 - [16] Cipolla D, Shekunov B, Blanchard J, Hickey A. Lipid-based carriers for pulmonary products: preclinical development and case studies in humans. *Adv Drug Deliv Rev* 2014;75:53–80.
 - [17] Pelgrift RY, Friedman AJ. Nanotechnology as a therapeutic tool to combat microbial resistance. *Adv Drug Deliv Rev* 2013;65:1803–15.
 - [18] Pastor M, Moreno-Sastre M, Esquisabel A, Sans E, Viñas M, Bachiller D, et al. Sodium colistimethate loaded lipid nanocarriers for the treatment of *Pseudomonas aeruginosa* infections associated with cystic fibrosis. *Int J Pharm* 2014;477:485–94.
 - [19] Obeidat WM, Schwabe K, Müller RH, Keck CM. Preservation of nanostructured lipid carriers (NLC). *Eur J Pharm Biopharm* 2010;76:56–67.
 - [20] Belouqui A, Solinís MÁ, Gascón AR, del Pozo-Rodríguez A, des Rieux A, Pr  at V. Mechanism of transport of saquinavir-loaded nanostructured lipid carriers across the intestinal barrier. *J Control Release* 2013;166:115–23.
 - [21] Clinical and Laboratory Standards Institute. M100-S20. Performance standards for antimicrobial susceptibility testing. 20th informational supplement. Wayne, PA: CLSI; 2010.
 - [22] Moskowitz SM, Foster JM, Emerson J, Burns JL. Clinically feasible biofilm susceptibility assay for isolates of *Pseudomonas aeruginosa* from patients with cystic fibrosis. *J Clin Microbiol* 2004;42:1915–22.
 - [23] Fern  ndez-Olmos A, Garc  a-Castillo M, Maiz L, Lamas A, Baquero F, Cant  n R. In vitro prevention of *Pseudomonas aeruginosa* early biofilm formation with antibiotics used in cystic fibrosis patients. *Int J Antimicrob Agents* 2012;40:173–6.
 - [24] Yapa WS, Patel K, Li J, Wilson JW, Dooley MJ, George J, et al. Pulmonary and systemic pharmacokinetics of inhaled and intravenous colistin methanesulfonate in cystic fibrosis patients: targeting advantage of inhalational administration. *Antimicrob Agents Chemother* 2014;58:2570–9.
 - [25] Dorobantu LS, Bhattacharjee S, Foght JM, Gray MR. Atomic force microscopy measurement of heterogeneity in bacterial surface hydrophobicity. *Langmuir* 2008;24:4944–51.
 - [26] Martins S, Sarmiento B, Ferreira DC, Souto EB. Lipid-based colloidal carriers for peptide and protein delivery-liposomes versus lipid nanoparticles. *Int J Nanomedicine* 2007;2:595–607.
 - [27] Weber S, Zimmer A, Pardeike J. Solid lipid nanoparticles (SLN) and nanostructured lipid carriers (NLC) for pulmonary application: a review of the state of the art. *Eur J Pharm Biopharm* 2014;86:7–22.
 - [28] Pamp SJ, Gjermansen M, Johansen HK, Tolker-Nielsen T. Tolerance to the antimicrobial peptide colistin in *Pseudomonas aeruginosa* biofilms is linked to metabolically active cells, and depends on the pmr and mexAB-oprM genes. *Mol Microbiol* 2008;68:223–40.
 - [29] Gooderham WJ, Hancock RE. Regulation of virulence and antibiotic resistance by two-component regulatory systems in *Pseudomonas aeruginosa*. *FEMS Microbiol Rev* 2009;33:279–94.
 - [30] Dubrovina EV, Voloshin AG, Kraevsky SV, Ignatyuk TE, Abramchuk SS, Yaminsky IV, et al. Atomic force microscopy investigation of phage infection of bacteria. *Langmuir* 2008;24:13068–74.
 - [31] Veiga-Crespo P, Fust   E, Vinuesa T, Vi  as M, Villa TG. Synergism between outer membrane proteins and antimicrobials. *Antimicrob Agents Chemother* 2011;55:2206–11.
 - [32] Gould IM, Bal AM. New antibiotic agents in the pipeline and how they can help overcome microbial resistance. *Virulence* 2013;4:185–91.

PAPER 4



Stability study of sodium colistimethate-loaded lipid nanoparticles

M. Moreno-Sastre, M. Pastor, A. Esquisabel, E. Sans, M. Viñas, D. Bachiller & J. L. Pedraz

To cite this article: M. Moreno-Sastre, M. Pastor, A. Esquisabel, E. Sans, M. Viñas, D. Bachiller & J. L. Pedraz (2016) Stability study of sodium colistimethate-loaded lipid nanoparticles, Journal of Microencapsulation, 33:7, 636-645, DOI: [10.1080/02652048.2016.1242665](https://doi.org/10.1080/02652048.2016.1242665)

To link to this article: <http://dx.doi.org/10.1080/02652048.2016.1242665>



Accepted author version posted online: 28 Sep 2016.
Published online: 14 Oct 2016.



Submit your article to this journal [↗](#)



Article views: 43



View related articles [↗](#)



View Crossmark data [↗](#)

RESEARCH ARTICLE

Stability study of sodium colistimethate-loaded lipid nanoparticles

M. Moreno-Sastre^{a,b,*}, M. Pastor^{a,b,*}, A. Esquisabel^{a,b}, E. Sans^c, M. Viñas^{c,d}, D. Bachiller^{e,f} and J. L. Pedraz^{a,b}

^aNanoBioCel Group, Laboratory of Pharmaceutics, School of Pharmacy, University of the Basque Country (UPV/EHU), Vitoria-Gasteiz, Spain; ^bBiomedical Research Networking Centre in Bioengineering, Biomaterials and Nanomedicine (CIBER-BBN), Vitoria-Gasteiz, Spain; ^cDepartment of Pathology and Experimental Therapeutics, Medical School, University of Barcelona – IDIBELL, Barcelona, Spain; ^dINFACTS, CESPU, Gandra, Portugal; ^eDevelopment and Regeneration Programme, Fundación Investigaciones Sanitarias Islas Baleares (FISIB), Bunyola (Balearic Islands), Spain; ^fConsejo Superior de Investigaciones Científicas (CSIC), Bunyola (Balearic Islands), 7110, Spain

ABSTRACT

In the last decades, the encapsulation of antibiotics into nanoparticulate carriers has gained increasing attention for the treatment of infectious diseases. Sodium colistimethate-loaded solid lipid nanoparticles (Colist-SLNs) and nanostructured lipid carriers (Colist-NLCs) were designed aiming to treat the pulmonary infection associated to cystic fibrosis patients. The nanoparticles were freeze-dried using trehalose as cryoprotectant. The stability of both nanoparticles was analysed over one year according to the International Conference of Harmonisation (ICH) guidelines by determining the minimum inhibitory concentration (MIC) against clinically isolated *Pseudomonas aeruginosa* strains and by studying their physico-chemical characteristics. The results showed that Colist-SLNs lost their antimicrobial activity at the third month; on the contrary, the antibacterial activity of Colist-NLCs was maintained throughout the study within an adequate range (MIC $\leq 16 \mu\text{g/mL}$). In addition, Colist-NLCs exhibited suitable physico-chemical properties at 5 °C and 25 °C/60% relative humidity over one year. Altogether, Colist-NLCs proved to have better stability than Colist-SLNs.

ARTICLE HISTORY

Received 22 February 2016
Revised 18 September 2016
Accepted 27 September 2016
Published online 13 October 2016

KEYWORDS

Stability; solid lipid nanoparticle; nanocarriers; sodium colistimethate; antimicrobial activity



Introduction

Over the last decades, the use of lipid nanoparticles (NPs) for drug delivery in pharmaceutical technology has been extensively investigated (Das and Chaudhury, 2011). Lipid nanoparticles show interesting features concerning their therapeutic application as they are able to incorporate a great variety of substances. In this regard, solid lipid nanoparticles (SLNs) have emerged as promising nanosystems to encapsulate drugs in the submicron range, from about 50 to 1000 nm. SLNs are composed of biocompatible and biodegradable lipids building a solid lipid matrix core but due to their low drug loading and unpredictable drug release, nanostructured lipid carriers (NLCs) have been developed as a second generation of lipid nanoparticles (Muller et al., 2000). The main difference between them is the structure of the lipid matrix that in the NLCs is composed of a mixture of solid and liquid lipids resulting in a less-ordered matrix with many imperfections that permit the increase of drug loading and prevent its leakage (Muller et al., 2007).

In principle, these NPs present some advantages over other drug delivery systems such as a controlled drug delivery, specific targeting, good tolerability, the ability to incorporate lipophilic and hydrophilic drugs and the possibility to protect the drug from degradation (Weber et al., 2014). Nevertheless, the major obstacle that limits the use of these nanoparticles is their physical or chemical instability in aqueous suspensions (Chacon et al., 1999). To overcome this drawback, the water content must be removed to convert the nanoparticle suspension into a solid-phase formulation able to display suitable stability for long-term storage.

For this purpose of improving stability, freeze-drying, also known as lyophilisation, is the technique usually applied in the pharmaceutical and technological industry (Abdelwahed et al., 2006). This process consists on removing the water from a frozen sample by sublimation and desorption under vacuum, hence decreasing hydrolysis phenomena (Jennings, 1999). Before freezing the sample, the addition of cryoprotectants might be required to protect the nanoparticles against mechanical stress of ice crystals or to prevent their aggregation. The most commonly used cryoprotectants are sugars like glucose, trehalose, sucrose and mannitol. Trehalose is widely used as it possesses low hygroscopicity, very low chemical reactivity and also high glass transition temperature (Crowe et al., 1996; Schwarz and Mehnert, 1997). It has been shown that samples lyophilised in the presence of sugars with high transition temperature (T_g) show less tendency to aggregate during storage as compared to sugars with lower T_g , such as sucrose or glucose (Molina et al., 2004).

Sodium colistimethate, which is rapidly hydrolysed to its active form (colistin), is a polypeptide antibiotic known to have potential bactericidal activity against a broad range of Gram-negative bacteria that is being administered in patients with pulmonary infections, particularly those suffering from with cystic fibrosis (Dijkmans et al., 2014). *Pseudomonas aeruginosa* is the main pathogen that affects cystic fibrosis patients showing a significant increase in its resistance to antimicrobial drugs in the last years. Sodium colistimethate has demonstrated its efficiency in combating this bacterium (minimum inhibitory concentration (MIC) susceptibility data $\leq 0.06\text{--}16 \mu\text{g/mL}$); however, its clinical use is limited due to its toxic effects such as nephrotoxicity and

CONTACT J. L. Pedraz  joseluis.pedraz@ehu.es  NanoBioCel Group, Laboratory of Pharmaceutics, School of Pharmacy, University of the Basque Country (UPV/EHU), Paseo de la Universidad 7, 01006 Vitoria-Gasteiz, Spain

*Both authors contributed equally.

© 2016 Informa UK Limited, trading as Taylor & Francis Group

neuromuscular blockade (Falagas and Kasiakou, 2005). It has been reported that nano-antibiotics administered by the pulmonary route may increase local drug concentration and avoid systemic adverse effects (Moreno-Sastre et al., 2015). In that sense, SLNs and NLCs have emerged as alternative vehicles for antibiotic delivery to the lungs as they can protect the drug from chemical and enzymatic degradation and gradually release it from the lipid matrix in the target site, thus minimising the toxicity and improving the antimicrobial effect (Huh and Kwon, 2011).

In our previous work, the preparation and characterisation of sodium colistimethate-loaded SLNs (Colist-SLNs) and NLCs (Colist-NLCs) were described (Pastor et al., 2014). In the present study, the stability of Colist-SLNs and Colist-NLCs after freeze-drying was investigated by determining their antimicrobial activity against several strains of *P. aeruginosa* (ATCC 27853, 056 SJD, 086 SJD) and the maintenance of their physicochemical properties over one year. NPs were stored for 12 months under four different conditions, selected as recommended in the International Conference on Harmonisation (ICH) guidelines: (a) long-term refrigerator at $5 \pm 3^\circ\text{C}$, (b) long-term room temperature at $25 \pm 2^\circ\text{C}/60 \pm 5\%$ relative humidity (RH), (c) intermediate at $30 \pm 2^\circ\text{C}/65\% \pm 5\%$ RH and (d) accelerated at $40 \pm 2^\circ\text{C}/75 \pm 5\%$ RH (Grimm, 1998; Guideline, 2003).

Materials and methods

Materials

Precirol® ATO 5 was kindly provided by Gattefossé (Madrid, Spain). Koliphor® P188 (Poloxamer 188) was a kind gift from BASF (Ludwigshafen, Germany). Tween® 80 was purchased from Panreac Química (Castell del Vallès, Barcelona, Spain). Miglyol® 812 was provided by Sasol (Johannesburg, South Africa). Sodium colistimethate was purchased from Sigma Aldrich (St. Louis, MO). All the chemicals were of analytical grade.

Preparation of colistimethate-loaded SLNs and NLCs

SLNs and NLCs containing sodium colistimethate were prepared as previously reported methods (Pastor et al., 2014). Colist-SLNs were elaborated by an emulsion-solvent-evaporation technique. Briefly, 10 mg of sodium colistimethate (drug loading at 10%) were mixed with Precirol® ATO 5 as lipid phase and dissolved in dichloromethane solution (5%, w/v). An aqueous solution containing Poloxamer 188 (1%, w/v) and Tween® 80 (1%, w/v) was also prepared (organic/aqueous phase SLN: 1:5). The aqueous phase was added into the lipid phase and then the mixture was sonicated at 20 W for 30 seconds (Branson Sonifier 250 Danbury, CT). The resulting emulsion was stirred for 2 h allowing the evaporation of the solvent. Subsequently, SLNs were washed by centrifugation in Amicon® centrifugal filtration units (100 000 Da MWCO) at 2500 rpm for 15 min three times.

On the other hand, Colist-NLCs were elaborated by the hot melt homogenisation technique. In brief, solid (Precirol® ATO 5) and liquid (Miglyol® 812) lipids at 10:1 were first weighed along with sodium colistimethate at a drug loading of 10% (w/w) and heated above the melting temperature of the solid lipid (at 60°C). In a separate container, Tween® 80 (1.3%, w/v) and Poloxamer 188 (0.6%, w/v) were dissolved in Milli-Q water and heated at the same temperature as the lipid phase. The hot aqueous surfactant solution was poured into the lipid phase and emulsified by sonication for 15 seconds at 20 W. This step produced a nano-emulsion that was stored at low temperature ($5 \pm 3^\circ\text{C}$) for 12 h to allow the recrystallisation of the lipids for NLCs formation. After that period,

the nanoparticles were washed by centrifugation at 2500 rpm in Amicon® centrifugal filtration units (100 000 Da MWCO) three times. Finally, all the nanoparticles prepared were freeze-dried.

Freeze-drying of the nanoparticles

Lyophilisation of the nanoparticles was used to prolong the stability of Colist-SLNs and Colist-NLCs during storage. Prior to freeze-drying, trehalose (15%, w/w of the lipid solid) was added to the nanoformulations as a cryoprotectant, and thereafter were freeze dried for 40 h (Telstar Lyobeta freeze-dryer, Terrasa, Spain). Freeze-drying cycle can be divided into three steps: freezing, primary drying and secondary drying. The primary drying took place for 24 h and the secondary drying step was maintained for 12 h in order to low humidity in the sample. Milli-Q water was used for redispersing the nanoparticles for NP characterisation.

Stability study

Each different batch of Colist-SLNs and Colist-NLCs was divided into four different sample sets. All samples were stored in plain glass vials (USP type I) in environmental simulation chambers for constant climatic conditions (Binder, Tuttlingen, Germany) according to ICH Q1 A (R2) guidelines (CPMO/ICH/2736/99) that were: $5 \pm 3^\circ\text{C}$, $25 \pm 2^\circ\text{C}/60 \pm 5\%$ RH, $30 \pm 2^\circ\text{C}/65 \pm 5\%$ RH and $40 \pm 2^\circ\text{C}/75 \pm 5\%$ RH (Table 1).

Parameters such as size, zeta potential, morphological characteristics and antimicrobial activity were studied over the time until 12 months of storage and compared to the fresh formulations (after freeze-drying, time 0) so that the changes observed of these characteristics could be attributed to sample exposure to different temperatures and humidity conditions. In addition, a drug release study testing Colist-NLCs was performed at 12 months to ensure the sustained release of the drug by that time. The specifications of the freeze-dried product are described in Table 2, these have been established according to the results of the fresh nanoparticles (time 0) and based on previous experience with this type of nanoformulations.

At the beginning of the stability study, an acceptance criterion was established for the microbiological assay stating the

Table 1. Stability test store conditions of temperature and relative humidity (RH) intervals and sampling time for all the four experiments.

Samples	Groups	Storage conditions	Time points
Colist-NLC	Long-term refrigerated	$5 \pm 3^\circ\text{C}$	0,1,3,6,9 and 12 months
Colist-SLN	Long-term room temperature	$25 \pm 2^\circ\text{C}$	0,1,3,6,9 and 12 months
		$60 \pm 5\%$ RH	
	Intermediate	$30 \pm 2^\circ\text{C}$	0,1,3,6,9 and 12 months
		$65 \pm 5\%$ RH	
	Accelerated	$40 \pm 2^\circ\text{C}$	0,1,3,6,9 ^a and 12 ^a months
		$75 \pm 5\%$ RH	

^aAdditional sampling time points not established by the ICH CPMO/ICH/2736/99.

Table 2. Specifications of the freeze-dried nanoparticles.

Parameters	Specifications
Size	≤ 500 nm
PDI	≤ 0.5
Zeta potential	≤ -20 mV
Macroscopic appearance	White powder
Microscopic morphology (TEM)	Spherical shape
Antibacterial activity (MIC)	≤ 16 µg/mL
Drug release profile	$\geq 80\%$ at 24 h

PDI: polydispersity index; TEM: transmission electron microscopy; MIC: minimum inhibitory concentration.

maximum MIC at 16 µg/mL. As Colist-SLNs formulations displayed a value higher than 16 µg/mL at the third month, meaning a loss of activity against bacteria, Colist-SLNs were set aside for the stability study for the following months. This is the reason why the drug release test was not carried out for this formulation at the end of the stability study.

Characterisation

Encapsulation efficiency

The encapsulation efficiency (EE) of sodium colistimethate into NPs was calculated by the following equation:

$$EE(\%) = \frac{(\text{initial drug amount} - \text{non-encapsulated drug})}{\text{initial drug amount}} \times 100$$

In this method the non-entrapped drug was determined by a high-performance liquid chromatography (HPLC) analysis from the supernatants collected after centrifugation. The HPLC technique was performed using a Waters 1525 HPLC Binary Pump (Waters Corp., Milford, CT) with a UV-detector Waters 2487 and Waters 717 plus autosampler adapted, as described in our previous work (Pastor et al., 2014). The system was controlled by the Empower 3 software. A Novapak C18 × 150 mm column with a 4 µm pore size was used as the stationary phase, whereas mixture of acetonitrile and an aqueous solution 23:77 (v/v) was used as mobile phase. The aqueous phase consisted of sodium sulphate (7.1 g/L), acetic (0.6 g/L) and phosphoric acid (2.2 g/L) and adjusted with triethylamine at pH 2.5. The column temperature, flow rate of mobile phase, injection volume for isocratic elution and detection wavelength were set as 65 °C, 1.5 mL/min, 50 µL and 206 nm, respectively. This analytic technique was previously validated following EMA guidance for bioanalytical methods. The calibration curve was linear ($r^2 > 0.9991$) within the concentration range 100–800 µg/mL. The mobile phase and surfactant presented no interference under the assessed conditions.

Particle size and zeta potential

The mean particle size and polydispersity index (PDI) were assessed by photon correlation spectroscopy (also known as dynamic light scattering) and Zeta potential (ZP) was determined by laser doppler velocimetry using a Zetasizer Nano ZS (Malvern Instruments, Ltd., Worcestershire, UK). Prior to the measurements, all samples were diluted with purified water to reach a suitable scattering intensity. Measurements were performed at 25 °C. Time 0 is considered as the time just after the lyophilisation step. All the measurements of each nanoparticle formulation were performed in triplicate.

Nanoparticle morphology study

Macroscopic characteristics. The physical appearance of Colist-NPs was studied over the time by visual inspection.

Microscopic appearance. Nanoparticles morphology was examined by a transmission electron microscope (TEM, Philips CM120 BioTWIN TEM, Eindhoven, Holland) at an accelerating voltage of 120 kV. Samples were prepared by drying a dispersion of the nanoparticles on a copper grid coated with an amorphous carbon film and then negative staining with 1% uranyl acetate for observation.

Measurement of antimicrobial activity

Pseudomonas aeruginosa strains were used to test the antimicrobial activity of the nanoparticles. Microbiological and biochemical

assays were performed in order to select and identify the different bacteria, i.e. morphology and colony observation in McConkey agar, Blood agar, TSA (Tryptone Soy Agar) and MHA (Mueller Hinton Agar) at 37 °C for 24–48 h, oxidase test, oxidative/fermentative test (O/F), and Kliger medium assay. Among the isolated strains, 056 SJD and 086 SJD that were recovered from the sputum of cystic fibrosis patients were selected for the stability study, presenting non-mucoid and mucoid characteristics, respectively. Additionally, the *P. aeruginosa* ATCC 27853 strain was also assessed.

The MIC of the free drug and nanoformulations was determined by the broth microdilution method. A bacterial inoculum was prepared from an overnight culture in Mueller–Hinton II Broth Cation-Adjusted (MHBCA) and adjusted to yield 10^4 CFU/well (colony-forming units). The inoculum was then delivered onto 96-well plates containing two-fold serial dilutions of formulations starting from 32 µg/mL. Finally, the plates were incubated for 24 h at 37 °C. Free antibiotic (sodium colistimethate), Colist-SLNs and Colist-NLCs were tested simultaneously against all bacterial strains. The lowest concentration of antibiotic that prevented the appearance of a visible growth was defined as the MIC. All measurements were performed in triplicate.

In vitro release profile

A release study was carried out for Colist-NLCs at time 0 and after 12 months to test the effect of the storage at all conditions of temperature and humidity. An accurate amount of the formulation was placed in a tube and incubated at 37 °C in phosphate buffer saline (PBS) as the release medium. The tube was kept on a rotary shaker at 100 rpm. Samples were withdrawn at pre-established time intervals being subsequently centrifuged in Amicon® centrifugal filtration units (100 000 Da MWCO) for 15 min. The medium withdrawn was replaced with fresh PBS. The supernatants were then analysed by HPLC for drug quantification as mentioned in the Section “Encapsulation efficiency”. Results were expressed as percentage of drug released from the NLCs at different time points. The assay was run in triplicate.

Results and discussion

Encapsulation efficiency

The encapsulation efficiency (EE) was calculated indirectly by determining the amount of drug in the supernatants collected after the washing step. High EEs were achieved for Colist-SLNs, $79.70 \pm 6.06\%$ and for Colist-NLCs $94.79 \pm 4.20\%$, thus leading to actual drug loadings of 7.9% and 9.4% for Colist-SLNs and Colist-NLCs, respectively. As sodium colistimethate is a hydrophilic drug, no lipid solubility would be achieved and it was dispersed in the molten lipids (Kaur et al., 2015). However, high encapsulation efficiencies have been reported also for hydrophilic drugs when encapsulating into SLNs or NLCs.

In agreement with this finding, Gainza et al. (2013) found that recombinant human epidermal growth factor (rh-EGF)-loaded NLCs presented higher encapsulation efficiencies than SLN-rhEGF (95.7% versus 73.9%). Similarly, Pardeike et al. (2011) achieved a high EE up to 98% for intraconazole in NLCs. It is postulated that the high drug payload described for NLCs is related to the blending of a solid lipid with a liquid lipid leading to a less ordered solid lipid matrix providing the possibility for a high drug encapsulation (Hu et al., 2006). Moreover, the presence of liquid lipids in NLCs could improve drug solubility and therefore, increase drug encapsulation. As Müller and colleagues stated (Müller et al., 2002), the presence of liquid lipid with different fatty acid C-chains produces NLC with

less organised crystalline structure and therefore provides better loading capacity for drug accommodation. Liquid lipids are better solubilizers of drugs than solid lipids. It is also important to take into account the chemical nature of the lipid, as lipids which form highly crystalline particles with a perfect lattice (e.g. monoacid triglycerides) lead to drug expulsion. More complex lipids containing mixtures of mono-, di- and triglycerides, such as the Miglyol used to prepare NLCs, form less perfect crystals that could lead to a better accommodation of drugs (Vivek et al., 2007). In the case of SLNs, only a solid lipid was used giving rise to an ordered internal structure minimising loading capacity.

Particle size and PDI

The maintenance of the nanoparticle diameter size after freeze-drying is considered as a good indication of physical stability (Uner, 2006). The particle size is presented as z-average diameter in nanometric scale over the time (Figure 1). The particle size measurement after the elaboration of the nanoparticles was assigned as "time 0" being around 303 nm and 412 nm for Colist-SLNs and Colist-NLCs, respectively.

Colist-SLNs (Figure 1(A)) met the specifications during the first month of storage at all temperatures ranging from 245 to 336 nm.

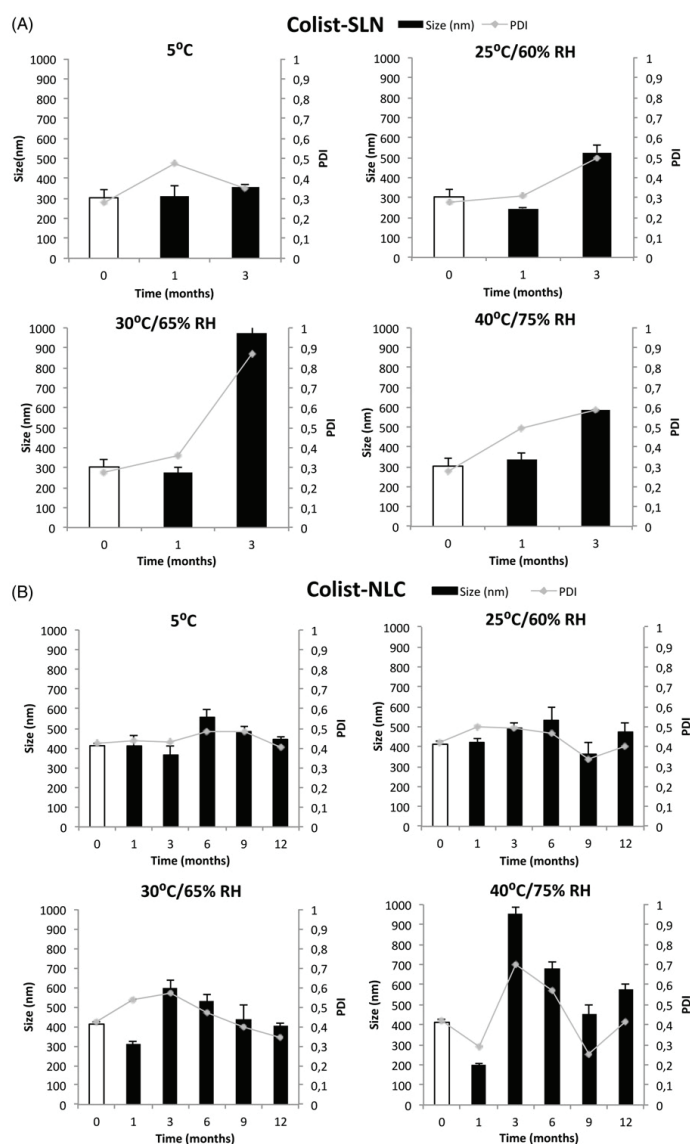


Figure 1. (A) Particle size and polydispersity index (PDI) of Colist-SLNs stored at ICH recommendations of temperature and relative humidity (RH) during 3 months. (B) Particle size and PDI of Colist-NLCs stored under the same conditions for 12 months ($n=3$).

However, the size requirement (below 500 nm) was only preserved for SLNs stored at 5 °C and 25 °C after the 3 months. It was observed that there was a progressive increase in size for all temperatures tested, being more remarkable at 30 °C and 40 °C. In a similar study carried out by Venkateswarlu and Manjunath (2004), clozapine-SLNs increased their size two-fold, from 40 to 78.8 nm, after 6 month-storage at 25 °C. In relation with our findings, Freitas and Müller (1998) showed a rapid particle growth within 3 days when storing SLN dispersions (consisting of 10% Compritol 888 stabilised with 1.2% poloxamer 188) at 50 °C. This fact was due to the high film rigidity of the emulsifier (also named microviscosity) that avoided the fusion of the film layers after particle collision. However, at room temperature (20 °C) improved stability for 3 months and stored the nanoparticles in darkness at 8 °C prolong their stability over 3 years. By this time the mean diameter remained almost unchanged from 276 to 297 nm. del Pozo-Rodríguez et al. (2009) found that SLNs for gene therapy lyophilised with trehalose were physically stable during 9 months at 25 °C/60% RH and 6 months at 30 °C/65% RH. However, the stability was lost when harder conditions were employed, for example at 40 °C/75% RH the size was twice higher than at time 0 resulting in unmeasured aggregates at 6 months.

On the other hand, Colist-NLCs (Figure 1(B)) met the requirements set for size at 5 °C and 25 °C, ranging around 400 nm overall but with a slight growth at the sixth month. However, when Colist-NLCs were stored at higher temperatures, a size enlargement was detected over the third month, exceeding 600 nm at 30 °C and 40 °C. The particle size fluctuations at the highest temperatures tested indicated that the size of the nanoparticles was influenced by the storage conditions.

Moreover, Das et al. (2012) reported that clotrimazole-loaded NLCs showed better stability in terms of size than SLNs at 5 °C and 25 °C after 3 months of storage, especially when a high amount of drug is incorporated to the formulation (10% versus 4% drug to lipid ratio). Kim et al. (2010) elaborated itraconazole-loaded NLCs with the solid lipid tristearin and the liquid lipid triolein at different ratios and found sizes less than 500 nm during 90 days of storage at room temperature.

It is known that the average particle diameter of NPs can be influenced by different factors, such as the composition of the formulation, the production technique or the parameters of the process such as time, temperature, pressure, equipment type, lyophilisation and storage conditions (Cavalli et al., 1997; Zimmermann et al., 2000). Well-formulated nanosystems should display a narrow particle size distribution in the submicron range. Particles greater than 1 µm and a particle growth over the time can be indicators of physical instability (Haskell et al., 1998). Depending on the application and route of administration, a particular attention should be paid in size control, for example, particle above 5 µm might cause embolism if they are administered by intravenous injection (Wissing et al., 2004). Furthermore, particle size can modulate the capture mechanism by macrophages and influence their biological stability, as phagocytosis increases when particle size increases; hence, it could influence the biodistribution behaviour of the particles. Due to the small size of the NPs developed, they have a greater chance to escape from the clearance mechanism by alveolar macrophages, compared to a microparticulate form (Chono et al., 2006). Moreover, after using a nebulisation system, pulmonary deposition depends on the particle size, shape and ventilation parameters; with decreasing particle diameters below 500 nm, the deposition increases in all regions of the lung due to their diffusional mobility (Yang et al., 2008) and they should also be able to diffuse through the mucus

pores of chronically infected lungs that typically fall in the range of around 200–500 nm (Suk et al., 2009).

The measurement of the polydispersity index (PDI) indicates the wide distribution of the particle size with values ranging from 0 to 1, and it is also a parameter that is used to evaluate the preservation of nanoparticles. As expected, there were more variations in the PDI at higher temperatures for both formulations (Figure 1). In general, as the particle size increased, the PDI also augmented. The PDI of Colist-SLNs was higher when increasing time and temperature, for instance, in the third month at 30 °C and 40 °C, the PDI reached the highest values, 0.87 and 0.59, respectively. Only samples stored under 5 °C and 25 °C displayed PDI values below 0.5. This is in concordance with the PDI values (<0.5) obtained by Ridolfi et al. (2012) when testing chitosan-SLN-tretinoin over one year period at room temperature.

The PDI of Colist-NLCs at the third month rose up to 0.57 and 0.75 at 30 °C and 40 °C, respectively, indicating a heterogeneous distribution of the nanoparticles that could be related to an increase of agglomerates. However, at lower temperatures, all PDIs were less than 0.5 meeting the criteria requirement for the storage conditions, meaning that the samples were monodisperse and homogenous (Zhang et al., 2009). Similarly, Das et al. (2012) reported that the PDI of clotrimazole-NLC formulations remained practically unchanged during the 3 months of the stability study at 2–8 °C and 25 °C. Altogether, the storage conditions at 5 °C and 25 °C met the specifications of size and PDI for Colist-SLNs and Colist-NLCs after three months and one year of storage, respectively.

Zeta potential

The measurement of zeta potential (ZP) is a good method to evaluate the state of nanoparticle surface and to detect any eventual modification during storage. It is also a useful indicator to predict physical stability of the NPs (Freitas and Müller, 1998). Positive and negative ZP indicates the degree of repulsion between close and similar particles in the dispersion; this repulsion prevents the aggregation process of particles (Heurtault et al., 2003).

After the lyophilisation step (time 0), the charge for Colist-SLNs and Colist-NLCs was almost identical, −20.8 and −21.97 mV, respectively. These zeta potential values could lead to a decreased risk of particle aggregation and enlargement after re-dispersion due to electric repulsion (Heurtault et al., 2003).

The ZP for all Colist-SLNs formulations ranged from −20 to −30 mV during the three months of the study (Figure 2(A)). Similarly, Radomska-Soukharev (2007) reported no changes in zeta potential of their SLNs formulations (−20 to −30 mV) after two years of storage at 5 °C, 25 °C and 40 °C, as the values at all three temperatures were identical to those of the day of preparation being the most stable ones the SLNs obtained with triglycerides compared to mono- and di-glycerides. It could be noticed that when the temperature increased, the zeta potential of Colist-SLNs was more negative, reaching −30.20 mV at 30 °C. In contrast, Freitas and Müller (1998) stated that the ZP of their SLN formulations decreased with increasing the input of energy (light and temperature) and only the samples stored at 8 °C in the dark were physically stable up to 3 years (−22 to −24 mV). They suggested that the energy input increases the kinetic energy of a system and can lead to changes in the crystalline structure of the lipid. In that study only SLN dispersions (without drug) were analysed.

Figure 2(B) shows the zeta potential values obtained for Colist-NLCs that remained below −20 mV (inside the limits of the specification values) at all conditions tested after one year indicating

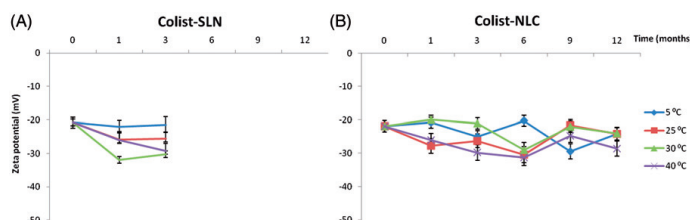


Figure 2. Representation of the zeta potential for Colist-nanoparticles during the stability study, at $5 \pm 3^\circ\text{C}$, $25 \pm 2^\circ\text{C}/60 \pm 5\%$ RH and $30 \pm 2^\circ\text{C}/65 \pm 5\%$ RH and $40 \pm 2^\circ\text{C}/75 \pm 5\%$ RH. (A) Colist-SLNs: The time points were set according to ICH CPMO/ICH/2736/99, but for Colist-SLNs the study was stopped at 3 months as the antibacterial activity specifications were not met. (B) Colist-NLCs.

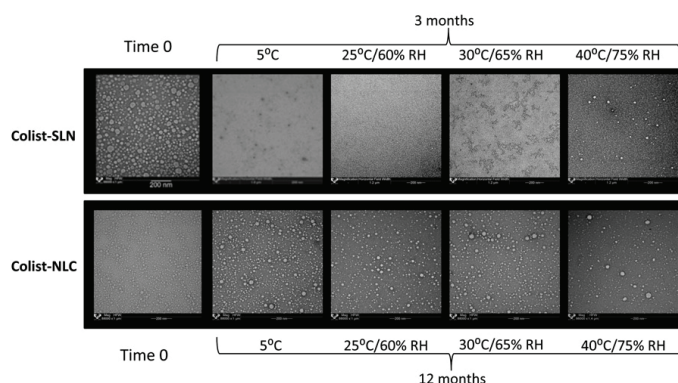


Figure 3. Upper row, transmission electron microscopy (TEM) images of Colist-SLNs at time 0 and the third month at ICH conditions. Lower row, TEM images of Colist-NLCs at time 0 and after 12 months at ICH conditions.

long-term stability. Generally, zeta potential value above $+20$ mV or below -20 mV combined with steric stabilisation predicts good stability of the nanoparticle dispersion; therefore, the NLCs prepared are expected to be stable (Das et al., 2012). Pardeike et al. (2011) found that the zeta potential of itraconazole-loaded NLCs stayed unchanged (around -31 mV) at room temperature and refrigerated conditions after 6-months of storage.

As instability such as aggregation or agglomeration of lipid nanoparticles are indicated by a decrease of the absolute zeta potential value, Colist-NLCs are expected to be stable beyond the observation period (Freitas and Müller, 1998). Moreover, surface electrostatic charge is an important factor influencing the deposition of inhaled nanoparticles. For example, charged NPs have higher deposition efficiencies as compared to neutrally ones (Yang et al., 2008). In addition, anionic liposomes exhibited longer retention in the lung compared to the neutral liposomes that was attributed to being less prone to aggregate *in vivo* (Beaulac et al., 1997).

Macroscopic and microscopic observation

A critical analysis of freeze-dried products normally includes the visual observation of the final volume and appearance of the cake. An attentive examination of the macroscopic aspect of the nanoparticles was carried out to detect any degradability of the formulation. The freeze-drying process led to a fine white powder at time 0 for both formulations. Colist-SLNs at the third month (when the stability study was stopped for Colist-SLNs as a result of the MIC data) showed a shrinkage appearance with a rubbery aspect and yellowish-white colour, especially after

undergoing 40°C storage conditions. However, Colist-NLCs maintained the desired characteristics of a freeze-dried pharmaceutical formulation with a powdery aspect at each sample time and until the end of the study. Accordingly, the white colour and consistency of nanoparticles remained unaltered. As a result, the effect of storing Colist-NLCs samples during 12 months at 5°C , 25°C and 60% RH, 30°C and 65% RH or as well as 40°C and 75% RH was negligible for their physical appearance. Similarly, Zhou and Zhou (2015) reported that lovastatin-loaded NLC dispersions maintained excellent stability without exhibiting any aggregation, precipitation or phase separation at 4°C for 6 months of storage and also any significant changes in appearance.

The microscopic visualisation of the particles allows the observation of the structure of the matrix, the conservation of nanoparticle integrity and to check whether any modifications took place on their morphology during storage. At the beginning of the study (time 0), both NPs were spherical as other authors described. For instance, Sanjula et al. (2009) used TEM to study the shape of the lyophilised carvediol-loaded SLNs prepared with stearic acid (oil phase) and Poloxamer 188 (surfactant), revealing that particles were spherical, smooth and uniformly distributed. However, in that case they used mannitol (5%) as cryoprotectant. In another study, spherical and uniform particle sizes were reported for chitosan-coated NLCs (Gartziandia et al., 2015).

TEM images revealed that Colist-SLNs at the third month (Figure 3, upper row) presented aggregation of particles or modifications in particle morphology in all temperatures tested. Scanning electron microscopy (SEM) pictures of amikacin-loaded SLNs dispersions developed by Ghaffari et al. (2011) showed that the particles stored at 4°C for 60 days did not present aggregation, however,

when stored at 25 °C and 40 °C they showed aggregation and particle size enlargement due to the melting of cholesterol used in their composition. On the other hand, SEM photos of redispersed lyophilised particles confirmed that the freeze-drying process did not have any impact on the shape and size of SLNs after 60 days stored at high temperature (40 °C).

On the contrary, Colist-NLCs (Figure 3, lower row) showed a different behaviour compared to Colist-SLNs. The resulting formulation exhibited spherical particles with a homogeneous particle size distribution meaning that Colist-NLCs were well preserved without aggregation or significant changes in morphology after

12 months at different conditions of temperature and humidity. TEM observation confirmed that the size distribution was uniform, which is an important technological property for powders regarding drug release kinetics.

Minimum inhibitory concentration (MIC)

The antimicrobial activity of both types of nanoparticles was analysed during the stability study for each sample time. For the data analysis, the following acceptance criterion was pre-established: as the MIC of the free antibiotic always led to 8–16 µg/mL

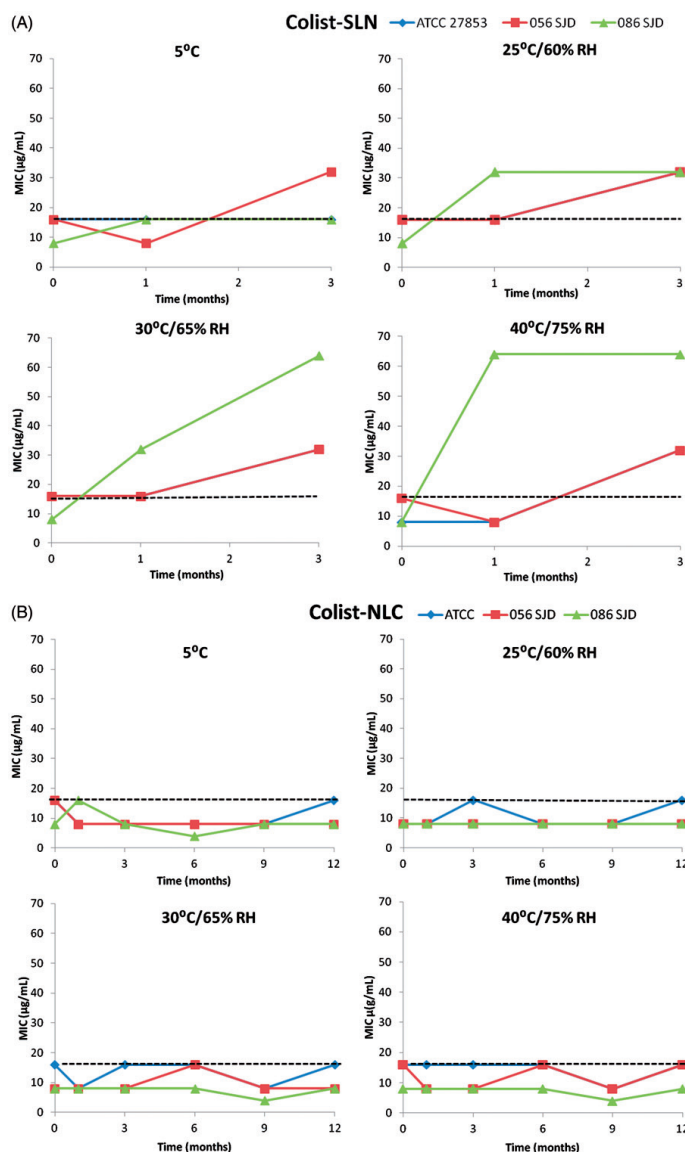


Figure 4. Minimum inhibitory concentration (MIC) of Colist-SLNs for 3 months (A) and Colist-NLCs for 12 months (B) against three strains of *Pseudomonas aeruginosa*, ATCC27853, 056SJD and 086 SJD at ICH conditions.

throughout all the study; 16 µg/mL MIC was set as the critical concentration. Samples outside that value were dropped off for the stability study.

At the beginning of the study, the MIC values of Colist-SLNs and Colist-NLCs were the same as the free drug. Solleti et al. (2015) found that the MIC and minimum bactericidal concentration (MBC) values of liposomal azithromycin (with an average diameter around 406 nm) were significantly lower than those of free azithromycin against *P. aeruginosa* (Solleti et al., 2015). Furthermore, other researchers observed better antimicrobial effects testing a liposomal polymyxin B formulation in comparison with the free antibiotic against *P. aeruginosa* strains (Omri et al., 2002) and clinical isolates (Alipour et al., 2008). This enhanced antimicrobial activity could be attributed to the fusional interaction between the membrane phospholipids of the liposomes and the bacterial cells (Alipour et al., 2008). Ghaffari et al. (2011) evaluated the antimicrobial activity against *P. aeruginosa* of free amikacin and amikacin-loaded SLN after freeze drying, obtaining MIC values of 8 and 16 µg/mL, respectively.

By the microbiological experiments it could be demonstrated that Colist-SLNs presented antimicrobial activity against ATCC 27853 and 056 SJD strains after one month of storage at different conditions. However, in the third month the MIC exerted was 32 or 64 µg/mL for all temperatures tested except at 5 °C (MIC of 16 µg/mL) against two out of the three *P. aeruginosa* strains, i.e., ATCC-27853 and 086 SJD (Figure 4(A)); it should point out that mucoid isolate was less susceptible to Colist-SLN than non-mucoid strains. Overall, it could be inferred that Colist-SLNs were not able to keep their antimicrobial activity after three months of storage and the stability study was stopped for sodium colistimethate-loaded SLNs. It has been previously reported that SLN are less stable than NLC (Kaur et al., 2015). This finding might have played a major role in the antimicrobial activity of the SLN. Probably, the lipid modification during storage led to drug degradation giving rise to activity loss.

On the other hand, the antimicrobial efficiency of Colist-NLCs was retained during 12 months against all the strains tested as the MIC values always were ≤ 16 µg/mL, even during storage under harder conditions of temperature and humidity (Figure 4(B)). These results demonstrated that sodium colistimethate encapsulated into NLCs was capable of preserving the antimicrobial activity during the storage period at ICH conditions.

Drug release study

Figure 5 shows the percentage of the drug release from Colist-NLCs at the beginning of the study and after one year storage under the conditions previously described. At time 0, the NLCs released the drug in a control manner reaching $91.53 \pm 7\%$ at 24 h and almost 100% at 48 h. The initial fast release of the NPs may be due to the presence of the drug in the surface of the nanoparticles, while the drug incorporated into the particulate core is released in a prolonged way (Misra et al., 2009).

Colist-NLCs demonstrated a sustained drug release also after 12 months under 5 °C and 25 °C as they showed similar release profile as the fresh nanoparticles. Similar findings were reported by Das et al. when working with clotrimazole-loaded NLCs. The release profile of their nanoparticles was the same as the fresh formulation, however, in that occasion only the refrigerated condition was tested and the storage duration was fixed in three months (Das et al., 2012). A slightly slower profile was detected at 30 °C of storage, but achieving around 83% of drug release at 24 h and the complete released at 48 h, meeting the specification requirements. On the contrary, Colist-NLCs at 40 °C showed a

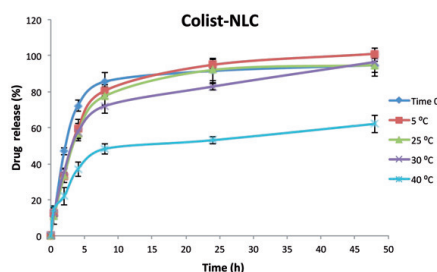


Figure 5. Sodium colistimethate release profile from NLCs before storage conditions (time 0) and after storage at 5 ± 3 °C, 25 ± 2 °C/60 \pm 5% RH, 30 ± 2 °C/65 \pm 5% RH and 40 ± 2 °C/75 \pm 5% RH after 12 months.

significantly slower drug release rate than their counterparts reaching only 62% at the end of the study, suggesting drug degradation.

The results obtained in our study confirmed the stability of the drug entrapped in nanoparticles as 100% of the drug (total encapsulated drug) was able to be released from the NLCs at 5 °C, 25 °C/60% RH and 30 °C/65% RH, indicating that the antibiotic was able to exert its antipseudomonal activity. The sustained release of a drug incorporated in a delivery system is an important characteristic quite often correlated with improved pharmacokinetics and efficacy (Chen et al., 2010). According to the prolonged release profile of the NLCs, it could be suggested that sodium colistimethate delivered as lipid nanocarrier might be administered in lower doses or longer intervals, thus reducing its undesirable side effects.

Conclusions

On the basis of these results, sodium colistimethate-loaded NLCs exhibited improved stability and shelf-life compared to Colist-SLNs, in terms of physico-chemical characteristics, biopharmaceutical properties and antimicrobial activity. The stability of NPs depended on temperature and humidity, but long-term stability of Colist-NLCs over one year can be achieved at the optimised storage conditions of 5 °C and 25 °C/60% RH. On these premises, room temperature would be the most attractive one for the storage of Colist-NLCs as it eases supply chain management.

Acknowledgements

Technical and human support provided by SGiker (UPV/EHU, MICINN, GV/EJ, ERDF and ESF) is gratefully acknowledged. The authors acknowledge the support of the University of the Basque Country UPV/EHU (UFI11/32) and University of Barcelona (UB). Authors also wish to thank the intellectual and technical assistance from the Platform for Drug Formulation (NANBIOSIS) CIBER-BBN.

Disclosure statement

The authors report no declarations of interest.

Funding

This work was carried out by TERFIQEC Project, Comprehensive Research On Effective Therapies For The Treatment of Cystic Fibrosis And Associated Diseases; IPT-2011-1402-900000 funded

by the Ministry of Economy and Competitiveness. M. Moreno-Sastre gratefully acknowledges the UPV/EHU for the fellowship grant.

References

- Abdelwahed W, Degobert G, Stainmesse S, Fessi H. Freeze-drying of nanoparticles: Formulation, process and storage considerations. *Adv Drug Deliv Rev*, 2006;58:1688–713.
- Alipour M, Halwani M, Omri A, Suntres ZE. Antimicrobial effectiveness of liposomal polymyxin B against resistant Gram-negative bacterial strains. *Int J Pharm*, 2008;355:293–8.
- Beaulac C, Clement-Major S, Hawari J, Lagace J. In vitro kinetics of drug release and pulmonary retention of microencapsulated antibiotic in liposomal formulations in relation to the lipid composition. *J Microencapsul*, 1997;14:335–48.
- Cavalli R, Caputo O, Carlotti ME, Trotta M, Scarnecchia C, Gasco MR. Sterilisation and freeze-drying of drug-free and drug-loaded solid lipid nanoparticles. *Int J Pharm*, 1997;148:47–54.
- Chacon M, Molpeceres J, Berges L, Guzman M, Aberturas MR. Stability and freeze-drying of cyclosporine loaded poly(D,L-lactide-glycolide) carriers. *Eur J Pharm Sci*, 1999;8:99–107.
- Chen C, Tsai T, Huang Z, Fang J. Effects of lipophilic emulsifiers on the oral administration of lovastatin from nanostructured lipid carriers: Physicochemical characterisation and pharmacokinetics. *Eur J Pharm Biopharm*, 2010;74:474–82.
- Chono S, Tanino T, Seki T, Morimoto K. Influence of particle size on drug delivery to rat alveolar macrophages following pulmonary administration of ciprofloxacin incorporated into liposomes. *J Drug Target*, 2006;14:557–66.
- Crowe LM, Reid DS, Crowe JH. Is trehalose special for preserving dry biomaterials? *Biophys J*, 1996;71:2087–93.
- Das S, Chaudhury A. Recent advances in lipid nanoparticle formulations with solid matrix for oral drug delivery. *AAPS PharmSciTech*, 2011;12:62–76.
- Das S, Ng WK, Tan RB. Are nanostructured lipid carriers (NLCs) better than solid lipid nanoparticles (SLNs): development, characterisations and comparative evaluations of clotrimazole-loaded SLNs and NLCs? *Eur J Pharm Sci*, 2012;47:139–51.
- del Pozo-Rodriguez A, Solinis MA, Gascon AR, Pedraz JL. Short- and long-term stability study of lyophilised solid lipid nanoparticles for gene therapy. *Eur J Pharm Biopharm*, 2009;71:181–9.
- Dijkmans AC, Wilms EB, Kamerling IM, Birkhoff W, Ortiz-Zacarias NV, van Nieuwkoop C, Verbrugh HA, Touw DJ. Colistin: Revival of an old polymyxin antibiotic. *Ther Drug Monit*, 2014;37:419–27.
- Falagas ME, Kasiakou SK. Colistin: The revival of polymyxins for the management of multidrug-resistant gram-negative bacterial infections. *Clin Infect Dis*, 2005;40:1333–41.
- Freitas C, Müller RH. Effect of light and temperature on zeta potential and physical stability in solid lipid nanoparticle (SLNTM) dispersions. *Int J Pharm*, 1998;168:221–9.
- Gainza G, Aguirre JJ, Pedraz JL, Hernández RM, Igartua M. rhEGF-loaded PLGA-Alginate microspheres enhance the healing of full-thickness excisional wounds in diabetised Wistar rats. *Eur J Pharm Sci*, 2013;50:243–52.
- Gartzandia O, Herran E, Pedraz JL, Carro E, Igartua M, Hernandez RM. Chitosan coated nanostructured lipid carriers for brain delivery of proteins by intranasal administration. *Colloids Surf B Biointerfaces*, 2015;134:304–13.
- Ghaffari S, Varshosaz J, Saadat A, Atyabi F. Stability and antimicrobial effect of amikacin-loaded solid lipid nanoparticles. *Int J Nanomedicine*, 2011;6:35–43.
- Grimm W. Extension of the International Conference on Harmonisation Tripartite Guideline for Stability Testing of New Drug Substances and Products to countries of climatic zones III and IV. *Drug Dev Ind Pharm*, 1998;24:313–25.
- Guideline ICH. 2003. Stability testing of new drug substances and products. Q1A (R2) [online]. Geneva, Switzerland: International Conference on Harmonization. Available from: http://www.ich.org/fileadmin/Public_Web_Site/ICH_Products/Guidelines/Quality/Q1A_R2/Step4/Q1A_R2_Guideline.pdf
- Haskell R, Shifflett J, Elzinga P. 1998. Particle-sizing technologies for submicron emulsions. Submicron emulsions in drug targeting and delivery. Amsterdam: Harwood Academic Publishers.
- Heurtault B, Saulnier P, Pech B, Proust JE, Benoit JP. Physico-chemical stability of colloidal lipid particles. *Biomaterials*, 2003;24:4283–300.
- Hu F, Jiang S, Du Y, Yuan H, Ye Y, Zeng S. Preparation and characteristics of monostearin nanostructured lipid carriers. *Int J Pharm*, 2006;314:83–9.
- Huh AJ, Kwon YJ. "Nanoantibiotics": A new paradigm for treating infectious diseases using nanomaterials in the antibiotics resistant era. *J. Control Release*, 2011;156:128–45.
- Jennings TA. 1999. Lyophilisation: Introduction and basic principles. Boca Raton, FL: CRC Press.
- Kaur S, Nautyal U, Singh R, Singh S, Devi A. Nanostructure Lipid Carrier (NLC): The new generation of lipid nanoparticles. *Asian Pac J Health Sci*, 2015;2:76–93.
- Kim J, Park J, Kim C. Development of a binary lipid nanoparticles formulation of itraconazole for parenteral administration and controlled release. *Int J Pharm*, 2010;383:209–15.
- Misra R, Acharya S, Dilnawaz F, Sahoo SK. Sustained antibacterial activity of doxycycline-loaded poly (D, L-lactide-co-glycolide) and poly (ε-caprolactone) nanoparticles. *Nanomedicine*, 2009;4:519–30.
- Molina M, Armstrong TK, Zhang Y, Patel MM, Lentz YK, Anchordoquy TJ. The stability of lyophilized lipid/DNA complexes during prolonged storage. *J Pharm Sci*, 2004;93:2259–73.
- Moreno-Sastre M, Pastor M, Salomon CJ, Esquisabel A, Pedraz JL. Pulmonary drug delivery: a review on nanocarriers for antibacterial chemotherapy. *J Antimicrob Chemother*, 2015;70:2945–55.
- Muller RH, Mader K, Gohla S. Solid lipid nanoparticles (SLN) for controlled drug delivery – A review of the state of the art. *Eur J Pharm Biopharm*, 2000;50:161–77.
- Müller RH, Radtke M, Wissing S. Nanostructured lipid matrices for improved microencapsulation of drugs. *Int J Pharm*, 2002;242:121–8.
- Muller RH, Petersen RD, Hommoss A, Pardeike J. Nanostructured lipid carriers (NLC) in cosmetic dermal products. *Adv Drug Deliv Rev*, 2007;59:522–30.
- Omri A, Suntres ZE, Shek PN. Enhanced activity of liposomal polymyxin B against *Pseudomonas aeruginosa* in a rat model of lung infection. *Biochem Pharmacol*, 2002;64:1407–13.
- Pardeike J, Weber S, Haber T, Wagner J, Zarfl HP, Plank H, Zimmer A. Development of an itraconazole-loaded nanostructured lipid carrier (NLC) formulation for pulmonary application. *Int J Pharm*, 2011;419:329–38.
- Pastor M, Moreno-Sastre M, Esquisabel A, Sans E, Viñas M, Bachiller D, Asensio VJ, Pozo AD, Gainza E, Pedraz JL. Sodium colistimethate loaded lipid nanocarriers for the treatment of *Pseudomonas aeruginosa* infections associated with cystic fibrosis. *Int J Pharm*, 2014;477:485–94.
- Radomska-Soukharev A. Stability of lipid excipients in solid lipid nanoparticles. *Adv Drug Deliv Rev*, 2007;59:411–18.
- Ridolfi DM, Marcato PD, Justo GZ, Cordi L, Machado D, Durán N. Chitosan-solid lipid nanoparticles as carriers for topical delivery of tretinoin. *Colloids Surf B Biointerfaces*, 2012;93:36–40.

- Sanjula B, Shah FM, Javed A, Alka A. Effect of poloxamer 188 on lymphatic uptake of carvedilol-loaded solid lipid nanoparticles for bioavailability enhancement. *J Drug Target*, 2009;17:249–56.
- Schwarz C, Mehnert W. Freeze-drying of drug-free and drug-loaded solid lipid nanoparticles (SLN). *Int J Pharm*, 1997;157: 171–9.
- Solleti VS, Alhariri M, Halwani M, Omri A. Antimicrobial properties of liposomal azithromycin for *Pseudomonas* infections in cystic fibrosis patients. *J Antimicrob Chemother*, 2015;70:784–96.
- Suk JS, Lai SK, Wang YY, Ensign LM, Zeitlin PL, Boyle MP, Hanes J. The penetration of fresh undiluted sputum expectorated by cystic fibrosis patients by non-adhesive polymer nanoparticles. *Biomaterials*, 2009;30:2591–7.
- Uner M. Preparation, characterisation and physico-chemical properties of solid lipid nanoparticles (SLN) and nanostructured lipid carriers (NLC): Their benefits as colloidal drug carrier systems. *Pharmazie*, 2006;61:375–86.
- Venkateswarlu V, Manjunath K. Preparation, characterisation and in vitro release kinetics of clozapine solid lipid nanoparticles. *J Control Release*, 2004;95:627–38.
- Vivek K, Reddy H, Murthy RSR. Investigations of the effect of the lipid matrix on drug entrapment, in vitro release, and physical stability of olanzapine-loaded solid lipid nanoparticles. *AAPS PharmSciTech*, 2007;8:E1–9.
- Weber S, Zimmer A, Pardeike J. Solid lipid nanoparticles (SLN) and nanostructured lipid carriers (NLC) for pulmonary application: A review of the state of the art. *Eur J Pharm Biopharm*, 2014;86:7–22.
- Wissing SA, Kayser O, Müller RH. Solid lipid nanoparticles for parenteral drug delivery. *Adv Drug Deliv Rev*, 2004;56:1257–72.
- Yang W, Peters JI, Williams RO. 3rd, Inhaled nanoparticles – A current review. *Int J Pharm*, 2008;356:239–47.
- Zhang J, Fan Y, Smith E. Experimental design for the optimization of lipid nanoparticles. *J Pharm Sci*, 2009;98:1813–19.
- Zhou J, Zhou D. Improvement of oral bioavailability of lovastatin by using nanostructured lipid carriers. *Drug Des Devel Ther*, 2015;9:5269.
- Zimmermann E, Müller RH, Mäder K. Influence of different parameters on reconstitution of lyophilized SLN. *Int J Pharm*, 2000;196:211–13.

PAPER 5

Determination of the spatiotemporal dependence of *Pseudomonas aeruginosa* biofilm viability after treatment with NLC-colistin

Eulalia Sans-Serramitjana¹
Marta Jorba¹
José Luis Pedraz²
Teresa Vinuesa¹
Miquel Viñas Ciordia¹

¹Laboratory of Molecular Microbiology and Antimicrobials, Department of Pathology and Experimental Therapeutics, University of Barcelona, Barcelona, ²Laboratory of Pharmaceutics, University of the Basque Country (UPV/EHU), (CIBER-BBN), Spain

Abstract: The emergence of colistin-resistant *Pseudomonas aeruginosa* in cystic fibrosis (CF) patients, particularly after long-term inhalation treatments, has been recently reported. Nanoencapsulation may enable preparations to overcome the limitations of conventional pharmaceutical forms. We have determined the time-dependent viability of *P. aeruginosa* biofilms treated with both free and nanoencapsulated colistin. We also examined the relationship between the optimal anti-biofilm activity of nanostructured lipid carrier (NLC)-colistin and the structural organization of the biofilm itself. The results showed the more rapid killing of *P. aeruginosa* bacterial biofilms by NLC-colistin than by free colistin. However, the two formulations did not differ in terms of the final percentages of living and dead cells, which were higher in the inner than in the outer layers of the treated biofilms. The effective anti-biofilm activity of NLC-colistin and its faster killing effect recommend further studies of its use over free colistin in the treatment of *P. aeruginosa* infections in CF patients.

Keywords: cystic fibrosis, colistin sulfate, lipid nanoparticles, *P. aeruginosa*, confocal laser scanning microscopy, anti-biofilm activity

Introduction

Pseudomonas aeruginosa is a gram-negative opportunistic pathogen that frequently infects the lungs of cystic fibrosis (CF) patients in the form of chronic biofilm infections.¹ The antimicrobial resistance of bacteria assuming a biofilm mode of growth poses challenges not only to host immune clearance mechanisms but also to health care settings, in the form of an increased risk of hospital-acquired infections.² The high level of antibiotic resistance that characterizes biofilms can be attributed to their structurally heterogeneous microenvironments, some of which contain metabolically inactive cell population,^{4,3} as well as to the differential expression of multiple gene networks and extracellular matrix by the resident bacterial species.⁴

Over the last decade, increasing attention has been paid to antimicrobial peptides (AMPs) as therapeutic agents, because resistance to them is thus far rare. Moreover, these peptides are able to modulate the innate immune response.⁵⁻⁷ The AMP colistin is a cyclic cationic decapeptide that attacks negatively charged bacterial membranes, thereby disrupting both the outer and inner membranes of gram-negative species.⁷ Although the use of colistin as an antimicrobial is restricted by its high nephrotoxicity, the increasing emergence of multiresistant pathogens has renewed interest in its therapeutic potential.⁸ In fact, nowadays, colistin is administered to CF patients and to other patients with chronic respiratory diseases for the treatment of lung infections

Correspondence: Miquel Viñas Ciordia
Laboratory of Molecular Microbiology,
University of Barcelona, Feixa Llarga s/n,
08907 Hospitalet de Llobregat, Spain
Tel +34 93 402 4265
Email mvinyas@ub.edu

caused by *P. aeruginosa*.⁹ However, colistin resistance, mediated by the post-translational modification of lipopolysaccharide, has emerged, perhaps driven by the increasing clinical use of this drug.^{10,11} Although resistance rates are still low in many countries, the recent identification of a plasmid-borne colistin resistance gene (*mcr-1*) in human, animal, and environmental isolates of Enterobacteriaceae may soon lead to rapid increases in resistance on a global scale.^{12,13} An awareness of this threat has catalyzed the search for less toxic antimicrobials as well as the development of synthetically modified forms enabling dose reductions, longer administration intervals, and reduced systemic toxicity. An alternative is new delivery strategies, such as the use of solid lipid nanoparticles and nanostructured lipid carriers (NLCs) to deliver colistin in CF patients with *P. aeruginosa* respiratory infections. The nebulization of antimicrobials carried in lipid nanoparticles improves drug bioavailability and allows a reduced dosing frequency.¹⁴ In principle, the administration of encapsulated drugs could overcome preexisting resistance mechanisms, including the decreased uptake and increased efflux of the drug, as well as biofilm formation.¹⁵ In a previous study, we demonstrated the higher anti-biofilm activity of NLC-colistin than of free colistin in both susceptible and resistant *P. aeruginosa* strains isolated from the sputum samples of CF patients.¹⁶ As biofilms play a key role in the natural history of *P. aeruginosa* respiratory infections in CF, the use of NLC-colistin may offer new approaches to their treatment. However, the mechanism underlying the improved efficiency of NLC-colistin in biofilm removal is unknown.¹⁶ Pamp et al¹⁷ showed that free colistin acts preferentially on bacteria with low metabolic rates; this is the case for bacteria in the deepest layers of a biofilm, as metabolic activity decreases with increasing distance from the biofilm surface. Whether the same differential response occurs with NLC-colistin has not been determined. Thus, this study explored the efficacy of NLC-colistin versus the free drug with respect to biofilm viability over time and across the different layers of the biofilm.

Materials and methods

Preparation of lipid nanoparticles

NLCs were prepared using the hot melt homogenization technique.¹⁸ The lipid core consisted of Precirol®ATO 5 (Gattefossé, Madrid, Spain) and Miglyol 812 (Sasol, Hamburg, Germany), which were mixed with colistin sulfate (Zhejiang Shenghua Biok Biology Co., Ltd., China). The temperature of the mixture was gradually increased to the melting temperature of the solid lipids. The surfactant solution was 1.3% (w/v) Polysorbate 80 (Panreac Química, Castellar del

Vallès, Barcelona, Spain) and 0.6% (w/v) Poloxamer 188 (BASF, Ludwigshafen, Rhineland-Palatinate, Germany). The mixture was emulsified by sonication for 15 s at 20 W. The nanoparticles were recrystallized by an overnight incubation at 4°C to stimulate particle formation. They were then washed three times by centrifugation at 2,500 rpm in Amicon centrifugal filtration units (100,000 MWCO). All prepared nanoparticles were freeze-dried with trehalose (15%).

Bacterial strain, culture conditions, and biofilm formation

P. aeruginosa strain PA01 in 20 mL of Mueller-Hinton II broth cation adjusted (Becton Dickinson Diagnostic Systems, Inc., Sparks, MD, USA) was grown overnight at 37°C with continuous shaking at 250 rpm. The culture was then adjusted to a concentration of $1-5 \times 10^8$ cfu/mL, and 200 μ L was used to inoculate μ -Slide 8 glass bottom wells (Ibidi, cat. num. 80827, Munich, Germany). Each well was previously coated with a 0.01% (w/v) poly-lysine hydrobromide (Sigma-Aldrich, Dorset, UK) solution to enhance bacterial cell adhesion and to prevent biofilm removal during the experiments. The slides were incubated at 37°C for 24 h to allow biofilm formation.

Confocal laser scanning microscopy imaging

Biofilms on the eight-well glass were washed once with Ringer $\frac{1}{4}$ to remove unfixed bacteria and then treated with free and NLC-colistin at a colistin concentration of 128 μ g/mL, based on previously published results.¹⁶ They were then incubated at 37°C for 20, 30, 40, 60, 80, and 100 min after which they were rinsed once with Ringer $\frac{1}{4}$. To stain the biofilms, a mixture of SYTO 9 and propidium iodide prepared at a dilution ratio of 1:2 (1.5 μ L of SYTO 9 and 3 μ L of propidium iodide in 1 mL of Ringer $\frac{1}{4}$) was applied to the entire biofilm. After 30 min of incubation in the dark at 37°C, the stained biofilms were washed once with Ringer $\frac{1}{4}$ to remove nonspecific staining. Fluorescence was observed using a Leica TCS-SL filter-free spectral confocal laser-scanning microscope (Leica Microsystems, Mannheim, Germany) equipped with a 488-nm argon laser, 543-nm and 633-nm He/Ne lasers (Scientific and Technological Centers, University of Barcelona, Bellvitge Campus, L'Hospitalet de Llobregat, Spain), and a 63 \times magnification oil immersion objective (1.4 numerical aperture). The image resolution was 1,024 \times 1,024 pixels. All experiments were performed in duplicate. Confocal laser scanning microscopy (CLSM) images were analyzed using ImageJ software (National

Institutes of health, Bethesda, MD, USA). The percentages of alive and dead bacterial cells were calculated from the total cell number.

Results and discussion

Time-dependent killing of strain PAO1 biofilms by free and NLC-colistin

Enumeration of the viable and dead bacteria for every treatment showed an increase in bacterial death over time in the strain PAO1 biofilms (Figure 1). In the control (untreated) biofilms, most of the cells were viable, with live/dead ratios of 78.2% (green) and 21.8% (red), respectively. This result was in agreement with a previous report.¹⁹ The baseline viability was taken into account in the interpretation of the experimental data. A nonlethal effect was observed in biofilms exposed for 20 min to free colistin, with the proportions of living and dead bacteria almost identical to that of the control (~80% and 20%, respectively). The killing efficiency reached a maximum of 80% after 60 min of treatment with the free formulation. By contrast, after 20 min of exposure to NLC-colistin, ~75% of the individual cells were dead (red fluorescence) and after 60 min of treatment almost 100%, thus demonstrating the rapid killing effect of the encapsulated drug.

The results shown in Figure 1 are in good agreement with the CLSM images of the untreated and treated biofilms (Figure 2). The latter mostly stained green (Figure 2A), indicating a high level of bacterial viability. After 20 and 40 min of exposure to NLC-colistin (Figure 2B.2 and 2C.4), the red population increased over time such that very few green-staining cells were observed, consistent with the significant damage of bacteria residing in the treated biofilm. After a

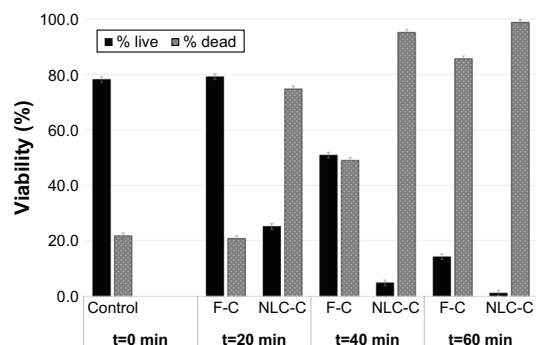


Figure 1 Graphical representation of living and dead bacteria treated or not treated with the different colistin formulations.

Note: Error bars represent the standard deviation of the mean (time: 0, 20, 40, and 60 min).

Abbreviations: F-C, free colistin; NLC-C, colistin nanoparticulated in nanostructured lipid carrier.

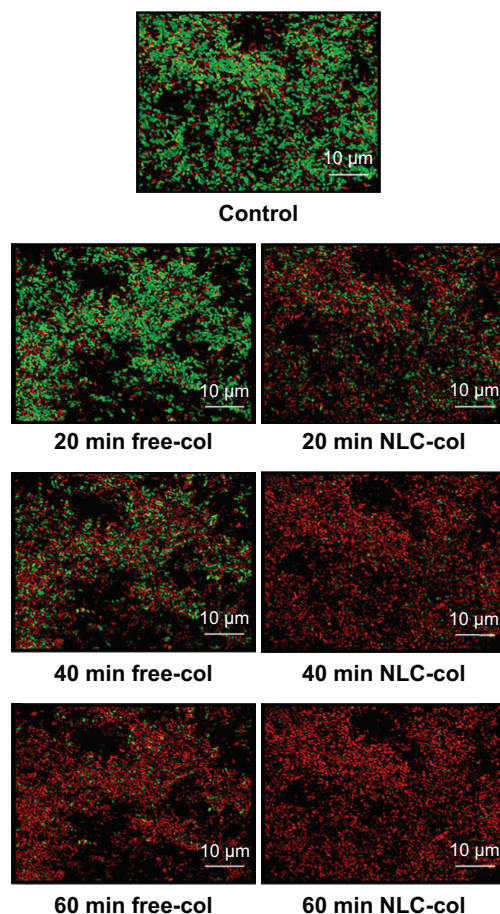


Figure 2 Confocal laser scanning microscopy images of *Pseudomonas aeruginosa* strain PAO1 biofilms.

Notes: Control: untreated biofilm. Drug exposure time: 20, 40, and 60 min. Green: viable bacteria; red: dead bacteria.

Abbreviations: free-col, free colistin; NLC-col, colistin nanoparticulated in nanostructured lipid carrier.

60-min incubation with NLC-colistin, all bacterial cells stained red. In the biofilms treated with free colistin (Figure 2B.1), the percentages of the red and green populations of bacteria after 20 min were almost identical to those of the control. After 40 and 60 min (Figure 2C.3, 2D.5), the red population in the free colistin treatment was always smaller than that in the NLC-colistin treatment, evidence of the faster killing of bacterial biofilms by the latter. This may reflect the ability of the lipid nanoparticles to easily penetrate the biofilm matrix, with the nanoparticulated drug then reaching the bacteria faster and more easily than free colistin.^{21,22} Islan et al²² reported similar results using levofloxacin-loaded lipid nanoparticles. In that study, rapid killing of *P. aeruginosa* biofilms by NLC-levofloxacin was achieved after 60 min of exposure.

Table 1 Percentage of the bacterial population living in the various layers and percentages of live and dead bacteria of the *Pseudomonas aeruginosa* strain PAOI biofilm after 20, 40, and 60 min of treatment with F-C and NLC-C

Treatment	Biofilm layer	Percentage of the bacterial population (%)											
		t=0 min			t=20 min			t=40 min			t=60 min		
		Total	Live	Dead	Total	Live	Dead	Total	Live	Dead	Total	Live	Dead
C+	Outer	28.5	22.5	6.1									
	Inner	71.5	55.8	15.7									
F-C	Outer				32.4	29.0	3.4	35.2	20.9	14.3	37.9	6.6	31.3
	Inner				60.3	50.3	9.9	64.8	30.1	34.8	62.1	7.6	54.5
NLC-C	Outer				20.8	5.5	15.3	17.4	0.9	16.5	19.6	0.2	19.5
	Inner				79.2	19.7	59.6	82.6	3.9	78.7	80.4	0.9	79.5

Abbreviations: C+, untreated biofilm; F-C, free colistin; NLC-C, colistin nanoparticulated in nanostructured lipid carrier.

Differentiation of distinct bacterial subpopulations in the strain PAOI biofilm

Biofilms are a complex, multicellular structure that favors the generation of physiologically distinct subpopulations of bacteria that together form a community able to adapt to rapidly changing environmental conditions.²³ To explore whether free and nanoencapsulated colistin differentially act on the subpopulations residing within the biofilm, the viability of bacteria in the different layers of the biofilm was determined. As seen in Table 1, the bacterial density was much higher in the inner layers of the biofilm, consistent with the previously reported high density of cells located close to the substratum in *P. aeruginosa* biofilms.²⁴ The biofilms were investigated in greater detail by dividing them in half, which revealed that 71% of the total number of cells occupied the inner layers (Table 1). This was essentially the case in all three types of biofilms (control, free colistin, and NLC-colistin) despite the demonstrated heterogeneity among biofilms with respect to their thickness and the strength of their surface attachment.²⁵ Nonetheless, our results can be explained by the initiation of cell detachment in the upper layers of the biofilm²⁶ as well as the accumulation of high densities of smaller cells in deeper parts of the biofilm in response to external stress conditions. Also, it is likely that the washing step with buffer altered the external parts of the biofilm while leaving its deeper parts relatively undisturbed. Although weakly attached bacteria will be discarded by carefully washing the biofilms after 24 h of incubation, simultaneous disruption of the superficial layers of the biofilm is difficult to avoid.

The two colistin formulations did not differ in their effects on the various biofilm subpopulations, as the percentages of living and dead cells were higher in the inner than in the outer layers of biofilms treated with free colistin or NLC-colistin (Table 1). Our results demonstrate that both formulations are able to penetrate the deeper layers of the biofilm and thus access a dormant and anaerobically

growing subpopulation.^{27,28} A reduction of the free colistin concentration, the delayed penetration of the free drug into the deeper portions of the multilayered biofilm, and the lack of specificity of NLC-colistin in killing metabolically active bacteria versus starved cells may account for our results, as proposed in similar studies.^{17,29} Further experiments will be aimed at improving the experimental conditions to optimize the performance of NLC-colistin.

Conclusion

In the previous works, we demonstrated the identical antimicrobial activity of free colistin and NLC-colistin. Here we have shown that NLC-colistin was clearly more effective than its free form in eradicating biofilms of *P. aeruginosa*, the most relevant pathogen in CF patients. Thus, the use of lipid nanoparticles may be an interesting strategy to prevent the growth and development of microbial biofilms in the clinical setting. NLC-colistin was much faster than free colistin in killing *P. aeruginosa*, based on the ability of the encapsulated drug to reach both the superficial and the deep regions of the biofilm. Further experiments are needed to identify the precise mechanism underlying the efficient removal of biofilms by NLC-colistin.

Acknowledgments

We thank Wendy Ran for copy editing the English version of the manuscript. This work was carried out under the Comprehensive Research on Effective Therapies for the Treatment of Cystic Fibrosis and Associated Diseases (IPT-2011-1402-900000) funded by the Spanish Ministry of Economy and Competitiveness. The authors gratefully acknowledge the support of the Scientific and Technological Centers (University of Barcelona, Bellvitge Campus, L'Hospitalet de Llobregat, Spain) and particularly the technical assistance of Dr Benjamin Torrejón in the CLSM study. MV is a member of the ENABLE (European Gram Negative Antibacterial Engine) European consortium (IMI-ND4BB).

Disclosure

The authors report no conflicts of interest in this work.

References

- Lyczak JB, Cannon CL, Pier GB. Lung infections associated with cystic fibrosis lung infections associated with cystic fibrosis. *Clin Microbiol Rev.* 2002;15(2):194–222.
- Drenkard E, Ausubel FM. *Pseudomonas* biofilm formation and antibiotic resistance are linked to phenotypic variation. *Nature.* 2002; 416(6882):740–743.
- Machineni L, Rajapantula A, Nandamuri V, et al. Influence of nutrient availability and quorum sensing on the formation of metabolically inactive microcolonies within structurally heterogeneous bacterial biofilms: an individual-based 3D cellular automata model. *Bull Math Biol.* 2017;79(3):594–618.
- Taylor PK, Yeung AT, Hancock RE. Antibiotic resistance in *Pseudomonas aeruginosa* biofilms: towards the development of novel anti-biofilm therapies. *J Biotechnol.* 2014;191:121–130.
- Hancock REW, Sahl HG. Antimicrobial and host-defense peptides as new anti-infective therapeutic strategies. *Nat Biotechnol.* 2006; 24(12):1551–1557.
- Hancock RE. Cationic peptides: effectors in innate immunity and novel antimicrobials. *Lancet Infect Dis.* 2001;1(3):156–164.
- Haney EF, Mansour SC, Hancock RE. Antimicrobial peptides: an introduction. *Methods Mol Biol.* 2017;1548:3–22.
- Li J, Nation RL, Milne RW, et al. Evaluation of colistin as an agent against multi-resistant Gram-negative bacteria. *Int J Antimicrob Agents.* 2005;25(1):11–25.
- Döring G, Flume P, Heijerman H, Elborn JS; Consensus Study Group. Treatment of lung infection in patients with cystic fibrosis: Current and future strategies. *J Cyst Fibros.* 2012;11(6):461–479.
- Gales AC, Jones RN, Sader HS. Contemporary activity of colistin and polymyxin B against a worldwide collection of Gram-negative pathogens: Results from the SENTRY antimicrobial surveillance program (2006–2009). *J Antimicrob Chemother.* 2011;66(9):2070–2074.
- Carmeli Y, Troillet N, Eliopoulos GM, Samore MH. Emergence of antibiotic-resistant *Pseudomonas aeruginosa*: comparison of risks associated with different antipseudomonal agents. *Antimicrob Agents Chemother.* 1999;43(6):1379–1382.
- Liu YY, Wang Y, Walsh TR, et al. Emergence of plasmid-mediated colistin resistance mechanism MCR-1 in animals and human beings in China: a microbiological and molecular biological study. *Lancet Infect Dis.* 2016;16(2):161–168.
- Jeannot K, Bolard A, Plésiat P. Resistance to polymyxins in Gram-negative organisms. *Int J Antimicrob Agents.* 2017;49(5): 526–535.
- Cipolla D, Shekunov B, Blanchard J, Hickey A. Lipid-based carriers for pulmonary products: Preclinical development and case studies in humans. *Adv Drug Deliv Rev.* 2014;75:53–80.
- Pelgrift RY, Friedman AJ. Nanotechnology as a therapeutic tool to combat microbial resistance. *Adv Drug Deliv Rev.* 2013;65(13–14): 1803–1815.
- Sans-Serramitjana E, Fusté E, Martínez-Garriga B, et al. Killing effect of nanoencapsulated colistin sulfate on *Pseudomonas aeruginosa* from cystic fibrosis patients. *J Cyst Fibros.* 2016;15(5):611–618.
- Pamp SJ, Gjermansen M, Johansen HK, Tolker-Nielsen T. Tolerance to the antimicrobial peptide colistin in *Pseudomonas aeruginosa* biofilms is linked to metabolically active cells, and depends on the *pmr* and *mexAB-oprM* genes. *Mol Microbiol.* 2008;68(1):223–240.
- Pastor M, Moreno-sastre M, Esquisabel A, et al. Sodium colistimethate loaded lipid nanocarriers for the treatment of *Pseudomonas aeruginosa* infections associated with cystic fibrosis. *Int J Pharm.* 2014; 477(1–2):485–494.
- Singh R, Monnappa AK, Hong S, Mitchell RJ, Jang J. Effects of carbon dioxide aerosols on the viability of *Escherichia coli* during biofilm dispersal. *Sci Rep.* 2015;5:13766.
- Klodzińska SN, Priemel PA, Rades T, et al. Inhalable antimicrobials for treatment of bacterial biofilm-associated sinusitis in cystic fibrosis patients: challenges and drug delivery approaches. *Int J Mol Sci.* 2016; 17(10). pii: E1688.
- Nafee N, Husari A, Maurer CK, et al. Antibiotic-free nanotherapeutics: ultra-small, mucus-penetrating solid lipid nanoparticles enhance the pulmonary delivery and anti-virulence efficacy of novel quorum sensing inhibitors. *J Control Release.* 2014;192:131–140.
- Islan GA, Tornello PC, Abraham GA, et al. Smart lipid nanoparticles containing levofloxacin and DNase for lung delivery. Design and characterization. *Colloids Surfaces B Biointerfaces.* 2016;143:168–176.
- Moormeier DE, Bayles KW. *Staphylococcus aureus* biofilm: a complex developmental organism. *Mol Microbiol.* 2017;104(3):365–376.
- Yang L, Nilsson M, Gjermansen M, Givskov M, Tolker-Nielsen T. Pyoverdine and PQS mediated subpopulation interactions involved in *Pseudomonas aeruginosa* biofilm formation. *Mol Microbiol.* 2009; 74(6):1380–1392.
- Flemming HC, Wingender J, Szewzyk U, Steinberg P, Rice SA, Kjelleberg S. Biofilms: an emergent form of bacterial life. *Nat Rev Microbiol.* 2016;14(9):563–575.
- Rollet C, Gal L, Guzzo J. Biofilm-detached cells, a transition from a sessile to a planktonic phenotype: a comparative study of adhesion and physiological characteristics in *Pseudomonas aeruginosa*. *FEMS Microbiol Lett.* 2009;290(2):135–142.
- Kim J, Hahn JS, Franklin MJ, Stewart PS, Yoon J. Tolerance of dormant and active cells in *Pseudomonas aeruginosa* PA01 biofilm to antimicrobial agents. *J Antimicrob Chemother.* 2009;63(1):129–135.
- Bjarnsholt T, Ciofu O, Molin S, Givskov M, Høiby N. Applying insights from biofilm biology to drug development – can a new approach be developed? *Nat Rev Drug Discov.* 2013;12(10):791–808.
- Haagensen JAJ, Klausen M, Ernst RK, et al. Differentiation and distribution of colistin- and sodium dodecyl sulfate-tolerant cells in *Pseudomonas aeruginosa* biofilms. *J Bacteriol.* 2007;189(1):28–37.

International Journal of Nanomedicine

Publish your work in this journal

The International Journal of Nanomedicine is an international, peer-reviewed journal focusing on the application of nanotechnology in diagnostics, therapeutics, and drug delivery systems throughout the biomedical field. This journal is indexed on PubMed Central, MedLine, CAS, SciSearch®, Current Contents®/Clinical Medicine,

Submit your manuscript here: <http://www.dovepress.com/international-journal-of-nanomedicine-journal>

Dovepress

Journal Citation Reports/Science Edition, EMBASE, Scopus and the Elsevier Bibliographic databases. The manuscript management system is completely online and includes a very quick and fair peer-review system, which is all easy to use. Visit <http://www.dovepress.com/testimonials.php> to read real quotes from published authors.

PAPER 6



Article

Free and nanoencapsulated tobramycin: Effects on planktonic and biofilm forms of *Pseudomonas*

Sans-Serramitjana E¹, Jorba M¹, Fusté E^{1,2}, Pedraz JL³, Vinuesa T¹, Viñas M^{1*}.¹ Laboratory of Molecular Microbiology and Antimicrobials. Dept. of Pathology and Experimental Therapeutics. Faculty of Medicine & Health Sciences. University of Barcelona. Spain² School of Nursing. Faculty of Medicine & Health Sciences. University of Barcelona. Spain³ Laboratory of Pharmaceuticals, University of the Basque Country and Biomedical Research Networking Center in Bioengineering, Biomaterials and Nanomedicine (CIBER-BBN). Spain* Correspondence: mvinyas@ub.edu; Tel.: +34-934-024265

Academic Editor: name

Received: date; Accepted: date; Published: date

Abstract: Cystic fibrosis (CF) is a genetic disorder in which frequent pulmonary infections develop secondarily. One of the major pulmonary pathogens colonizing the respiratory tract of CF patients and causing chronic airway infections is *Pseudomonas aeruginosa*. Although tobramycin was initially effective against *P. aeruginosa*, tobramycin-resistant strains have emerged. Among the strategies for overcoming resistance to tobramycin and other antibiotics is encapsulation of the drugs in nanoparticles. In this study, we explored the antimicrobial activity of nanoencapsulated tobramycin, both in solid lipid nanoparticles (SLN) and in nanostructured lipid carriers (NLC), against clinical isolates of *P. aeruginosa* obtained from CF patients. We also investigated the efficacy of these formulations in biofilm eradication. In both experiments, the activities of SLN and NLC were compared with that of free tobramycin.

The susceptibility of planktonic bacteria was determined using the broth microdilution method and by plotting bacterial growth. The minimal biofilm eradication concentration (MBEC) was determined to assess the efficacy of the different tobramycin formulations against biofilms.

The activity of tobramycin-loaded SLN was less than that of either tobramycin-loaded NLC or free tobramycin. The minimum inhibitory concentration (MIC) and MBEC of nanoencapsulated tobramycin were slightly lower (1–2 logs) than the corresponding values of the free drug when determined in tobramycin-susceptible isolates. However, in tobramycin-resistant strains, the MIC and MBEC did not differ between either encapsulated form and free tobramycin. Our results demonstrate the efficacy of nanoencapsulated formulations in killing susceptible *P. aeruginosa* from CF and from other patients.

Keywords: Tobramycin; lipid nanoparticles; antibacterial and antibiofilm effects; *P. aeruginosa*; cystic fibrosis.

1. Introduction

Cystic fibrosis (CF) is the most common genetic disorder in the Caucasian population and it is characterized by a high morbidity and mortality. The CF lung is compromised by the production of viscous mucus secretions, resulting in a debilitated mucociliary clearance that promotes bacterial infection and inflammation [1]. *Pseudomonas aeruginosa* is the predominant opportunistic pathogen infecting the respiratory tract of CF patients. Once chronic lung colonization occurs, *P. aeruginosa* changes phenotypically to produce alginate, which allows the bacterium to become established within mucoid biofilms and thus highly resistant to multiple antimicrobials [2][3]. Indeed, the emergence of multidrug-resistant phenotypes and treatment failure were shown to correlate with the reduced permeability of the outer membrane of *P. aeruginosa* to most antimicrobials and the acquisition of genes encoding antimicrobial resistance [4][5].

Tobramycin is a hydrophilic, cationic antibiotic administered as an aerosol in the treatment of *P. aeruginosa* lung infections in CF patients [6]. Like other aminoglycosides, tobramycin targets the bacterial ribosome, such that bacterial resistance, although rare, mainly involves impermeability and the acquisition of aminoglycoside-modifying enzymes, encoded either on a plasmid or within the genome by transposable elements [7]. However, despite their chemical stability, fast bactericidal effect, synergy with β -lactam antibiotics, and low incidence of resistance, aminoglycosides are of limited utility because of their nephrotoxicity [8][9]. While tobramycin is less nephrotoxic than gentamicin and other aminoglycosides and has been successfully used against *P. aeruginosa* [10], planktonic bacteria are much more sensitive than bacteria in biofilms, the growth form occurring in the lower respiratory tract of CF patients. The reduced efficacy of tobramycin and other antimicrobials is due to poor mucus penetration, the resilience of the extracellular matrix of the biofilm, and inactivation of the drug through various binding interactions in the infected CF lung [11].

Nanoformulations such as lipid nanoparticles could improve the delivery of tobramycin and thus enhance its activity. Lipid nanoparticles with a solid matrix are available as solid lipid nanoparticles (SLN) and as newer-generation lipid nanostructured lipid carriers (NLC). SLN are composed of solid lipids. NLC are prepared from a blend of a solid lipid with a liquid lipid. Both are stabilized by surfactants and are able to incorporate lipophilic and hydrophilic drugs [12].

Among the key benefits of lipid nanoparticles in the pulmonary delivery of antibiotics are the improved bioavailability and rapid distribution of the drug, precise targeting of the site of infection, the need for a lower dose, the longer administration intervals, thereby reducing the risk of serious dose-related side effects, and the scaling-up feasibility of nanoparticle production [13]. The specific advantages of SLN and NLC over other delivery systems include their higher stability compared to liposomes, both in vitro and in vivo [12] [14], as well as their better biocompatibilities and lower potential toxicity (both acute and chronic) compared to polymeric nanoparticles and other synthetic formulations [15]. Moreover, the use of nanoparticles could overcome pre-existing drug resistance mechanisms, including those involving the decreased uptake and increased efflux of the drug, to achieve better biofilm penetration. Previous studies testing the effectiveness of aminoglycosides against clinical isolates of *P. aeruginosa* reported better results with compounds loaded in nanoformulations than with the free drug [16] [17] [18].

Based on these findings and our own results demonstrating the antimicrobial activity of colistin loaded into lipid nanoparticles [19] [20], in this work we explored the activity of nanoencapsulated (both SLN and NLC) tobramycin versus that of the free drug against *P. aeruginosa* clinical isolates obtained from CF patients. We then investigated the efficacy of these novel formulations in the eradication of *P. aeruginosa* biofilms.

2. Materials and Methods

2.1. Bacterial isolates

The 34 clinical isolates of *P. aeruginosa* (17 non-mucoid and 17 mucoid) included in this study were obtained from the sputum samples and pharyngeal exudates of CF patients seen at the Hospital de la Vall d'Hebron and Hospital Sant Joan de Déu (Barcelona, Spain) between January and April 2012. The patients (59% female, 41% male) ranged in age from 9 to 50 years (mean: 27 years). *P. aeruginosa* strains ATCC 27853 and PAO1 served as the control strains in the drug susceptibility assays and biofilm studies, respectively. Two CF clinical isolates, *P. aeruginosa* strain 362VH (tobramycin-resistant) and strain 056SJD (tobramycin-susceptible), were used to evaluate the ability of free and nanoencapsulated tobramycin to inhibit bacterial growth and eradicate bacterial biofilms.

2.2. Chemicals and bacteriological media

Tobramycin was purchased from Sigma-Aldrich Chemicals (St.Louis,MO,USA). Mueller-Hinton II broth cation-adjusted (MHBCA) was from Becton Dickinson (Sparks, MD, US). Tryptone soy agar (TSA) was purchased from Sharlau (Sentmenat, Barcelona, Spain). Precirol ATO 5 was kindly

provided by Gattefossé (Madrid, Spain), and poloxamer 188 by BASF (Ludwigshafen, Rhineland-Palatinate, Germany). Polysorbate and Tween 80 were purchased from Panreac Química (Castellar del Vallès, Barcelona, Spain). Miglyol 812 was provided by Sasol (Hamburg, Germany).

2.3. Preparation of lipid nanoparticles

Tobramycin-loaded SLN was prepared using an emulsion solvent evaporation technique, following a procedure reported elsewhere [20]. In SLN formulations, emulsifiers constitute the aqueous phase of the emulsions, stabilizing the lipid dispersion of the nanoparticles and preventing their agglomeration [21]. Thus, the influence of the emulsifier on the bioactivity of the lipid nanoparticles was examined in two different types of SLN. SLN-tobramycin nanoparticles were prepared using the emulsifiers poloxamer 188 and polysorbate 80, each at 1% w/v. SLN-SDS-tobramycin nanoparticles were prepared using 2% sodium dodecyl sulfate (SDS) as the co-emulsifier. NLC loaded with tobramycin (NLC-tobramycin) were prepared using a hot melt homogenization technique, following the method described by Pastor et al. [20].

All three types of nanoparticles used in this work (SLN-tobramycin, SLN-SDS-tobramycin, and NLC-tobramycin) were stabilized by trehalose, since in previous research we determined that it was a better cryoprotectant than mannitol [19].

2.4. Drug susceptibility assay in planktonic bacteria

Susceptibility to free tobramycin and to the three formulations of nanoencapsulated tobramycin was determined using the broth microdilution method in accordance with the Clinical Laboratory Standards Institute [22]. Briefly, the isolates were grown overnight at 37°C in MHBCA, after which 2 mL of the culture was used to inoculate 20 mL of fresh MHBCA medium. After 2 h at 37°C and 200 rpm, the bacterial cultures were adjusted to an optical density at 625 nm (OD_{625nm}) of 0.08–0.1 and diluted 1:1000 in fresh MHBCA medium. Five µL of each diluted suspension was added to the wells of 96-well microtiter plates previously filled with MHBCA and serially diluted antibiotic (free and nanoencapsulated). The plates were incubated at 37°C for 24 h, after which the minimal inhibitory concentration (MIC) was determined macroscopically, based on the visually assessed turbidity of the wells. All experiments were performed in triplicate with three technical replicates.

2.5. Effect of free and nanoencapsulated tobramycin on *P. aeruginosa* growth

Two *P. aeruginosa* CF isolates, tobramycin-susceptible strain 056SJD and tobramycin-resistant strain 362VH, were used to examine the effect of free and nanoencapsulated (SLN and NLC) tobramycin. The antimicrobials were added to exponentially growing liquid cultures (1×10⁸ cfu/mL, in MHBCA) at concentrations above and below the MIC. Samples were taken aseptically at 0, 1, 2, 3, 4 and 5 h from bacterial cultures incubated at 37°C with shaking (250 rpm). Bacterial growth was measured optically to determine the OD_{625nm}. All measurements were carried out in triplicate.

2.6. Antimicrobial susceptibility of sessile bacteria

The minimal biofilm eradication concentration (MBEC), defined in this study as the minimal antibiotic concentration required to eliminate > 90% of the non-treated biofilm, was determined as described by Moskowitz et al. [23], with modifications. Briefly, the formation of bacterial biofilms was promoted as follows: The pegs of a modified polystyrene microtiter lid (catalog no. 445497; Nunc TSP system) were immersed into 96-well microtiter plates containing inoculated 200 µL MHBCA/well. The modified plates were left undisturbed at 37°C for 24 h. The pegs were then gently rinsed in 0.9 % NaCl and the bacterial biofilms exposed to different concentrations of free and nanoencapsulated tobramycin for 24 h at 37°C. The pegs were then rinsed again with 0.9% NaCl and the biofilms removed by centrifugation (2000 rpm, 10 min). Bacteria recovered from the biofilms were incubated for 24 h at 37°C. The OD_{625nm} was measured to determine the MBEC values. All experiments were performed in triplicate on at least three occasions.

2.7. Statistical analysis

The antimicrobial susceptibilities of the tested *P. aeruginosa* strains to free and nanoencapsulated tobramycin were statistically analyzed using Cochran's Q test. A p value < 0.05 was considered to indicate statistical significance.

3. Results and discussion

3.1 Antimicrobial activity of free and nanoencapsulated tobramycin

Nearly all the isolates tested in this study were susceptible ($MIC \leq 4 \mu g/mL$) to both the free and nanoencapsulated tobramycin formulations (Fig. 1). The MIC of free tobramycin tested against the isolates was $0.5 \mu g/mL$, whereas that of NLC-tobramycin was slightly lower (between $0.25 \mu g/mL$ and $0.5 \mu g/mL$) and was also lower than the MICs of SLN- and SLN-SDS-tobramycin ($0.5 \mu g/mL$ and between 1 and $4 \mu g/mL$, respectively) type.

In addition, NLC were much more active than either of the SLN preparations, as evidenced by MIC values of 0.5 and 1–4 $\mu g/mL$ ($p < 0.05$), respectively. Among the two types of SLN, the formulation prepared without SDS lost antimicrobial activity (2-fold higher MICs) (Fig. 1). Thus, further experiments were conducted using NLC and SLN-SDS.

The efficient antibacterial activity of lipid nanoparticles loaded with tobramycin may be due to their small size, which facilitates diffusion of the drug into the bacterial cell [24]. Similar results were reported by Ghaffari et al. [18] in their study of *P. aeruginosa* clinical isolates obtained from CF patients. The authors showed that tobramycin loaded in lipid nanoparticles had the same or higher antimicrobial activity than the free form of the drug. The slightly higher bioactivity of tobramycin-loaded NLC than SLN can be attributed to the higher drug-loading capacity of these nanoparticles and the avoidance of drug loss during storage [13] [25]. As demonstrated by Moreno-Sastre et al. [26], second-generation NLC are more stable than first-generation SLN and they can be stored at a wider range of temperatures without relevant modifications of their antimicrobial activity.

The improved antibacterial activity of SLN-SDS vs. the SLN particles suggests that SDS, when used as a co-emulsifier, confers improved drug stability and release. SDS may also facilitate contact between the lipid nanoparticles and water, resulting in a better distribution equilibrium of the drug. Of relevance to our findings is the major challenge posed by ensuring drug stability in the development of colloidal drug carriers, which offer a high surface area and short diffusion pathways [27]. Figure 1b shows the data separated for mucoid and non-mucoid strains of *P. aeruginosa*.

3.2 Effect of free and nanoencapsulated tobramycin on bacterial growth

The susceptibilities of non-mucoid, susceptible (isolate 056SJD) and mucoid, resistant (isolate 362VH) *P. aeruginosa* to free and nanoencapsulated tobramycin were similar at all concentrations of the antibiotic tested (Figure 2). At sub-inhibitory concentrations ($1/2 \times MIC$), the effect of the tobramycin-loaded lipid formulations on the growth kinetics of susceptible isolate was slightly lower than that of the free drug (Figure 2a) whereas the response of the resistant isolate did not differ (Figure 2d). At the MIC, greater inhibition of the susceptible isolate was achieved, since after 5 h of antimicrobial exposure none of the formulations was able to fully inhibit the growth of the resistant isolate (Figure 2b, e). At concentrations above the MIC, the growth of the susceptible isolate was inhibited immediately after the addition of the antimicrobial (Figure 2c), but, again, none of the formulations fully inhibited the growth of the resistant isolate (Figure 2f). Empty lipid nanoparticles had no antibacterial activity in either isolate (data not shown).

Taken together, our results demonstrate that the loading of tobramycin into lipid nanoparticles does not adversely affect the antimicrobial activity of the drug against planktonic *P. aeruginosa*. The preserved potency of lipid nanoparticles containing tobramycin may be due to their facilitated diffusion across the bacterial cell membrane. Mugabe et al. [28] showed that the effective antimicrobial activity of gentamicin loaded into liposomes involved fusion of the particles with the

bacterial membrane, leading to its deformation. Further experiments are needed to better understand the interactions between the lipids in nanoformulations and the cellular membrane of microorganisms that promote drug diffusion.

The slower killing of the mucoid, resistant strain of *P. aeruginosa* than of the non-mucoid, susceptible strain by free as well as nanoencapsulated tobramycin can be explained by the additional time needed for outer membrane permeabilization by the drug, regardless of its method of preparation, and the subsequent delay in its reaching its intracellular target.

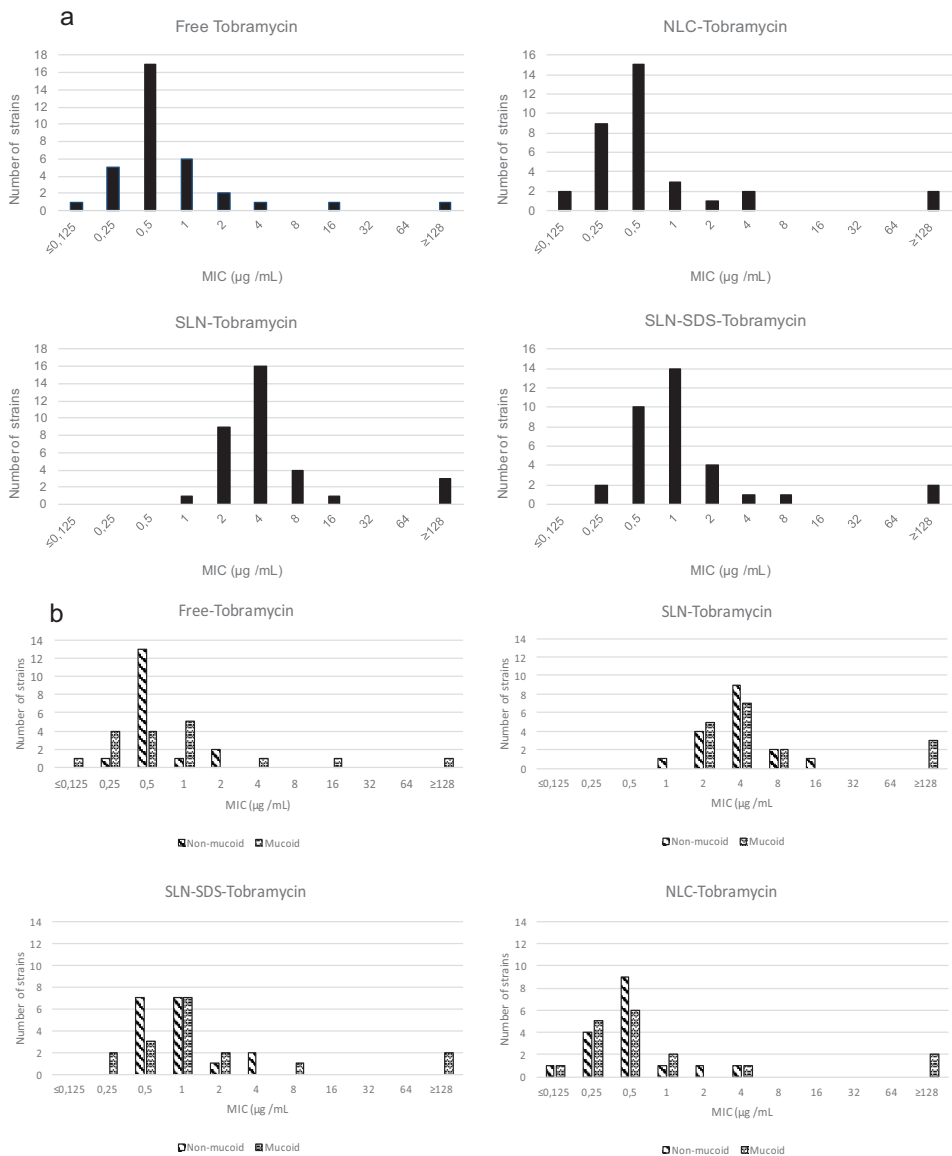


Figure 1. a) The bioactivity (minimum inhibitory concentration, MIC) of lipid nanoparticles loaded with tobramycin in 34 strains of *Pseudomonas aeruginosa* isolated from the clinical samples of cystic fibrosis patients. b) The same as in (a) but separated according to the 17 mucoid and 17 non-mucoid strains of the bacterium. For an explanation of the nanoparticles, see the text.

A previous study showed an immediate effect of tobramycin against most of the susceptible populations tested but not against the resistant population [29].

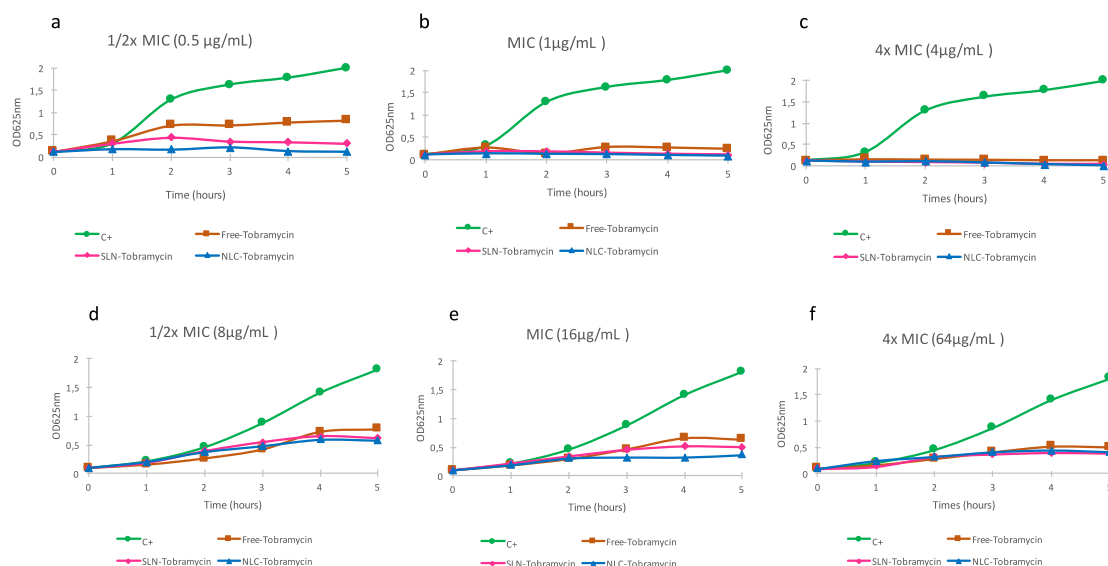


Figure 2. The effect of free and nanoencapsulated (SLN and NLC) tobramycin on the growth of *P. aeruginosa*. (a–c) Strain 056SJD at: (a) 1/2× MIC (0.5 µg/mL); (b) the MIC (1 µg/mL), and (c) 4× MIC (4 µg/mL). (d–f) Strain 362VH at (d) 1/2× MIC (8 µg/mL); (e) the MIC (16 µg/mL); and (d) 4× MIC (64 µg/mL).

3.3 Anti-biofilm efficacy of free and nanoencapsulated tobramycin

To test the influence of the lipid nanoparticles on tobramycin's ability to kill sessile bacteria, biofilms of four *P. aeruginosa* strains were exposed to free and nanoencapsulated (SLN and NLC) tobramycin at antibiotic concentrations between 0 and 256 µg/mL. ATCC strain 27853 and strain PAO1 were used as controls, and strains 056SJD (non-mucoid, tobramycin-susceptible) and 362VH (mucoid, tobramycin-resistant) as the *P. aeruginosa* CF isolates. All *P. aeruginosa* strains used in this experiment formed adequate biofilms (data not shown). The MIC and MBEC values of the four strains are shown in Table 1. Among the isolates susceptible to tobramycin, the MIC and MBEC values of the nanoencapsulated drug were slightly lower (1–2 logs) than those of the free drug. However, for the clinical isolate resistant to tobramycin, there were no differences in the MIC and MBEC values obtained with the nanoparticles and free tobramycin. The exception was NLC-tobramycin, in which the MBEC was slightly lower than the value obtained with the free form. The much higher MBEC vs. MIC values of both free and nanoencapsulated tobramycin likely reflected the interaction between the anionic mucopolysaccharide of the biofilm and the cationic aminoglycoside, such that the amount of free tobramycin available to act against the resident bacteria was limited [30]. Among the two types of nanoparticles (SLN and NLC), NLC were slightly more active than SLN (1 log) for all strains tested. Specifically, the concentrations of free tobramycin required to completely eradicate

the *P. aeruginosa* biofilm were 8–16 µg/mL (tobramycin-susceptible strains) and 32 µg/mL (tobramycin-resistant strain), but the effective NLC-tobramycin concentration was lower (2–4 µg/mL and 16 µg/mL, respectively). The better results obtained with the NLC formulation of tobramycin was in agreement with our previously published results showing that colistin-loaded NLCs were highly effective in biofilm eradication [19].

Although the mechanisms underlying the efficacy of tobramycin in NLC are not fully understood, a role for charge distribution seems likely. Tobramycin loaded into NLC has a negative net charge because of the negatively charged nanoparticles, in contrast to the positive net charge of free tobramycin. The superior mucus penetration of negatively charged nanoparticles has been reported [31] and suggests the greater ability of NLC-tobramycin to penetrate the exopolysaccharide matrix surrounding the biofilm structure. Increased penetration would better allow tobramycin to reach its cellular target, in contrast to its free form. Alternatively, the fast-antimicrobial release reported by Pastor et al. [20] would ensure an initial antimicrobial concentration that is high enough to inhibit the biofilm growth of *P. aeruginosa*. Moreover, a sustained antimicrobial concentration higher than the MIC value would enable the eradication of surviving cells. However, further experiments are needed to determine which, if any, of our hypotheses is the correct one.

	ATCC 27853		PAO1		056SJD		362 VH	
	MIC (µg/ml)	MBEC (µg/ml)	MIC (µg/ml)	MBEC (µg/ml)	MIC (µg/ml)	MBEC (µg/ml)	MIC (µg/ml)	MBEC (µg/ml)
Free Tobramycin	0.5	8	0.5	16	1	16	16	32
SLN-SDS- Tobramycin	0.25	4	0.25	8	0.5	8	16	32
NLC- Tobramycin	≤0.0625	2	0.25	4	0.25	4	16	16

Table 1. Minimal biofilm eradication concentration (MBEC) and minimum inhibitory concentration (MIC) of free and NLC-encapsulated tobramycin. *P. aeruginosa* ATCC 27853 and strain PAO1 were used as controls. Strains 056SJD (non-mucoid, tobramycin-susceptible) and 362VH (mucoid, tobramycin-resistant) served as the *Pseudomonas*

4. Conclusions

New antimicrobial formulations, such as lipid nanoparticles, can improve the transfer of antimicrobials to their sites of action, potentially allowing a dose reduction and therefore the avoidance of adverse side effects. Our study of planktonic cultures and biofilms of *P. aeruginosa* demonstrated the greater antimicrobial activity of nanoencapsulated tobramycin (both SLN and NLC), including a more efficient eradication of bacteria growing in biofilms. Given the key role of biofilms in respiratory infections of *P. aeruginosa* in CF patients, the results obtained in this study, and especially with NLC-tobramycin, may provide new options in the treatment of these infections.

Acknowledgments: The bacterial strains used in this study were generously provided by the Hospital Vall d'Hebron and Hospital Sant Joan de Déu. This work was carried out under the Comprehensive Research on Effective Therapies for the Treatment of Cystic Fibrosis and Associated Diseases (TERFIQEC); IPT-2011-1402-900000 funded by the Spanish Ministry of Economy and Competitiveness. The authors gratefully acknowledge the support of University of the Basque Country UPV/EHU (UFI11/32) and the support of the Basque Government by IT 428-10 consolidated group.

MV is member of the ENABLE (European Gram Negative Antibacterial Engine) European consortium (IMI-ND4BB, <http://www.imi.europa.eu/content/enable>).

Author Contributions: E.S-S, M.J. and E.F. did the experiments; J.L.P. prepare the nanoformulations, M.V. and T.V. conceived the research and did the interpretation of data, E.S-S. and M.V. wrote the paper.

Conflicts of Interest: The authors declare no conflict of interest

References

1. Lyczak, J.B.; Cannon, C.L.; Pier, G.B. Lung infections associated with cystic fibrosis. *Clin Microbiol Rev.* 2002,15,194–222.
2. Wei, Q.; Ma, L.Z. Biofilm matrix and its regulation in *Pseudomonas aeruginosa*. *Int J Mol Sci.* 2013,14,20983–1005.
3. Drenkard, E.; Ausubel, F.M. *Pseudomonas* biofilm formation and antibiotic resistance are linked to phenotypic variation. *Nature.* 2002,416,740–3.
4. Li, X.Z.; Plésiat, P.; Nikaido, H. The challenge of efflux-mediated antibiotic resistance in Gram-negative bacteria. *Clin Microbiol Rev.* 2015,28,337–418.
5. Fusté, E.; López-Jiménez, L.; Segura, C.; Gainza, E.; Vinuesa, T.; Viñas, M. Carbapenem-resistance mechanisms of multidrug-resistant *Pseudomonas aeruginosa*. *J Med Microbiol.* 2013,62,1317–25.
6. Döring, G.; Flume, P.; Heijerman, H.; Elborn, J.S. Treatment of lung infection in patients with cystic fibrosis: Current and future strategies. *J Cyst Fibros.* 2012,11,461–79.
7. MacLeod, D.L.; Nelson, L.E.; Shawar, R.M.; Lin, B.B.; Lockwood, L.G.; Dirk, J.E.; Miller, G.H.; Burns, J.L.; Garber, R.L. Aminoglycoside-resistance mechanisms for cystic fibrosis *Pseudomonas aeruginosa* isolates are unchanged by long-term, intermittent, inhaled tobramycin treatment. *J Infect Dis.* 2000,181,1180–4.
8. Stehling, F.; Büscher, R.; Grosse-Onnebrink, J.; Hoyer, P.F.; Mellies, U. Glomerular and tubular renal function after repeated once-daily tobramycin courses in cystic fibrosis patients. *Pulm Med.* 2017,2017,1–6.
9. Wargo, K.A.; Edwards, J.D. Aminoglycoside-Induced Nephrotoxicity. *J Pharm Pract.* 2014,27,573–7.
10. Weintraub, R.G.; Duggin, G.G.; Horvath, J.S.; Tiller, D.J. Comparative nephrotoxicity of two aminoglycosides: gentamicin and tobramycin. *Med J Aust.* 1982,2,129–32.
11. Cao, B.; Christophersen, L.; Kolpen, M.; Jensen, P.Ø.; Sneppen, K.; Høiby, N.; Moser, C.; Sams, T. Diffusion retardation by binding of tobramycin in an alginate biofilm model. *PLoS One.* 2016,11,1–11.
12. Das, S.; Chaudhury, A. Recent advances in lipid nanoparticle formulations with solid matrix for oral drug delivery. *AAPS Pharm Sci Tech.* 2011,12,62–76.
13. Weber, S.; Zimmer, A.; Pardeike, J. Solid Lipid Nanoparticles (SLN) and Nanostructured Lipid Carriers (NLC) for pulmonary application: A review of the state of the art. *Eur J Pharm Biopharm.* 2014,86,7–22.
14. Puri, A.; Loomis, K.; Smith, B.; Lee, J.H.; Yavlovich, A.; Heldman, E.; Blumenthal, R. Lipid-based nanoparticles as pharmaceutical drug carriers: from concepts to clinic. *Crit Rev Ther Drug Carrier Syst.* 2009,26,523–80.
15. Hwang, T.L.; Aljuffali, I.A.; Lin, C.F.; Chang, Y.T.; Fang, J.Y. Cationic additives in nanosystems activate cytotoxicity and inflammatory response of human neutrophils: Lipid nanoparticles versus polymeric nanoparticles. *Int J Nanomedicine.* 2015,10,371–85.
16. Abdelghany, S.M.; Quinn, D.J.; Ingram, R.J.; Gilmore, B.F.; Donnelly, R.F.; Taggart, C.C.; Scott, C.J. Gentamicin-loaded nanoparticles show improved antimicrobial effects towards *Pseudomonas aeruginosa* infection. *Int J Nanomedicine.* 2012,7,4053–63.
17. Deacon, J.; Abdelghany, S.M.; Quinn, D.J.; Schmid, D.; Megaw, J.; Donnelly, R.F.; Jones, D.S.; Kissenpfennig, A.; Elborn, J.S.; Gilmore, B.F.; Taggart, C.C.; Scott, C.J. Antimicrobial efficacy of tobramycin polymeric nanoparticles for *Pseudomonas aeruginosa* infections in cystic fibrosis: Formulation, characterisation and functionalisation with dornase alfa (DNase). *J Control Release.* 2015,198,55–61.
18. Ghaffari, S.; Varshosaz, J.; Saadat, A.; Atyabi, F. Stability and antimicrobial effect of amikacin-loaded solid lipid nanoparticles. *Int J Nanomedicine.* 2011,6,35–43.
19. Sans-Serramitjana, E.; Fusté, E.; Martínez-Garriga, B.; Merlos, A.; Pastor, M.; Pedraz, J.L.; Esquisabel, A.; Bachiller, D.; Vinuesa, T.; Viñas, M. Killing effect of nanoencapsulated colistin sulfate on *Pseudomonas aeruginosa* from cystic fibrosis patients. *J Cyst Fibros.* 2016,15,611–8.

20. Pastor, M.; Moreno-sastre, M.; Esquisabel, A.; Sans, E.; Viñas, M.; Bachiller, D.; Asensio, V.J.; Pozo, A.D.; Gainza, E.; Pedraz, J.L. Sodium colistimethate loaded lipid nanocarriers for the treatment of *Pseudomonas aeruginosa* infections associated with cystic fibrosis. *Int J Pharm.* 2014, 477, 485–94.
21. Attama, A.; Momoh, M.A.; Builders, P.F. Lipid Nanoparticulate Drug Delivery Systems: A Revolution in Dosage Form Design and Development. *Recent Adv Nov Drug Carr Syst.* 2012, 107–40.
22. Clinical and Laboratory Standards Institute. Performance standards for antimicrobial susceptibility testing; 27th informational supplement CLSI document M100-S27. Wayne, PA Clin Lab Stand Inst. 2017.
23. Moskowitz, S.M.; Foster, J.M.; Emerson, J.; Burns, J.L. Clinically Feasible Biofilm Susceptibility Assay for Isolates of *Pseudomonas aeruginosa* from Patients with Cystic Fibrosis. *J Clin Microbiol.* 2004, 42, 1915–22.
24. De Jong, W.H.; Borm, P.J. Drug delivery and nanoparticles: applications and hazards. *Int J Nanomedicine.* 2008, 3, 133–49.
25. Martins, S.; Sarmiento, B.; Ferreira, D.C.; Souto, E.B. Lipid-based colloidal carriers for peptide and protein delivery - liposomes versus lipid nanoparticles. *Int J Nanomedicine.* 2007, 2, 595–607.
26. Moreno-Sastre, M.; Pastor, M.; Esquisabel, A.; Sans, E.; Viñas, M.; Bachiller, D.; Pedraz J.L. Stability study of sodium colistimethate-loaded lipid nanoparticles. *J Microencapsul.* 2016, 33, 636–645.
27. Yadav, N.; Khatak, S.; Vir, U.; Sara, S. Solid lipid nanoparticles - a review. *Int J Appl Pharm.* 2013, 5, 8–18.
28. Mugabe, C.; Azghani, A.O.; Omri, A. Liposome-mediated gentamicin delivery: Development and activity against resistant strains of *Pseudomonas aeruginosa* isolated from cystic fibrosis patients. *J Antimicrob Chemother.* 2005, 55, 269–71.
29. Bulitta, J.B.; Ly, N.S.; Landersdorfer, C.B.; Wanigaratne, N.A.; Velkov, T.; Yadav, R.; Oliver, A.; Martin, L.; Shin, B.S.; Forrest, A.; Tsuji, B.T. Two mechanisms of killing of *Pseudomonas aeruginosa* by tobramycin assessed at multiple inocula via mechanism-based modeling. *Antimicrob Agents Chemother.* 2015, 59, 2315–27.
30. Khan, W.; Bernier, S.P.; Kuchma, S.L.; Hammond, J.H.; Hasan, F.; O'Toole, G.A. Aminoglycoside resistance of *Pseudomonas aeruginosa* biofilms modulated by extracellular polysaccharide. *Int Microbiol.* 2010, 13, 207–12.
31. Forier, K.; Messiaen, A.S.; Raemdonck, K.; Deschout, H.; Rejman, J.; De Baets, F.; Nelis, H.; De Smedt, S.C.; Demeester, J.; Coenye, T.; Braeckmans, K. Transport of nanoparticles in cystic fibrosis sputum and bacterial biofilms by single-particle tracking microscopy. *Nanomedicine.* 2013, 8, 935–49.



© 2017 by the authors. Submitted for possible open access publication under the terms and conditions of the Creative Commons Attribution (CC BY) license (<http://creativecommons.org/licenses/by/4.0/>).

4. DISCUSSION

4. DISCUSSION

Cystic fibrosis (CF) lung surrounded by viscous mucus, and affected by a debilitated mucociliary clearance, promotes bacterial infection and inflammation (33). *P. aeruginosa* is one of the major opportunistic pathogen colonizing the respiratory tract of CF patients and causing chronic airways infection. Once *P. aeruginosa* established chronically in the CF lung, bacterial density increases and the microorganism switches to a mucoid form and to a stable biofilm mode of growth in which susceptibility to antimicrobials decreases (99). The high resistance of *P. aeruginosa* to multiple antimicrobials led to scenarios in which almost no treatment options are available. In this regard, the research on the introduction of less toxic antimicrobials as well as the use of pharmaceutical forms enabling dose reductions, longer administration intervals, and reduced systemic toxicity has been stimulated (118)(115).

Along this doctorate period we have succeed in developing antibiotic-loaded lipid nanoparticles such as solid lipid nanoparticles (SLN) and nanostructured lipid carriers (NLC), as pulmonary delivery system focusing on the treatment of *P. aeruginosa* infections in CF patients.

Two antimicrobial agents have been assayed: tobramycin and mostly colistin. On one hand, tobramycin was included since it was selected as inhaled antibiotic of choice in the treatment of CF associated with *P. aeruginosa* CF infections (119). However, despite its effectiveness, the emergence of tobramycin-resistant *P. aeruginosa* clinical isolates due to the low permeability of the outer membrane as well as the acquisition of genes encoding antimicrobial resistance has been noted in several studies (120). Moreover, the reduced efficacy of tobramycin is also correlated with poor mucus penetration and drug inactivation through various binding interactions in the infected CF lung (121). On the other hand, colistin was selected since nowadays inhaled colistin is considered a useful therapeutic option for early antibiotic intervention in periodically colonized CF patients and in critically ill patients, resulting in one of the most active antimicrobials to combat multidrug-resistant bacteria (76). Nevertheless, recent studies have reported

the emergence of colistin-resistant bacteria mediated by the post-translational modification of lipopolysaccharide in CF patients treated with long-term by inhalations (103). Despite the fact that both antimicrobials are effective against *P. aeruginosa*, they produce local side effects. Furthermore, their administration is time consuming, is conditioned by unpredictable systemic drug absorption and needs education and training. All these facts together induce poor adherence to the treatment (29).

An awareness of this threat has initiated the search for new treatment options. An alternative is the use of lipid nanoparticles (SLN and NLC) to improve the drug delivery and enhance its activity. The first generation of lipid nanoparticles (SLN), are composed of solid lipids, whereas NLC, the second generation of lipid nanoparticles, are prepared from a blend of a solid lipid with a liquid lipid. Both are stabilized by surfactants and are able to incorporate lipophilic and hydrophilic drugs (122). Among the key benefits of lipid nanoparticles in the pulmonary delivery of antimicrobials are the improved bioavailability and rapid distribution of the drug, precise targeting of the site of infection, the need for a lower dose, the longer administration intervals, thereby reducing the risk of serious dose-related side effects, and the scaling-up feasibility of nanoparticle production (108). Some advantages of these nanoparticles over other delivery systems include their higher stability compared to liposomes, both in vitro and in vivo (122)(123), as well as their better biocompatibilities and lower potential toxicity (both acute and chronic) compared to polymeric nanoparticles and other synthetic formulations (124). In principle, the administration of encapsulated drugs could overcome pre-existing resistance mechanisms, including those involving the decreased uptake and increased efflux of the drug, as well as achieve better biofilm penetration (115).

Therefore, the aim of this thesis was to develop nanoencapsulated colistin and tobramycin in both SLN and NLC and explore their antimicrobial activity versus free drug against *P. aeruginosa* clinical isolates from CF patients and to investigate the efficacy of these novel formulations in the eradication of biofilms, one of the most relevant mechanisms involved in persistence and in chronic infections.

Elaboration and characterization

The main objective of the first part of this thesis was to elaborate and characterize lipid nanoparticles (SLN and NLC) as colistin and tobramycin carriers to treat *P. aeruginosa* lung infection. Specifically, the physicochemical properties of lipid nanoparticles, their toxicity effect, and the *in vivo* distribution of these nanoformulations in lungs were determined. Moreover, nebulization and mucus penetration experiments were also performed. The results of these studies have been reported in **Papers 1 and 2**.

Firstly, colistin loaded lipid nanoparticles were prepared focusing on the treatment of *P. aeruginosa* in CF patients. The use of lipid nanoparticles gave rise to a potential enhancement of treatment. High encapsulation efficiencies (EE) (SLN 79.7% and NLC 94.8%) were obtained which are in accordance with the results reported by Martins et al. (125) who also described high EE values (>90%) for camptothecin-loaded SLN. Their slightly higher results are likely to be associated with the higher lipophilicity of camptothecin compared to colistin. Likewise, Patlolla et al. (126) reported similar encapsulation efficiency (EE) values (>90%) when encapsulating Celecoxib in NLCs. Therefore, the lipid nanoparticles described in this work presented acceptable EE values, comparable to those reported previously. Turning to the release profile of the nanoparticles, NLCs released an 86% of colistin in 8 hours and SLNs a 50%, data that were similar to those reported by Silva et al. (127) for risperidone loaded SLN, i.e., 40% drug released by the 8th hour, similarly, Zheng et al. (128) also detected almost a 100% of drug release from their NLCs. Remarkably, it could be observed that almost all the drug was released from the Colistin-NLC under the assayed conditions. This sustained release, especially the one presented by the Colistin-NLC, could reduce the number of doses, improving patient adherence to the treatment and, thus, life quality. The release profile of the dye was much slower than that observed for colistin, very likely due to its lipophilicity (129). Indeed, this delayed release is very helpful for the *in vivo* imaging in order to ensure that the infrared (IR) dye detected in mice is closely related to the dye incorporated into the NLCs. Regarding the cell experiments, it should be remarked that, in agreement with

our findings, Nassimi et al. (130) reported that blank SLN displayed very high IC₅₀ values (analyzed by MTT, (3-(4,5-dimethylthiazole-2-yl)-2,5-diphenyltetrazolium bromide, and NRU, Neutral Red Uptake), that is 2–3 mg/ml. Although the assays were conducted under the same cell line, the results could not be directly compared as they used other techniques for determination of cell viability. On an average, as reported by Doktorovova et al. (131) after the analysis of their published data concerning IC₅₀, this value is usually within 0.1–1 mg/ml for lipid nanoparticles, being in our case slightly superior for Colistin- NLC, 2.82 mg/ml and 1.08 mg/ml for A549 and H441, respectively. In terms of cell viability, Ribeiro de Souza et al. (132) describe that praziquantel-loaded SLN presented a time and dose-dependent cell viability in a hepatoma cell line, reaching up to a 70% decrease of cell viability for the free drug and 45% decrease for the loaded SLN. Overall, it could be concluded that colistin encapsulation led to lower toxicity values. Lately, due to the Gram-negative resistance, the use of colistin has re-emerged despite its side effects and toxicity (133). Hence, based on these *in vitro* results, it could be hypothesized that inserting colistin into lipid nanoparticles decreases the toxicity of the drug, mainly because it is released in a controlled manner over time. As far as the *in vivo* biodistribution experiments are related, NLCs displayed a suitable tissue disposition, spreading extensively throughout the lungs. Similarly, Taratula et al. (134) reported that NLC presented a uniform distribution through the lungs 24 hours post-nebulization, whereas intravenous administration led to only 23% of NLCs retained in the lungs.

Secondly, following the encouraging results obtained with colistin loaded in lipid nanoparticles, primarily with the second generation of lipid nanoformulations, we decided to encapsulate tobramycin in SLN and NLC. Nanoparticles displayed a diameter size ranging from 250 to 300 nm using trehalose or mannitol as cryoprotectants. The particle size of the nanoparticles prevents the phagocytosis of the particles by macrophages. It is generally assumed that particles of 0.5–3 μ m in diameter are captured by macrophages being these dimensions the maximal and minimum size (135). It should be stated that maximal encapsulation efficiencies (93%) were

achieved for both (SLN and NLC) nanoparticles. As it was observed with colistin, the nanoparticles loaded with tobramycin also had the ability to release the antibiotic in *in vitro* experiments. According to the release studies, a biphasic profile, characterized by an initial rapid release followed by a modulated and progressive release of antibiotics were observed. Total release lasted at least for three days, in both types of formulations. This profile release is almost identical to the one reported by Patlolla et al. (126). It is remarkable that the number of doses could be reduced or longer the dosing interval and therefore enhance patient compliance.

To determine whether tobramycin loaded in NLC exerted cell toxicity, *in vitro* cytotoxicity and viability assays using human epithelial cell (A549 and H441) lines was performed after 24 h of exposition. None of the formulations tested presented toxicity, at least at the concentrations studied. This finding is in accordance with other reports that demonstrated the good tolerability of lipid nanoparticles *in vitro* using A549 cell lines (126)(136). Furthermore, the concentration of 1 mg/ mL is 2000 times higher than the MIC of tobramycin-NLCs against *P. aeruginosa* (MIC 0.5 µg/mL). In the next step, cell viability was analyzed under fluorescent microscopy where the predominance of green color in all the samples confirmed the safety of the lipid nanoparticles. Mucus covers many body surfaces forming a gel-like barrier to protect the body from pathogens and other kind of environmental ultrafine particles (137). However, in CF patients this natural mucus becomes tenacious housing many bacterial pathogens that hinder the penetration of antibiotics and the efficiency of therapies. Therefore, in order to overcome this abnormal mucus barrier and to prolong the NLCs retention in the lung two mucolytic agents (mannitol and carboxymethylcysteine) were selected. It was tested whether our nanoparticles could cross the mucus and facilitate the drug transport through it using the artificial mucus (AM) model, reported before by Yang et al. (138). Coomassie blue (CB) dye was chosen as the active ingredient because the gelatin interfered with the amino groups of the tobramycin and it was impossible to quantify. As the nanoparticle diffusion across the mucus is dictated by the size of the mucus pores, tobramycin-NLCs particles with an approximate diameter of 250 nm, theoretically, should be able to overcome the mucus barrier as they are small enough to diffuse across the mucus pores

which typically fall in the range of 200–500 nm in chronically infected lungs (139). As expected, the penetration of the particles across the mucus layer was improved by the addition of mucolytic agents that facilitated the drug transport through it. Suk et al. (140) also demonstrated an increased in particle penetration through CF sputum when using another mucolytic, N-acetylcysteine. Complementary studies incubating *P. aeruginosa* with AM are needed in order to find out what could happen in an infection scenario such as in CF patient sputum. The permeability assay revealed that the maximum drug permeation across the mucus layer was observed for the tobramycin-NLC PC (precinol + compritol) incorporating carboxymethylcysteine (CMC), whereas the addition of mannitol did not improve significantly the drug permeability at 7 hours. Similarly, Suk et al. (140) also reported a close to 13-fold improvement in the diffusion velocity of nanoparticles through a sputum layer upon the addition of N-acetylcysteine. The presence of tobramycin in the receptor compartment suggests that the drug from NLCs may slowly release, permeate and distribute into the abnormal mucus layer being locally available for its antimicrobial activity. According to these results, we developed a mucus penetrating drug carrier that after formulate with appropriate mucolytic agents, could offer sustained levels of antibiotic at the mucus barrier. Finally, the administration of IR-NLCs exerted a strong IR signal in the lungs of the mice lasting until 48 hours allowing the drug release from the lipid matrix. The intra-tracheal instillation by Penn Century1 device provides a fast and quantifiable technique for drug delivery directly to the lungs presenting large distribution and minimal drug loss during application compared to nebulization processes (141). However, intra-tracheal instillation does not reflect the natural inhalation mechanism because the formulation is required to be administered to anesthetized animals (142). Regarding to the free drug, Poyner et al. (106) reported that the endotracheal administration of radiolabeled tobramycin led to a higher dissemination to the kidney and in a lower extent at the lung tissue compared to liposomal and microcapsular tobramycin which were primarily retained in the lungs, thus decreasing nephrotoxicity. Similar results were reported by Varshosaz et al. (143) who confirmed that amikacin-loaded SLNs remained 6 hours longer in lungs after pulmonary administration by microsyringe compared to intravenous route. Therefore, it might be concluded

that tobramycin encapsulation within nanoparticulate drug delivery systems (DDSs) may represent an advantage for prolonging lung residence time of the encapsulated drug that would be slowly released to the media allowing continuous bacterial killing.

Stability

The second essential point of this work concerns the stability of both type of lipid nanoparticles after freeze-drying. The maintenance of their physicochemical properties over time, the effect of the storage temperature of nanoparticles over time, as well as the action of trehalose and mannitol as cryoprotectants in freeze-dried formulations were extensively studied. The stability studies were carry out on lipid nanoparticles loaded with colistin. The results of these studies have been reported in **Papers 1, 3 and 4**.

It is suggested that the high drug loading capacity described for NLCs is related to the blending of a solid lipid with a liquid lipid leading to a less ordered solid lipid matrix providing the possibility for a high drug encapsulation (144). Additionally, the presence of liquid lipids in NLCs could improve drug solubility and therefore, increase drug encapsulation (145). Liquid lipids are better solubilizers of drugs than solid lipids. It is important to note that the chemical nature of the lipid, as lipids which form highly crystalline particles with a perfect lattice (e.g. monoacid triglycerides) lead to drug expulsion. More complex lipids containing mixtures of mono-, di- and triglycerides, such as the Miglyol used to prepare NLCs, form less perfect crystals that could lead to a better accommodation of drugs (146). In the case of SLNs, only a solid lipid was used giving rise to an ordered internal structure minimizing loading capacity. In regard to the effect of the storage temperature on nanoparticles stability over time, it was observed that there was a progressive increase in size for all temperatures tested, being more remarkable at 30°C and 40°C. In a similar study carried out by Venkateswarlu et al. (147), clozapine-SLNs increased their size two-fold, from 40 to 78.8 nm, after 6 month-storage at 25°C. It was found that SLNs for gene therapy lyophilized with trehalose were physically stable during 9 months at 25°C/60%

relative humidity (RH) and 6 months at 30°C/65% RH (148). However, the stability was lost when harder conditions were employed. In fact, colistin-NLCs presented a size of around 400 nm at 5°C and 25°C but with a slight growth at the sixth month. Nevertheless, when Colistin-NLCs were stored at higher temperatures, a size increase was detected over the third month, exceeding 600 nm at 30°C and 40°C. The particle size fluctuations at the highest temperatures tested indicated that the size of the nanoparticles was influenced by the storage conditions. Interestingly, Das et al. (149) reported that clotrimazole-loaded NLCs showed better stability in terms of size than SLNs at 5°C and 25°C after 3 months of storage, especially when a high amount of drug is incorporated to the formulation (10% versus 4% drug to lipid ratio). It is reported that the average particle diameter of lipid nanoparticles can be influenced by different factors, such as the composition of the formulation, the production technique or the parameters of the process such as time, temperature, pressure, equipment type, lyophilisation and storage conditions (150). The particle size can modulate the capture mechanism by macrophages and influence their biological stability, as phagocytosis increases when particle size increases; hence, it could influence the biodistribution behavior of the particles. Due to the small size of the nanoparticles developed, they have a greater chance to escape from the clearance mechanism by alveolar macrophages, compared to a microparticulate form (151). Moreover, after using a nebulization system, pulmonary deposition depends on the particle size, shape and ventilation parameters; with decreasing particle diameters below 500 nm, the deposition increases in all regions of the lung due to their diffusional mobility and they should also be able to diffuse through the mucus pores of chronically infected lungs that typically fall in the range of around 200–500 nm (139)(152). The measurement of the polydispersity index (PDI) indicates the wide distribution of the particle size with values ranging from 0 to 1, and it is also a parameter that is used to evaluate the preservation of nanoparticles. As expected, more variations in the PDI at higher temperatures for both formulations were observed. In general, as the particle size increased, the PDI also augmented. On one hand, the PDI of colistin-SLNs was higher when increasing time and temperature, for instance, in the third month at 30 °C and 40 °C, the PDI

reached the highest values, 0.87 and 0.59, respectively. Only samples stored under 5°C and 25°C displayed PDI values below 0.5. This is in agreement with the PDI values (<0.5) obtained by Ridolfi et al. (153) when testing chitosan-SLN-tretinoin over one year period at room temperature. On the other hand, the PDI of colistin-NLCs at the third month rose up to 0.57 and 0.75 at 30°C and 40°C, respectively, indicating a heterogeneous distribution of the nanoparticles that could be related to an increase of agglomerates. However, at lower temperatures, all PDIs were less than 0.5 meeting the criteria requirement for the storage conditions, meaning that the samples were monodisperse and homogenous. Altogether, the storage conditions at 5°C and 25°C met the specifications of size and PDI for colistin-SLNs and colistin-NLCs after three months and one year of storage, respectively. The measurement of zeta potential (ZP) is a good method to evaluate the state of nanoparticle surface, detect any eventual modification during storage, as well as to predict physical stability of the nanoparticles. Positive and negative ZP indicates the degree of repulsion between close and similar particles in the dispersion; this repulsion prevents the aggregation process of particles (154). At time 0 (after the lyophilisation step) the charge for colistin-SLNs and colistin-NLCs was almost identical, -20.8 and -21.97 mV, respectively. These zeta potential values could lead to a decreased risk of particle aggregation and enlargement after re-dispersion due to electric repulsion (154). The ZP for all colistin-SLNs formulations ranged from -20 to -30 mV during the three months of the study. Similarly, Radomska-Soukharev (155) reported no changes in zeta potential of their SLNs formulations (-20 to -30 mV) after two years of storage at 5°C, 25°C and 40°C, as the values at all three temperatures were identical to those of the day of preparation being the most stable ones the SLNs obtained with triglycerides compared to mono- and diglycerides. It could be noticed that when the temperature increased, the ZP of colistin-SLNs was more negative, reaching -30.20 mV at 30°C. Turning to the issue of colistin-NLCs, the ZP values below -20 mV at all conditions tested after one year indicating long-term stability. Generally, ZP value above +20 mV or below -20 mV combined with steric stabilization predicts good stability of the nanoparticle dispersion. Therefore, the NLCs prepared are expected to be stable beyond the observation period (149). Some authors found that the

zeta potential of itraconazole-loaded NLCs stayed unchanged (around -31 mV) at room temperature and refrigerated conditions after 6 months of storage (156). By the drug release experiments, it was observed that at time 0, the NLCs released the drug in a control manner reaching $91.53 \pm 7\%$ at 24 hours and almost 100% at 48 hours. The initial fast release of the nanoparticles may be due to the presence of the drug in their surface, while the drug incorporated into the particulate core is released in a prolonged way. Colistin-NLCs demonstrated a sustained drug release also after 12 months under 5°C and 25°C as they showed similar release profile as the fresh nanoparticles. Similar findings were reported by Das et al. (149) when working with clotrimazole-loaded NLCs. The results obtained in our study confirmed the stability of the drug entrapped in nanoparticles as 100% of the drug (total encapsulated drug) was able to be released from the NLCs at 5°C, 25°C/60% RH and 30°C/65% RH, indicating that the antimicrobial was able to exert its antipseudomonal activity. The sustained release of a drug incorporated in a delivery system is a relevant characteristic quite often correlated with improved pharmacokinetics and efficacy (157). According to the prolonged release profile of the NLCs, it could be suggested that colistin delivered as lipid nanocarriers might be administered in lower doses or longer intervals, thus reducing its undesirable side effects. By the microbiological experiments, it could be demonstrated that all *P. aeruginosa* isolates tested were susceptible ($\text{MIC} \leq 4 \mu\text{g/mL}$) to free colistin and to NLC-colistin prepared by using trehalose as cryoprotectant. When comparing both types of nanoparticles (SLN and NLC) stabilized by mannitol, it becomes apparent that NLC were much more active than SLN accounting 3 and 19% of survival ($p < 0.05$). Moreover, the comparison between SLN-colistin stabilized by mannitol and trehalose, one can conclude that differences were also significant ($p < 0.05$). In conclusion, it was demonstrated that NLC were more active than SLN and that trehalose was more adequate to be used as cryoprotectant in the preparation of nanoparticulated colistin (lyophilization process). Consequently, the effect of the temperatures of storage over time was only tested for nanoparticles stabilized with trehalose. After storages of 3 months at 25 °C, 30 °C, and 40 °C, SLN nanoparticles loose antimicrobial activity (MICs increased between 1 and 2 dilutions). In contrast, NLC

maintained similar levels of activity after storage at different conditions for 9 months. Overall, it could be deduced that colistin-SLNs were not able to keep their antimicrobial activity after three months of storage and the stability study was stopped for colistin-loaded SLNs. It has been previously reported that SLN are less stable than NLC (158). This finding could be explained by the fact that the SLNs lipid modification during storage led to drug degradation giving rise to activity loss. It should be pointed out that mucoid isolate was less susceptible to colistin-SLN than non-mucoid strains, suggesting that the mucoid state could alter the effect of SLN but not NLC. After 3 months, storage at different temperatures, MICs of isolates to NLC-colistin became lower than those of SLN-colistin. Antibacterial activity of NLC-colistin remained stable for all isolates and tested temperatures, giving MIC values similar to those of fresh nanoparticles. Our results showed that NLC were more stable than SLN and that they can be employed in a wider range of storage temperatures without relevant modifications on their antimicrobial activity. Thus, NLC stabilized with trehalose was the chosen formulation for further experiments. According to some authors (159), NLC, which are a second generation of lipid nanoparticles, have higher drug loading capacity than SLN (first generation of lipid nanoparticles) and do not present drug expulsion during storage. Finally, it was observed that the antimicrobial efficiency of colistin-NLCs was retained during 12 months against all the strains tested as the MIC values always were 16 µg/mL, even during storage under harder conditions of temperature and humidity. These results demonstrated that colistin encapsulated into NLCs was capable of preserving the antimicrobial activity during the storage period at ICH conditions.

Antimicrobial activity

The last part focuses on the study of the antimicrobial activity of SLN and NLC loaded with colistin and tobramycin against *P. aeruginosa* isolates from Sant Joan de Déu and Vall d'Hebrón hospitals CF patients. For this reason, we determined the antimicrobial effect and analyzed the key role of both antimicrobials loaded in lipid nanoparticles on *P. aeruginosa* planktonic and biofilm mode of growth.

The results of these studies have been reported in **Papers 1, 2, 3, 5 and 6.**

CF patients usually suffer for chronic infections caused by *P. aeruginosa*, which frequently become resistant to many antimicrobial agents. For that reason, the efficacy of colistin and tobramycin loaded in lipid nanoparticles was evaluated.

Initially, the antibacterial activity of colistin nanoencapsulated on *P. aeruginosa* planktonic cultures was extensively studied. It should be underlined that the lipid nanoparticles loaded with colistin described in this work presented MIC values similar to its free form around 1–2 µg/mL and were active against the mucoid strains. Although both lipid formulations had antimicrobial effect, NLCs were much more active than SLNs. This is in agreement with our previous stability results demonstrating that second-generation NLC are more stable than first-generation SLN and they can be stored at a wider range of temperatures without relevant modifications of their antimicrobial activity (160). Moreover, our empty lipid nanoparticles did not have antibacterial activity. Other authors, such as Omri et al. reported much higher MIC values for *P. aeruginosa* ATCC 27853 (between 4.0 and 1.0 µg/mL) when incorporating Polymixin B in liposomes. However, the MIC values were even higher when the free Polymixin B was assessed (161). The effect of free and nanoencapsulated colistin on *P. aeruginosa* growth was also evaluated. On this point, both CF isolates used in this study (056SJD colistin-susceptible strain and P19 colistin-resistant strain) presented similar susceptibilities to free colistin, nanoencapsulated colistin, and empty nanoparticles with free colistin at all concentrations tested. At subinhibitory concentrations of antimicrobials ($1/4 \times \text{MIC}$), no differences were observed among the formulations tested, being rates of growth slightly lower than those of the drug-free control. At MIC, the inhibitory effect was higher on the susceptible isolate although none of the formulations were able to fully inhibit bacterial growth of the resistant isolate after 4 h of antimicrobial exposure. At concentrations above MIC, bacterial growth was immediately inhibited after the addition of the antimicrobial. There are no previously reported data on the antimicrobial activity of colistin nanoencapsulated in lipid nanoparticles against *P. aeruginosa* biofilms. After observing that colistin nanoencapsulated

did not lose its bioactivity, we decided to focus on the capability of tobramycin loaded in lipid nanoparticles to act against *P. aeruginosa* CF isolates. It was found that almost all isolates tested in this study were susceptible ($MIC \leq 4 \mu\text{g/mL}$) to both the free and nanoencapsulated tobramycin formulations. The MIC of free tobramycin tested against the isolates was $0.5 \mu\text{g/mL}$, whereas that of NLC-tobramycin was slightly lower (between $0.25 \mu\text{g/mL}$ and $0.5 \mu\text{g/mL}$) and was also lower than the MICs of SLN- and SLN-SDS-tobramycin ($0.5 \mu\text{g/mL}$ and between 1 and $4 \mu\text{g/mL}$, respectively) type. Thus, NLC were much more active than either of the SLN preparations, as evidenced by MIC values of 0.5 and $1\text{--}4 \mu\text{g/mL}$ ($p < 0.05$), respectively. Among the two types of SLN, the formulation prepared without SDS lost antimicrobial activity (2-fold higher MICs).

The efficient antibacterial activity of tobramycin-loaded in SLN and NLC may be due to their small size, which facilitates diffusion of the drug into the bacterial cell (162). Ghaffari et al. reported that tobramycin loaded in lipid nanoparticles had the same or higher antimicrobial activity than its free form against *P. aeruginosa* clinical isolates obtained from CF patients (163). The slightly higher bioactivity of tobramycin-loaded NLC than SLN can be attributed to the higher drug-loading capacity of these nanoparticles and the avoidance of drug loss during storage (108)(164). The improved antibacterial activity of SLN-SDS vs. the SLN particles suggests that SDS, when used as a co-emulsifier, confers improved drug stability and release. SDS may also facilitate contact between the lipid nanoparticles and water, resulting in a better distribution equilibrium of the drug. The encouraging results obtained to date led us to optimize the NLC-tobramycin formulation, as well as to determine its MIC value finding the same or higher antipseudomonal activity than free tobramycin (165). The effect of free and nanoencapsulated tobramycin on *P. aeruginosa* growth was also evaluated. In this regard, it was observed that the susceptibilities of non-mucoid, susceptible (isolate 056SJD) and mucoid, resistant (isolate 362VH) *P. aeruginosa* to free and nanoencapsulated tobramycin were similar at all concentrations of the antibiotic tested. At sub-inhibitory concentrations ($1/2 \times MIC$), the effect on the growth kinetics of susceptible isolate was slightly lower than that of the free drug whereas the response of the resistant isolate did not differ. At the MIC,

greater inhibition of the susceptible isolate was achieved, since after 5 h of antimicrobial exposure none of the formulations was able to fully inhibit the growth of the resistant isolate. At concentrations above the MIC, the growth of the susceptible isolate was inhibited immediately after the addition of the antimicrobial, but, again, none of the formulations fully inhibited the growth of the resistant isolate. In this case, empty lipid nanoparticles had either antibacterial activity in either isolate.

Taken together, our results demonstrate that the loading of antibiotics into lipid nanoparticles does not adversely affect the antimicrobial activity of the drug against planktonic *P. aeruginosa*. The preserved potency of lipid nanoparticles containing antibiotic may be due to their facilitated diffusion across the bacterial cell membrane. Mugabe et al. showed that the effective antimicrobial activity of gentamicin loaded into liposomes involved fusion of the particles with the bacterial membrane, leading to its deformation (166). Further experiments are needed to better understand the interactions between the lipids in nanoformulations and the cellular membrane of microorganisms that promote drug diffusion. The slower killing of the mucoid, resistant strain of *P. aeruginosa* than of the non-mucoid, susceptible strain by free as well as nanoencapsulated antimicrobial can be explained by the additional time needed for outer membrane permeabilization by the drug, regardless of its method of preparation, and the subsequent delay in its reaching its intracellular target.

To test the influence of the lipid nanoparticles on colistin's ability to kill sessile bacteria, NLCs were the chosen formulation due to their higher efficacy in comparison with that one showed by SLNs. It was directly observed that whereas concentrations of free colistin as well as when empty nanoparticles and free colistin were used together, colistin concentrations required to completely eradicate biofilm ranged from 640 to 2560 µg/mL, in contrast, concentrations of NLC-colistin needed for biofilm removal were much lower (160 and 320 µg/mL, respectively). These values were quite similar either in mucoid, non-mucoid, and reference strain as well. Since it seems clear than biofilms play a key role in respiratory infections in CF patients by *P. aeruginosa*, NLC-colistin could open new frontiers in the treatment of such infections. Despite the intimate mechanism by which colistin in NLC is so

efficient in biofilm removal remains unknown, data clearly show that it is directly derived from the pharmaceutical nanoform since free colistin plus empty NLC do not have significant effect on MBEC values (at maximum one dilution) whereas NLC-colistin gave MBEC values up to four dilutions. As Pamp et al. (167) pointed out, free colistin acts preferentially on bacteria with low metabolic rates, that is to say in a biofilm free colistin is going to be more active on the microbes located deep in the multilayered biofilm, since metabolic activity decreases when distance to surface increases. It could be also feasible that nanoencapsulated colistin would not distinguish between metabolically active bacteria and starved individuals. Another possibility is in close relation with the charge distribution. NLC-colistin has a negative net charge, whereas free colistin has a positive net charge. Lipopolysaccharide has also negative charge, and this charge is higher at stationary phase of growth, than at exponential phase; subsequently, NLC-colistin (negatively charged) action on exponentially growing bacteria would be favored. It is well known that *P. aeruginosa* exposed for long periods to colistin exhibits a mechanism of resistance based on the up-regulation of a two-component system (or more). This leads to the addition of 4-aminoarabinose to lipid A of the LPS molecule reducing the net negative charge of LPS and limiting its interaction with polycationic antibiotics (adaptive resistance) (168). When resistant strains (P19 and P20) were tested by their susceptibility to free and nanoencapsulated colistin, results demonstrate that also in this case nanoencapsulated colistin was more active against biofilms than free colistin. This is in agreement with the hypothesis that net charge would be the main reason of different activities. In addition to that, we also tested the efficacy of NLC-colistin to prevent the biofilm formation. For all the isolates tested, BPC values of NLC-colistin were identical to values for free colistin and the mixture of empty NLC and free colistin. All formulations had BPCs coincident with MICs. Whereas NLC-colistin was more effective than free colistin in eradicating biofilms, both free and nanoencapsulated colistin did not show any differences on the prevention of biofilm formation. AFM experiments were also performed in order to study the biofilm surface and structure after treatment with NLC-colistin. Topography images gave information about surface and structure differences whereas amplitude images allowed a better observation

of surface characteristics and fine details (169). Based on AFM images, untreated biofilms were compared to a control and presented the typical *P. aeruginosa* bacilli shape without alterations in its surface. After both free and nanoencapsulated colistin treatment, biofilm forming bacteria resulted severely altered. Moreover, these alterations in biofilm gradually increased over time. However, it was also observed that non-relevant differences existed between free and nanoencapsulated colistin. AFM is an excellent tool widely used to shed some light not only in imaging parameters—topography, error signal, phase—but also in cell mechanics at the nanoscale resolution—adhesion forces, elasticity, etc.—and roughness, being extremely sensitive due to its ability to detect a large range of forces, from nN to pN. One of the main goals of the fight against biofilm is to induce changes that could decrease the physical stability of biofilm. We used such measurements to explore the eventual differences in adhesion forces due to the treatment with colistin and nanoencapsulated colistin. It was observed that surface nanoroughness varied being the lower those of control whereas both free and NLC-colistin induce drastic increases in cellular surface roughness. Tip-cell-surface adhesion force of untreated, as well as NLC-colistin- and free-colistin-treated bacteria resulted to be 145 ± 33 , 885 ± 195 , and 701 ± 239 , respectively. We found that values in NLC-colistin-treated bacteria were higher than those of control and that colistin-treated were even higher than those measured in NLC-colistin-treated biofilms although very similar. This is in agreement with the hypothesis that nanoparticles do not have direct effect on biofilm but facilitate the direct antimicrobial effect of colistin, and also with the results recorded when empty nanoparticles were tested. It is important to note that, in case of a biofilm development, the biphasic release profile might be beneficial, where the fast-antibiotic release in the beginning ensures a high initial antibiotic concentration enough to inhibit the biofilm growth, followed by a sustained antibiotic concentration above the MIC value that permits the eradication of the surviving cells minimizing the exacerbation (170). For that reason, we decided to explore the efficacy of NLC-colistin vs. the free drug with respect to biofilm viability over time and across the different layers of the biofilm. After 20 and 40 min of exposure to NLC-colistin, the red population increased over time such that very few green-staining cells were observed,

consistent with the significant damage of bacteria residing in the treated biofilm. After 60 min incubation with NLC-colistin, all bacterial cells stained red. In the biofilms treated with free colistin, the percentages of the red and green populations of bacteria after 20 min were almost identical to those of the control. After 40 and 60 min, the red population in the free colistin treatment was always smaller than that in the NLC-colistin treatment, evidence of the faster killing of bacterial biofilms by the latter. This may reflect the ability of the lipid nanoparticles to easily penetrate the biofilm matrix, with the nanoparticulated drug then reaching the bacteria faster and more easily than free colistin (171)(172). Islan et al. (173) reported similar results using levofloxacin-loaded lipid nanoparticles. In that study, rapid killing of *P. aeruginosa* biofilms by NLC-levofloxacin was achieved after 60 min of exposure.

Biofilms are a complex, multicellular structure that favors the generation of physiologically distinct subpopulations of bacteria that together form a community able to adapt to rapidly changing environmental conditions (174). To explore whether free and nanoencapsulated colistin differentially act on the subpopulations residing within the biofilm, the viability of bacteria in the different layers of the biofilm was determined. It was observed that bacterial density was much higher in the inner layers of the biofilm, consistent with the previously reported high density of cells located close to the substratum in *P. aeruginosa* biofilms (175). Our results can be explained by the initiation of cell detachment in the upper layers of the biofilm (176) as well as the accumulation of high densities of smaller cells in deeper parts of the biofilm in response to external stress conditions. Also, it is likely that the washing step with buffer altered the external parts of the biofilm while leaving its deeper parts relatively undisturbed. Although weakly attached bacteria will be discarded by carefully washing the biofilms after 24 h of incubation, simultaneous disruption of the superficial layers of the biofilm is difficult to avoid. The two colistin formulations did not differ in their effects on the various biofilm subpopulations, as the percentages of living and dead cells were higher in the inner than in the outer layers of biofilms treated with free colistin or NLC-colistin. Our results demonstrate that both formulations are able to penetrate the deeper layers of the biofilm and thus access a dormant and

anaerobically growing subpopulation (177)(178). A reduction of the free colistin concentration, the delayed penetration of the free drug into the deeper portions of the multilayered biofilm, and the lack of specificity of NLC-colistin in killing metabolically active bacteria vs. starved cells may account for our results, as proposed in similar studies (167)(179). Further experiments will be aimed at improving the experimental conditions to optimize the performance of NLC-colistin. It was also studied the influence of the lipid nanoparticles on tobramycin's ability to kill sessile bacteria. All *P. aeruginosa* strains used in this experiment formed adequate biofilms. Among the isolates susceptible to tobramycin, the MIC and MBEC values of the nanoencapsulated drug were slightly lower (1–2 logs) than those of the free drug. However, for the clinical isolate resistant to tobramycin, there were no differences in the MIC and MBEC values obtained with the nanoparticles and free tobramycin. The exception was NLC-tobramycin, in which the MBEC was slightly lower than the value obtained with the free form. The much higher MBEC vs. MIC values of both free and nanoencapsulated tobramycin likely reflected the interaction between the anionic mucopolysaccharide of the biofilm and the cationic aminoglycoside, such that the amount of free tobramycin available to act against the resident bacteria was limited (180). Among the two types of nanoparticles (SLN and NLC), NLC were slightly more active than SLN (1 log) for all strains tested. Specifically, the concentrations of free tobramycin required to completely eradicate the *P. aeruginosa* biofilm were 8–16 µg/mL (tobramycin-susceptible strains) and 32 µg/mL (tobramycin-resistant strain), but the effective NLC-tobramycin concentration was lower (2–4 µg/mL and 16 µg/mL, respectively). The better results obtained with the NLC formulation of tobramycin was in agreement with our previously published results showing that colistin-loaded NLCs were highly effective in biofilm eradication (181). Although the mechanisms underlying the efficacy of tobramycin in NLC are not fully understood, a role for charge distribution seems likely. Tobramycin loaded into NLC has a negative net charge because of the negatively charged nanoparticles, in contrast to the positive net charge of free tobramycin. The superior mucus penetration of negatively charged nanoparticles has been reported and suggests the greater ability of NLC-tobramycin to penetrate the exopolysaccharide matrix surrounding the biofilm structure (182). Increased

penetration would better allow tobramycin to reach its cellular target, in contrast to its free form. Alternatively, the fast-antimicrobial release reported by Pastor et al. (183) would ensure an initial antimicrobial concentration that is high enough to inhibit the biofilm growth of *P. aeruginosa*. Moreover, a sustained antimicrobial concentration higher than the MIC value would enable the eradication of surviving cells. However, further experiments are needed to determine which, if any, of our hypotheses is the correct one.

5. CONCLUSIONS

5. CONCLUSIONS

1. Lipid nanoparticles presented a diameter size ranging from 250 to 300 nm preventing their phagocytosis by macrophages. High encapsulation efficiencies were achieved for both (SLN and NLC) nanoparticles. However, the NLCs drug loading capacity was higher than that of SLNs.
2. NLCs had the ability to release an 86% of the drug in 8 hours and SLNs a 50%. The sustained release, especially the one presented by the antimicrobial-NLC, could reduce the number of doses improving patient adherence to the treatment and, thus, life quality.
3. None of the formulations tested presented toxicity confirmed the safety of the lipid nanoparticles. Moreover, they displayed a suitable tissue disposition, spreading extensively throughout the lungs.
4. The penetration of the particles across the mucus layer was improved by the addition of mucolytic agents that facilitated the drug transport through it.
5. A progressive increase in size as well as variations in the PDI at higher temperatures were observed, being more remarkable at 30 °C and 40 °C.
6. On one hand, the ZP of colistin-SLNs was more negative when the temperature increased, reaching -30.20 mV values at 30 °C. On the other hand, the ZP value of colistin-NLCs below -20 mV at all concentrations tested after one year indicating long-term stability. Moreover, colistin-NLCs demonstrated a sustained drug release after 12 months under 5 °C and 25 °C as they showed similar release profile as the fresh nanoparticles.
7. Colistin-SLNs were not able to keep their antimicrobial activity after three months, while NLC maintained similar levels of bioactivity after storage under different conditions for 9 months.

8. Mucoid isolates were less susceptible to colistin-SLN than non-mucoid strains, suggesting that the mucoid state could alter the effect of SLN but not that of NLC. Moreover, trehalose was more adequate to be used as cryoprotectant in the preparation of the nanoparticles during the lyophilization process.
9. Colistin and tobramycin in lipid nanoparticles presented MIC values similar to their free form, being NLCs more active than SLN. In addition, these nanoformulations presented antimicrobial activity against the mucoid strains.
10. Among the two types of SLN used in the tobramycin susceptibility assay, the formulation prepared without SDS lost antimicrobial activity.
11. Among the isolates susceptible to tobramycin, the MIC and MBEC values of the nanoencapsulated drug were slightly lower (1–2 logs) than those of the free drug. However, for the clinical isolate resistant to tobramycin, there were no differences in the MIC and MBEC values obtained with the nanoparticles and free tobramycin. The exception was NLC-tobramycin, in which the MBEC was slightly lower than the value obtained with the free form.
12. Whereas NLC-colistin was more effective than free colistin in eradicating biofilms, both free and nanoencapsulated colistin did not show any differences on the prevention of biofilm formation. Based on AFM images, after both free and nanoencapsulated colistin treatment, biofilm forming bacteria resulted severely altered. Moreover, these alterations in biofilm gradually increased over time. The surface nanoroughness of *P. aeruginosa* PAO1 biofilm varied being the lower those of control whereas both free and NLC-colistin induce drastic increases in cellular surface roughness.

13. We found that tip-cell-surface adhesion force values in NLC-colistin-treated biofilm were higher than those of control and that colistin-treated were even higher than those measured in NLC-colistin-treated biofilms although very similar.
14. The results obtained with the confocal microscopy showed the more rapid killing of *P. aeruginosa* bacterial biofilms by NLC-colistin than by free colistin. However, the two formulations did not differ in terms of the final percentages of living and dead cells, which were higher in the inner than in the outer layers of the treated biofilms.
15. GENERAL CONCLUSION: The use of nanoparticulated antibiotics for nasal instillation in CF patients and chronic respiratory infections is regarded as a promising strategy. This PhD work reports data useful to provide basis for future exploration.

6. REFERENCES

6. REFERENCES

1. Ryan KJ, Ray CG. Sherris medical microbiology, 6th Ed. Sherris medical microbiology. 2014.
2. Murray PR, Baron EJ, Jorgensen JH, Pfaller MA. Manual of Clinical Microbiology. 9th Edition. American Society for Microbiology. 2007.
3. Sivaprakasam S, Mahadevan S, Sekar S, Rajakumar S. Biological treatment of tannery wastewater by using salt-tolerant bacterial strains. Microb Cell Fact. 2008;7:15.
4. Goldberg JB, Pier GB. The role of the CFTR in susceptibility to *Pseudomonas aeruginosa* infections in cystic fibrosis. Trends Microbiol. 2000;8:514–20.
5. Bueno E, Mesa S, Bedmar EJ, Richardson DJ, Delgado MJ. Bacterial adaptation of respiration from oxic to microoxic and anoxic conditions: redox control. Antioxid Redox Signal. 2012;16:819–52.
6. Arat S, Bullerjahn GS, Laubenbacher R. A network biology approach to denitrification in *Pseudomonas aeruginosa*. PLoS One. 2015;10:1–12.
7. Delcour AH. Outer Membrane Permeability and Antibiotic Resistance. Biochim Biophys Acta. 2009;1794:808–16.
8. Cohen TS, Prince A. Cystic fibrosis: a mucosal immunodeficiency syndrome. Nat Med . 2012;18:2715-11.
9. Miyazaki S, Matsumoto T, Tateda K, Ohno A. Role of exotoxin A in inducing severe *Pseudomonas aeruginosa* infections in mice. J.Med.Microbiol. 1995;43:169–75.
10. Kamath S, Kapatral V, Chakrabarty AM. Cellular function of elastase in *Pseudomonas aeruginosa*: Role in the cleavage of nucleoside diphosphate kinase and in alginate synthesis. Mol Microbiol. 1998;30:933–41.
11. Rabin SDP, Veessenmeyer JL, Bieging KT, Hauser AR, Lee VT, Smith RS, et al. Activities of *Pseudomonas aeruginosa* Effectors Secreted by the Type III Secretion System In Vitro and during Infection. Infection and Immunity. 2005;73:2598–605.
12. Rossolini GM, Mantengoli E. Treatment and control of severe

- infections caused by multiresistant *Pseudomonas aeruginosa*. Clin Microbiol Infect. 2005;11:17–32.
13. Szczotka-Flynn LB, Pearlman E, Ghannoum M. Microbial contamination of contact lenses, lens care solutions, and their accessories: a literature review. Eye Contact Lens. 2010; 36:116-29.
 14. Weber DJ, Rutala WA, Sickbert-Bennett EE. Outbreaks associated with contaminated antiseptics and disinfectants. Antimicrob Agents Chemother. 2007;51:4217–24.
 15. Jadhav S, Sahasrabuddhe T, Kalley V, Gandham NR. The microbial colonization profile of respiratory devices and the significance of the role of disinfection: A blinded study. J Clin Diagnostic Res. 2013;7:1021–6.
 16. Kazmierczak BI, Schniederberend M, Jain R. Cross-regulation of *Pseudomonas* motility systems: the intimate relationship between flagella, pili and virulence. Curr Opin Microbiol. 2015;28:78–82.
 17. Jimenez PN, Koch G, Thompson JA, Xavier KB, Cool RH, Quax WJ. The multiple signaling systems regulating virulence in *Pseudomonas aeruginosa*. Microbiol Mol Biol Rev. 2012;76:46–65.
 18. Howell HA. Early Expression of Type III Secretion is Critical for Bacterial Survival in Acute *Pseudomonas aeruginosa* Pneumonia. 2013;4:1–9.
 19. Maldonado RF, Sá-Correia I, Valvano MA. Lipopolysaccharide modification in Gram-negative bacteria during chronic infection. FEMS Microbiol Rev. 2016;40:480–93.
 20. Bodey GP, Bolivar R, Fainstein V, Jadeja L. Infections caused by *Pseudomonas aeruginosa*. Rev Infect Dis. 1983;5:279–313.
 21. Williams BJ, Dehnbostel J, Blackwell TS. *Pseudomonas aeruginosa*: Host defence in lung diseases. Respirology. 2010;15:1037–56.
 22. Cornelis P, Dingemans J. *Pseudomonas aeruginosa* adapts its iron uptake strategies in function of the type of infections. Front Cell Infect Microbiol. 2013;3:75.
 23. Gibson RL, Burns JL, Ramsey BW. Pathophysiology and Management of Pulmonary Infections in Cystic Fibrosis. Am J Respir Crit Care Med. 2003;168:918–51.

24. Welsh MJ, Smith AE. Molecular mechanisms of CFTR chloride channel dysfunction in cystic fibrosis. *Cell*. 1993;73:1251–4.
25. Andersen D. Cystic fibrosis of the pancreas and its relation to celiac disease: a clinical and pathologic study. *Am J Dis Child*. 1938;56:344–99.
26. Cutting GR. Cystic fibrosis genetics: from molecular understanding to clinical application. *Nat Rev Genet*. 2015;16:45–56.
27. Sims EJ, McCormick J, Mehta G, Mehta A. Neonatal screening for cystic fibrosis is beneficial even in the context of modern treatment. *J Pediatr*. 2005;147:S42–6.
28. Schmidt BZ, Haaf JB, Leal T, Noel S. Cystic fibrosis transmembrane conductance regulator modulators in cystic fibrosis: Current perspectives. *Clin Pharmacol Adv Appl*. 2016;8:127–40.
29. Heijerman H, Westerman E, Conway S, Touw D. Inhaled medication and inhalation devices for lung disease in patients with cystic fibrosis: A European consensus. *J Cyst Fibros*. 2009;8:295–315.
30. Adler FR, Aurora P, Barker DH, Barr ML, Blackwell LS, Bosma OH, et al. Lung Transplantation for Cystic Fibrosis. *Proc Am Thorac Soc*. 2009;6:619–33.
31. Hauser AR, Jain M, Bar-Meir M, McColley SA. Clinical significance of microbial infection and adaptation in cystic fibrosis. *Clin Microbiol Rev*. 2011;24:29–70.
32. Döring G, Flume P, Heijerman H, Elborn JS. Treatment of lung infection in patients with cystic fibrosis: Current and future strategies. *J Cyst Fibros*. 2012;11:461–79.
33. Lyczak JB, Cannon CL, Pier GB. Lung Infections Associated with Cystic Fibrosis Lung Infections Associated with Cystic Fibrosis. *Clin Microbiol Rev*. 2002;15:194–222.
34. Oliver A, Baquero F, Blázquez J. The mismatch repair system (*mutS*, *mutL* and *uvrD* genes) in *Pseudomonas aeruginosa*: Molecular characterization of naturally occurring mutants. *Mol Microbiol*. 2002;43:1641–50.
35. Mandsberg LF, Ciofu O, Kirkby N, Christiansen LE, Poulsen HE, Høiby N. Antibiotic resistance in *Pseudomonas aeruginosa* strains with

- increased mutation frequency due to inactivation of the DNA oxidative repair system. *Antimicrob Agents Chemother*. 2009;53:2483–91.
36. Ciofu O, Mandsberg LF, Bjarnsholt T, Wassermann T, Høiby N. Genetic adaptation of *Pseudomonas aeruginosa* during chronic lung infection of patients with cystic fibrosis: Strong and weak mutators with heterogeneous genetic backgrounds emerge in *mucA* and/or *lasR* mutants. *Microbiology*. 2010;156:1108–19.
 37. Sousa AM, Pereira MO. *Pseudomonas aeruginosa* Diversification during Infection Development in Cystic Fibrosis Lungs-A Review. *Pathog* . 2014;3:680–703.
 38. Firoved AM, Boucher JC, Deretic V. Global Genomic Analysis of AlgU (σ^E)-Dependent Promoters (Sigmulon) in *Pseudomonas aeruginosa* and Implications for Inflammatory Processes in Cystic Fibrosis. *J Bacteriol*. 2002;184:1057–64.
 39. Hentzer M, Teitzel GM, Balzer GJ, Molin S, Givskov M, Matthew R, et al. Alginate Overproduction Affects *Pseudomonas aeruginosa* Biofilm Structure and Function. *J Bacteriol*. 2001;183:5395–401.
 40. Ciofu O, Lee B, Johannesson M, Hermansen NO, Meyer P, Høiby N. Investigation of the *algT* operon sequence in mucoid and non-mucoid *Pseudomonas aeruginosa* isolates from 115 Scandinavian patients with cystic fibrosis and in 88 in vitro non-mucoid revertants. *Microbiology*. 2008;154:103–13.
 41. Silhavy TJ, Kahne D, Walker S. The bacterial cell envelope. *Cold Spring Harb Perspect Biol*. 2010;2:1–16.
 42. Cullen L, McClean S. Bacterial Adaptation during Chronic Respiratory Infections. *Pathog*. 2015;4:66–89.
 43. Moskowitz SM, Ernst RK. Endotoxins: Structure, Function and Recognition. 2010;53:241–53.
 44. Hauser AR. The Type III Secretion System of *Pseudomonas aeruginosa*: Infection by Injection. *Nat Rev Microbiol*. 2009;7:654–65.
 45. Dasgupta N, Ferrell EP, Kanack KJ, West SE, Ramphal R. *fleQ*, the gene encoding the major flagellar regulator of *Pseudomonas aeruginosa*, is σ^{70} dependent and is downregulated by Vfr, a homolog of *Escherichia coli* cyclic AMP receptor Protein. *J Bacteriol*.

- 2002;184:5240–50.
46. Baynham PJ, Ramsey DM, Gvozdyev B V., Cordonnier EM, Wozniak DJ. The *Pseudomonas aeruginosa* ribbon-helix-helix DNA-binding protein AlgZ (AmrZ) controls twitching motility and biogenesis of type IV pili. *J Bacteriol.* 2006;188:132–40.
 47. D'Argenio DA, Wu M, Hoffman LR, Kulasekara HD, Smith EE, Nguyen H, et al. *Mol Microbiol.* 2007;64:512–33.
 48. Taylor RF, Hodson ME, Pitt TL. Adult cystic fibrosis: association of acute pulmonary exacerbations and increasing severity of lung disease with auxotrophic mutants of *Pseudomonas aeruginosa*. *Thorax.* 1993;48:1002–5.
 49. Malone JG. Role of small colony variants in persistence of *Pseudomonas aeruginosa* infections in cystic fibrosis lungs. *Infect Drug Resist.* 2015;8:237–47.
 50. Wei Q, Tarighi S, Dötsch A, Häussler S, Müsken M, Wright VJ, et al. Phenotypic and genome-wide analysis of an antibiotic-resistant small colony variant (SCV) of *Pseudomonas aeruginosa*. *PLoS One.* 2011;6.
 51. Houston LS, Burns JL, Ramsey BW, Miller SI. *Pseudomonas aeruginosa lasr* mutants are associated with cystic fibrosis lung disease progression. 2010;8:66–70.
 52. Bjarnsholt T, Jensen PØ, Jakobsen TH, Phipps R, Nielsen AK, Rybtke MT, et al. Quorum sensing and virulence of *Pseudomonas aeruginosa* during lung infection of cystic fibrosis patients. *PLoS One.* 2010;5:1–10.
 53. Palmer KL, Mashburn LM, Singh PK, Whiteley M. Cystic Fibrosis Sputum Supports Growth and Cues Key Aspects of *Pseudomonas aeruginosa* Physiology Cystic Fibrosis Sputum Supports Growth and Cues Key Aspects of *Pseudomonas aeruginosa* Physiology. *J Bacteriol.* 2005;187:5267–77.
 54. Collier DN, Anderson L, McKnight SL, Noah TL, Knowles M, Boucher R, et al. A bacterial cell to cell signal in the lungs of cystic fibrosis patients. *FEMS Microbiol Lett.* 2002;215:41–6.
 55. Lee J, Zhang L. The hierarchy quorum sensing network in *Pseudomonas aeruginosa*. *Protein Cell.* 2014;6:26–41.

56. Döring G, Parameswaran IG, Murphy TF. Differential adaptation of microbial pathogens to airways of patients with cystic fibrosis and chronic obstructive pulmonary disease. *FEMS Microbiol Rev.* 2011;35:124–46.
57. Donlan RM, Costerton JW. Biofilms: survival mechanisms of clinically relevant microorganisms. *ClinMicrobiol Rev.* 2002;15:167–19.
58. Donlan RM. Biofilms: Microbial life on surfaces. *Emerg Infect Dis.* 2002;8:881–90.
59. Ciofu O, Tolker-Nielsen T, Jensen PØ, Wang H, Høiby N. Antimicrobial resistance, respiratory tract infections and role of biofilms in lung infections in cystic fibrosis patients. *Adv Drug Deliv Rev.* 2015;85:7–23.
60. Hengge R. Principles of c-di-GMP signalling in bacteria. *Nat Rev Microbiol.* 2009;7:263–73.
61. Kim SK, Lee JH. Biofilm dispersion in *Pseudomonas aeruginosa*. *J Microbiol.* 2016;54:71–85.
62. Klausen M, Heydorn A, Ragas P, Lambertsen L, Aaes-Jørgensen A, Molin S, et al. Biofilm formation by *Pseudomonas aeruginosa* wild type, flagella and type IV pili mutants. *Mol Microbiol.* 2003;48:1511–24.
63. Høiby N. Understanding bacterial biofilms in patients with cystic fibrosis: Current and innovative approaches to potential therapies. *J Cyst Fibros.* 2002;1:249–54.
64. Sun Yoon S, Hennigan RF, Hilliard GM, Ochsner UA, Parvatiyar K, Kamani MC, et al. *Pseudomonas aeruginosa* Anaerobic Respiration in Biofilms: Relationships to Cystic Fibrosis Pathogenesis. *Dev Cell.* 2002;3:593–603.
65. Gellatly SL, Hancock REW. *Pseudomonas aeruginosa*: New insights into pathogenesis and host defenses. *Pathog Dis.* 2013;67:159–73.
66. Allesen-Holm M, Barken KB, Yang L, Klausen M, Webb JS, Kjelleberg S, et al. A characterization of DNA release in *Pseudomonas aeruginosa* cultures and biofilms. *Mol Microbiol.* 2006;59:1114–28.
67. Häussler S, Becker T. The pseudomonas quinolone signal (PQS) balances life and death in *Pseudomonas aeruginosa* populations. *PLoS Pathog.* 2008;4.

68. Kaplan JB. Biofilm dispersal: mechanisms, clinical implications, and potential therapeutic uses. *J Dent Res*. 2010;89:205–18.
69. Rasamiravaka T, Labtani Q, Duez P, El Jaziri M. The formation of biofilms by *Pseudomonas aeruginosa*: A review of the natural and synthetic compounds interfering with control mechanisms. *Biomed Res Int*. 2015;2015:759348.
70. Cantón R, Cobos N, de Gracia J, Baquero F, Honorato J, Gartner S, et al. Antimicrobial therapy for pulmonary pathogenic colonisation and infection by *Pseudomonas aeruginosa* in cystic fibrosis patients. *Clin Microbiol Infect*. 2005;11:690–703.
71. Fusté E, López-Jiménez L, Segura C, Gainza E, Vinuesa T, Viñas M. Carbapenem-resistance mechanisms of multidrug-resistant *Pseudomonas aeruginosa*. *J Med Microbiol*. 2013;62:1317–25.
72. Döring G, Conway SP, Heijerman HG, Hodson ME, Høiby N, Smyth A, et al. Antibiotic therapy against *Pseudomonas aeruginosa* in cystic fibrosis: a European consensus. *Eur Respir J*. 2000;16:749–67.
73. Bergen PJ, Landersdorfer CB, Zhang J, Zhao M, Lee HJ, Nation RL, et al. Pharmacokinetics and pharmacodynamics of “old” polymyxins: What is new? *Diagn Microbiol Infect Dis*. 2012;74:213–23.
74. Beringer P. The clinical use of colistin in patients with cystic fibrosis. *Curr Opin Pulm Med*. 2001;7:434–40.
75. Lim LM, Ly N, Anderson D, Yang JC, Macander L, Jarkowski A, et al. Resurgence of colistin: a review of resistance, toxicity, pharmacodynamics, and dosing. *Pharmacotherapy*. 2010;30:1279–91.
76. Döring G, Høiby N, Assael B, Ballmann M, Bush A, Button B, et al. Early intervention and prevention of lung disease in cystic fibrosis: A European consensus. *J Cyst Fibros*. 2004;3:67–91.
77. Canton R, Maiz L, Escribano A, Oliveira C, Oliver A, Asensio O, et al. Spanish Consensus on the Prevention and Treatment of *Pseudomonas aeruginosa* Bronchial Infections in Cystic Fibrosis Patients. 2015;51:140–50.
78. Poole K. *Pseudomonas aeruginosa*: resistance to the max. *Front Microbiol*. 2011;2:65.
79. Fernandez L, Hancock REW. Adaptive and Mutational Resistance:

- Role of Porins and Efflux Pumps in Drug Resistance. Clin Microbiol Rev. 2012;25:661–81.
80. Poole K. Efflux pumps as antimicrobial resistance mechanisms. Ann Med. 2007;39:162–76.
 81. Dreier J, Ruggerone P. Interaction of antibacterial compounds with RND efflux pumps in *Pseudomonas aeruginosa*. Front Microbiol. 2015;6:1–21.
 82. Tian ZX, Yi XX, Cho A, O’Gara F, Wang YP. CpxR Activates MexAB-OprM Efflux Pump Expression and Enhances Antibiotic Resistance in Both Laboratory and Clinical *nalB*-Type Isolates of *Pseudomonas aeruginosa*. PLoS Pathog. 2016;12.
 83. Masuda N, Ohya S. Cross-resistance to meropenem, cephems, and quinolones in *Pseudomonas aeruginosa*. Antimicrob Agents Chemother. 1992;36:1847–51.
 84. Ziha-Zarifi I, Llanes C, Köhler T, Pechere JC, Plesiat P. *In vivo* emergence of multidrug-resistant mutants of *Pseudomonas aeruginosa* overexpressing the active efflux system mexA-mexB-OprM. Antimicrob Agents Chemother. 1999;43:287–91.
 85. Masuda N, Sakagawa E, Ohya S, Gotoh N, Tsujimoto H, Nishino T. Substrate specificities of MexAB-OprM, MexCD-OprJ, and MexXY-OprM efflux pumps in *Pseudomonas aeruginosa*. Antimicrob Agents Chemother. 2000;44:3322–7.
 86. N Gotoh, H Tsujimoto, K Poole, J Yamagishi TN. The outer membrane protein OprM of *Pseudomonas aeruginosa* is encoded by *oprK* of the *mexA-mexB-oprK* multidrug resistance operon. Antimicrob Agents Chemother. 1995;39:2567–9.
 87. Sobel ML, McKay GA, Poole K. Contribution of the MexXY Multidrug Transporter to Aminoglycoside Resistance in *Pseudomonas aeruginosa* Clinical Isolates. Antimicrob Agents Chemother. 2003;47:3202–7.
 88. Ciofu O. *Pseudomonas aeruginosa* chromosomal beta-lactamase in patients with cystic fibrosis and chronic lung infection. Mechanism of antibiotic resistance and target of the humoral immune response. APMIS Suppl. 2003;1–47.

89. Carsenti-Etesse H, Cavallo JD, Roger PM, Zih-Zarifi I, Plesiat P, Garrabe E, et al. Effect of beta-lactam antibiotics on the in vitro development of resistance in *Pseudomonas aeruginosa*. Clin Microbiol Infect. 2001;7:144–51.
90. Rodríguez-Martínez JM, Poirel L, Nordmann P. Molecular epidemiology and mechanisms of carbapenem resistance in *Pseudomonas aeruginosa*. Antimicrob Agents Chemother. 2009;53:4783–8.
91. Akasaka T, Tanaka M, Yamaguchi A, Sato K. Type II topoisomerase mutations in fluoroquinolone-resistant clinical strains of *Pseudomonas aeruginosa* isolated in 1998 and 1999: Role of target enzyme in mechanism of fluoroquinolone resistance. Antimicrob Agents Chemother. 2001;45:2263–8.
92. Poole K. Efflux-mediated resistance to fluoroquinolones in gram-negative bacteria. Antimicrob Agents Chemother. 2000;44:2233–41.
93. Poole K. Aminoglycoside Resistance in *Pseudomonas aeruginosa*. Antimicrob Agents Chemother. 2005;49:479–87.
94. Krahm T, Gilmour C, Tilak J, Fraud S, Kerr N, Lau CHF, et al. Determinants of intrinsic aminoglycoside resistance in *Pseudomonas aeruginosa*. Antimicrob Agents Chemother. 2012;56:5591–602.
95. Barclay ML BE. Aminoglycoside adaptive resistance: importance for effective dosage regimens. Drugs. 2001;61:713–21.
96. Macfarlane EL, Kwasnicka A, Hancock REW. Role of *Pseudomonas aeruginosa* Phop-PhoQ in resistance to antimicrobial cationic peptides and aminoglycosides. Microbiology. 2000;146:2543–54.
97. Moskowitz SM, Ernst RK, Miller SI. PmrAB, a Two-Component Regulatory System of *Pseudomonas aeruginosa* that Modulates Resistance to Cationic Antimicrobial Peptides and Addition of Aminoarabinose to Lipid A. J Bacteriol. 2004;186:575–9.
98. Poole K. Mechanisms of bacterial biocide and antibiotic resistance. J Appl Microbiol. 2002;92:55S–64S.
99. Drenkard E. Antimicrobial resistance of *Pseudomonas aeruginosa* biofilms. Microbes Infect. 2003;5:1213–9.
100. Su S, Hassett DJ. Anaerobic *Pseudomonas aeruginosa* and other

- obligately anaerobic bacterial biofilms growing in the thick airway mucus of chronically infected cystic fibrosis patients: an emerging paradigm or “Old Hat”? *Expert Opin Ther Targets*. 2012;16:859–73.
101. Kolpen M, Appeldorff CF, Brandt S, Mousavi N, Kragh KN, Aydogan S, et al. Increased bactericidal activity of colistin on *Pseudomonas aeruginosa* biofilms in anaerobic conditions. *Pathog Dis* . 2016;74:ftv086.
 102. Wood TK, Knabel SJ, Kwan BW. Bacterial persister cell formation and dormancy. *Appl Environ Microbiol*. 2013;79:7116–21.
 103. Gales AC, Jones RN, Sader HS. Contemporary activity of colistin and polymyxin B against a worldwide collection of Gram-negative pathogens: Results from the SENTRY antimicrobial surveillance program (2006-09). *J Antimicrob Chemother*. 2011;66:2070–4.
 104. Carmeli Y, Troillet N, Eliopoulos GM, Samore MH. Emergence of antibiotic-resistant *Pseudomonas aeruginosa*: Comparison of risks associated with different antipseudomonal agents. *Antimicrob Agents Chemother*. 1999;43:1379–82.
 105. Gould IM, Bal AM. New antibiotic agents in the pipeline and how they can help overcome microbial resistance. *Virulence*. 2013;4:185–91.
 106. Poyner, E.A., Alpar, H.O., Almeida, A.J., Gamble, M.D., Brown MR. A comparative study on the pulmonary delivery of tobramycin encapsulated into liposomes and PLA microspheres following intravenous and endotracheal delivery. *J Control Release*. 1995;35:41–8.
 107. Andrade F, Rafael D, Videira M, Ferreira D, Sosnik A, Sarmento B. Nanotechnology and pulmonary delivery to overcome resistance in infectious diseases. *Adv Drug Deliv Rev*. 2013;65:1816–27.
 108. Weber S, Zimmer A, Pardeike J. Solid Lipid Nanoparticles (SLN) and Nanostructured Lipid Carriers (NLC) for pulmonary application: A review of the state of the art. *Eur J Pharm Biopharm*. 2014;86:7–22.
 109. M. Iler RH, Mehnert W, Lucks JS et al. Solid lipid nanoparticles (SLN) – An alternative colloidal carrier system for controlled drug delivery. *Eur J Pharm Biopharm*. 1995;41:62–9.
 110. MR G. Method for producing solid lipid microspheres having a narrow

- size distribution. US Pat. 1993;5:250–236.
111. Siekmann B WK. Submicron-sized parenteral carrier systems based on solid lipids. *Pharm Pharmacol Lett*. 1992;1:123–6.
 112. Mäder K, Mehnert W. Solid lipid nanoparticles: production, characterization and applications. *Adv Drug Deliv Rev*. 2001;47:165–96.
 113. Abdelghany SM, Quinn DJ, Ingram RJ, Gilmore BF, Donnelly RF, Taggart CC, et al. Gentamicin-loaded nanoparticles show improved antimicrobial effects towards *Pseudomonas aeruginosa* infection. *Int J Nanomedicine*. 2012;7:4053–63.
 114. Cipolla D, Shekunov B, Blanchard J, Hickey A. Lipid-based carriers for pulmonary products: Preclinical development and case studies in humans. *Adv Drug Deliv Rev*. 2014;75:53–80.
 115. Pelgrift RY, Friedman AJ. Nanotechnology as a therapeutic tool to combat microbial resistance. *Adv Drug Deliv Rev*. 2013;65:1803–15.
 116. Obeidat WM, Schwabe K, Müller RH, Keck CM. Preservation of nanostructured lipid carriers (NLC). *Eur J Pharm Biopharm*. 2010;76:56–67.
 117. Belouqui A, Solinís MÁ, Gascón AR, Del Pozo-Rodríguez A, Des Rieux A, Préat V. Mechanism of transport of saquinavir-loaded nanostructured lipid carriers across the intestinal barrier. *J Control Release*. 2013;166:115–23.
 118. Rudilla H, Fusté E, Cajal Y, Rabanal F, Vinuesa T, Viñas M. Synergistic antipseudomonal effects of synthetic peptide AMP38 and carbapenems. *Molecules*. 2016;21:1–12.
 119. Smyth AR, Bell SC, Bojcin S, Bryon M, Duff A, Flume P, et al. European cystic fibrosis society standards of care: Best practice guidelines. *J Cyst Fibros*. 2014;13 Suppl 1:S23–42.
 120. Li XZ, Plésiat P, Nikaido H. The challenge of efflux-mediated antibiotic resistance in Gram-negative bacteria. *Clin Microbiol Rev*. 2015;28:337–418.
 121. Cao B, Christophersen L, Kolpen M, Jensen PØ, Sneppen K, Høiby N, et al. Diffusion retardation by binding of tobramycin in an alginate biofilm model. *PLoS One*. 2016;11:1–11.

122. Das S, Chaudhury A. Recent advances in lipid nanoparticle formulations with solid matrix for oral drug delivery. *AAPS PharmSciTech*. 2011;12:62–76.
123. Puri A, Loomis K, Smith B, Lee J-H, Yavlovich A, Heldman E, et al. Lipid-based nanoparticles as pharmaceutical drug carriers: from concepts to clinic. *Crit Rev Ther Drug Carrier Syst*. 2009;26:523–80.
124. Hwang TL, Aljuffali IA, Lin CF, Chang YT, Fang JY. Cationic additives in nanosystems activate cytotoxicity and inflammatory response of human neutrophils: Lipid nanoparticles versus polymeric nanoparticles. *Int J Nanomedicine*. 2015;10:371–85.
125. Martins S, Tho I, Reimold I, Fricker G, Souto E, Ferreira D, et al. Brain delivery of camptothecin by means of solid lipid nanoparticles: Formulation design, in vitro and in vivo studies. *Int J Pharm*. 2012;439:49–62.
126. Patlolla RR, Chougule M, Patel AR, Jackson T, Tata PN V, Singh M. Formulation, characterization and pulmonary deposition of nebulized celecoxib encapsulated nanostructured lipid carriers. *J Control Release*. 2010;144:233–41.
127. Silva AC, Kumar A, Wild W, Ferreira D, Santos D, Forbes B. Long-term stability, biocompatibility and oral delivery potential of risperidone-loaded solid lipid nanoparticles. *Int J Pharm*. 2012;436:798–805.
128. Zheng M, Falkeborg M, Zheng Y, Yang T, Xu X. Formulation and characterization of nanostructured lipid carriers containing a mixed lipids core. *Colloids Surfaces A Physicochem Eng Asp*. 2013;430:76–84.
129. Yue C, Liu P, Zheng M, Zhao P, Wang Y, Ma Y, et al. IR-780 dye loaded tumor targeting theranostic nanoparticles for NIR imaging and photothermal therapy. *Biomaterials*. 2013;34:6853–61.
130. Nassimi M, Schleh C, Lauenstein HD, Hussein R, Hoymann HG, Koch W, et al. A toxicological evaluation of inhaled solid lipid nanoparticles used as a potential drug delivery system for the lung. *Eur J Pharm Biopharm*. 2010;75:107–16.
131. Doktorovova S, Souto EB, Silva AM. Nanotoxicology applied to solid lipid nanoparticles and nanostructured lipid carriers - A systematic

- review of in vitro data. Eur J Pharm Biopharm. 2014;87:1–18.
132. Souza ALR De, Andreani T, De Oliveira RN, Kiill CP, Santos FK Dos, Allegretti SM, et al. *In vitro* evaluation of permeation, toxicity and effect of praziquantel-loaded solid lipid nanoparticles against *Schistosoma mansoni* as a strategy to improve efficacy of the schistosomiasis treatment. Int J Pharm. 2014;463:31–7.
 133. Sukhadeve K, Apte M, Waghmare P. Colistin for bad bugs. Pediatr Infect Dis. 2013;4:168–71.
 134. Taratula O, Kuzmov A, Shah M, Garbuzenko OB, Minko T. Nanostructured lipid carriers as multifunctional nanomedicine platform for pulmonary co-delivery of anticancer drugs and siRNA. J Control Release. 2013;171:349–57.
 135. Mansour HM, Rhee YS, Wu X. Nanomedicine in pulmonary delivery. Int J Nanomedicine. 2009;4:299–319.
 136. Liu J, Gong T, Fu H, Wang C, Wang X, Chen Q, et al. Solid lipid nanoparticles for pulmonary delivery of insulin. Int J Pharm. 2008;356:333–44.
 137. Cone RA. Barrier properties of mucus. Adv Drug Deliv Rev. 2009;61:75–85.
 138. Yang Y, Tsifansky MD, Shin S, Lin Q, Yeo Y. Mannitol-Guided delivery of ciprofloxacin in artificial cystic fibrosis mucus model. Biotechnol Bioeng. 2011;108:1441–9.
 139. Suk JS, Lai SK, Wang YY, Ensign LM, Zeitlin PL, Boyle MP, et al. The penetration of fresh undiluted sputum expectorated by cystic fibrosis patients by non-adhesive polymer nanoparticles. Biomaterials. 2009;30:2591–7.
 140. Suk JS, Lai SK, Boylan NJ, Dawson MR, Boyle MP, Hanes J. Rapid transport of muco-inert nanoparticles in cystic fibrosis sputum treated with N-acetyl cysteine. Nanomedicine. 2011;6:365–75.
 141. Bivas-Benita M, Zwier R, Junginger HE, Borchard G. Non-invasive pulmonary aerosol delivery in mice by the endotracheal route. Eur J Pharm Biopharm. 2005;61:214–8.
 142. Nahar K, Gupta N, Gauvin R, Absar S, Patel B, Gupta V, et al. *In vitro*, *in vivo* and *ex vivo* models for studying particle deposition and drug

- absorption of inhaled pharmaceuticals. *Eur J Pharm Sci.* 2013;49:805–18.
143. Varshosaz J, Ghaffari S, Mirshojaei SF, Jafarian A, Atyabi F, Kobarfard F, et al. Biodistribution of amikacin solid lipid nanoparticles after pulmonary delivery. *Biomed Res Int.* 2013;2013:136859.
 144. Huh AJ, Kwon YJ. “Nanoantibiotics”: A new paradigm for treating infectious diseases using nanomaterials in the antibiotics resistant era. *J Control Release.* 2011;156:128–45.
 145. Müller RH, Radtke M, Wissing SA. Nanostructured lipid matrices for improved microencapsulation of drugs. *Int J Pharm.* 2002;242:121–8.
 146. Vivek K, Reddy H, Murthy RS. Investigations of the effect of the lipid matrix on drug entrapment, *in vitro* release, and physical stability of olanzapine-loaded solid lipid nanoparticles. *AAPS PharmSciTech.* 2007;8:E83.
 147. Venkateswarlu V, Manjunath K. Preparation, characterization and *in vitro* release kinetics of clozapine solid lipid nanoparticles. *J Control Release.* 2004;95:627–38.
 148. Del Pozo-Rodríguez A, Solinis MA, Gascón AR, Pedraz JL. Short- and long-term stability study of lyophilized solid lipid nanoparticles for gene therapy. *Eur J Pharm Biopharm.* 2009;71:181–9.
 149. Das S, Ng WK, Tan RBH. Are nanostructured lipid carriers (NLCs) better than solid lipid nanoparticles (SLNs): Development, characterizations and comparative evaluations of clotrimazole-loaded SLNs and NLCs? *Eur J Pharm Sci.* 2012;47.
 150. Zimmermann E, Souto EB, Mu RH. Physicochemical investigations on the structure of drug-free and drug- loaded solid lipid nanoparticles (SLN) by means of DSC and ¹H NMR. 2005;60:508-13.
 151. Chono S, Tanino T, Seki T, Morimoto K. Influence of particle size on drug delivery to rat alveolar macrophages following pulmonary administration of ciprofloxacin incorporated into liposomes. *J Drug Target.* 2006;14:557–66.
 152. Yang W, Peters JI, Williams RO. Inhaled nanoparticles-A current review. *Int J Pharm.* 2008;356:239–47.
 153. Ridolfi DM, Marcato PD, Justo GZ, Cordi L, Machado D, Durán N.

- Chitosan-solid lipid nanoparticles as carriers for topical delivery of tretinoin. *Colloids Surfaces B Biointerfaces*. 2012;93:36–40.
154. Heurtault B, Saulnier P, Pech B, Proust JE, Benoit JP. Physico-chemical stability of colloidal lipid particles. *Biomaterials*. 2003;24:4283–300.
 155. Radomska-Soukharev A. Stability of lipid excipients in solid lipid nanoparticles. *Adv Drug Deliv Rev*. 2007;59:411–8.
 156. Pardeike J, Weber S, Haber T, Wagner J, Zarfl HP, Plank H, et al. Development of an Itraconazole-loaded nanostructured lipid carrier (NLC) formulation for pulmonary application. *Int J Pharm*. 2011;419:329–38.
 157. Chen CC, Tsai TH, Huang ZR, Fang JY. Effects of lipophilic emulsifiers on the oral administration of lovastatin from nanostructured lipid carriers: Physicochemical characterization and pharmacokinetics. *Eur J Pharm Biopharm*. 2010;74:474–82.
 158. Kaur S, Nautyal U, Singh R, Singh S, Devi A. Nanostructure Lipid Carrier (NLC): the new generation of lipid nanoparticles. *Asian Pac J Heal Sci*. 2015;2:76–93.
 159. Martins S, Sarmento B, Ferreira DC, Souto EB. Lipid-based colloidal carriers for peptide and protein delivery - Liposomes versus lipid nanoparticles. *Int J Nanomedicine*. 2007;2:595–607.
 160. Moreno-Sastre M, Pastor M, Esquisabel A, Sans E, Viñas M, Bachiller D, Pedraz L, et al. Stability study of sodium colistimethate-loaded lipid nanoparticles. *J Microencapsul*. 2016;33:636-645.
 161. Omri A, Suntres ZE, Shek PN. Enhanced activity of liposomal polymyxin B against *Pseudomonas aeruginosa* in a rat model of lung infection. *Biochem Pharmacol*. 2002;64:1407–13.
 162. De Jong WH, Borm PJ. Drug delivery and nanoparticles: applications and hazards. *Int J Nanomedicine*. 2008;3:133–49.
 163. Ghaffari S, Varshosaz J, Saadat A, Atyabi F. Stability and antimicrobial effect of amikacin-loaded solid lipid nanoparticles. *Int J Nanomedicine*. 2011;6:35–43.
 164. Martins SM, Ferreira D, Sarmento B, Souto EB. Lipid-based colloidal carriers for peptide and protein delivery — Liposomes versus lipid

- nanoparticles. *Int J Nanomedicine*. 2007;2:595–607.
165. Moreno-Sastre M, Pastor M, Esquisabel A, Sans E, Viñas M, Fleischer A, et al. Pulmonary delivery of tobramycin-loaded nanostructured lipid carriers for *Pseudomonas aeruginosa* infections associated with cystic fibrosis. *Int J Pharm*. 2016;498:263–73.
 166. Mugabe C, Azghani AO, Omri A. Liposome-mediated gentamicin delivery: Development and activity against resistant strains of *Pseudomonas aeruginosa* isolated from cystic fibrosis patients. *J Antimicrob Chemother*. 2005;55:269–71.
 167. Pamp SJ, Gjermansen M, Johansen HK, Tolker-Nielsen T. Tolerance to the antimicrobial peptide colistin in *Pseudomonas aeruginosa* biofilms is linked to metabolically active cells, and depends on the *pmr* and *mexAB-oprM* genes. *Mol Microbiol*. 2008;68:223–40.
 168. Gooderham WJ, Hancock REW. Regulation of virulence and antibiotic resistance by two-component regulatory systems in *Pseudomonas aeruginosa*. *FEMS Microbiol Rev*. 2009;33:279–94.
 169. Dubrovin E V, Voloshin AG, Kraevsky S V, Ignatyuk E, Abramchuk SS, Yaminsky I V, et al. Atomic Force Microscopy Investigation of Phage Infection of Bacteria. *Langmuir*. 2008;24:13068–74.
 170. Cheow WS, Chang MW, Hadinoto K. Antibacterial efficacy of inhalable antibiotic-encapsulated biodegradable polymeric nanoparticles against *E. coli* biofilm cells. *J Biomed Nanotechnol*. 2010;6:391–403.
 171. Klodzińska SN, Priemel PA, Rades T, Nielsen HM. Inhalable antimicrobials for treatment of bacterial biofilm-associated sinusitis in cystic fibrosis patients: Challenges and drug delivery approaches. *Int J Mol Sci*. 2016;17.
 172. Nafee N, Husari A, Maurer CK, Lu C, De Rossi C, Steinbach A, et al. Antibiotic-free nanotherapeutics: Ultra-small, mucus-penetrating solid lipid nanoparticles enhance the pulmonary delivery and anti-virulence efficacy of novel quorum sensing inhibitors. *J Control Release*. 2014;192:131–40.
 173. Islan GA, Tornello PC, Abraham GA, Duran N, Castro GR. Smart lipid nanoparticles containing levofloxacin and DNase for lung delivery. Design and characterization. *Colloids Surfaces B Biointerfaces*.

- 2016;143:168–76.
174. Moormeier DE, Bayles KW. *Staphylococcus aureus* biofilm: a complex developmental organism. *Mol Microbiol.* 2017;0:1–12.
 175. Yang L, Nilsson M, Gjermansen M, Givskov M, Tolker-Nielsen T. Pyoverdine and PQS mediated subpopulation interactions involved in *Pseudomonas aeruginosa* biofilm formation. *Mol Microbiol.* 2009;74:1380–92.
 176. Rollet C, Gal L, Guzzo J. Biofilm-detached cells, a transition from a sessile to a planktonic phenotype: A comparative study of adhesion and physiological characteristics in *pseudomonas aeruginosa*. *FEMS Microbiol Lett.* 2009;290:135–42.
 177. Kim J, Hahn JS, Franklin MJ, Stewart PS, Yoon J. Tolerance of dormant and active cells in *Pseudomonas aeruginosa* PA01 biofilm to antimicrobial agents. *J Antimicrob Chemother.* 2009;63:129–35.
 178. Bjarnsholt T, Ciofu O, Molin S, Givskov M, Høiby N. Applying insights from biofilm biology to drug development - can a new approach be developed? *Nat Rev Drug Discov.* 2013;12:791–808.
 179. Haagensen JAJ, Klausen M, Ernst RK, Miller SI, Folkesson A, Tolker-Nielsen T, et al. Differentiation and distribution of colistin- and sodium dodecyl sulfate-tolerant cells in *Pseudomonas aeruginosa* biofilms. *J Bacteriol.* 2007;189:28–37.
 180. Khan W, Bernier SP, Kuchma SL, Hammond JH, Hasan F, O'Toole GA. Aminoglycoside resistance of *Pseudomonas aeruginosa* biofilms modulated by extracellular polysaccharide. *Int Microbiol.* 2010;13:207–12.
 181. Sans-Serramitjana E, Fusté E, Martínez-Garriga B, Merlos A, Pastor M, Pedraz JL, et al. Killing effect of nanoencapsulated colistin sulfate on *Pseudomonas aeruginosa* from cystic fibrosis patients. *J Cyst Fibros.* 2016;15:611–8.
 182. Forier K, Messiaen A-S, Raemdonck K, Deschout H, Rejman J, De Baets F, et al. Transport of nanoparticles in cystic fibrosis sputum and bacterial biofilms by single-particle tracking microscopy. *Nanomedicine.* 2013;8:935–49.

183. Pastor M, Moreno-sastre M, Esquisabel A, Sans E, Viñas M, Bachiller D, et al. Sodium colistimethate loaded lipid nanocarriers for the treatment of *Pseudomonas aeruginosa* infections associated with cystic fibrosis. Int J Pharm. 2014;477:485.

7. ANNEXES

7.1. ANNEX I

Part of the experimental data presented in this published article was obtained during my undergraduate internship (Sep 2010 – Mar 2011) in Prof.Dr. Roland Benz's lab at the DFG-research center for experimental biomedicine (University of Würzburg, Germany). While I was there, I studied some protein channels of the external membrane of different species of *Borrelia* by using molecular microbiology and electrophysiology techniques: FPLC, SDS-Page, Blue Native Page and black lipid bilayer.

Study of the Protein Complex, Pore Diameter, and Pore-forming Activity of the *Borrelia burgdorferi* P13 Porin^{*§}

Received for publication, November 30, 2013, and in revised form, May 10, 2014. Published, JBC Papers in Press, May 13, 2014, DOI 10.1074/jbc.M113.539528

Iván Bárcena-Uribarri^{†§1}, Marcus Thein[‡], Mariam Barbot[‡], Eulalia Sans-Serramitjana[‡], Mari Bonde[¶], Reinhard Mentle^{||}, Friedrich Lottspeich^{||}, Sven Bergström[¶], and Roland Benz^{‡§}

From the [†]Rudolf-Virchow-Center, Deutsche Forschungsgemeinschaft Research Center for Experimental Biomedicine, University of Würzburg, Versbacher Strasse 9, D-97078 Würzburg, Germany, [‡]School of Engineering and Science, Jacobs University Bremen, Campusring 1, D-28759 Bremen, Germany, [¶]Department of Molecular Biology, Umeå University, S-90187 Umeå, Sweden, and ^{||}Max-Planck Institute of Biochemistry, Protein Analysis Department, Am Klopferspitz 18, D-82152 Martinsried, Germany

Background: *B. burgdorferi* P13 has unique characteristics compared with other porins.

Results: P13 is a homo-oligomer with a 0.6 nS conductance in 1 M KCl and a substrate cut-off of 400 Da.

Conclusion: P13 represents a general diffusion pathway for small solutes into *Borrelia*.

Significance: Understanding the molecular transport through P13 may play a role in designing more efficient antibiotic treatments against *Borrelia* infections.

P13 is one of the major outer membrane proteins of *Borrelia burgdorferi*. Previous studies described P13 as a porin. In the present study some structure and function aspects of P13 were studied. P13 showed according to lipid bilayer studies a channel-forming activity of 0.6 nanosiemens in 1 M KCl. Single channel and selectivity measurements demonstrated that P13 had no preference for either cations or anions and showed no voltage-gating up to ± 100 mV. Blue native polyacrylamide gel electrophoresis was used to isolate and characterize the P13 protein complex in its native state. The complex had a high molecular mass of about 300 kDa and was only composed of P13 monomers. The channel size was investigated using non-electrolytes revealing an apparent diameter of about 1.4 nm with a 400-Da molecular mass cut-off. Multichannel titrations with different substrates reinforced the idea that P13 forms a general diffusion channel. The identity of P13 within the complex was confirmed by second dimension SDS-PAGE, Western blotting, mass spectrometry, and the use of a *p13* deletion mutant strain. The results suggested that P13 is the protein responsible for the 0.6-nanosiemens pore-forming activity in the outer membrane of *B. burgdorferi*.

the most well studied species in this genus, is one of the causative agents of the Lyme disease, a multisystemic disease that can affect different organs during infection, such as skin, joints, and nervous system (5, 6).

Borrelia species are found associated with various hosts, which is attributed to their limited metabolic capacity (7). *Borrelia* sp. lack genes involved in the biosynthesis of amino acids, fatty acids, and nucleotides pointing to the need of getting additional nutrients from their different hosts (8). These molecules must be taken up from the vertebrate hosts including birds or the invertebrate tick vector (9, 10). The first step in nutrient uptake in Gram-negative bacteria is accomplished by porins. Bacterial porins are water-filled channels that facilitate the transport of essential molecules across the outer membrane (11). Most of the porins found in the outer membranes of Gram-negative bacteria are composed of antiparallel β -sheets forming β -barrel cylinders. Frequently, they are arranged as oligomers, usually trimers, which provide a high stability to the protein complex (11, 12). Porins can be classified in two groups depending on their function; as general diffusion porins when they sort simply according to the molecular mass of the solutes or as substrate-specific porins when facilitating the transport of classes of molecules such as carbohydrates, nucleotides, or phosphate (11, 13–17).

Three porins have previously been described in *Borrelia* sp. P66 and P13 were found in Lyme disease *B. burgdorferi*, whereas Oms38 was first discovered in relapsing fever spirochetes. Subsequently, an Oms38 homologue, called DipA, has been found in *B. burgdorferi*. P66 has a remarkably high single channel conductance, and it is the best studied pore-forming protein in *Borrelia* sp. (18–21). Oms38/DipA has been identified to be a porin-specific for dicarboxylates (22, 23).

P13, the subject of this study, represents an atypical type of porin. It forms channels in the outer membrane of *Borrelia* despite its small 13-kDa molecular mass and its α -helical secondary structure (24). The occurrence and function of a

The genus *Borrelia* belongs to the Spirochetes phylum, which is distantly related to Gram-negative bacteria (1). *Borrelia* sp. are pathogenic bacteria that can cause two diseases, Lyme disease and relapsing fever (2–4). *Borrelia burgdorferi*,

^{*} This work was supported by a joint project between Stint (Sweden) and Deutscher Akademischer Austauschdienst (DAAD) (Germany) (to S. B. and R. B.), the Deutsche Forschungsgemeinschaft (Be 864/15-1; to R. B.), Wi 933 (to Mathias Winterhalter), and Swedish Medical Research Council Grant 07922 (to S. B.).

[§] This article contains supplemental Fig. S1–S4.

¹ Supported by the Alfonso Martín Escudero Foundation. To whom correspondence should be addressed: School of Engineering and Science, Jacobs University Bremen, Campusring 1, D-28759 Bremen, Germany. Tel.: 49-421-200-3583; Fax: 49-421-200-3249; E-mail: i.barcenauribarri@jacobs-university.de.

periplasmic peptide derived from cleavage of its C-terminal end is not completely understood and is unique among porins (25, 26). Another very remarkable feature of P13 is the presence of up to eight paralogues in the genome of *B. burgdorferi* (27). The only paralogue further studied is BBA01, also showing pore forming activity (28). The reason for the high copy number of genes coding for P13-like proteins is still not understood, but it reinforces the idea that P13 could be an indispensable outer membrane protein.

Another protein called Oms28, which is exported to the periplasm, was initially described as a porin with a 0.6-nanosiemens (nS)² single channel conductance (29). Afterward, its function as a porin was questioned due to its periplasmic membrane-associated location (30, 31).

In the present study structure and composition of the P13 protein complex was studied with blue native PAGE (BN-PAGE). Furthermore, the biophysical properties of the complex were investigated. In particular, we studied its single channel activity in different salt solutions, ion selectivity, voltage-gating, and the possibility of substrate specificity. Similarly, the diameter of the P13 channel was evaluated using different non-electrolytes. Surprisingly, the 0.6-nS single channel conductance of P13 described in this study was completely different to the 3.5-nS conductance previously reported (24).

EXPERIMENTAL PROCEDURES

Bacterial Strains and Isolation of the Outer Membrane Proteome

B. burgdorferi B31 (ATCC35210) high passage, and *B. burgdorferi* P13–18 (32) were cultivated in BSKII medium as previously described (33). The isolation of outer membrane proteins (B-Fraction) was performed following a previously published protocol (34).

Study of the P13 Complex by Blue Native PAGE and SDS-PAGE

BN-PAGE in First Dimension—Approximately 1.8 μ g of B-fraction was solubilized in 25 μ l of 10 mM digitonin by incubation for 15 min at room temperature. After solubilization the sample was centrifuged at 20,000 \times g for 20 min at 4 °C. The remaining insolubilized proteins in the pellet were discarded. The supernatant was mixed 5:1 v/v with 50% glycerol and then 15:1 v/v with 5% Coomassie G-250 right before loading the BN-PAGE.

NativePAGETM Novex® 4–16% Bis-Tris gels 1.0 mm (Invitrogen) were used. The conditions recommended by the manufacturers were used for electrophoresis (150 V constant). One-third of the run was performed in the presence of deep blue cathode buffer, and the remaining two-thirds were run using light blue cathode buffer. The corresponding P13 band was eluted from the gel and run again on a BN-PAGE to eliminate the remaining proteins from the membrane extract that tended to smear on the first BN-PAGE. To extract the P13 complex, the

corresponding band was excised with a clean scalpel. The gel was crushed into pieces and mixed 1:2 w/v with 0.1% digitonin. The mixture was incubated overnight in a shaker at 4 °C. For reloading the sample on another BN-PAGE, the protein solution was mixed 5:1 v/v with 50% glycerol and then 30:1 v/v with 5% Coomassie solution before the sample was loaded on the gel. The conditions for electrophoresis remained the same as for the first BN-PAGE.

Tricine SDS-PAGE—The P13 complex eluted from a native gel was resolved in Tricine gels (Novex® 16% Tricine gels 1.0 mm, Invitrogen) after mixing with SDS sample buffer and heating the sample for 10 min at 95 °C. The gels were run using MES SDS running buffer following the instructions of the manufacturer.

SDS-PAGE in Second Dimension—Second dimension SDS-PAGE (NuPAGE® Novex 12% Bis-Tris gel 1.0-mm 2D Well, Invitrogen) was used to dissect the P13 complex after BN-PAGE. A lane of the BN-PAGE was cut and incubated in three denaturing solutions according to manufacturer's instructions (Invitrogen). The lane of the gel was incubated for 30 min in the reducing and alkylating solutions and then 15 min in the quenching solution. Electrophoresis was performed as recommended by the manufacturer (Invitrogen) using MES SDS running buffer. BN- and SDS-PAGE were stained with silver nitrate following protocols described elsewhere (35, 36).

Western Blots (WB)—BN- and SDS-PAGE were blotted onto 0.2- μ m pore size PVDF membranes (Immobilon®-P^{5Q} Transfer Membrane, Millipore). The membranes were fixed in 8% acetic acid after transferring the proteins in the case of BN-PAGE. Excess Coomassie Blue in the membranes was removed by incubating the membrane several minutes in methanol and then rinsing with water. Membranes were blocked using 5% skim milk in TBS buffer overnight. P13 (25) and BBA01 (27) antibodies were dissolved in 2.5% skim milk TBS buffer. For the secondary antibody an anti-rabbit antibody coupled to an alkaline phosphatase was used (anti-rabbit IgG alkaline phosphatase antibody produced in goat; Sigma). 5-bromo-4-chloro-3-indolyl phosphate/nitro blue tetrazolium (SIGMAFASTTM BCIP®/NBT, Sigma) was used to develop the membranes.

Mass Spectroscopy

For MALDI analysis a Proteomics analyzer 4700 (MALDI-TOF/TOF, Applied Biosystems, Darmstadt, Germany) was used. Matrix was α -Matrix (α -cyano-4-hydroxy-cinnamic acid) in overlay technique at 5 mg/ml in 50% acetonitrile, 0.1% TFA, 0.45- μ l sample, and 0.45- μ l matrix solution. The MALDI-MS and MS/MS measurements were performed with a 355-nm Nd:YAG laser in positive reflector mode with a 20-kV acceleration voltage.

Planar Lipid Bilayer

Two approaches were used in this study to characterize the pore-forming activity of the P13 porin; multichannel solvent-containing membranes (37) and single channel solvent-free membranes (38). The single channel conductance of P13 was studied using both methods, whereas ion selectivity, voltage-gating, and substrate specificity were studied using multichannel solvent-containing membranes.

² The abbreviations used are: nS, nanosiemens; BN-PAGE, blue native PAGE; Bis-Tris, 2-bis(2-hydroxyethyl)amino-2-(hydroxymethyl)propane-1,3-diol; Tricine, N-[2-hydroxy-1,1-bis(hydroxymethyl)ethyl]glycine; WB, Western blot; DPhPC, 1,2-diphytanoyl-sn-glycero-3-phosphocholine; DPhPG, 1,2-diphytanoyl-sn-glycero-3-phospho-1'-rac-glycerol; NE, nonelectrolyte.

Properties of P13 Borrelia Porin

Single Channel Conductance in Multichannel Solvent-containing Membranes—The planar lipid bilayer method has been described previously (39). The membranes were formed from a 1% (w/v) solution of DPhPC (1,2-diphytanoyl-*sn*-glycero-3-phosphocholine) or 1% DPhPG (1,2-diphytanoyl-*sn*-glycero-3-phospho-1'-rac-glycerol) (Avanti Polar Lipids, Alabaster, AL) in *n*-decane. The membranes had a surface of $\sim 0.5 \text{ mm}^2$, and they were formed using a Teflon loop to spread the lipid over the aperture. The porin-containing protein fractions were 1:1 diluted in 1% Genapol (Roth) and added to the aqueous phase after the membrane had turned black. The membrane current was measured with a pair of reference Ag^+/AgCl electrodes with salt bridges switched in series with a voltage source and a highly sensitive current amplifier (Keithley 427). The signal was recorded by an analog strip chart recorder (Rikandenki). The temperature was kept at 20°C throughout.

Single Channel Conductance at the Single Unit Level in Solvent-free Planar Lipid Bilayers—This approach has been described in detail previously (38, 40). Membranes were formed with DPhPC by employing the classic Montal and Mueller technique (38) where the solvent is depleted. Membranes had a surface of $\sim 0.008 \text{ mm}^2$. Standard Ag^+/AgCl electrodes (World Precision Instruments) were placed in each chamber to measure the ion current. For single-channel measurements, small amounts of porin were added to the chamber. Spontaneous channel insertions were usually obtained applying 50-mV voltages. Conductance measurements were performed using an Axopatch 200B amplifier (Axon Instruments) in the voltage clamp mode. Signals were filtered by an on-board low pass Bessel filter at 600 Hz and recorded onto a computer hard drive with a sampling frequency of 2.5 kHz. The analysis of the conductance of the channels was performed using Clampfit (Axon Instruments) and Origin (Microcal Software Inc.).

Ion Selectivity—Zero-current membrane potential measurements were performed as described earlier (37). The membranes were formed in 0.1 M salt solution. A salt concentration gradient was gradually established across the membrane after porin insertions reached a stationary phase by the addition of 0.1 M salt solution to one side and 3 M salt solution to the other. Ions with a higher permeability through P13 cause charge separation across the membrane. As a result, a zero-current membrane potential is established when the electrochemical equilibrium is reached. Potentials were measured at the diluted side with a high impedance electrometer (Keithley 617) and analyzed using the Goldman-Hodgkin-Katz equation (37).

Voltage Gating—Voltage gating of the P13 porin was checked following the method described elsewhere (41) using membrane potentials in a range between -100 and $+100 \text{ mV}$. The membrane conductance (G) as a function of voltage (V_m) was measured when the opening and closing of channels reached equilibrium after the membrane current decay due to the voltage step. The initial value of the conductance (G_o) obtained immediately after the onset of the voltage (which follows a linear function of the voltage) was divided by conductance (G) to analyze the gating of the channel.

Substrate Specificity—Blocking of P13 conductance by different substrates was investigated in the same way as the titration experiments to measure binding of maltotigosaccharides to

carbohydrate-specific porins (15, 42). The measurements were performed with multi-channel membranes under stationary conditions obtained about 60–90 min after the addition of the protein to the planar lipid membranes. At that point, different solutes were added in defined concentrations to both sides of the membrane while stirring to allow equilibration. Specific transport of substances should create a block of the channel conductance due to an impaired ion flux through the channel caused by the binding of the solutes to the channel interior.

Channel Diameter Estimation Using Nonelectrolytes—The estimation of channel diameters using NEs is a method that has successfully been used previously (43). This method is based on the fact that small non-electrolytes that penetrate a channel will reduce its conductance due to an increase in the solution viscosity inside the channel. The conductance of the P13 channel was measured in 1 M KCl solutions each time containing a different NE (20% w/v) with increasing hydrodynamic radii (43–45). When the diameter of the NEs is increased, a point may be reached where bigger NEs cannot enter the channel, and its interior will be free of NEs. In these cases the conductance will be about the same as that measured in 1 M KCl solution free of nonelectrolytes. Following this protocol, the channel diameter should be approximately equal to the smallest NE that does not enter the channel and, therefore, does not reduce its conductance.

The size of a possible constriction inside the channel can be guessed using the channel filling concept. The filling of the channel (F) and its value in percentage ($\%F$) were calculated as described elsewhere (43). The filling (F) is given by

$$F = [(G_o - G_i)/G_i]/[(X_o - X_i)/X_i] \quad (\text{Eq. 1})$$

where G_o is the single-channel conductance in a solution without NE (1 M KCl), and G_i is the single-channel conductance in the presence of a solution containing 20% (w/v) of an NE. X_o and X_i correspond to the conductivity of the salt solution without NE and with 20% (w/v) of a defined NE, respectively. Assuming that the filling of the channel by two of the smallest NEs (in our study ethylene glycol and glycerol) is close to the maximum possible level, the filling can be calculated in terms of percentage ($\%F$),

$$\%F = 2F_i/(F_1 + F_2)100\% \quad (\text{Eq. 2})$$

where F_i is the filling in the presence of a given NE and F_1 and F_2 represent filling in the presence of ethylene glycol and glycerol in the bathing solution respectively. The radius of the constriction zone should be equal to the radius of the smallest NE that does not pass freely through the channel and, therefore, does not fill it by 100%.

The following NEs were used: ethylene glycol, glycerol, sorbitol, (all obtained from Sigma), polyethylene glycol (PEG) 200, PEG 300, PEG 400, PEG 600, and PEG 1,000 (all obtained from Fluka; Munich, Germany). Polyethylene glycols were the molecules of choice in our studies because in aqueous solutions they have a spherical shape (46, 47). At least 100 hundred P13 channels reconstituted into lipid membranes were analyzed to estimate the single channel conductance in the presence of the different NEs.

RESULTS

Composition of the Protein Complex—The B-fraction of *B. burgdorferi* was studied using BN-PAGE to identify possible formation of outer membrane complexes. Several protein complexes appeared on the BN-PAGE stained with silver nitrate. To further investigate if any of these complexes was related to P13, WBs were carried out using polyclonal antibodies against P13. A band with an apparent molecular mass of 300 kDa reacted strongly with the P13 antibody (Fig. 1A, left).

Faint traces of the P13 protein were also observed in Western blots of this first BN-PAGE especially in the low molecular mass range. To minimize this effect and increase the homogeneity of the sample, the P13 complex was extracted from the first BN-PAGE and reloaded again on a BN-PAGE of identical characteristics. The extraction of the P13 protein complex from the gel did not have any effect on its apparent molecular mass, which remained stable at 300 kDa. Western blots of the second BN-PAGE again confirmed the presence of P13 within the complex (Fig. 1A, center).

To study the protein complex in more detail, the band was also excised and extracted from the second BN-PAGE and resolved on a Tricine SDS-PAGE under denaturing conditions. A main band of 13 kDa was observed, which clearly reacted with the P13 antibody (Fig. 1A, right). Small amounts of other proteins were also observed in the gel when the staining procedure was prolonged.

Second dimension SDS-PAGE was also performed to differentiate between proteins smearing along the gel, which appear like lines crossing the gel horizontally, and well-defined components of the complex, which appear like small spots. Some proteins smeared along the first dimension and appeared in the second dimension as horizontal bands faintly stained. Those proteins were not considered as possible components of the complex. The gel also showed several spots apart from the one corresponding to the 13-kDa P13 protein with molecular masses of ~72 and 95 kDa (Fig. 1B, SDS-PAGE). When a gel of identical characteristics was used to perform a Western blot, the P13 antibody reacted with all these spots. Furthermore, other spots in the same vertical lane, which were not visible in the silver-stained gel, reacted also with the antibody (Fig. 1B, WB).

The outer membrane fraction of a *p13* knock-out mutant (*B. burgdorferi* P13-18; Ref. 32) was separated on a BN-PAGE in the same way as performed above for the wild type membrane fraction to confirm the role of P13 in the formation of the protein complex. The 300-kDa band was not visible after staining the gel with silver nitrate. The corresponding signal in the WB was also completely missing. That means not only that P13 was not expressed but also that the P13 antibody did not react with any other protein in the sample, for instance with the P13 paralogues (Fig. 2).

To study a possible role of the other proteins within the P13 paralogue protein family 48, especially the close-related protein BBA01, in the co-formation of the complex, an immunoblot against this paralogue was performed. However, BBA01 could not be detected in the 300-kDa complex eluted from a second BN-PAGE, which indicates that P13 forms the complex with-

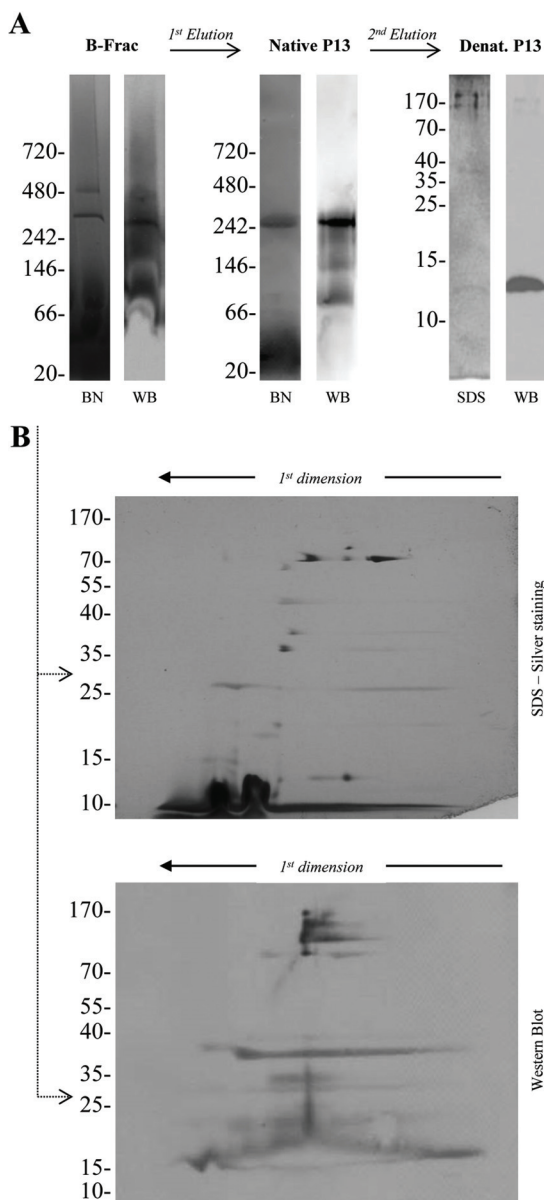


FIGURE 1. BN- and SDS-PAGE analysis of the *B. burgdorferi* P13 complex. A, the B-fraction-containing outer membrane proteins from *B. burgdorferi* B31 were separated on a BN-PAGE 4–16% acrylamide (Invitrogen), and P13 was detected by immunoblot (left). The band was excised from the gel and eluted with 0.1% digitonin, and the procedure was repeated in a second BN-PAGE/Western blot (center). The band was again excised and eluted and resolved on a Tricine SDS-PAGE plus Western blot (right). B, the first BN-PAGE containing the B-fraction of *B. burgdorferi* was also resolved in a second dimension SDS-PAGE with its correspondent P13 WB.

out requiring other P13 paralogues (results not shown). As discussed later, all other paralogues were absent in the sample tested.

Properties of P13 *Borrelia* Porin

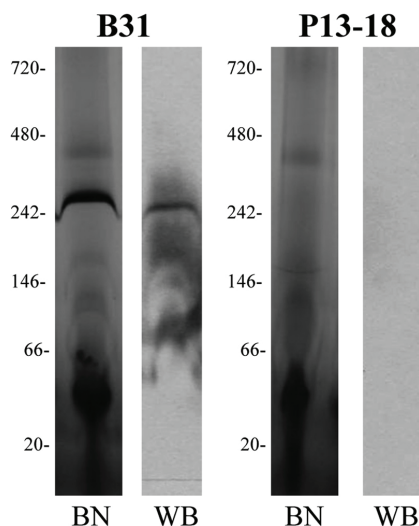


FIGURE 2. Comparison of BN-PAGE and Western blot between *B. burgdorferi* wild type (B31) and a P13 knock out mutant (P13-18). Approximately 0.8 μ g of B-fraction from both strains was solubilized in digitonin and loaded in the BN-PAGE. The Western blots were performed using an antibody against P13.

To further analyze the protein complex, it was subjected to mass spectrometry. Three samples were prepared for this analysis (supplemental Fig. S1). Sample 1 was obtained by excising the 300-kDa band from a second BN-PAGE, and samples 2 and 3 were obtained by cutting two pieces from a two-dimensional SDS-PAGE from a second BN-PAGE where the complex was resolved. Sample 2 covered several spots in an approximate horizontal range from 60 to 100 kDa, and sample 3 was a spot within an approximate range from 12–17 kDa. The proteins were trypsin-digested, and the masses obtained from the spectral data of these peptides (supplemental Figs. S2–S4) were compared with expected values computed from sequence database entries (NCBI, taxonomy bacterial proteins) according to the enzyme's cleavage specificity. The peptide identified with a higher intensity (>70%) in all three samples had a molecular mass of 1898.92 Da. This peptide was recognized as a P13 peptide with the sequence LTEILPFTFANSYNR. In samples 1 and 2 a 1940.85-Da peptide was also observed with high intensity. This peptide was identified as a degradation product of pig trypsin, and it was not taken into consideration. In sample 2 other peptides with intensities between 40 and 70% were observed (masses 1306.50; 1492.70 and 1597.76 Da), but the search in the database did not report any significant matches for those peptides. The observation of the sequence of the BBA01 paralogue reported significant differences in trypsinization of this protein, and therefore, the peptide with a mass of 1898.92 is specific for P13 within the components of the paralogue family 48.

Single Channel Conductance—The P13 complex was run on two consecutive BN-PAGES, and after the second elution the pore forming activity of this porin was studied. The addition of small amounts of the purified P13 complex (~ 10 ng/ml) to one

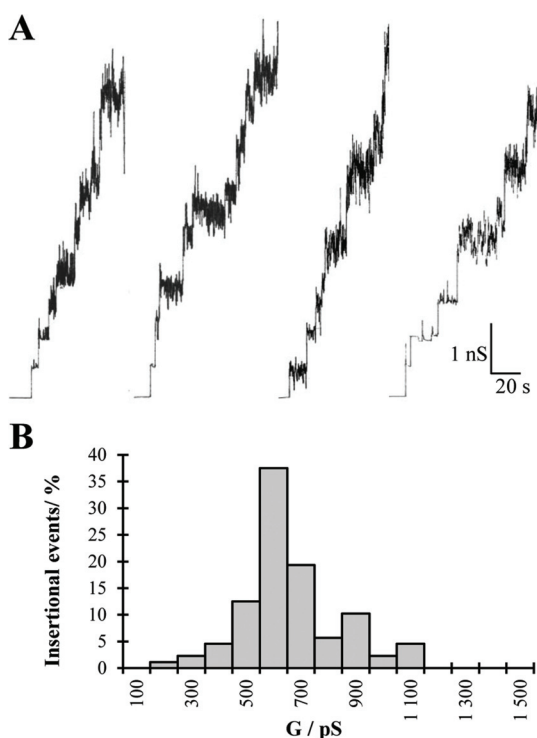


FIGURE 3. Pore forming activity of *B. burgdorferi* P13 extracted from a secondary BN-PAGE. Shown are four independent records of single channel insertions in a newly formed DPhPC membrane (1 M KCl, 20 mV) (A) and the corresponding histogram of the pore forming activity of the P13 protein complex using the planar lipid bilayer assay (B).

or both sides of a planar lipid membrane made of phosphocholine/*n*-decane resulted after some delay in observation of step-like conductance increases with a value of 0.6 nS in 1 M KCl. Most of the steps were directed upward, indicating that the channels were in an open state under low voltage conditions (20 mV). The P13 channel had an intrinsic high noise that made it impossible after reconstitution of a few pores to identify the conductance of additional insertions (Fig. 3A). Therefore, only the first insertions in each membrane with clear conductance values were used to estimate the conductance of the P13 complex (Fig. 3B).

The pore-forming activity of the P13 complex was also measured in different KCl concentrations and in different electrolytes (LiCl and KCH₃COO) to gain some insight into the ion transport properties. The linear correlation between KCl concentration and the pore conductance is typical for general diffusion porins, which have no binding sites for anions or cations and where no net charges influence the pore conductance (Table 1). Comparison of measurements done in 1 M lithium chloride and in 1 M potassium acetate, where anions and cations differ inversely in hydrodynamic radius, with measurements done in 1 M KCl showed a similar decrease (0.2 and 0.25 nS, respectively) for the P13 single channel conductance. The comparable results obtained by exchanging the mobile ions K⁺ and

TABLE 1

Single channel measurements of *B. burgdorferi* P13 in different KCl concentrations and different electrolytes

The P13 conductance (G) in each salt solution was taken from the highest conductance value observed in a Gaussian distribution of single channel conductance. To analyze P13 conductance, in each case at least 100 channels were reconstituted in DPhPC membranes at 20 mV voltage. The solutions were used unbuffered with a pH close to 6 unless otherwise indicated. The conductivity of each salt solution (χ) was measured at room temperature with a conductometer (Knick 703). The ion activities (γ) of the salts at 25 °C are given in parentheses (51).

Electrolyte	Concentration (γ)	χ	P13 G
	<i>M</i>	<i>mS/cm</i>	<i>nS</i>
KCl	0.1 (0.77)	13.1	0.05
	0.3 (0.68)	37.1	0.075
	1 (0.60)	106.5	0.6
	3 (0.56)	291.8	1.5
LiCl	1 (0.77)	70.3	0.2
KCH ₃ COO (pH 7)	1 (0.78)	68.6	0.25

Cl[−] by the less mobile ions Li⁺ and CH₃COO[−] indicates that cations and anions have a similar permeability through the P13 complex, *i.e.* its selectivity is low if any (Table 1).

Two are the major lipids in the outer membrane of *B. burgdorferi*, phosphatidylcholine and phosphatidylglycerol. To study the possible influence of lipids, the P13 porin was as well measured in DPhPG membranes and 1 M KCl salt solution. P13 displayed in this type of membranes a very similar behavior to the one observed using DPhPC membranes. The sample was very active, and after several insertions the current noise hindered an accurate resolution of new insertions (Fig. 4A). Using the first insertions, a histogram was produced where the major conductance step was 0.6 nS in 1 M KCl (Fig. 4B).

Another reconstitution approach using solvent-free membranes was performed to study this porin at the single unit level. A single P13 channel was recorded with a high sampling digitizer (2.5 kHz) and a 600-Hz filter. Interestingly, the channel displayed some sub-states as well as short upwards spike-like fluctuations that shortly increased the conductance (Fig. 5A). These sub-states and fluctuations upward (Fig. 5A, conductance states 2 and 3, respectively) seem to be independent from the applied voltage as it is shown in the voltage-gating experiments (see below). A histogram summarizing the conductance data points revealed a predominant conductance of ~0.65 nS in 1 M KCl (Fig. 5B, conductance state 1). These results are somehow preliminary, and further analysis of this dynamic channel is required to clarify its several conductance states.

Ion Selectivity—Zero-current membrane potential measurements were also carried out to measure the ion selectivity of P13 in more detail. Membranes with >100 inserted P13 pores were used to perform these measurements. 5-Fold gradients of KCl, LiCl, and KCH₃COO were established across the membranes. Consequently, the zero-current potential for KCl was slightly negative (−3.4 mV) at the more diluted side of the membranes, which reflects some low anion selectivity. When LiCl was used, the diluted side was more negative (−11.9 mV), and when KCH₃COO was used, a positive potential was observed at the diluted side (17 mV). The ratios of the permeability P_{cation} and P_{anion} as calculated using the Goldman-Hodgkin-Katz equation were 0.8 for KCl, 0.40 for LiCl, and 3.5 for KCH₃COO, which means that the selectivity followed the mobility sequence of anions and cations in the aqueous phase, *i.e.* it is indeed water-filled (see Table 2). This supported the idea of a general diffu-

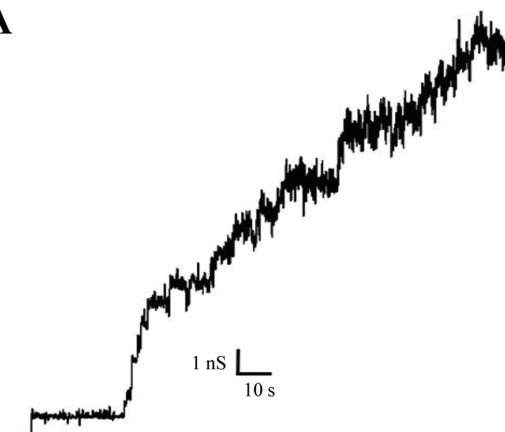
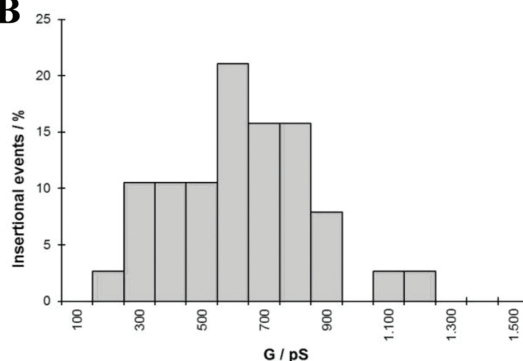
A**B**

FIGURE 4. Pore forming activity of *B. burgdorferi* P13 in DPhPG/*n*-decane membranes. Shown are single channel recording of P13 extracted from a secondary BN-PAGE in 1 M KCl and 20 mV applied voltage (A) and the corresponding histogram of the pore forming activity of the P13 complex in DPhPG/*n*-decane membranes (B).

sion channel with some minor selectivity for ions with a similar aqueous mobility.

Voltage Gating—The effect of the voltage in the P13 pore was studied in a DPhPC membrane containing many P13 channels. Increasing positive and negative voltages were applied to study a possible gating of the pore. P13 showed a very low voltage-gating tendency between −100 and +100 mV (Fig. 6). For voltages up to ±40 mV the channel showed no decrease of the conductance at all. For higher voltages up to ±100 mV the P13 channel displayed minor gating, and the conductance values remained 85% or higher of its initial one.

Substrate Specificity—In these experiments we studied a possible substrate specificity of P13. In a first run we tested some physiologically important sugars such as glucose, fructose, galactose, ribose, maltose, lactose, and glucosamine. Similarly, we studied the effect of some amino acids such as glycine, cysteine, phenylalanine, histidine, arginine, or other molecules like ATP, ascorbic acid, or sodium phosphate on the conductance of P13. Interestingly, none of these molecules displayed any

Properties of P13 *Borrelia* Porin

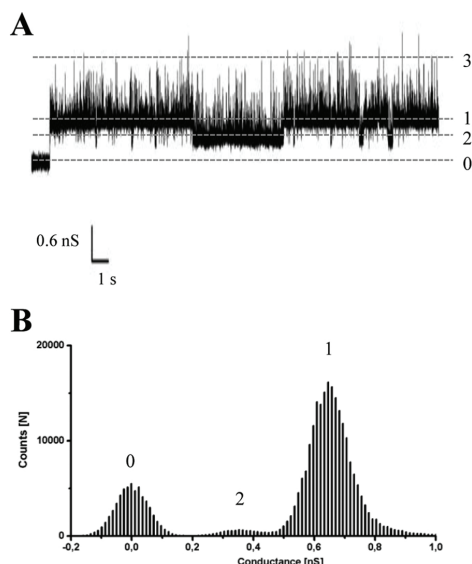


FIGURE 5. Typical conductance through a single *B. burgdorferi* P13 channel (1 M KCl and 50 mV of applied voltage). A, recording of a single P13 channel in a solvent-free DPhPC membrane. The different conductance states are indicated by the dashed lines. B, histogram summarizing its conductance from a 200-s measurement (400 μ s sampling rate). The conductance state 3 is not appreciable in the histogram because the time in this conformation is very low in comparison with states 1 and 2. State 0 corresponds to the membrane with no pore inserted upon which a 50-mV voltage was already applied.

TABLE 2

Zero-current membrane potentials of PC/*n*-decane membranes in the presence of *B. burgdorferi* P13 measured for a 5-fold gradient of different salts (100 mM versus 500 mM)

The zero-current membrane potentials V_m are defined as the difference between the potential at the dilute side and the potential at the concentrated side. The aqueous salt solutions were used unbuffered and had a pH of 6 if not indicated otherwise; $T = 20^\circ\text{C}$. The permeability ratio $P_{\text{cation}}/P_{\text{anion}}$ was calculated using the Goldman-Hodgkin-Katz equation (37) from at least three individual experiments.

Salt	V_m mV	$P_{\text{cation}}/P_{\text{anion}}$
KCl	-3.4	0.8
LiCl	-11.9	0.4
KCH ₃ COO (pH 7)	17.0	3.5

effect on the P13 channel conductance when added in a concentration range between 0.5 and 100 mM.

Channel Diameter—The estimation of a channel diameter using NEs is a method based on the fact that small non-electrolytes that penetrate a channel will reduce its conductance due to an increase in the viscosity of the solution in the channel interior that will modulate the ion flux (43). The conductance of the P13 channel was measured in a 1 M KCl solution supplemented with 20% (w/v) of different NEs with increasing hydrodynamic radii. Increasing the diameter of the NEs will lead to a point where the NEs will not be able to enter the channel and the channel interior will be free of NEs. In such a case the conductance of the P13 channel will be equal to the one measured in pure salt solution. By plotting the channel conductance as a function of the radii of the NEs, it is possible to correlate the hydrodynamic radius of the smallest NE that does not enter the

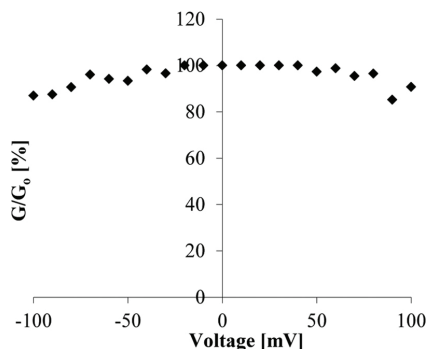


FIGURE 6. Voltage-gating of *B. burgdorferi* P13. Increasing positive and negative voltages were applied on a membrane saturated with P13 to study its gating. After applying the voltage and reaching equilibrium, the decrease in the membrane conductance (G/G_0) was calculated individually for each applied voltage. G_0 = initial conductance right after applying voltage; G = conductance after reaching equilibrium.

pore with the diameter of the pore. The conductance of P13 as derived from the measurements with different NEs is summarized in Table 3. Molecular masses and hydrodynamic radii of the NEs and the specific aqueous conductivity of the solutions are also included in this table.

In the presence of ethylene glycol, glycerol, sorbitol, PEG 200, and PEG 300, the conductance of P13 was reduced to some extent (30–52% that of the original) (Fig. 7A). This decrease was correlated with the decrease of the specific conductivity of the salt solution in presence of the NEs. The P13 channel did not show any conductance reduction in the presence of PEG 400, PEG 600, and PEG 1,000 (Fig. 7A). This means that NEs with a hydrodynamic radius of 0.7 nm or larger were not able to enter the channel. In contrast to this, NEs with a hydrodynamic radius of 0.6 nm or smaller could enter the channel, which resulted in a conductance decrease. The results obtained suggested that the entrance of the P13 channel has approximately the size of PEG 400, *i.e.* its radius is estimated to be around 0.7 nm.

The channel-filling concept was also used here to analyze the idea of a possible constriction zone inside the channel. The radius of the constriction could be calculated using a previously proposed equation calculating the portion of the channel filled by each one of the NEs (43). This concept suggested that the radius of a constriction zone should be close to the radius of the smallest NE that does not fill the channel completely and, therefore, does not pass freely through the channel.

NEs such as ethylene glycol, glycerol, sorbitol, PEG 200, and PEG 300 showed an almost complete filling of the P13 channel, whereas PEG 400 and bigger had filling values close to 0 (Table 3 and Fig. 7B). NEs that filled the channel only partially could not be identified among the different NEs, which means that the channel has no obvious constriction, *i.e.* looks more like a cylinder. The channel filling with sorbitol and PEG 300 was somewhat >100%. To test if that effect was due to a special interaction of the sorbitol or PEG 300 with the channel interior, we performed titration experiments of multichannel membranes with these molecules in the millimolar range as previ-

TABLE 3

Average single channel conductance of *B. burgdorferi* P13 in the presence of different NEs in the bath solution

Average single channel conductances (G) and their S.D. ($G \pm \text{S.D.}$) were calculated from at least 100 conductance steps. The aqueous phase contained 1 M KCl and the corresponding nonelectrolyte at a concentration of 20% (w/v). $V_m = 20$ mV; $T = 20$ °C; Mr = molecular mass; r = hydrodynamic radius (M_r and r of the nonelectrolytes were taken from previous publications (43–45)); χ is the conductivity of the aqueous solutions. Channel filling (F) and percentage of channel filling (% F) were calculated as described elsewhere (43). Et.Gl, ethylene glycol.

NEs	Mr	r	χ	P13			
				$G \pm \text{S.D.}$	% G	F	% F
	g/mol	nm	mS cm ⁻¹	nS			
None			110.30	0.6 ± 0.18	100		
Et.Gl	62	0.26	57.20	0.3 ± 0.09	50	1.08	114.63
Glycerol	92	0.31	49.10	0.3 ± 0.07	50	0.80	85.37
Sorbitol	182	0.39	57.80	0.2 ± 0.07	33	2.20	234.31
PEG 200	200	0.50	46.10	0.3 ± 0.09	50	0.72	76.40
PEG 300	300	0.60	45.50	0.2 ± 0.07	33	1.40	149.44
PEG 400	400	0.70	46.40	0.6 ± 0.07	100	0.00	0.00
PEG 600	600	0.80	54.10	0.6 ± 0.11	100	0.00	0.00
PEG 1000	1000	0.94	49.50	0.65 ± 0.09	108	-0.06	-6.66

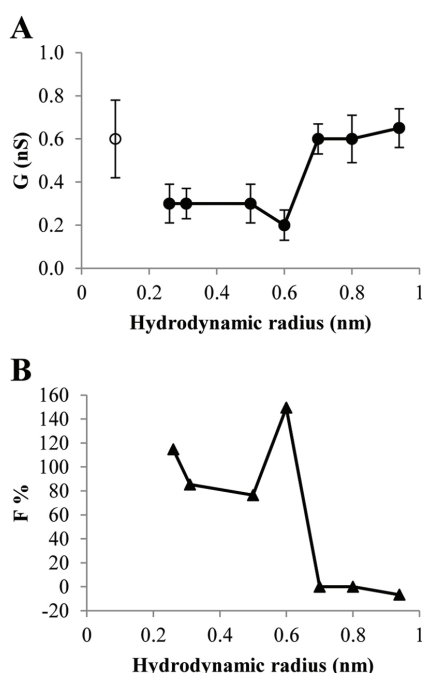


FIGURE 7. *B. burgdorferi* P13 conductance and channel filling in presence of different non-electrolytes. A, the conductance of P13 (G) was measured in 1 M KCl (open circles) and 1 M KCl containing 20% (v/v) of an NE (filled circles). B, the channel filling in percentage (% F) was calculated using the formula described elsewhere (43). The conductance and channel filling corresponding to sorbitol were not included in these diagrams due to its unreasonable values, which could indicate a possible interaction of this compound with the channel interior.

ously described in the substrate specificity section. In these experiments we could not detect any effect of PEG 300 or sorbitol on the P13 conductance.

A possible orientation of the P13 channel in planar bilayers was studied using different approaches. First, P13 was added only to one side of the membrane, and different positive and negative voltages were applied. P13 displayed a very similar gating behavior when applying positive or negative voltages. These results were as well very similar to those obtained when P13 was

added to both sides (Fig. 4), preventing any conclusion. In a second approach a possible orientation of P13 was studied while decreasing the pH. The pH was decreased only in one side of the membrane, whereas the other side remained around pH 6. As described previously for LamB (48), this decrease can cause a gating of the pores probably because the charged loops bend over the channel blocking its conductance. If the channel is oriented, the blockage of the channel will only occur when the pH is decreased in one of the sides. Unfortunately, the results decreasing the pH were not consistent, and neither approach led to a clear identification of an oriented insertion of the P13 channel into DPhPC membranes.

DISCUSSION

Structure of the P13 Pore-forming Complex—P13 isolated from the outer membrane of *B. burgdorferi* has been described as a protein with porin properties, although its structure differs considerably from those of typical Gram-negative bacterial porins (49).

We used BN-PAGE/WB to study the P13 protein complex in detail. Western blots demonstrated the presence of P13 in a 300-kDa band on the gels. Globular or elongated complexes may run with different speed in BN-PAGE. This issue is addressed in detail in a previous study, where a maximal molecular mass deviation of 15% was estimated for different kinds of proteins (50). This estimation seems to be valid as long as the proteins either bind Coomassie or have isoelectric points (pI) below or equal to 8.6 (50). According to this study, proteins with higher pI values, like P13, which binds Coomassie but has a pI close to 9.5, could show a molecular mass up to 30% higher than the real molecular mass (50). How much higher is difficult to predict. The apparent molecular mass of the P13 complex was ~ 300 kDa on BN-PAGE. If it is assumed that this could be at maximum 30% too high, the molecular mass of the complex could still be around 200 kDa. This estimation is supported by the Western blots of the two-dimensional gel where some P13 spots, probably complexes retaining the native conformation in the SDS-PAGE, appeared to have a molecular mass close to 200 kDa (Fig. 1B).

SDS-PAGE of the P13 complex in the second dimension was also used to study if other proteins were part of the protein complex (Fig. 1B). A clear spot of ~ 13 kDa was observed when the gel was stained with silver nitrate. Two additional spots

Properties of P13 *Borrelia* Porin

were usually observed on the gel with molecular masses around 72 and 95 kDa. The corresponding Western blots demonstrated that these three spots contained also P13. Additional protein spots in the upper molecular mass range reacted also with the P13 antibody (Fig. 1B, WB). Based on that, the P13 complex appeared to be resistant, at least partially, to denaturing agents like SDS or DTT. The different spots in the same vertical lane could, therefore, be different dissociation states of P13 from the P13 complex. A cross-reaction with other proteins was unlikely because antibodies against P13 did not interact with other proteins in the *p13*-deficient mutant.

It is noteworthy that the resolution of the P13 complex in two-dimensional SDS-PAGE and in Tricine SDS-PAGE after elution and heating of the sample showed that the P13 complex is a homo-oligomer. This fact is also supported by the MS analysis of the protein complex.

In the *B. burgdorferi* B31 genome eight paralogues have been found for the *p13* gene (bb0034), constituting the gene family 48. Two are pseudogenes (bbj02.1 and bbq81), one has an authentic frameshift producing a completely different peptide (bbg03), and another is located inside bbj02.1 (bbj03). The remaining four (BBA01, BBI31, BBH41, and BBQ06) show a higher similarity to P13 (25), and therefore, they may share a similar function. A previous study showed that in high passage *B. burgdorferi* B31 cultures the plasmids containing some of these paralogues are lost, and only BBA01 was still present (27). The high passage strain and an immunoblot against BBA01 contradict a possible presence of these polypeptides within the 300-kDa complex. Whether these paralogues form similar protein complexes as P13 or not is an open question, and further studies need to be done to clarify this issue in more detail.

Pore-forming Activity of the P13 Complex—The pore-forming activity of the P13 complex was measured in lipid bilayer experiments after gel elution. The conductance of the pore formed by P13 was estimated in previous studies to be 3.5 nS in 1 M KCl (24, 28). However, none of the samples isolated in this study from different BN-PAGEs showed such a pore-forming activity. The planar lipid bilayer measurements of the 300-kDa band and the realization of the corresponding histogram revealed a pore-forming activity of about 0.6 nS in 1 M KCl. This result is in some contradiction to the previous pore forming activity observed for P13 (24, 28). The pores obtained from the eluted 300-kDa band showed some intrinsic noise, and after reconstitution of some channels it was difficult to evaluate the exact conductance of new insertions (see Fig. 3A). Although the noise was very high from that point on, the membrane conductance increased constantly. To check the integrity of the eluted P13 complex, the protein was loaded on a second and even a third BN-PAGE that displayed the same molecular mass and, therefore, retained its native state. It is noteworthy that the P66 complex previously eluted from BN-PAGE also retained its pore-forming activity after elution from BN-PAGE (52).

A similar 0.6-nS pore-forming activity as the one found here was previously described together with 12.6-nS pores in outer membrane vesicles from *B. burgdorferi* B31 (53). This 0.6-nS pore-forming activity was afterward attributed to Oms28 (29). However, in another study the role of Oms28 as a porin was questioned because of its apparent location in the periplasmic

space (30). The existence of a channel-forming protein in the outer membrane of *Borrelia* with a conductance of 0.6 nS in 1 M KCl has been observed several times in our laboratory when B-fractions were analyzed. The 300-kDa complex isolated from BN-PAGE containing P13 has the same conductance and can, therefore, be considered as the complex responsible for such a pore-forming activity.

Previous studies of the B-fraction from a *p66* knock-out mutant and a *p13/p66* double knock-out could support this assumption (32). The B-fraction of the *p66* knock-out mutant did not show any 3.5-nS activity at all, and the double *p13/p66* knock-out reduced the conductance of the porins in the sample to 300 pS or below, where the 0.6-nS activity was also missing (32).

The kind of lipid used to form the membrane and the presence of solvents in it did not seem to influence the conductance of the P13 channel as demonstrated in the experiments of Figs. 4 and 5. Two phospholipids constitute the outer membrane of *Borrelia*, phosphatidylcholine, and phosphatidylglycerol (54). Side chain variants of these lipids, diphytanoyl phosphatidylcholine and diphytanoyl phosphatidylglycerol, were used to perform planar lipid membrane experiments. Phospholipids containing diphytanoyl fatty acid side chains are commonly used to form stable artificial lipid membranes within a wide temperature range without a phase transition (from -120 to $+80$ °C for DPhPC) (55). The channel displayed the same 0.6-nS conductance independently of the lipid used. In reference to the presence of solvents in the membrane the study of single P13 units in solvent-free membranes showed a very similar channel conductance of 0.65 nS. Furthermore, the study of a single P13 unit in solvent-free membranes allowed the observation of a high intrinsic noise of this channel. This noise differed to some extent from channel to channel.

Size of the Pore Formed by the P13 Complex—We used different NEs to determine the channel diameter of the P13 pore employing a previously suggested method (43, 45, 56). Because NEs are uncharged molecules, they avoid attraction/repulsion forces between ions and charges in the channel interior. In addition, the determination of the channel diameter using NEs is not influenced by the conformation of the pores when they represent oligomeric channels in particular trimers such as many porins in Gram-negative bacteria. From the experiments with NEs we calculated a diameter of about 1.4 nm for the P13 complex. These calculations include an estimated error of ± 0.1 nm caused by a certain smearing of the molecular masses of the individual NEs influencing their hydrodynamic radii (45, 56). According to our results, a constriction inside the P13 channel cannot be excluded completely, but this is rather unlikely because the constriction has a similar diameter as the channel opening as judged from the results of estimating the channel filling.

Small molecules up to 400 g/mol seem to have access to the channel interior and, therefore, could diffuse in the periplasmic space of *B. burgdorferi* through P13. It is well known that porins in Gram-negative bacteria represent a pathway for antibiotics to cross the outer membrane (57–59). Several antibiotics used in the treatment against *Borrelia* (60) such as amoxicillin (365 g/mol) are under the molecular weight cut-off described in this

paper for possible P13 substrates. Therefore, this channel could play a role in the translocation and action of antibiotics used to treat infections by *Borrelia*.

In this study we investigated structure and composition of the P13 complex from *B. burgdorferi* outer membrane. The results suggested that P13 forms a complex with a molecular mass of about 200 to 300 kDa. P13 is the only polypeptide that is present in the complex. The P13 complex is a homo-oligomer, and it is composed of a high number of P13 monomers, although further studies need to be done to assign the number of monomers and pores in the complex. Similarly we studied the pore-forming activity of the P13 complex in detail and could attribute it to a single channel conductance of 0.6 nS in 1 M KCl. The channel has minor selectivity for ions, is voltage-gating-independent up to ± 100 mV, and seems to be a general diffusion channel. The molecular mass cut-off of the P13 complex was estimated to be around 400 g/mol from experiments with NEs meaning the channel diameter is around 1.4 (± 0.1) nm.

REFERENCES

- Woese, C. R. (1987) Bacterial evolution. *Microbiol. Rev.* **51**, 221–271
- Obermeier, O. H. F., and Zeiss, H. (1873) *Die entdeckung von fadenförmigen gebilden im blut von rückfallfieberkranken (1873) Eingeleitet und herausgegeben von Dr. Heinz Zeiss*, Leipzig, J. A. Barth, 1926
- Burgdorfer, W. (1984) Discovery of the Lyme disease spirochete and its relation to tick vectors. *Yale J. Biol. Med.* **57**, 515–520
- Burgdorfer, W., Barbour, A. G., Hayes, S. F., Benach, J. L., Grunwaldt, E., and Davis, J. P. (1982) Lyme disease—a tick-borne spirochetosis? *Science* **216**, 1317–1319
- Steere, A. C. (2001) Lyme disease. *N. Engl. J. Med.* **345**, 115–125
- Steere, A. C. (2006) Lyme borreliosis in 2005, 30 years after initial observations in Lyme Connecticut. *Wien. Klin. Wochenschr.* **118**, 625–633
- Barbour, A. G., and Hayes, S. F. (1986) Biology of *Borrelia* species. *Microbiol. Rev.* **50**, 381–400
- Fraser, C. M., Casjens, S., Huang, W. M., Sutton, G. G., Clayton, R., Lathigra, R., White, O., Ketchum, K. A., Dodson, R., Hickey, E. K., Gwinn, M., Dougherty, B., Tomb, J. F., Fleischmann, R. D., Richardson, D., Peterson, J., Kerlavage, A. R., Quackenbush, J., Salzberg, S., Hanson, M., van Vugt, R., Palmer, N., Adams, M. D., Gocayne, J., Weidman, J., Utterback, T., Watthey, L., McDonald, L., Artiach, P., Bowman, C., Garland, S., Fuji, C., Cotton, M. D., Horst, K., Roberts, K., Hatch, B., Smith, H. O., and Venter, J. C. (1997) Genomic sequence of a Lyme disease spirochaete, *Borrelia burgdorferi*. *Nature* **390**, 580–586
- Hasle, G. (2013) Transport of ixodid ticks and tick-borne pathogens by migratory birds. *Front Cell Infect. Microbiol.* **3**, 48
- Mannelli, A., Bertolotti, L., Gern, L., and Gray, J. (2012) Ecology of *Borrelia burgdorferi* sensu lato in Europe: transmission dynamics in multi-host systems, influence of molecular processes and effects of climate change. *FEMS Microbiol. Rev.* **36**, 837–861
- Benz, R. (1994) Solute uptake through bacterial outer membranes. in *Bacterial Cell Wall* (Ghuysen, J. M., and Hakenbeck, R., eds.) pp. 397–423. Elsevier Science Publishing Co., Inc., New York
- Achouak, W., Heulin, T., and Pagès, J. M. (2001) Multiple facets of bacterial porins. *FEMS Microbiol. Lett.* **199**, 1–7
- Maier, C., Bremer, E., Schmid, A., and Benz, R. (1988) Pore-forming activity of the Tsx protein from the outer membrane of *Escherichia coli*. Demonstration of a nucleoside-specific binding site. *J. Biol. Chem.* **263**, 2493–2499
- Benz, R., Schmid, A., Maier, C., and Bremer, E. (1988) Characterization of the nucleoside-binding site inside the Tsx channel of *Escherichia coli* outer membrane. Reconstitution experiments with lipid bilayer membranes. *Eur. J. Biochem.* **176**, 699–705
- Benz, R., Schmid, A., and Vos-Scheperkeuter, G. H. (1987) Mechanism of sugar transport through the sugar-specific LamB channel of *Escherichia coli* outer membrane. *J. Membr. Biol.* **100**, 21–29
- Hancock, R. E., and Benz, R. (1986) Demonstration and chemical modification of a specific phosphate binding site in the phosphate-starvation-inducible outer membrane porin protein P of *Pseudomonas aeruginosa*. *Biochim. Biophys. Acta* **860**, 699–707
- Kim, B. H., Andersen, C., and Benz, R. (2001) Identification of a cell wall channel of *Streptomyces griseus*: the channel contains a binding site for streptomycin. *Mol. Microbiol.* **41**, 665–673
- Bárcena-Uribarri, I., Thein, M., Sacher, A., Bunikis, I., Bonde, M., Bergström, S., and Benz, R. (2010) P66 porins are present in both Lyme disease and relapsing fever spirochetes: a comparison of the biophysical properties of P66 porins from six *Borrelia* species. *Biochim. Biophys. Acta* **1798**, 1197–1203
- Skare, J. T., Mirzabekov, T. A., Shang, E. S., Blanco, D. R., Erdjument-Bromage, H., Bunikis, I., Bergström, S., Tempst, P., Kagan, B. L., Miller, J. N., and Lovett, M. A. (1997) The Oms66 (p66) protein is a *Borrelia burgdorferi* porin. *Infect. Immun.* **65**, 3654–3661
- Coburn, J., Chege, W., Magoun, L., Bodary, S. C., and Leong, J. M. (1999) Characterization of a candidate *Borrelia burgdorferi* β 3-chain integrin ligand identified using a phage display library. *Mol. Microbiol.* **34**, 926–940
- Coburn, J., and Cugini, C. (2003) Targeted mutation of the outer membrane protein P66 disrupts attachment of the Lyme disease agent, *Borrelia burgdorferi*, to integrin α v β 3. *Proc. Natl. Acad. Sci. U.S.A.* **100**, 7301–7306
- Thein, M., Bunikis, I., Denker, K., Larsson, C., Cutler, S., Drancourt, M., Schwan, T. G., Mentele, R., Lottspeich, F., Bergström, S., and Benz, R. (2008) Oms38 is the first identified pore-forming protein in the outer membrane of relapsing fever spirochetes. *J. Bacteriol.* **190**, 7035–7042
- Thein, M., Bonde, M., Bunikis, I., Denker, K., Sickmann, A., Bergström, S., and Benz, R. (2012) DipA, a pore-forming protein in the outer membrane of Lyme disease spirochetes exhibits specificity for the permeation of dicarboxylates. *PLoS ONE* **7**, e36523
- Ostberg, Y., Pinne, M., Benz, R., Rosa, P., and Bergström, S. (2002) Elimination of channel-forming activity by insertional inactivation of the *p13* gene in *Borrelia burgdorferi*. *J. Bacteriol.* **184**, 6811–6819
- Noppa, L., Ostberg, Y., Lavrinovich, M., and Bergström, S. (2001) P13, an integral membrane protein of *Borrelia burgdorferi*, is C-terminally processed and contains surface-exposed domains. *Infect. Immun.* **69**, 3323–3334
- Kumru, O. S., Bunikis, I., Sorokina, I., Bergström, S., and Zückert, W. R. (2011) Specificity and role of the *Borrelia burgdorferi* CtpA protease in outer membrane protein processing. *J. Bacteriol.* **193**, 5759–5765
- Pinne, M., Ostberg, Y., Comstedt, P., and Bergström, S. (2004) Molecular analysis of the channel-forming protein P13 and its paralogue family 48 from different Lyme disease *Borrelia* species. *Microbiology* **150**, 549–559
- Pinne, M., Denker, K., Nilsson, E., Benz, R., and Bergström, S. (2006) The BBA01 protein, a member of paralogue family 48 from *Borrelia burgdorferi*, is potentially interchangeable with the channel-forming protein P13. *J. Bacteriol.* **188**, 4207–4217
- Skare, J. T., Champion, C. L., Mirzabekov, T. A., Shang, E. S., Blanco, D. R., Erdjument-Bromage, H., Tempst, P., Kagan, B. L., Miller, J. N., and Lovett, M. A. (1996) Porin activity of the native and recombinant outer membrane protein Oms28 of *Borrelia burgdorferi*. *J. Bacteriol.* **178**, 4909–4918
- Mulay, V., Caimano, M. J., Liveris, D., Desrosiers, D. C., Radolf, J. D., and Schwartz, I. (2007) *Borrelia burgdorferi* BBA74, a periplasmic protein associated with the outer membrane, lacks porin-like properties. *J. Bacteriol.* **189**, 2063–2068
- Cluss, R. G., Silverman, D. A., and Stafford, T. R. (2004) Extracellular secretion of the *Borrelia burgdorferi* Oms28 porin and Bgp, a glycosaminoglycan binding protein. *Infect. Immun.* **72**, 6279–6286
- Pinne, M., Thein, M., Denker, K., Benz, R., Coburn, J., and Bergström, S. (2007) Elimination of channel-forming activity by insertional inactivation of the *p66* gene in *Borrelia burgdorferi*. *FEMS Microbiol. Lett.* **266**, 241–249
- Barbour, A. G. (1984) Isolation and cultivation of Lyme disease spirochetes. *Yale J. Biol. Med.* **57**, 521–525
- Magnarelli, L. A., Anderson, J. F., and Barbour, A. G. (1989) Enzyme-linked immunosorbent assays for Lyme disease: reactivity of subunits of *Borrelia burgdorferi*. *J. Infect. Dis.* **159**, 43–49

Properties of P13 *Borrelia* Porin

35. Schagger, H. (2006) Tricine-SDS-PAGE. *Nat. Protoc.* **1**, 16–22
36. Blum, H., Beier, H., and Gross, H. J. (1987) Improved silver staining of plant proteins, RNA and DNA in polyacrylamide gels. *Electrophoresis* **8**, 93–99
37. Benz, R., Janko, K., and Läuger, P. (1979) Ionic selectivity of pores formed by the matrix protein (porin) of *Escherichia coli*. *Biochim. Biophys. Acta* **551**, 238–247
38. Montal, M., and Mueller, P. (1972) Formation of bimolecular membranes from lipid monolayers and a study of their electrical properties. *Proc. Natl. Acad. Sci. U.S.A.* **69**, 3561–3566
39. Benz, R., Janko, K., Boos, W., and Läuger, P. (1978) Formation of large, ion-permeable membrane channels by the matrix protein (porin) of *Escherichia coli*. *Biochim. Biophys. Acta* **511**, 305–319
40. Mahendran, K. R., Hajjar, E., Mach, T., Lovelle, M., Kumar, A., Sousa, I., Spiga, E., Weingart, H., Gameiro, P., Winterhalter, M., and Ceccarelli, M. (2010) Molecular basis of enrofloxacin translocation through OmpF, an outer membrane channel of *Escherichia coli*: when binding does not imply translocation. *J. Phys. Chem. B* **114**, 5170–5179
41. Ludwig, O., De Pinto, V., Palmieri, F., and Benz, R. (1986) Pore formation by the mitochondrial porin of rat brain in lipid bilayer membranes. *Biochim. Biophys. Acta* **860**, 268–276
42. Benz, R., Schmid, A., Nakae, T., and Vos-Scheperkeuter, G. H. (1986) Pore formation by LamB of *Escherichia coli* in lipid bilayer membranes. *J. Bacteriol.* **165**, 978–986
43. Krasilnikov, O. V., Da Cruz, J. B., Yuldasheva, L. N., Varanda, W. A., and Nogueira, R. A. (1998) A novel approach to study the geometry of the water lumen of ion channels: colicin Ia channels in planar lipid bilayers. *J. Membr. Biol.* **161**, 83–92
44. Sabirov, R. Z., Krasilnikov, O. V., Ternovsky, V. I., and Merzliak, P. G. (1993) Relation between ionic channel conductance and conductivity of media containing different nonelectrolytes. A novel method of pore size determination. *Gen. Physiol. Biophys.* **12**, 95–111
45. Krasilnikov, O. V., Sabirov, R. Z., Ternovsky, V. I., Merzliak, P. G., and Muratkhodjaev, J. N. (1992) A simple method for the determination of the pore radius of ion channels in planar lipid bilayer membranes. *FEMS Microbiol. Immunol.* **5**, 93–100
46. Mark, J. E., and Flory, P. J. (1965) The configuration of the polyoxyethylene chain. *J. Am. Chem. Soc.* **87**, 1415–1422
47. Rempp, P. (1957) Contribution à l'étude des solution de molecules en chaine a squelette oxygene. *J. Chem. Phys.* **54**, 432–453
48. Andersen, C., Schiffer, B., Charbit, A., and Benz, R. (2002) PH-induced collapse of the extracellular loops closes *Escherichia coli* maltoporin and allows the study of asymmetric sugar binding. *J. Biol. Chem.* **277**, 41318–41325
49. Benz, R. (ed) (2001) *Porins: Structure and Function*, WILEY-VCH Verlag GmbH, Weinheim, Germany
50. Schagger, H., Cramer, W. A., and von Jagow, G. (1994) Analysis of molecular masses and oligomeric states of protein complexes by blue native electrophoresis and isolation of membrane protein complexes by two-dimensional native electrophoresis. *Anal. Biochem.* **217**, 220–230
51. Lide, D. R. (ed) (1998) *CRC Handbook of Chemistry and Physics*, 71st Edition, Section 5, p. 99, CRC Press, Inc., Boca Raton, FL
52. Bárcena-Uribarri, I., Thein, M., Maier, E., Bonde, M., Bergström, S., and Benz, R. (2013) Use of nonelectrolytes reveals the channel size and oligomeric constitution of the *Borrelia burgdorferi* P66 porin. *PLoS ONE* **8**, e78272
53. Skare, J. T., Shang, E. S., Foley, D. M., Blanco, D. R., Champion, C. I., Mirzabekov, T., Sokolov, Y., Kagan, B. L., Miller, J. N., and Lovett, M. A. (1995) Virulent strain associated outer membrane proteins of *Borrelia burgdorferi*. *J. Clin. Invest.* **96**, 2380–2392
54. Belisle, J. T., Brandt, M. E., Radolf, J. D., and Norgard, M. V. (1994) Fatty acids of *Treponema pallidum* and *Borrelia burgdorferi* lipoproteins. *J. Bacteriol.* **176**, 2151–2157
55. Tristram-Nagle, S., Kim, D. J., Akhuznada, N., Kucerka, N., Mathai, J. C., Katsaras, J., Zeidel, M., and Nagle, J. F. (2010) Structure and water permeability of fully hydrated diphytanoylPC. *Chem. Phys. Lipids* **163**, 630–637
56. Nablo, B. J., Halverson, K. M., Robertson, J. W., Nguyen, T. L., Panchal, R. G., Gussio, R., Bavari, S., Krasilnikov, O. V., and Kasianowicz, J. J. (2008) Sizing the *Bacillus anthracis* PA63 channel with nonelectrolyte poly(ethylene glycols). *Biophys. J.* **95**, 1157–1164
57. Nikaido, H. (2003) Molecular basis of bacterial outer membrane permeability revisited. *Microbiol. Mol. Biol. Rev.* **67**, 593–656
58. Hancock, R. E., and Bell, A. (1988) Antibiotic uptake into gram-negative bacteria. *Eur. J. Clin. Microbiol. Infect. Dis.* **7**, 713–720
59. Delcour, A. H. (2009) Outer membrane permeability and antibiotic resistance. *Biochim. Biophys. Acta* **1794**, 808–816
60. Sicklinger, M., Wienecke, R., and Neubert, U. (2003) *In vitro* susceptibility testing of four antibiotics against *Borrelia burgdorferi*: a comparison of results for the three genospecies *Borrelia afzelii*, *Borrelia garinii*, and *Borrelia burgdorferi* sensu stricto. *J. Clin. Microbiol.* **41**, 1791–1793

7.2. ANNEX II

QUORUM SENSING AND BIOFILM FORMATION IN *STREPTOCOCCUS* SPECIES

All data presented here were obtained during my internship (Dec 2015- Feb 2016) in Dr. Michael Federle's lab at University of Illinois at Chicago (UIC).

While I was there, I studied a targeted mutant of a putative cell wall hydrolase enzyme in *Streptococcus pyogenes*. I also cloned, expressed and purified a recombinant version of the enzyme and tested its activity in *S. pyogenes* biofilm biogenesis and in peptidoglycan hydrolysis. I also learned how they assess transcriptional activation and biofilm development of quorum sensing (QS) pathways. Thus, I partook in methodologies relating to bacteria culture, genetic cloning, protein purification, bioluminescence assays, and pheromone stimulation. It would be wonderful if these methodologies could help us in our work with antimicrobials loaded in lipid nanoparticles as an alternative therapeutic option to treat *Pseudomonas aeruginosa* respiratory infections. At the very least, we might have new perspectives on quorum sensing (QS) and how cell-cell signaling might contribute to susceptibility or resistance of *P. aeruginosa* to antibiotics.

1-FUNCTION OF 0186c: is it involved in *Streptococcus pyogenes* quorum sensing Rgg-Shp pathway?

1.1. BACKGROUND

The aim of this project was to study the 0186c activity and its contribution on biofilm formation. It was thought that 0186c protein was a transglutaminase like cysteine protease and it was from the same family as stcA protein of other streptococcus species (Fig.1). It was also thought that maybe, stcB and 0186c were working together and the activation of both genes could contribute in biofilm formation.

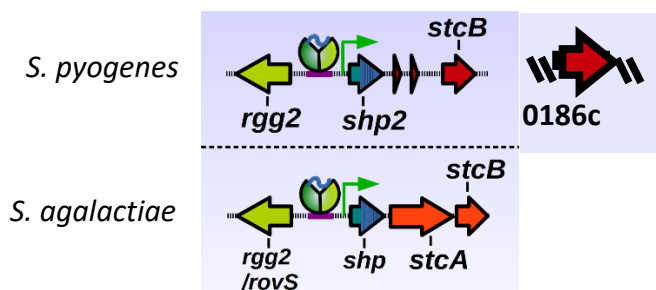


Fig.1. Rgg2/shp2 downstream region in *S.pyogenes*.

The downstream *rgg2* region is required for *shp*-dependent increase in biofilm formation seen in WT (wild type strain) when the *rgg2/3* system is activated (Jiménez JC, data not yet published). As can be seen in Figure 2, in the presence of *shp* (*rgg2/3* system is activated), WT strain presented high levels of biofilm. In contrast, the $\Delta 0186$ strain presented lower biofilm levels than WT.

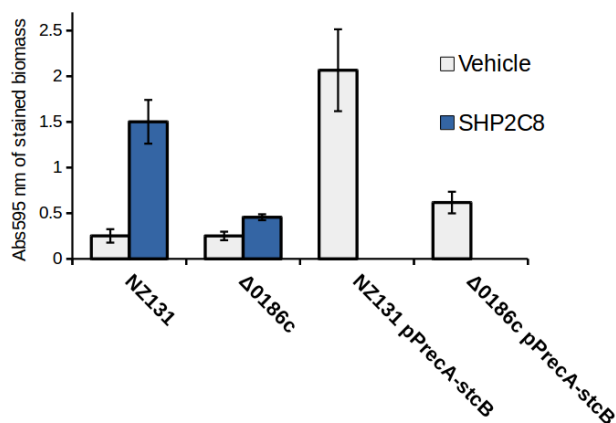


Fig.2. Biofilm levels of *S.pyogenes* cultures.

1.2. EXPERIMENTAL PROCEDURE

Bacterial strains, plasmids and culture media

Bacterial strains and plasmids used in this study are listed in Table 1(184). *S. pyogenes* was routinely grown in Todd-Hewitt Broth with yeast extract (THY) or in chemically defined medium (CDM) containing 1% glucose. Luciferase reporter assays were performed by growing *S. pyogenes* reporter strains in

CDM. When necessary, antibiotics were included at the following concentrations for *S. pyogenes*: chloramphenicol, 3 µg/mL; erythromycin, 0.5 µg/mL.

STRAIN/PLASMID	DESCRIPTION
NZ131	Wild-type <i>S.pyogenes</i> M49 strain
JCJ202	NZ131 Δ 0186; Cm ^r
JCC181	NZ131 Δ rgg2 integrated with pJC219 Pshp3-luxAB reporter; Erm ^r
JCC179	NZ131 integrated with pJC219 Pshp3-luxAB reporter; Erm ^r
JCJ488	NZ131 Δ 0186 integrated with pJC219 Pshp3-luxAB reporter; Erm ^r
P7INT	Shuttle-suicide vector that integrates at streptococcal bacteriophage T12 <i>attB</i> site; Erm ^r
pJC219	DNA fragment containing the shp3 promoter (384bp) fused to luxAB and cloned into p7INT; Erm ^r

Table 1. Bacterial strains and plasmids used in this study. Erm (erythromycin); Cm (chloramphenicol).

Escherichia coli strains NEB- α and BH10C were used for cloning purposes and were grown in LB or on LB agar with ampicillin 100 µg/mL. The *E. coli* expression strain BL21 (DE3) was maintained on LB agar with ampicillin.

Construction of Mutant Strains and Plasmids

Strains used in this study were derived from *S. pyogenes* serotype M49 strain NZ131. Construction of derivative strains and luciferase reporters has been detailed previously (Table1).

Purification of recombinant 0186c

Purification of recombinant 0186c was performed following the protocol described by Aggarwal et al. with a few modifications (185). The *S. pyogenes* NZ131 0186c gene was amplified using primers JJ376 and JJ372 and was cloned into the pEt21A expression vector downstream of the His6 tag; the resulting vector, pJJ292, was electroporated in *E. coli* BL21 (DE3) cells. Expression of His6-0186c was induced at an approximate optical density at 600 nm of 0.5 with 1 mM isopropyl- β -D-thiogalactopyranoside (IPTG) for 5 h at 30°C. Cells were pelleted and suspended in buffer A (PBS [7.4 pH], 20mM imidazole, 10mM β -mercaptoethanol). Cells were disrupted by sonication on ice, and cellular debris was removed by centrifugation at 45,000 x g for 20 min at 4°C. His6-0186c was then purified using a HisPur Ni-NTA Spin Column (Thermo Scientific) and eluted with 250mM imidazole. The purified protein was dialyzed in PBS followed by addition of glycerol to a final concentration of 20% glycerol. Aliquots were stored at -80 °C.

Azocasein assay

Azocasein assay was performed to check the protease activity on recombinant protease (0186c). Summarily, 0186c was diluted 1:1 in assay buffer (0.1 Phosphate Buffer, 0.01mM EDTA, 10mM DTT, pH 7.6) and incubated for 30 min at 37°C to activate enzyme. After activation, protease, azocasein solution (2% Azocasein in assay buffer) and assay buffer were mixed to obtain a final concentration of 1% azocasein, and 1 mg/mL of protease. Also, a no-enzyme control and a positive control (proteinase K) were included in this experiment. Samples were incubated at 37°C and taken very hour. To measure Azo release (as indicator of protease activity) in samples, immediately casein was precipitated with 2.5% TCA, incubated in ice for 10 min and samples were spinned down at 15,000 RPM for 5 min. The absorbance of the supernatant was read at 440 nm. The value of the no-enzyme control reading was subtracted.

BSA assay

BSA assay was performed as described by Dinella et al. (186) with a few modifications in order to check the transglutaminase activity on 0186c protein. Briefly, 1 mg/ml of our protein and 20 mg/mL of BSA were mixed together in a cell wall buffer and at regular intervals samples were taken from the reaction soluble. Then, the samples were run in a 5% acrylamide gel.

Luciferase transcriptional reporter assays

For luciferase assays, bacterial cells from overnight cultures grown at 30 °C were diluted 100-fold into CDM and incubated at 37 °C. In experiments containing synthetic peptides, reporter strains were diluted in fresh CDM containing 25 nM shp3c8 (synthetic peptide). At each time point, 50 µL of each culture was removed to an opaque 96-well plate, samples were exposed to decyl aldehyde (Sigma) fumes for 30 s, and luminescence (counts per second [CPS]) was quantified using a microplate luminometer. The optical density of the culture at OD_{600nm} was also measured at each time point using a spectrophotometer. Relative light units were calculated by normalizing CPS to OD.

Biofilm experiments

Bacterial strains were grown overnight in THY medium at 30 °C and then diluted 1:25 into fresh CDM media containing -/+25 nM shp3c8 or -/+ 80, 55.4 and 8 µg/mL 0186c and then plated in duplicate in cell culture-treated 24 well polystyrene plates.

Plates then were incubated at 37 °C with 5% of CO₂ for 20 h to promote biofilm growth. Medium was aspirated, wells were washed once with 0.9% NaCl, and biomass was dry-fixed overnight. Biofilms were stained with 0.2% crystal violet solution, washed three times with a solution containing 0.9% NaCl and 10% ethanol, and quantified by measurement of absorbance at λ₅₉₅ by an area scan of the wells in a Synergy 2 plate reader. Experiments were performed in duplicate per condition.

1.3. RESULTS AND DISCUSSION

Recombinant protease 0186c had not any effect on QS signaling of *S. pyogenes*

It was performed a light assay to study if the protein 0186c could alter the QS pathway in *S. pyogenes*. Three reporter strains were tested: NZ131, NZ131 Δ 0186c and NZ131 Δ rgg2. The results showed that the luminescence activity was high and similar for all strains and conditions (+/- shp3c8) tested (Fig.3). This point out that the protein had no any effect on the QS signaling, so that the QS is not affected by 0186c mutations.

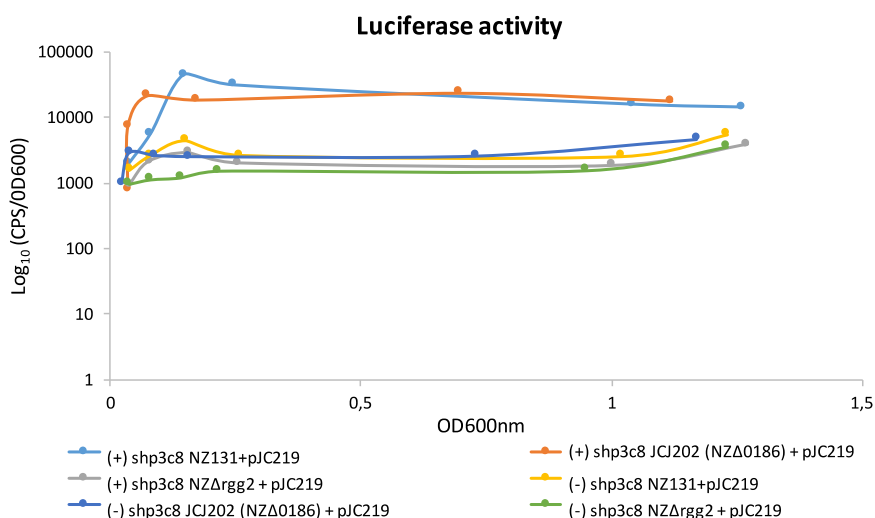


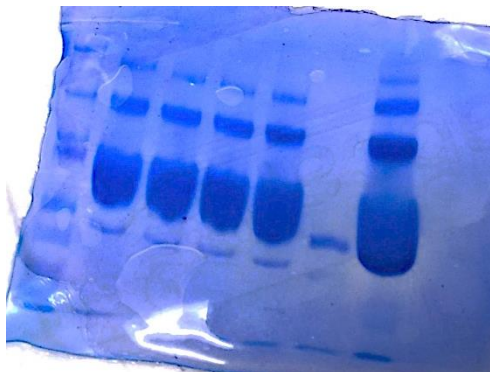
Fig.3. Luminescence activity of $P_{shp3^-}luxAB$ in *S.pyogenes* cultures in response to shp3c8 (25nM).

Recombinant protease 0186c had not present translutaminase nor protease activity

Azocasein assay and BSA assay were performed to check the protein activity. As can be seen in Figure 4.A., no protease activity on 0186c was observed even increasing the concentration. After that, the BSA assay was performed

and no changes were observed in the migration and the protein did not polymerize, so 0186c did not show any transglutaminase activity (Fig.4.B).

A



B

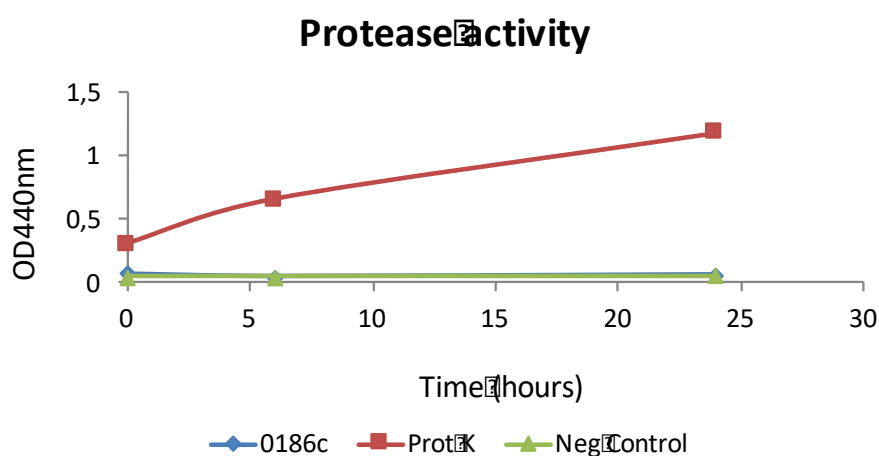


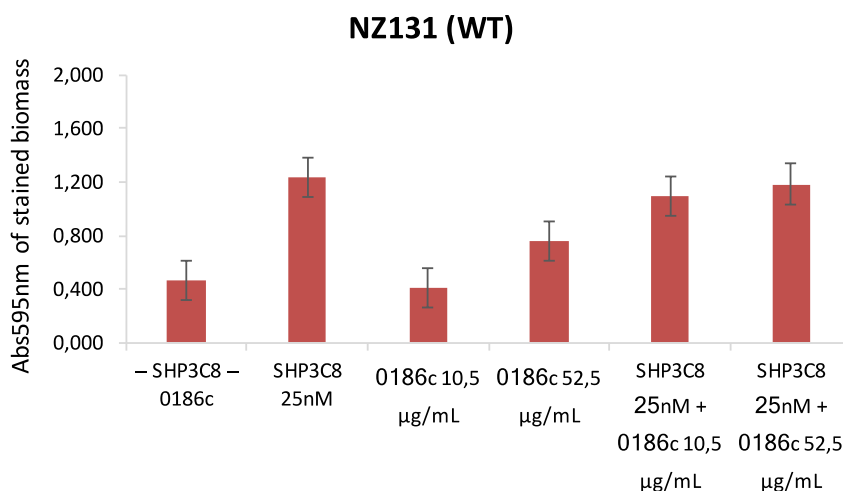
Fig.4. (A) SDS PAGE on 5% acrylamide gel of reaction mixture Tase-casein at different incubation times. (B) Azo releases as indicator of protease activity.

Recombinant protease 0186c in the presence of shp3c8 promotes biofilm formation

Biofilm experiments were performed to observe if 0186c contributes in biofilm formation. Two strains of *S. pyogenes* were tested (NZ131 and NZ131Δ0186) at different conditions. As shown in Figure 5, biofilm levels in the presence of

shp3c8 in the WT strain were higher than those without shp3c8. These results are in accordance with the results obtained by Jimenez JC (data not published yet). In addition, it was observed that biofilm levels in the presence of shp2c8 and 0186c at high concentrations in the mutant strain were so high, suggesting that maybe stcB and 0186c could work together.

A



B

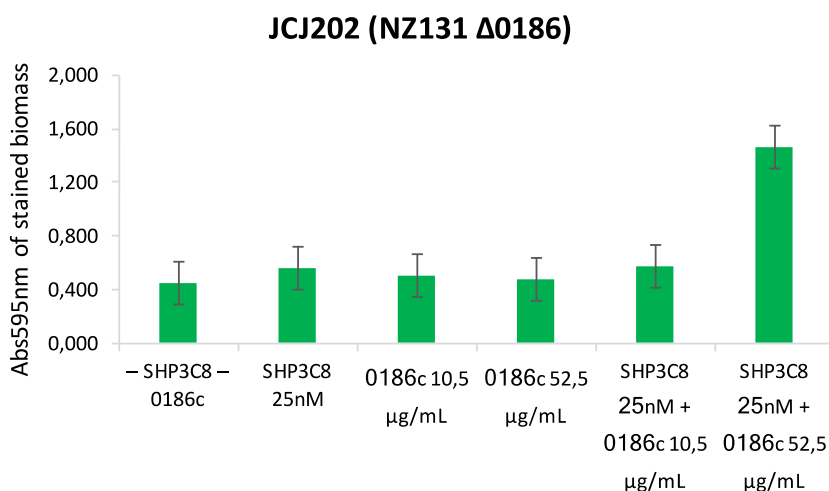


Fig.5. Biofilm levels of *S. pyogenes* cultures at different concentrations of +/- shp3c8 and +/-0186c tested. (A) *S. pyogenes* NZ131 (WT). (B) *S. pyogenes* NZ131 Δ 0186.

2-Study if *rgg2/shp2* system of *Streptococcus iniae* also contributes to biofilm formation.

2.1. BACKGROUND

The aim of this project was to study the function of Rgg2/shp2 system on the *S. iniae* behavior and the contribution to biofilm formation. *S. iniae* is a specie of the pyogenic group streptococci and normally it is a fish pathogen but occasionally has produced infection in humans. *S. iniae* has the homologous *S. pyogenes* loci encoding *rgg2-shp2* with its downstream associated genes (Fig.6 and 7) (187).

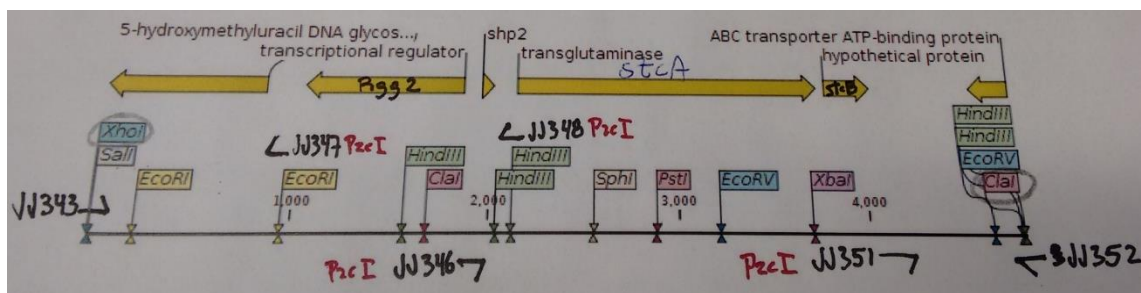


Fig.6. Rgg2/shp2 region in *S. iniae*.

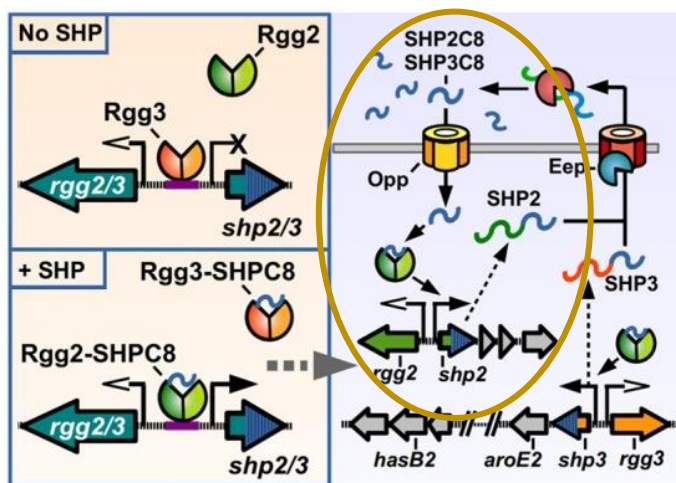


Fig.7. Rgg2/shp2 system in *S. pyogenes* (187).

2.2. EXPERIMENTAL PROCEDURE

Bacterial strains, plasmids and culture media

Bacterial strains and plasmids used in this study are listed in Table 2. *S. iniae* was routinely grown in THY or in CDM containing 1% glucose. Luciferase reporter assays were performed by growing *S. iniae* reporter strains in CDM and THY. When necessary, spectinomycin was included at a concentration of 100 ug/mL for *S. iniae*.

STRAIN/PLASMID	DESCRIPTION
9177	Wild-type <i>S. iniae</i> strain
9066	Wild-type <i>S. iniae</i> strain
JCC022	9177 integrated with pLC301 Pshp2-luxAB reporter; Spec ^r
pL2Sp	Shuttle-suicide vector that integrates at streptococcal bacteriophage T12 <i>attB</i> site; Spec ^r
pLC301	DNA fragment containing the shp2 promoter fused to luxAB and cloned into pL2Sp; Spec ^r

Table 2. Bacterial strains and plasmids used in this study. Spec (spectinomycin).

Construction of Mutant Strains and Plasmids

Strains used in this study were derived from *S. iniae* 9177 and 9066 strains. Construction of derivate strains and luciferase reporters has been detailed previously (Table 2).

Luciferase transcriptional reporter assays

For luciferase assays, bacterial cells from overnight cultures grown at 30 °C were diluted 100-fold into CDM and THY and incubated at 37 °C. In experiments containing synthetic peptides, reporter strains were diluted in THY and in fresh CDM containing 25 nM shp3c8 (synthetic peptide). In experiments containing cyclosporine A, reporter strains were diluted in fresh CDM containing 25 nM shp3c8 and 5 µM cyclosporine. At each time point, 50 µL of each culture was removed to an opaque 96-well plate, samples were exposed to decyl aldehyde (Sigma) fumes for 30 s, and luminescence (counts per second [CPS]) was quantified using a microplate luminometer. The optical density of the culture at OD_{600nm} was also measured at each time point using a spectrophotometer. Relative light units were calculated by normalizing CPS to OD.

Biofilm experiments

Bacterial strains were grown overnight in THY medium at 30 °C and then diluted 1:25 into fresh CDM media containing -/+25 nM shp3c8 and then plated in duplicate in cell culture-treated 24 well polystyrene plates.

Afterwards, plates were incubated at 37 °C with 5% of CO₂ for 20 h to promote biofilm growth. Medium was aspirated, wells were washed once with 0.9 % NaCl, and biomass was dry-fixed overnight. Biofilms were stained with 0.2 % crystal violet solution, washed three times with a solution containing 0.9 % NaCl and 10 % ethanol, and quantified by absorbance measures at λ₅₉₅ by an area scan of the wells in a Synergy 2 plate reader. Experiments were performed in duplicate per condition.

2.4. RESULTS AND DISCUSSION

S. iniae rgg2/shp2 system is activated in the presence of shp2

The luciferase assay was performed in order to check if the rgg2/shp2 system of *S. iniae* was involved in the QS pathway. The experiment was made under two different conditions: with and without shp2. As can be seen in Figure 8,

one could observe big increase in the luciferase activity and it means that without shp2, the rgg2/shp2 system is not activated. Moreover, it was observed that THY medium do not induce Pshp expression suggesting that *S. iniae* needs CDM with glucose as the primary carbon source to activate *shp* gene expression.

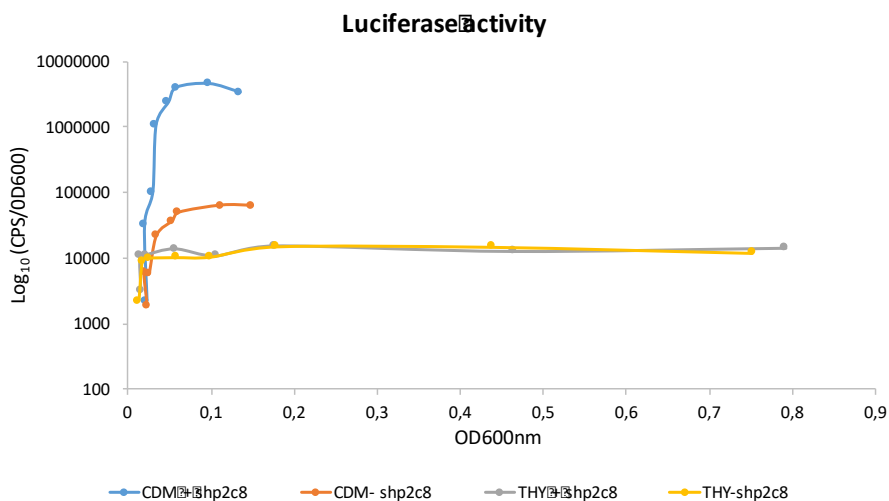


Fig.8. Luminescence activity of the P_{shp2} -*luxAB* reporter in response to a single concentration (25 nM) of shp2c8.

Cyclosporine A blocks quorum sensing in *S. iniae*

It was previously demonstrated that addition of SHP pheromones to cultures of *S. iniae* strain 9177 stimulates activation of rgg2/shp2, and therefore we wanted to elucidate if the Rgg antagonists (cyclosporine A) were capable of blocking this function. As shown in Figure 9, 5 μ M of CsA stopped activation of the P_{shp2} -*luxAB* reporter in strain 9177. These results agree with the ones published by Aggarwal et al. focusing on *S. pyogenes* (185).

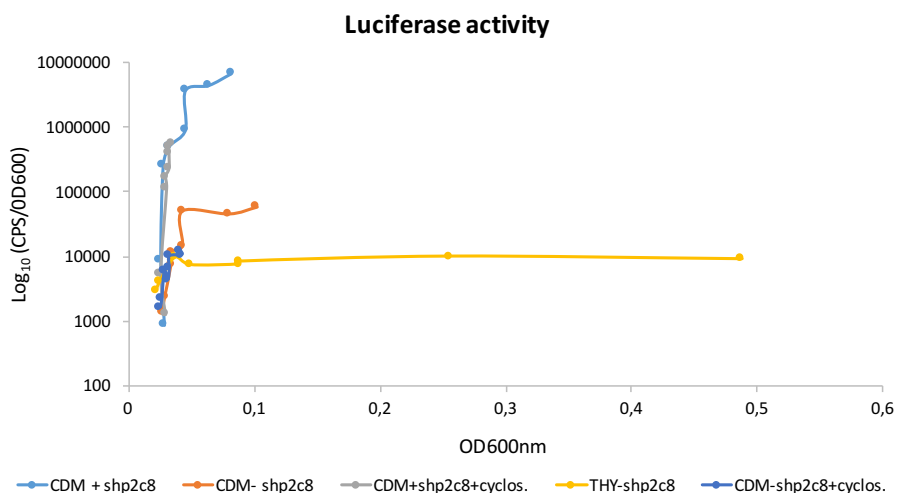


Fig.9. Luminescence activity of $P_{shp2-luxAB}$ in *S.iniae* cultures in response to CsA (5 μ M) and shp2c8 (25 nM).

SHP-dependent biofilm development

It was previously reported that addition of SHP pheromones to cultures of *S. pyogenes* strain NZ131 stimulates development of biofilms (184)(188), and therefore we investigated if this also occurs in *S. iniae*. The results of this experiment showed that biofilm levels were higher in the presence of pheromone (Fig.10)

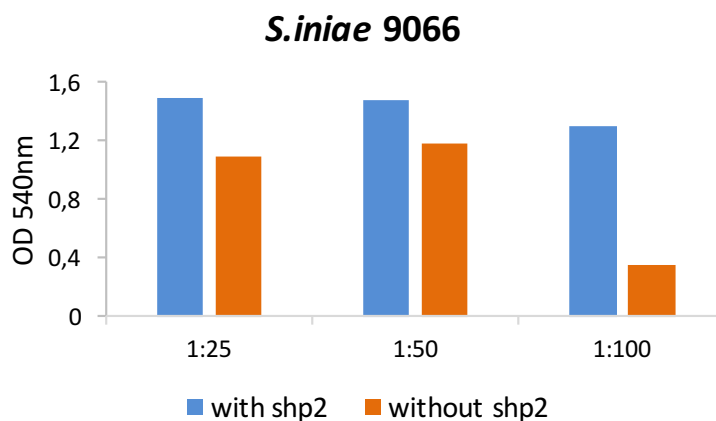


Fig.10. Biofilm levels of *S. iniae* strain 9066 at different concentrations of bacteria tested, with and without shp2c8.

CONCLUSIONS

- Recombinant protease 0186c had not any effect on QS signaling of *S.pyogenes*.
- Recombinant protease 0186c had not present transglutaminase nor protease activity.
- Recombinant protease 0186c in the presence of sph3c8 promotes biofilm formation.
- *S.iniae* rgg2/shp2 system is activated in the presence of shp2.
- Cyclosporine A blocks quorum sensing in *S.iniae*.
- The addition of SHP pheromones to cultures of *S.iniae* stimulates development of biofilms.
- The multiple QS systems of GAS offer interesting molecular targets to block or interfere in order to modulate the behavior of this pathogen as a way of future treatment.

REFERENCES

1. Aggarwal C, Jimenez JC, Nanavati D, Federle MJ. Multiple length peptide-pheromone variants produced by *Streptococcus pyogenes* directly bind Rgg proteins to confer transcriptional regulation. J Biol Chem. 2014;289:22427–36.
2. Aggarwal C, Jimenez JC, Lee H, Chlipala GE, Ratia K, Federle MJ. Identification of quorum-sensing inhibitors disrupting signaling between rgg and short hydrophobic peptides in Streptococci. MBio. 2015;6:1–11.
3. Dinnella C, Gargaro MT, Rossano R, Monteleone E. Spectrophotometric assay using o-phthaldialdehyde for the determination of transglutaminase activity on casein. Food Chem. 2002;78:363–8.
4. Jimenez JC, Federle MJ. Quorum sensing in group A Streptococcus. Front Cell Infect Microbiol. 2014;4:127.
5. Chang JC, LaSarre B, Jimenez JC, Aggarwal C, Federle MJ. Two group a Streptococcal peptide pheromones act through opposing Rgg regulators to control biofilm development. PLoS Pathog. 2011;7: e1002190.